2013

A Novel Globally Optimized Instantaneous Torque Ripple Minimization Method in Switched Reluctance Motors with Matrix Converter Drives

Syeda Fatima S. Ghousia
University of Windsor

A Novel Globally Optimized Instantaneous Torque Ripple Minimization Method in Switched Reluctance Motors with Matrix Converter Drives

By

Syeda Fatima Ghousia

A Dissertation
Submitted to the Faculty of Graduate Studies
through **the Department of Electrical and Computer Engineering**
in Partial Fulfillment of the Requirements for
the Degree of **Doctor of Philosophy**
at the University of Windsor

Windsor, Ontario, Canada

2013

A Novel Globally Optimized Instantaneous Torque Ripple Minimization Method in Switched Reluctance Motors with Matrix Converter Drives

by

Syeda Fatima Ghousia

APPROVED BY:

_____

Sheldon S. Williamson, External Examiner
Department of Electrical and Computer Engineering, University of Concordia

_____

Nadir Zamani,
Department of Mechanical Engineering, University of Windsor

_____

Govinda Raju,
Department of Electrical and Computer Engineering, University of Windsor

_____

Jonathan Wu,
Department of Electrical and Computer Engineering, University of Windsor

_____

Xiang Chen,
Department of Electrical and Computer Engineering, University of Windsor

_____

Narayan C. Kar, Advisor
Department of Electrical and Computer Engineering, University of Windsor

[May 14, 2013]

DECLARATION OF ORIGINALITY

I hereby certify that I am the sole author of this thesis and that no part of this thesis has been published or submitted for publication.

I certify that, to the best of my knowledge, my thesis does not infringe upon anyone's copyright nor violate any proprietary rights and that any ideas, techniques, quotations, or any other material from the work of other people included in my thesis, published or otherwise, are fully acknowledged in accordance with the standard referencing practices. Furthermore, to the extent that I have included copyrighted material that surpasses the bounds of fair dealing within the meaning of the Canada Copyright Act, I certify that I have obtained a written permission from the copyright owner(s) to include such material(s) in my thesis and have included copies of such copyright clearances to my appendix.

I declare that this is a true copy of my thesis, including any final revisions, as approved by my thesis committee and the Graduate Studies office, and that this thesis has not been submitted for a higher degree to any other University or Institution.

ABSTRACT

The tangential component of electromagnetic force in switched reluctance motors (SRM) produces the desired torque which fluctuates with rotor position due to the doubly saliency in physical structure of SRM. The conventional methods are insufficient to completely compensate for the intrinsic behavior due to double saliency.

This dissertation proposes a novel method of eliminating the torque ripple in the instantaneous torque profile of SRM and a method to generate the precise reference phase current waveforms for even open loop operational design through global optimization. For the purpose of implementation of the proposed method, a non-sinusoidal DC matrix converter is also proposed to generate such waveforms without using multiple source voltages and to be able to use the drive in electric vehicle applications where a battery system is available for DC voltage sources.

The experimentally-obtained characteristics are used for finding the optimal solution for torque ripple reduction. FEA is used to investigate the accurate EM force and its radial and tangential components using volume integration method. The proposed global optimization method can give a precise solution for this non-linear problem. Therefore a modified fast-filled method is proposed to balance out the crests and troughs of the torque ripples throughout the operation of SRMs. A set of novel reference current waveforms are generated for feed-forward torque control.

Comparative analyses with the torque and current profiles of conventional methods are performed to prove the elimination of ripple up to less than 1% by using the proposed method. Therefore, it is concluded that the advanced turn-on and delayed turn-off angles with gradual rise and fall significantly eliminate the ripple.

Inverter topology requirement for SRM is geometry-dependent. A multi-level converter is more suitable to generate the required position-dependent phase current. Matrix converters can be used for finer control on flexible current profiling. Therefore, a non-sinusoidal DC matrix converter is proposed to generate the required phase current waveforms from a single DC source and to accommodate the changes if required accurately. Three reduced-switching states schemes were tested with matrix converter resulting in the ripple elimination between 0.9% - 2% where 0.45% reduction is possible.

DEDICATION

This dissertation is dedicated to my incredibly wonderful husband, *Zulfiqar Ali Qureshi (ZAQ)*, and my beautiful and precious daughters Duaa and Michelle. Thank you for your love, support, patience, and numerous sacrifices throughout my PhD program. This thesis and the pursuit of my goals would not have been possible without you. I give my deepest expression of love and appreciation for the encouragement that you gave and the sacrifices you made during this graduate program. Thank you for the support and company during late nights work.

Duaa and Michelle: Thank you for your patience, encouragement, for making me laugh, and for providing great joy, beauty, and truth to my life. Both of you has shown me that learning is a life-long process. I have learned so much from both of you. I love you more than I can say, and I am extremely fortunate and proud to be your mother. Thank you for being there for each other too and listening to your daddy with remarkable patience whenever mommy was busy in the nights.

ZAQ: I cannot possibly thank you enough for all of your unconditional love, constant support, and encouragement from the beginning of our marriage. I am eternally grateful. You are everything to me. I love you, always and forever.

ACKNOWLEDGEMENTS

I am thankful to Allah (God) for his uncountable blessings and merciful guidance to finish this dissertation successfully. I am also thankful to my prophet Muhammad (peace be upon him and his family) for being the role model for me and teaching me the importance of seeking knowledge in a human life.

After that I am indebted to many people who have been an integral part of my research and supportive throughout my PhD program. I am most grateful to Dr. Narayan C. Kar for taking me under his wing as a Ph.D. student, his everlasting support and enthusiasm, his advices, humor and positive attitude when things did not go as planned (countless times!), handling with grace the delicate balance of guidance while allowing me to be independent with my research, and finally on a personal level, for being my academic big brother and supportive of my growing family, which includes my husband, my daughters and myself and for being such a wonderful mentor and providing me with support, guidance, and patience throughout this research.

I would like to express my gratitude to my other committee members Dr. Raju, Dr. Zamani, Dr. Wu, and Dr. Chen, for their valuable advice and feedback. I would also like to thank Andria Ballo, the Graduate Secretary, ECE department, for her resourceful support and friendliness. I am thankful to all my colleagues in the department and chargelabs specifically for their encouragements and supports.

And finally, I could not have done this without the love and support of my family. I would also like to thank my parents for visiting me and staying with me in Canada for the sake of completion of my dissertation. I can't thank my mom enough. She made me whaever I am. Thanks to my bundles of endless joy Duaa and Michelle. I also hope that as your curiosity grows, so will your love of knowledge, research and reasoning. At the end, I like to thank my husband, ZAQ who has been so incredibly supportive during my studies. He also has this uncanny ability to stay calm, hopeful, and patient in the midst of disaster, which has made the process of finishing a dissertation, searching for jobs, and always available for taking care of two young children while himself going through the same simultaneously i.e. busy with his own research and his own dissertation. Thank you, ZAQ. You are the greatest gift of Allah to me. I can only hope to bring you as much joy as you have given me.

TABLE OF CONTENTS

LIST OF TABLES

LIST OF FIGURES

LIST OF ABBREVIATIONS/ SYMBOLS

AC	:	Alternating Current
BDS	:	Bidirectional Switch
BLDC	:	Brushless DC motors
DAC	:	Dwell Angle Control
DC	:	Direct Current
DTC	:	Direct Torque Control
EMF	:	Electromagnetic Force
EMI	:	Electromagnetic Interference
EV	:	Electric Vehicles
FC	:	Frequency Converter
FEA	:	Finite Element Analysis
FEM	:	Finite Element Method
FPGA	:	Field Programmable Gate Arrays
HEV	:	Hybrid Electric Vehicle
HP	:	Horse Power
IGBT	:	Insulated Gate bipolar Transistor
IC	:	Integrated Circuits
IEC	:	International Electro-technical Commission
IM	:	Induction Machines
IPM	:	Interior Permanent magnet
ISO	:	International Standardization Organization
LF	:	Lorenz Force
MC	:	Matrix Converter
MLE	:	Multi-Level Excitation
MMF	:	Magneto Motive Force
MST	:	Maxwell's Stress Tensor
NLP	:	Non-Linear Problems
PM	:	Permanent Magnet
PWM	:	Pulse Width Modulation

RB	:	Reverse Blocking
RPM	:	Revolutions Per Minute
SF	:	Saliency Force
SM	:	Synchronous Machines
SRM	:	Switched Reluctance Motors
TSF	:	Torque Sharing Function

NOMENCLATURE

σ_t	:	Tangential stress
σ_n	:	Normal or radial stresses
B_t	:	Tangential flux density
B_n	:	Normal or radial flux density
J	:	Current density
Ψ	:	Magnetic flux
θ	:	Rotor position
i	:	Instantaneous phase current
θ_{pitch}	:	Dwell angle
m	:	modulation index
θ_c	:	Critical rotor position
j	:	Current phase
$T_{i,}(\theta)$	:	Instantaneous torque at $i_j(\theta)$
k	:	Torque constant ratio
$k_{T,j}$	:	Torque constant ratio for phase j
k_0	:	Torque constant ratio between neighboring phases
$R_t(\theta)$	:	Torque ripple at θ
θ_{on}	:	Turn-on angle
ω	:	Motor speed
θ_{off}	:	Turn-off angle
θ^x_c	:	Critical angle at equal x in neighboring phases

Chapter 1

INTRODUCTION

1.1 Research Background

Recently, Switched reluctance motor (SRM) drives have received more and more attention in the field of high performance drives because of their simple construction, robust design, lower weight and size due to the absence of rotor windings, variable speed operations, higher torque-to-inertia ratio, inexpensive, reliability, ruggedness, fault tolerance, reduced number of power switches requirement, and relatively low manufacturing costs leading to attractiveness for industrial and electrical vehicle (EV) applications [1], [2]. An SRM can produce high torque at low speed. Furthermore, these features make SR drives a viable alternative to other commonly used motors like AC, BLDC, PM Synchronous or universal motors for numerous applications[3], [4]. A well designed SRM drive system matches the performance of the conventional ac motor drives and it has several advantages over them due to unipolar rotor torque. However, it still needs broad industry acceptance due to his high torque ripple, excessive machine vibrations, and undesirable acoustic noise [5].

Any electrical machine has to be thoroughly studied in the design stage for its static and dynamic performance before the finalization of its design and/or control. Therefore, the first phase of the research work consists of the complete analysis of the electromagnetic characteristics of the machine in terms of its electromagnetic force, flux, current and torque profiles with respect to rotor angle between stator and rotor poles [6].

SRMs are basically characterized by a strongly non-linear behaviour due to its typical operation in a magnetic saturation region; there is no analytical equation to describe their behaviours [7]. The numerical determination can be based on finite-element method (FEM) analysis, conveniently used to obtain machine magnetic vector potential values in the presence of complex magnetic materials [8]. Therefore, significant research in the development of more appropriate numerical algorithms for a FEM study of SR machines has been done in the past years [9]. Many authors have proposed analytical methods to predict the unsaturated magnetic characteristics of SRM as in for an 8/6 SRM and in only for the unaligned inductance [10]. However these methods are quite laborious and cannot be used to predict the dynamic behaviour of the machine. Therefore an accurate FEA is required to match the fingerprints of the machine under study.

Due to the absence of windings on the rotor, stored energy in the air gap of the SRM is almost entirely converted into the mechanical form except for the iron losses in the rotor [11]. This magneto-mechanical energy conversion is manifested in the distribution of the radial and tangential force components around the circular air gap [12]. Tangential component of the force is acting on the rotor and stator poles resulting in generation of the electromagnetic torque on the rotor and tangential vibration of the stator poles. The radial component of the force, on the other hand, appears as a by-product and mainly contributes to the radial vibration of the stator which is known to be the main origin of acoustic noise in SRM drives [13], [14]. The ripple in the instantaneous torque profile decreases the efficiency [15]. Therefore, the study of electromagnetic force distribution in all directions is also important in order to keep the tangential component constant to eliminate the ripple in the torque and improve the drive efficiency.

The reduction of torque ripple is the main target in research for designing a variable drive system with switched reluctance motors (SRM) for higher torque density and better efficiency [5]. This ripple is mainly due to the transition of excitation current between the adjacent phases. Precise control of turn-on and turn off angle is required to smooth the torque [16]. Effects of selecting the turn-on and turn-off angles are studied in detail with simulation results. It is observed that with the extended turn-on and turn off angles, the precise selection of turn-on and turn off angle can alter the shape of the excitation current in the stator coil and its point of overlapping with the adjacent coil. Therefore the transition between different phases can be smoothed out. The impact of this alteration on the excitation current and torque ripple as a function of different parameters of dwell angle is also studied paper. It is found that a sinusoidal current shape can also be obtained with the proper selection of these parameters.

Keeping the tangential component of the EM force constant throughout the electrical and mechanical cycle requires constantly varying input current source as well as the freedom of choosing the rotor position because the amount of torque does not depend only on the input current but also on the rotor position [17]. A global optimization method is proposed to balance out the crests and troughs of the torque ripples throughout the operation. Open loop simulations with precise drive model in the form of its fingerprints are studied. These fingerprints are actually the intrinsic electromagnetic characteristics of the machine. It is suggested that the proposed reference current waveforms will improve the performance by compensating for the intrinsic behavior of the machine which is the non-linear relationships of torque with phase currents and rotor positions.

1.2 Research Objectives

Direct torque Control (DTC) methods [18] which are usually employed in feedback and control system of an electrical drive can only improve the average torque value in case of SRM and cannot improve the instantaneous torque ripple produced due to the double saliency structure. This is because when the feedback reaches the command signal, rotor has already change its position and the input signal requirement changes for the same EM force with respect to the geometrical structure of the machine [19].

Therefore, different approaches have been adopted by researchers to reduce the ripple in the torque to improve the percentage of torque ripple in the instantaneous torque and optimize the benefits of different methods employed for the torque the problem has to be solved with the adoption of non-linear problem solving approach [20].

There are many approaches to achieve the objectives. Some of them are as follows:

- Modification in the geometric structure of the machine such as increasing the number of poles shapes of poles etc. [21]-[33].
- Suggestions to alter the winding configuration such as short-pitch, concentrated coil etc. [34], [35]
- Variations in the dwell angle parameters [36]-[38]
- Multi-level phase excitation [39]
    1. Unipolar switching [40], [41]
    2. Bipolar switching [42]

However, among all these solutions, there is still no single solution which can exactly address all operating conditions and which can compensate for the ripples in all regions of the saturation curve. This is because usually the solution is based on the

machine modelling and requires an exact model of the machine which is quite impossible. Therefore, the research objective of this dissertation is to propose a global non-linear solution which can be applied under all operating conditions.

1.3 Research Approach and Key Contributions

In this section the contributions of this dissertation are presented to fulfil the objectives discussed in the previous section. Since the research approach is to use the experimental data instead of a mathematical or analytical model, the first contribution is the identification of regions of interests individually and the study of co-relation of geometry with the electromagnetic characteristics (chapter 3).

The second contribution is the evaluation of the deficiencies and inaccuracies of energy method which is usually employed for modelling and another method is evaluated to determine the accurate force distribution. On the basis of this accurate force distribution and its tanegntial component profile, the deffficiencies in each region and its possible local solutions are evaluated (chapter 4).

The third contribution is the comparative performance evaluation of each local solution when implemented individually and also simultaneously. Therefore, optimization of these local solutions is evaluated as a global solution to this non-linear problem, and the results are analyzed for the extent of their effectiveness and limitations for the simultaneous implementation. The results are quite desirable. However there are some adverse effects such as some other sources of ripple generation occurs which are quite lower as compared to initial problem but it exists. Hence it lowers the benefits from as compared to their indivdual use (chapter 5).

The forth contribution which is one of the two key contributions is the proposal of applying a modified version of a genetic optimization algorithm known as fast-filled method for fast filling colors in artificial intelligence which will give a fastest, accurate and more efficient solution to this problem (chapter 6). It is accurate because it is a model-free solution because it takes into account the experimental data instead of approximate models. In such case, there is no chance of propagating the modelling error into the solution. Since there is no model of the machine, no errors due to parameter sensitivity or uncertainty is expected. This is because the method is using the actual values of the machine characteristics and if any of the parameter is changed, for example, if the winding resistence increases with the passage of time, the machine EM characteristics will change automatically and only recaliberation will solve the problem. (FEA model is simply the rebuilding of the machine virtually with exact EM characteristics for cold test runs).

The fast fill algorithm is a generic algorithm for global optimization techniques. Therefore, the term global for this solution is significant solution which can work on all regions of electromagnetic characteristics curves of the machine equally. This will make the solution geometric-dependent instead of drive operating conditions and speed dependent. As a result, it also generates a set of exact and unique input phase current profiles for switching. It also optimizes the results for the minimum variations in input current.

The last and the other key contribution is the proposal of a design of a non-sinusoidal matrix converter for the drive to implement these input phase currents. Matrix converter is an ac-ac converter which can ideally produce any ac-output with any ac-input

through modulation and usually works for sinusoidal input and output. However, many researchers have proposed it for non-sinusoidal output. With no energy storage element or passive components, the number of active switches and considering the switching losses and frequency determines the efficieny of the converter. Therefore, the efficiency is analyzed by reducing the number of switches (using sparse MC) and switching states. by reducing the number of DC level sensitivity.

The classical matrix converter topology is modified not only for the non-sinusoidal output but also for the DC input source. A DC source instead of a 3-phase sinusoidal input source is chosen for feasibility analysis of SRM drive for electric vehicles whichs run on batteries to be able to achieve any desirable DC level. Since matrix converters donot have any energy storage element and its power factor can be fully controlled, it gives a motivation to eliminate the DC link energy storage elements in electric vehicles by using the matrix converters.

1.4 Thesis Organization

This thesis consists of eight chapters and four appendices. The appendices consist of matrix data in the form of tables generated to implement the global optimization method. The raw experimental data set and the processed data set cannot be plotted as a function and can not be presented accurately in the graph form for detailed study or future work.

Chapter 2 provides an introduction to a typical market-available traditional SRM including its distinctive features, motor design, its construction, and basic operation. It also provides the identifying characteristics of the machine and its typical control methods. In summary, the theoretical study of the SRM is provided.

Chapter 3 presents the details of the development finite element analysis (FEA) model of the SRM to study the non-linear electromagnetic characteristics of the SRM in terms of flux and torque with respect to the excitation current and rotor position. Therefore, comparative analyses of the proposed torque ripple minimization technique with other typical methods can be performed on this FE model. FEM simulations require complete information about the geometrical parameters of SRM. It could be used as a prior stage during the development of the electromechanical system.

Chapter 4 consists of a comprehensive study of the electromagnetic force and its distribution in tangential and radial directions as well as their desired and adverse effects on instantaneous torque profile. It also provides the regions of torque profile where tangential force decreases significantly, therefore, keeping a constant torque profile is not possible and thus causing ripple. Also the accurate EM force has been calculated using tunable volume integration method.

Chapter 5 discusses the effects of the dwell angle control parameters in terms of advanced angle, delayed tail angle and duration of the conduction angle. An optimization procedure is also adopted for the best possible results in terms of torque ripple minimization. The results are compared with the effects of these parameters individually as well as in optimized situation not only in terms of the percentage of the torque ripple reduction but also the amount of total average generated torque.

Chapter 6 describes the proposed global NLP optimization method for the torque ripple minimization in detail. Since the torque at any instant is not only dependent on the position of the rotor but also on the amount of current in the excitation coil. Therefore, an optimization between dwell angle parameters and multi-phase multi-level

current excitation can provide a better control on keeping the desired instantaneous torque level constant. It also includes the comparative analysis of the results of global NLP optimization method with conventional methods. A set of reference excitation current waveforms are also generated for feed-forward and open-loop operations of SRM.

Chapter 7 proposes the use of the popular ac-ac matrix converter for this proposed method requirement of variable reference current waveform. A sparse-matrix converter is simulated to give an example of how a single power source can be used for multiple levels of required current in different phases of the SRM at the same time as required. The comparative analysis in terms of torque ripple reduction of the results obtained by selection of a few of the allowable switching states of the sparse matrix model is presented with the proposed excitation current waveforms in FEA machine model.

Chapter 8 presents the conclusions of this research.

Appendix A contains the experimental data obtained from the Lab SRM

Appendix B contains database constructed for the proposed method.

Appendix C contains the instantaneous torque profile obtained by the most efficient of the typical methods of torque ripple minimization i.e. advanced angle etc.

Appendix D contains the instantaneous torque and phase current profiles obtained by the matrix converter design after the implementation of the global NLP optimization method.

Chapter 2

OVERVIEW OF SWITCHED RELUCTANCE MOTORS

2.1 Introduction

Since, switched reluctance motors (SRM) are gaining wider popularity among variable-speed drives, some of the SRM design parameters, identifying characteristics and FEA analyses are presented. SRM has currently been given a considerable attention in the field of high performance drives. The research work has globally been done in both industrial and university sectors. They offer the advantages of simple structure, low-cost construction characterized by an absence of magnets and rotor winding, high level of performance over a wide range of speeds fault tolerance, and mechanical robustness, leading to attractiveness for industrial and electrical vehicle (EV) applications. Furthermore, the availability and the moderate cost of the necessary electronic components make SR drives a viable alternative to other commonly used motors like AC, BLDC, PM Synchronous or universal motors for numerous applications. After the design verification methods some of the modern control techniques of SRM are also discussed.

2.2 Distinctive Features of SRM

From the literature review, these are some unique features of the traditional SRM configurations in comparison to other motors available.

- Lowest construction complexity, many stamped metal elements especially helpful for the size and weight restrictions on HEV
- Like a BLDC or stepper without the permenant magnets

- High reliability (no brush wear), failsafe for Inverter (it eliminates the possibility of a rail-to-rail short circuit) but acoustically noisy
- High efficiency
- Fault tolerant [43]
- Motor EMI good but terrible EMI from Inverter
- Driven by multi-phase Inverter controllers [44]-[49]
- Sensor-less speed control possible [50]
- Higher total system cost than for DC motors.
- Inverter 'shoot-through' not possible so higher reliability for automotive
- Torque ripple can be reduced by advanced control techniques [51]-[57]
- Very Robust and high speed operation is possible
- High start-up torque and high torque density.
- Intrinsically high torque ripple (i.e. high torque pulsation at low speed) may cause noise and vibration if mechanical tolerances are not held to close limits.

However, it can be reduced by different operational and advanced control techniques such as electronic switching control for its operation because torque in the switched reluctance machine is produced by pulses of phase current synchronized with rotor position. The timing and regulation of these current pulses are controlled by the drive circuit and the torque control scheme. Several power stage topologies are being implemented, according to the number of motor phases and the desired control algorithm. A power stage with two independent power switches per motor phase is the most used topology. This particular topology of SRM power stage is fault tolerant in contrast to

power stages of AC induction motors because it eliminates the possibility of a rail-to-rail short circuit. SRM requires position feedback for motor phase commutation. In many cases, this requirement is addressed by using position sensors, like encoders, Hall sensors, etc. The result is that the implementation of mechanical sensors increases costs and decreases system reliability.

Traditionally, developers of motion control products have attempted to lower system costs by reducing the number of sensors. A variety of algorithms for sensor-less control have been developed, most of which involve evaluation of the variation of magnetic circuit parameters that are dependent on the rotor position.

2.3 Traditional SRM Design

SRM is a rotating electric machine where both stator and rotor have salient poles (Figures 2.1 and 2.2). Traditional switching can be described as follows:

- The motor is excited by a sequence of current pulses applied at each phase of the stator which are consequently excited, forcing the motor to rotate.
- The current pulses need to be applied to the respective phase at the exact rotor position relative to the excited phase.
- The inductance profile of SRM is triangular shaped, with maximum inductance at fully aligned position and minimum inductance at unaligned.
- The motor creates torque in the direction of increasing inductance. When the phase is energized in its minimum inductance position, the rotor moves to the forthcoming position of maximal inductance.
- The excitation phase current profiles together with the magnetization characteristics define the generated torque and thus the speed of the motor.

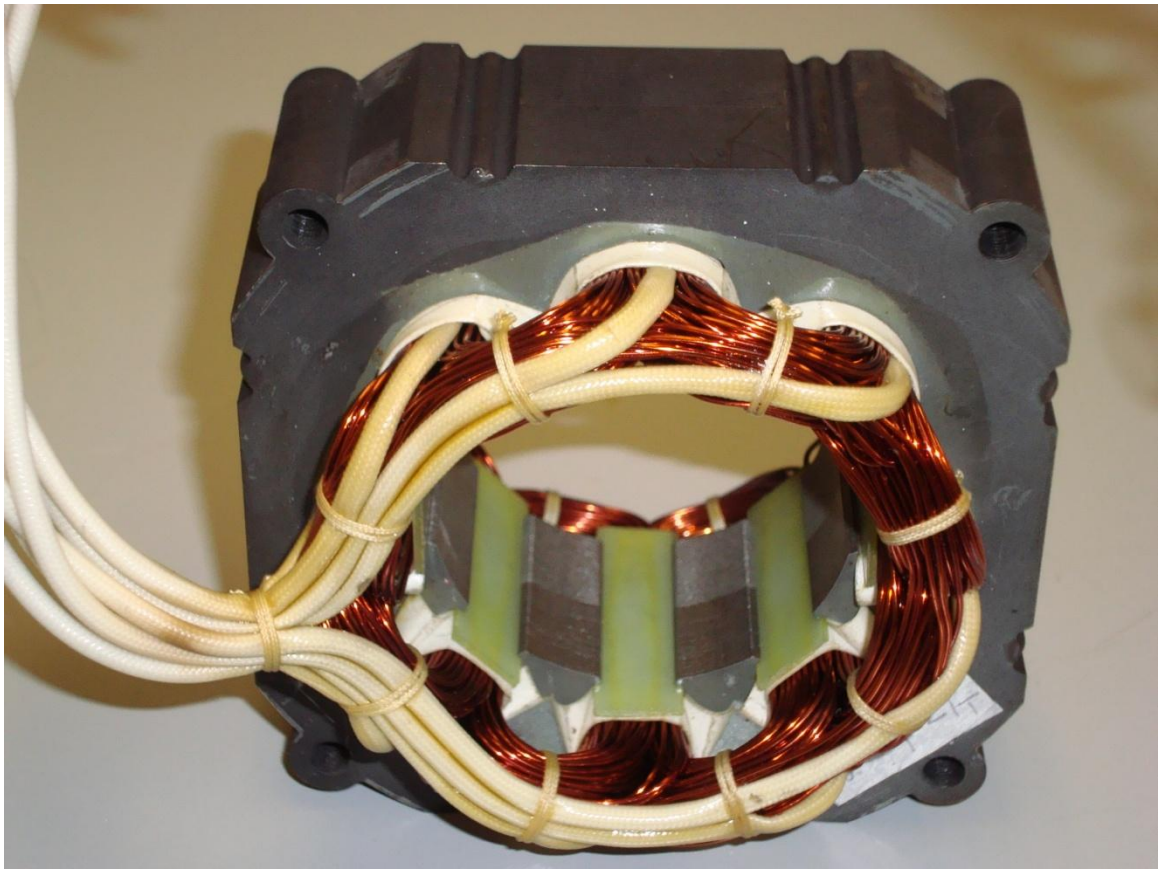

Figure 2.1 Snapshot of 1 hp, 8/6 laboratory switched reluctance motor.

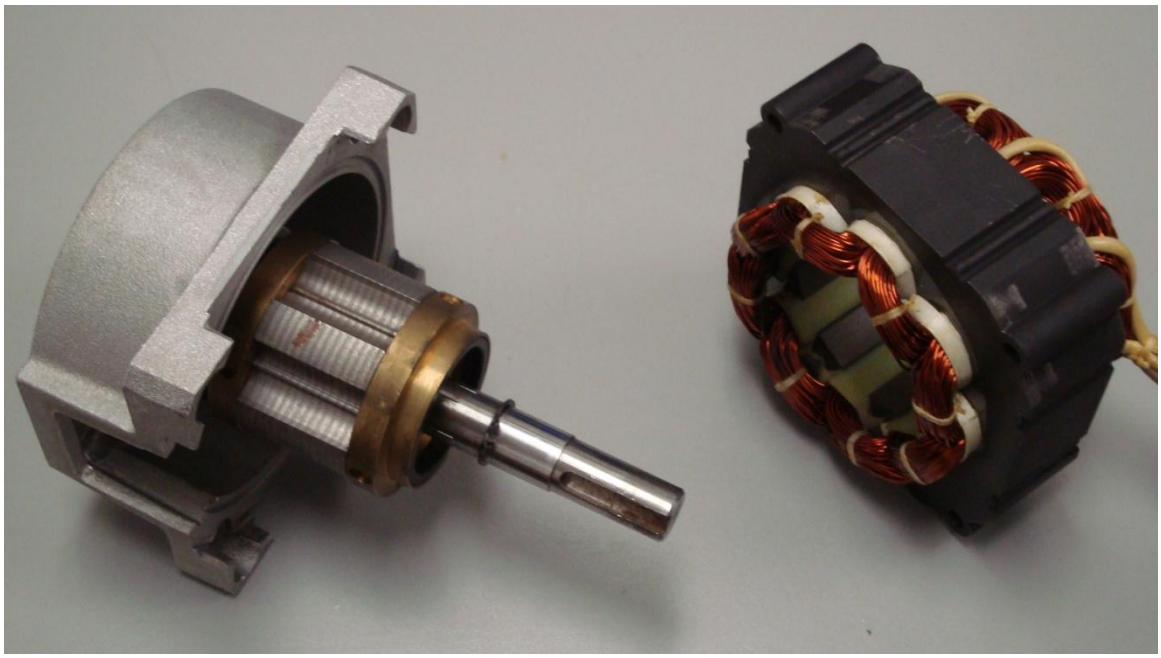

Figure 2.2 Interior of an 8/6 switched reluctance motor used in laboratory.

2.4 Identifying SRM Mechanical Design

The stator winding is comprised of a set of coils, each of which is wound on one pole. SRMs differ in the number of phases wound on the stator. Each of them has a certain number of suitable combinations of stator and rotor poles.

Machine Specifications i.e. required Power Output (hp), Speed N (rpm), peak phase current (A), and ac supply voltage (V). Speed and power output will also fix the torque to be developed.

- Frame Size Selection i.e. IEC standards fix physical dimensions for all electrical machines according to ISO regulations. Selection of Frame size fixes all other physical design parameters automatically.
- Pole Selection
- Stator and Rotor Pole Angle Selection
- Preliminary Design Process and Winding Design
- Calculation of Average Torque and Minimum Inductance

2.5 Identifying SRM Electrical Design

Analyzing the dynamic behavior requires to determine the following factors

1. Governing Equations: To predict the dynamic performance (average and peak torques and currents, speed, etc.) of an SRM, it is necessary to solve a set of differential circuit equations for the appropriate switched conditions including the mechanical equations.
2. Modeling of non-linear Inductance
3. Modeling Speed as there is no built-in provision for it.

2.6 SRM Electromagnetic Characterization

A basic traditional mathematical model of SRMs is usually based on the electrical diagram of the motor, incorporating phase resistance and phase inductance. Any voltage applied to a phase of the SRM can be described as a sum of voltage drops in the phase resistance and induced voltages on the phase inductance. The required machine Specifications i.e. required Power Output (hp), Speed N (rpm), peak phase current (A), and ac supply voltage (V). Decision of Speed and power output also fix the torque. An idealized non-linear theory describing the behavior of the motor is readily available, and a mathematical model is created based on the theory. On one hand, it is assumed to enable simulation of the SRM system and, on the other hand, development and implementation of sophisticated algorithms for controlling the SRM is feasible. The mathematical model of an SRM is then represented by a system of equations, describing the conversion of electromechanical energy.

The SRM electromagnetic circuit is characterized by non-linear magnetization. Figure 2.3 describes the dwell angle with respect to magnetic flux, ψ, the phase current, i, and the motor position, θ. The influence of the phase current is most apparent in the aligned position, where saturation effects can be observed. In the idealized triangular inductance profile of a 3-phase of SRM, the individual phases A, B, and C are shifted by 120 electrical degrees relative to each other. The interval, when the respective phase is powered, is called the dwell angle, θ_{dwell}. It is defined by the turn-on angle, θ_{on}, and the turn-off angle, θ_{off}.

2.7 Basic Principles of Operation

The motor itself is a low-cost, simply constructed machine. Variable especially high speed operation is possible, making the motor suitable for high-speed applications, like hybrid electric vehicles, vacuum cleaners, fans, white goods, etc. However, the disadvantage of the SRM is the need for shaft position information for proper switching of individual phases.

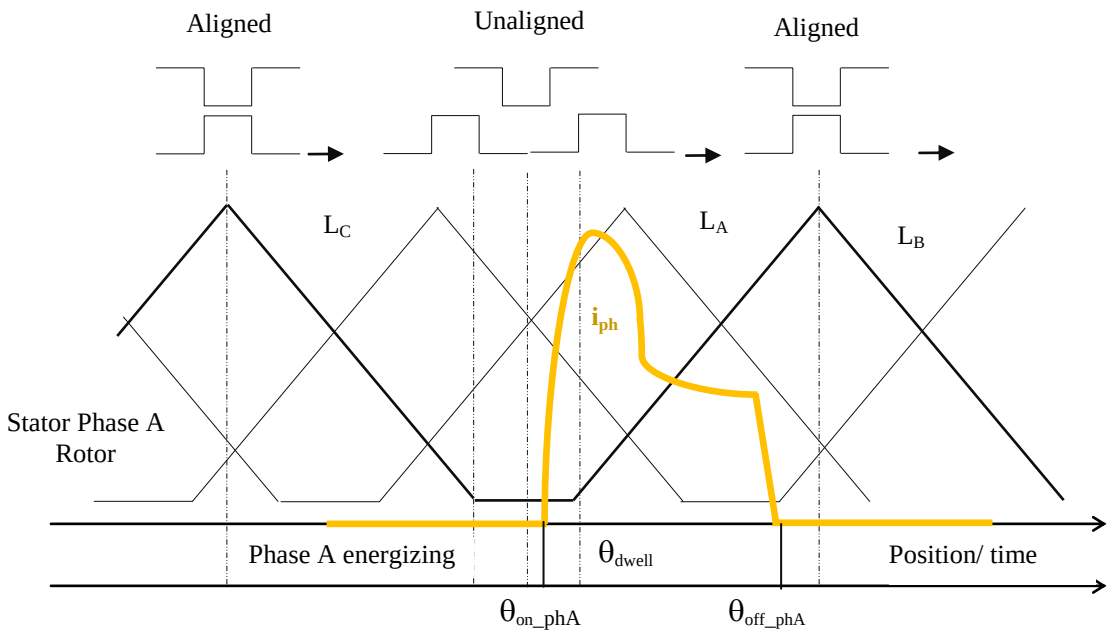

Figure 2.3 Dwell angle illustrations in a 3-phase SRM.

Also, the motor structure causes noise and torque ripple. The higher the number of poles, the smoother the torque ripple, but motor construction and control electronics become more expensive. In general, torque ripple can also be reduced by advanced control techniques, such as phase current profiling. Its basic principles of operation are:

- ❑ The motor is excited by a sequence of current pulses applied at each phase

- The current pulses need to be applied to the respective phase at the exact rotor position
- The inductance profile of SRM is triangular shaped, with maximum inductance when it is in an aligned position and minimum inductance when unaligned.
- When the current pulse is applied to the stator phase, the motor creates torque in the direction of increasing inductance and the rotor moves to the forthcoming position of maximum inductance.
- The profile of the phase current and the magnetization characteristics define the generated torque and thus the speed of the motor.
- The influence of the phase current is most apparent in the aligned position, where saturation effects can be observed.

During a standard operation in the commutation phase, just one phase is powered at a time. The control technique uses fixed turn-on and turn-off angles for switching the phases. The speed of the motor is controlled by the voltage, applied to the motor phase using the PWM technique.

2.8 Basic Switching Techniques for PWM Control

At low-speed operation, the pulse width modulation (PWM), applied on the corresponding switches, modulates the voltage level. Two basic switching techniques which can be applied are:

- ***Soft Switching***, where one transistor is left turned on during the entire commutation period and PWM is applied to the other transistor
- ***Hard Switching***, where PWM is applied simultaneously to both transistors

There are a number of control techniques for SRM, which differ in the structure of the control algorithm and in position evaluation. Two basic techniques for controlling SRM can be distinguished, according to the motor variables that are being controlled.

- ***Voltage control*** is where phase voltage is a controlled variable. In voltage control techniques, the voltage applied to the motor phases is constant during the complete sampling period of the speed-control loop. The commutation of the phases is linked to the position of the rotor. The voltage applied to the phase is directly controlled by a speed controller. The speed controller processes the speed error (the difference between the desired speed and the actual speed) and generates the desired phase voltage. The phase voltage is defined by a PWM duty cycle
- ***Current control*** is where phase current is a controlled variable. In current control techniques, the voltage applied to the motor phases is modulated to reach the desired current at the powered phase. For most applications, the desired current is constant during the complete sampling period of the speed control loop. The voltage applied to the phase is controlled by a current controller with an external speed control loop. The speed controller processes the speed error (the difference between the desired speed and the actual speed) and generates the desired phase current. The current controller evaluates the difference between actual and desired phase current and calculates the appropriate PWM duty cycle. Thus, the phase voltage is modulated at the rate of the current control loop.

2.9 Control Techniques for SRM

Many techniques are available for SRM complex control methods. They can mainly be categorized as position sensor techniques e.g. Encoder Technique, Hall position sensor technique or sensor-less techniques e.g. sensor-less position estimation using flux linkage estimation, DTC (direct torque control). DTC is becoming popular due to the following reasons.

The basic principle of DTC is to directly select stator voltage vectors according to the differences between the reference and actual values of torque and stator flux linkage. The DTC uses the concept of voltage space vectors to maintain stator flux linkage within a suitable range. Stator flux vector is known and rotor position can be estimated, thus the torque angle can be rapidly maintained so that the electromagnetic torque is always at its maximum point.

2.10 Feasibility Analysis for HEV Applications

Table 2.1 compares the feasibility of different electrical machines for electric and hybrid electric vehicles. EV & HEV traction is best served by a drive with long constant power speed range [58]. Other attributes of the motor drives for traction are:

- Safe operation (no locked rotor accidents)
- Reliable (soft failures) and fault tolerant.
- Low cost
- Efficient and compact.
- Induction and permanent magnet motor drives are considered as main players in this area.

- Exhibiting a long constant power region makes SRM drives a good candidate for this strategic application.

Hotel loads include air conditioning, compressor drive, active suspension, pumps, utility motors.

- These need motors that are low cost, reliable, and efficient.
- They should be able to operate under harsh ambient conditions.
- These machines need to be fault tolerant.
- Some of these machines need to be low noise

DC brush PM machines have been extensively used in the past. It is anticipated that new art of electronically driven drives such as SRM, BLDC be used for some of these applications.

2.11 Options in Research Directions for SRM Drives

- Modification in the physical design of the machine such as increasing the number of poles, shapes of poles etc.
- Suggestions to alter the winding configuration such as short-pitch, concentrated coil etc.
- Variation in the switching angle and the turn-on and off timings to reduce the torque ripple, noise and vibration e.g. multiphase excitation
    1. Unipolar
    2. Bipolar
    3. 4-level converters [59].

Table 2.1 Comparative Analysis of Feasibility of Various Motors for HEV Applications.

	IM	BLDC- SM	BLDC-IPM	SRM
Closed loop Simplicity		+		+
Open loop Simplicity	+		+	
Wide Speed Range	+			++
Need for Position Sensor		-	-	-
Acoustic Noise				-
Torque Pulsation	+		+	-
Motor Cost	+			+
Efficiency		+	+	
Fault Tolerance				+
Safety				+

Chapter 3

DEVELOPMENT OF FINITE ELEMENT ANALYSIS MODEL

3.1 Introduction

SRMs are basically characterized by a strongly non-linear behaviour due to its typical operation in a magnetic saturation region; there is no analytical equation to describe their behaviours. Thus, the flux linkage and static torque characteristics are indispensable fundamental data (also called 'finger prints" of SRM) required in modeling the machine behaviour for both simulation and control purposes. These finger prints can be obtained numerically or experimentally [8].

SRMs portray a modern rotating electromechanical energy conversion device by a doubly salient machine geometry and power electronics-based excitation. A power electronic controller is used to shape the input electrical energy for optimal performance. The electromagnetic torque is generated due to the tendency of the polarized rotor pole in reaching a full alignment with the excited stator pole [42]. Due to the absence of magnetic source i.e. permanent magnets or coils on the rotor, the stored energy in the air gap of the SRM is almost entirely converted into the mechanical form (except for the iron losses in the rotor). The numerical determination can be based on finite-element method (FEM) analysis, conveniently used to obtain machine magnetic vector potential values in the presence of complex magnetic materials. Therefore, significant research in the development of more appropriate numerical algorithms for a FEM study of SR machines has been done in the past years.

For simulation purposes, SRMs are usually modeled on a per phase basis. The flux linkage data utilized for the electrical equation are obtained with current flowing in only one phase winding. The torque generated by each phase is computed as the derivative of co-energy associated with that phase. However, in the case of multiple-phase excitation, the total torque is then computed as the sum of the individual phase torques [5].

SRM has traditionally been controlled using sequential single phase excitation. Recently several SRM configurations and control methods employing multiphase excitation have been developed claiming performance improvements in terms of torque density, torque ripple, efficiency and acoustic noise. This claim is based on shorter flux path reducing the eccentric forces between the stator and rotor poles. It also decreases the core losses.

Dealing with an SRM that has an 8/6 structure for stator/ rotor poles, a finite-element analysis using MagNet is first performed to obtain the magnetic characteristics of the machine, considering the saturation and mutual inductance effects. From the results of Magnet 2D-static solutions, the performance parameters of the machine (such as flux linkage per phase, static torque per phase, average torque and phase inductance and mutual inductances) are determined. These results have been verified with the experimental results presented in [59]. The flux linkages and the static torque (the fingerprints) of the machine in comparison with experimental values have been demonstrated. This model is then be used to study the impact of multiphase excitation on key characteristics of the machine and also the effects of hysteresis and eddy current losses on the dynamic performance.

3.2 Finite Element Modelling of the 8/6 SRM

As mentioned, SRM modeling consists of the determination of its magnetic characteristics: magnetic flux and electromagnetic torque using as parameters, the angular rotor position, θ and phase current, *i*. The model described in this section uses the results obtained with a two-dimensional (2D) finite element analysis of the machine cross section. It is well known that this technique can be used to compute the magnetic vector potential on structures with a complex geometry and with nonlinear magnetic material characteristics. This ability to deal with such problems has become essential to the analysis of SRM due to its double salient structure and the intense saturation effects that occur in the partially aligned stator–rotor poles.

A number of assumptions have been made to simplify the FEM modeling problem. The computed quantities were assumed to remain constant when considering different sections of the machine, thus allowing the problem to be solved with 2D analysis. It has also been assumed that the materials of which the machine is made are isotropic. Regarding the ferromagnetic material characteristics of the SRM, it becomes necessary to specify its *B*–*H* curve, which includes magnetic saturation, to obtain a reliable FEM model. A linear model becomes inappropriate for a dynamic analysis of an SRM (for SRM drives to be efficient, the machine material must be saturated) and is therefore valid only for low phase current operations.

3.3 Machine Geometrical Model

The Infolytica Corp's MagNet software has been used for electromagnetic solutions e.g. 2D static solution. The magnetic field distribution in the machine has been

obtained from the computed values. The first step in building the model consists of specifying the geometry of the machine section to the MagNet software.

Figure 3.1 shows the 3D FEM solid geometrical model while Fgure 3.2 shows the 2D structure (cross-sectional area) of the SRM considering the symmetry along the length of the machine. These Figures also show the areas representing the windings around each pole and the area representing the air around the machine. Table 3.1 shows the main dimensions of the machine. Several geometries have been set to be analyzed, one for each rotor angular position θ. This is defined as the angle between a certain pole stator (which is taken as reference) and one of the rotor poles. The angular positions considered were between -28° and $+28^{\circ}$ in 4° increment steps. This covers the underlap to–overlap and overlap to underlap sequence between machine poles and takes into account the precision of the position sensor to be used in the experimental tests. Thus, it covers the rotor position from fully unaligned position to fully aligned position and again to fully unaligned position. In other words, covering the flux profile versus rotor position of maximum inductance to minimum inductance and then again to maximum inductance.

It is also necessary to specify the area where the magnetic field is confined. The magnetic field was confined within the motor and also in a surrounding area of free air space with its borderline set at a zero potential vector. There is an air box surrounding the machine as seen in geometrical model. There is negligible flux leakage outside the stator, so there is no need to leave a gap between the air box and stator.

3.4 Machine Magnetic Properties

After defining the geometry, it is necessary to attribute to each area the magnetic properties of the corresponding material. The areas of air and copper winding are set with

a unitary relative magnetic permeability. It is important to note that the central circular area shown in Figure 3.2 is not filled by air but corresponds to the machine shaft made of aluminum and also with a unitary relative magnetic permeability. For the stator and rotor areas, the experimentally obtained magnetization curve, which was found quite closer to malleable iron castings material has been attributed [60]. Table 3.2 gives the material type for each component. Figure 3.3 shows the experimentally obtained *B-H* curve for the rotor and stator material. To compute the magnetic flux in a phase, it is necessary to define a path. As an example, Figure 3.4 shows the path for phase 1.

3.5 FEM Discretization

In 2D FEA, the elements are shaped like triangles defined by three vertices (nodes). The potential in each element of the mesh is modeled as a polynomial in the spatial coordinates. The accuracy of the solution depends upon the nature of the field and the size of the mesh elements. In regions where the direction or magnitude of the field is changing rapidly, high accuracy requires small elements or high polynomial orders (or a combination of both). In general, higher order polynomials give greater accuracy, but involve longer solution times.

The size of the elements for either the entire model or any of its components can be changed. MagNet provides the control over the size of the mesh elements automatically through an adaption process (h-adaption in case of 2D) which automatically identifies and refines the areas of the mesh where one expects a higher degree of changing the magnetic quantities. The mesh grid size around the air gap is smaller than the other adjacent regions, which allows greater mesh refinement there. Figure 3.5(a) shows the 2D of the SRM at 0° rotor position. The initial mesh in Figure

3.5(b) is the mesh before solution. The fineness of the initial mesh is based upon the model extent (the smallest and largest dimensions of a cross-section of the model normal to the sweep direction which can differ by up to five orders of magnitude).

The 2D initial mesh shows the mesh only at the solving plane (XY plane, Z=0) for the 2D solution. The mesh density of the initial mesh can be increased by subdividing edges into segments or by specifying a new maximum element size. This Mesh improvement option minimizes the aspect ratio of the elements. The solution mesh as shown in Figure 3.5 is created from the initial mesh during the solution process. The solution mesh includes the changes specified by mesh edge subdivisions and maximum element edge size as well as the changes created by *h*-adaption. If the field discontinuity error of an element is higher than a specified tolerance, the element is subdivided. The Delaunay algorithm is then applied to the mesh to produce optimum aspect ratio elements in the vicinity of the subdivided element.

Due to adaptive mesh refinement technique used, there is neither the same size nor the same number of elements (or nodes) generated for each value of excitation current or even for the same excitation current but at different rotor positions. A long range of different sizes of the element is present in each case as can be seen in Figure 3.5. The maximum size in each component is related to the physical dimensions of that component. As the value converges according to the set tolerance level and iterations, it may take the same solution time generating different number of triangles and degrees of freedom for different order polynomials. For example, in the case of 6 A excitation current at 0° rotor angle with a first-order polynomial, the initial mesh contains 2,068 and the final solution mesh contains 5,966 triangles. However, for the second-order

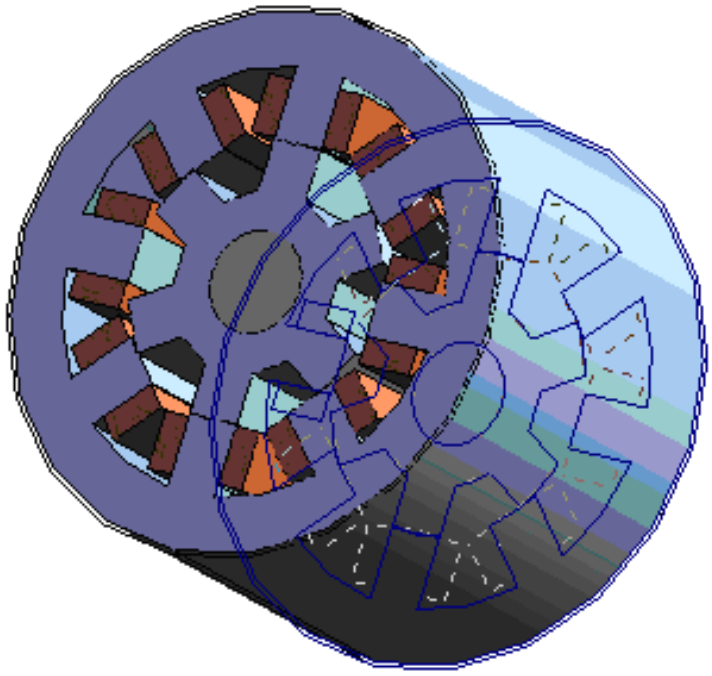

Figure 3.1 3D FEM solid geometrical model ignoring end-winding effects.

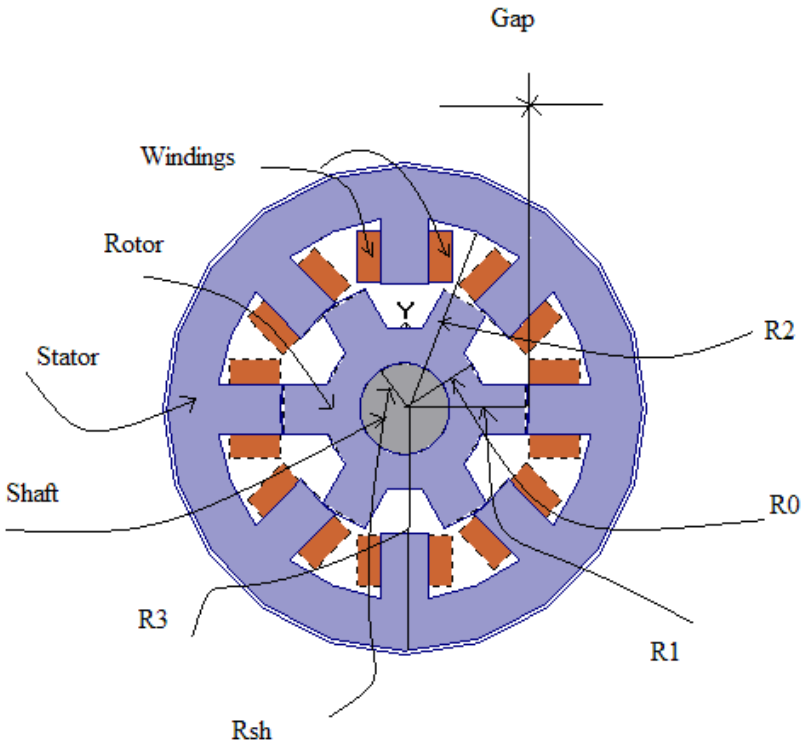

Figure 3.2 Cross-sectional geometry of the 8/6 SRM and respective dimensions.

Table 3.1 8/6 SRM Geometrical Dimensions.

Radius Type	Radius (cm)
R_{sh}	1.49 cm
R_0	2.67 cm
R_1	4.13 cm
R_2	6.22 cm
R_3	7.87 cm
Gap	0.31 mm
Beta-s	22.3˚
Beta-r	22.5˚
Motor length	11.96 cm
Turns per pole (N)	100

Table 3.2 8/6 SRM Component Materials.

Component	Material
Shaft	Aluminium
Rotor	Iron
Stator	Iron
Windings	Copper
Gap	Air
Surrounding	Air

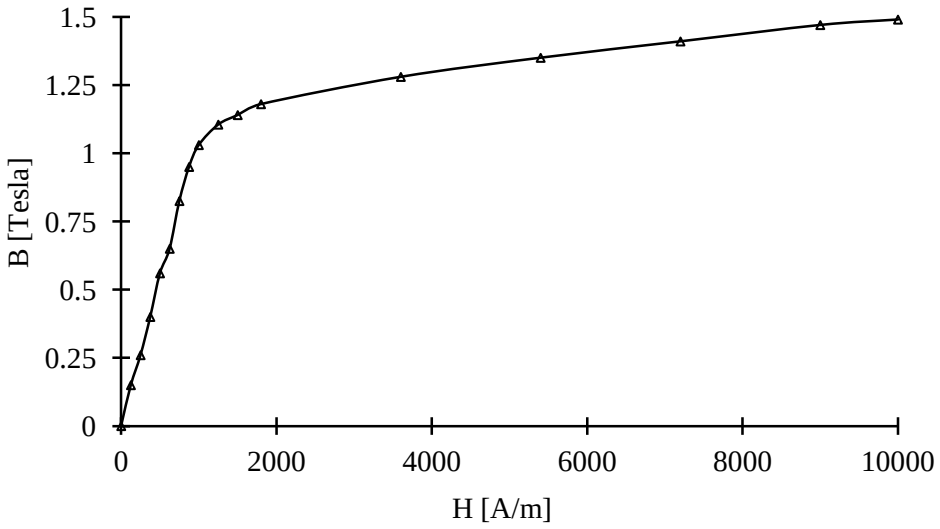

Figure 3.3 Measured magnetization curve used in the analysis.

polynomial under the same conditions, initial mesh contains the same 2,068 triangles and only 6,734 triangles were generated for the final solution mesh. The maximum degrees of freedoms in the case of the first-order polynomial were 3,061 and, in the case of the second-order polynomial, it was 13,618.

The FEA was performed for both the polynomial orders 1 and 2 at different values of excitation currents and at different rotor angles. The flux linkages and torques do not change significantly due to an increase in the polynomial order. For example, they differ only after the 3rd decimal value if the order is increased to 2 (from 1).

In the Dirichlet, or *flux tangential*, boundary condition, the flux function is constant over any portion of the boundary with this condition, so the portion becomes part of a flux line. Since for most problems this is the best choice. So this choice has been adopted for the analysis in this paper. It is equivalent to putting the model in a cavity of a material with zero permeability (air), so that no flux can escape from the model. Usually, if the boundary condition is taken sufficiently far away from the components of the model, it is a good approximation to an open boundary. However, in this case, there is a negligible flux leakage outside the stator, so there is no need to leave a gap between the air box and the stator.

3.6 Finite Element Analysis Results

The next step consists of specifying the phase current for which a solution is to be obtained. This is done by applying a current driven source for the stranded coil (current per turn and number of turns and using a simple AC/DC source) on the elements that correspond to the windings of a certain phase. The phase current values used to obtain the model are between 3 A and 18 A with a 3 A increment. The direction of

current flow in the coils must be made in such a way that one establishes the direction and magnitude of the magnetic field in the respective stator pole. Besides, it is also necessary that the magnetic field direction generated by both phase windings be coherent.

Once a solution is obtained, i.e. the magnetic potential vector distribution along the machine is known, it is possible to calculate the value of the magnetic flux in each phase. The phases are defined according to the sequential scheme i.e. here phase 1 is defined as the one in which the excitation current is applied. Phase 2 and phase 4 (negative) are the phases will be switched according to sequence on adjacent stator pole windings of phase 1 winding. It should be noted that the flux values computed above are only for the cross-section of the machine, and it is necessary to multiply these by the motor length in order to obtain the total magnetic flux considering the symmetry. The Magnetic flux linkage in phase 1 as a function of rotor position and excitation current as obtained by the finite element model is shown in Figure 3.6, Figure 3.7 and Figure 3.8 along with the measured values. As can be seen from these figures, the results obtained by the FEA are in good agreement with the measured ones.

The air-gap torque produced on phase 1 as a function of the rotor position and excitation current as calculated by the finite- element model is shown in Figure 3.9, Figure 3.10, and Figure 3.11 along with the measured values. As can be seen from these Figures, the results obtained by the FEA are in good agreement with the measured ones. Figure 3.12 shows the measured and calculated average air-gap torque produced in phase 1 as a function of the phase 1 excitation current. Although both the curves evolve similarly, the air-gap torque by the FEA is always greater than the corresponding experimental value because the leakage fluxes have been ignored in a 2D FEA model.

The reduced Chi-squared goodness-of-fit technique has been used to analyze the discrepancies between the torque values obtained experimentally and the ones computed using FEM for the full range of the excitation current values. These values are calculated using the equations (3.1) and (3.2)

$$\chi_j^{\,2} = \sum_i^n \frac{\left(T_{FEM,i} - T_{EXP,i}\right)^2}{T_{EXP,i}} \tag{3.1}$$

Where $T_{FEM,\,i}$ is the torque calculated from the FEM for *i*th rotor position and *j*th current value and $T_{EXP,\,i}$ is the torque from the experiment for *i*th rotor position and *j*th current value. The reduced chi-squared value can be calculated using (3.2).

$$\chi^2_{reduced} = \frac{\chi^2}{No.of\ rotor\ positions} \tag{3.2}$$

Table 3.3 presents the results of the discrepancies among the torque values obtained from the experiment and the torque values computed using the FEA technique. The higher value of reduced chi-squared test represents the higher discrepancy. It can be seen from Table 3.3, at lower excitation current, the discrepancy is low and at higher excitation current, the torque discrepancy is higher. Table 3.3 also specifies the maximum instantaneous torque error (considering only the sampled rotor angle positions) for each current with the corresponding rotor angle. This quantity is calculated as the difference between the experimentally obtained and FEA computed torque values. It is found that the maximum instantaneous torque error occur at -20^o rotor angle for all excitation currents. This rotor angle is the transition point where the rotor and stator poles are just aligned and the rotor will move towards the full alignment. Smoothing of this starting torque is one of the major issues and an interesting research area in SRM design and configurations. It is also seen that as the excitation current increases the absolute value of

maximum torque error increases. However, in terms of percentage value with respect to the experimental values of the torque at higher values of excitation current, maximum torque error percentage decreases except at 6 A. Figure 3.12 shows that as the excitation current increases, the discrepancy between the average torque value obtained from the experiment and the one computed using FEM also increases. This increase is due to the fact that the torque is directly proportional to the square of the current.

Table 3.3 Torque Profile Discrepansies Between the Experimental Values and FEA Model.

Phase Current (A)	Reduced Chi-squared value	Max. Torque Error at -20 ˚ (%)
3	0.03	73%
6	0.30	104%
9	0.48	68%
12	0.51	65%
15	0.57	51%
18	0.52	47%

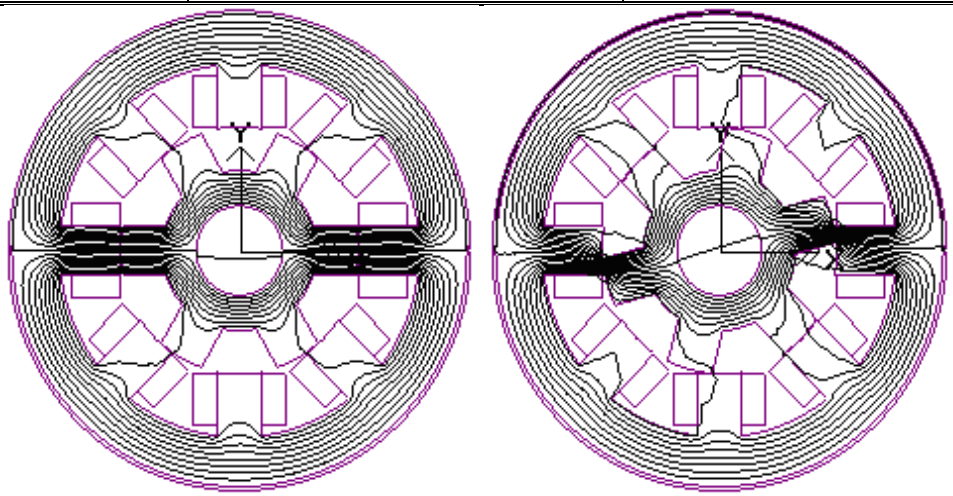

(a) (b)

Figure 3.4 Magnetic flux distribution at the two rotor positions for phase 1 excitation. (a) 0° rotor position. (b) 16° rotor position.

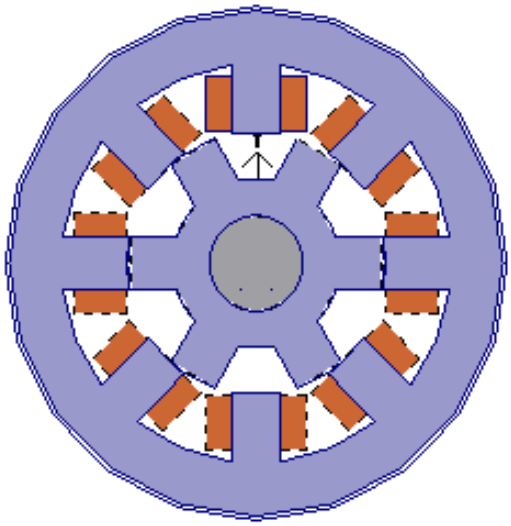

(a)

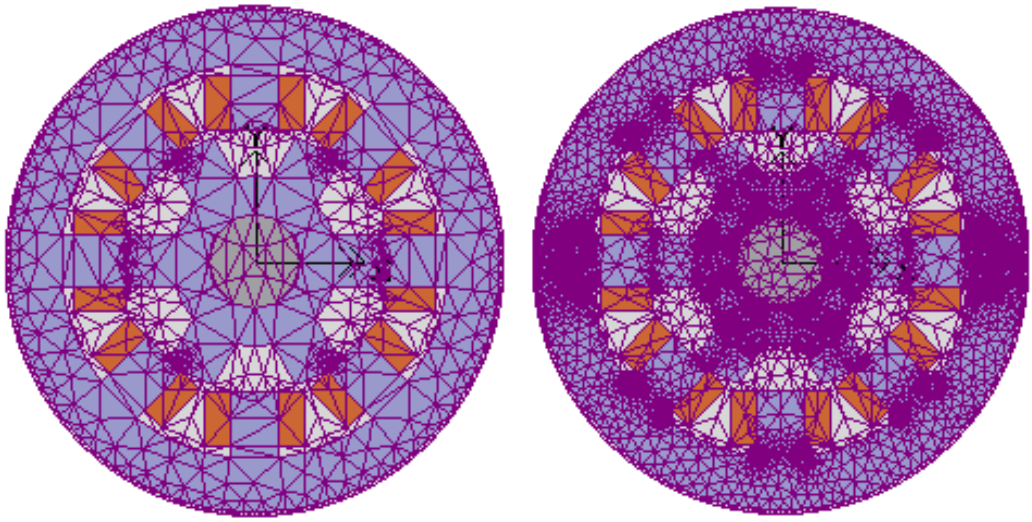

(b) (c)

Figure 3.5 Initial and solution mesh for FEM analysis. (a) 2D-view of SRM at 0° rotor position. (b) Initial 2D mesh. (c) Solution mesh.

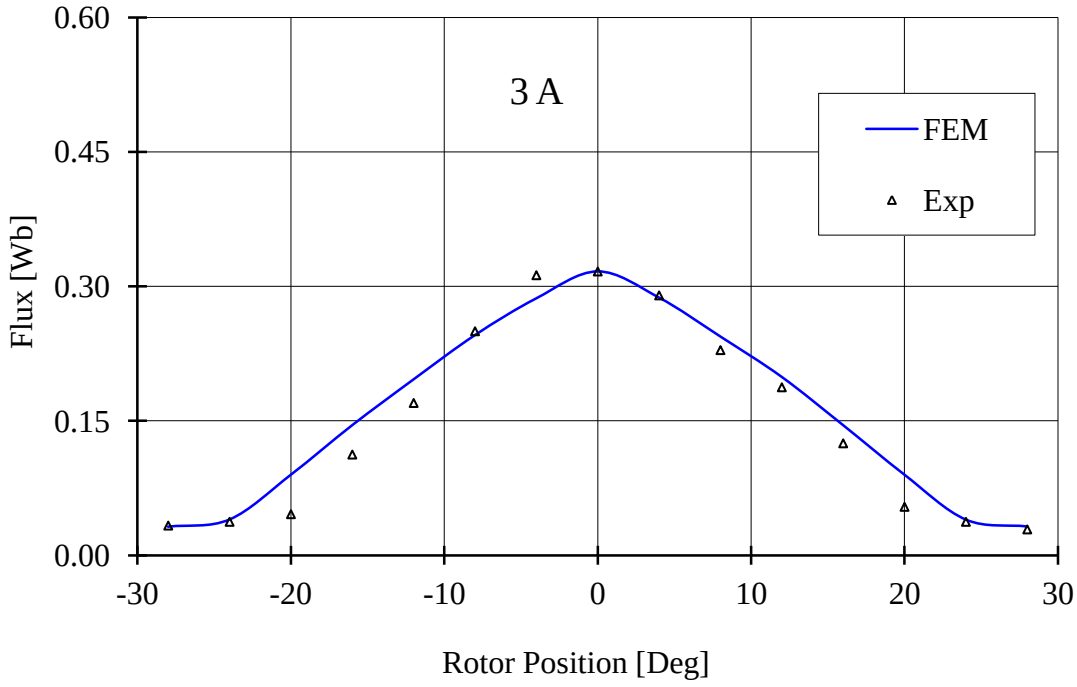

(a)

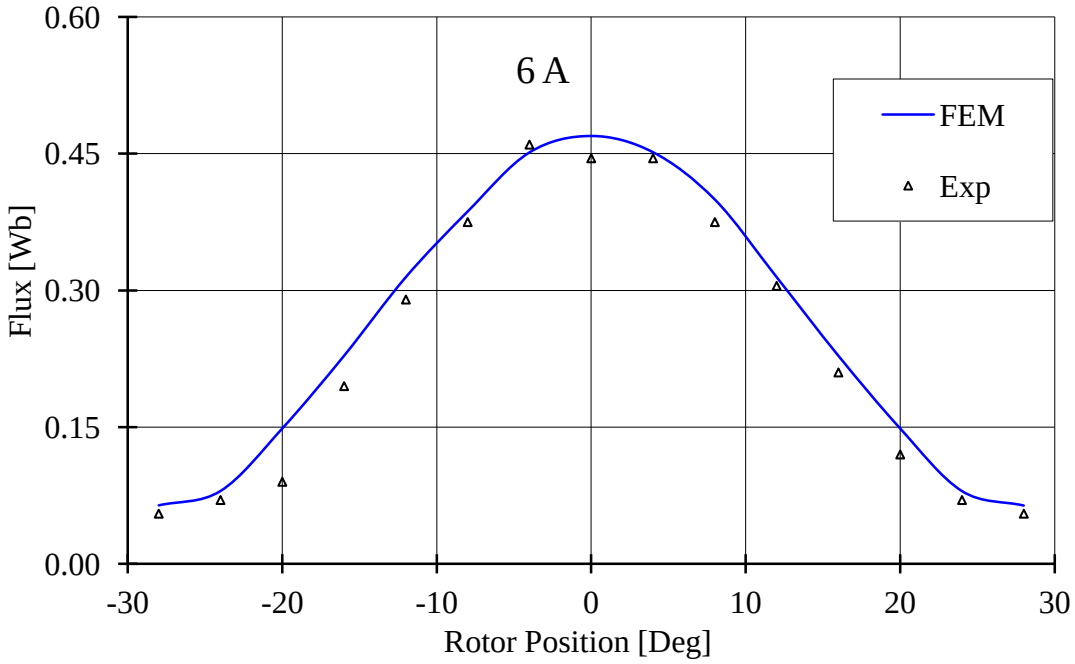

(b)

Figure. 3.6 Magnetic flux linkage in phase 1 as a function of the rotor position and excitation current obtained by the FEM and experiments. (a) 3 A. (b) 6 A.

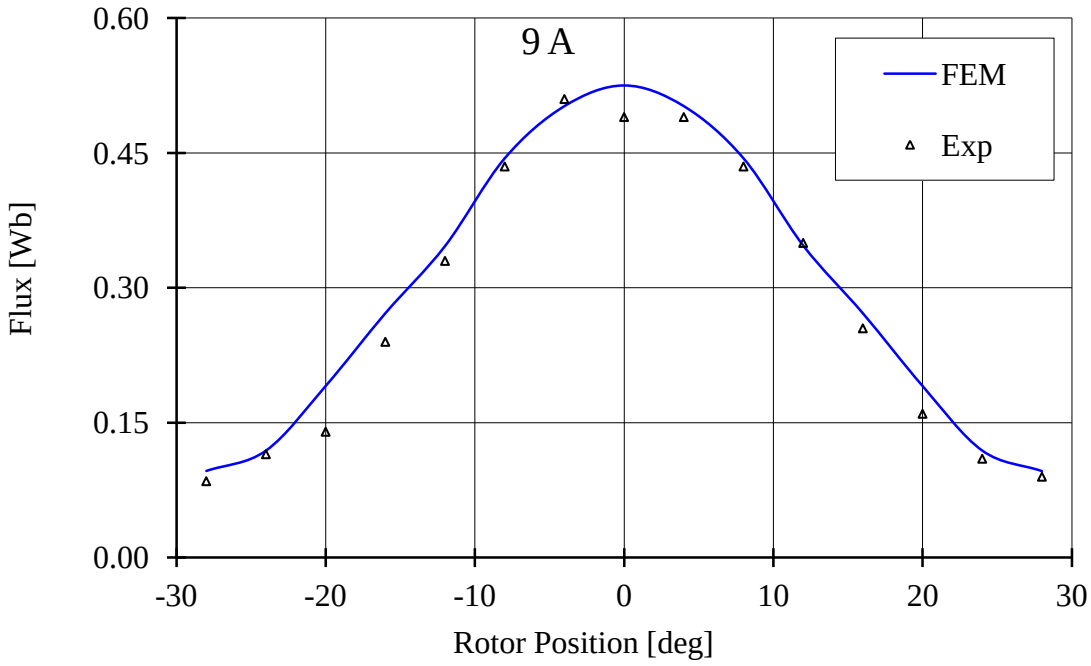

(a)

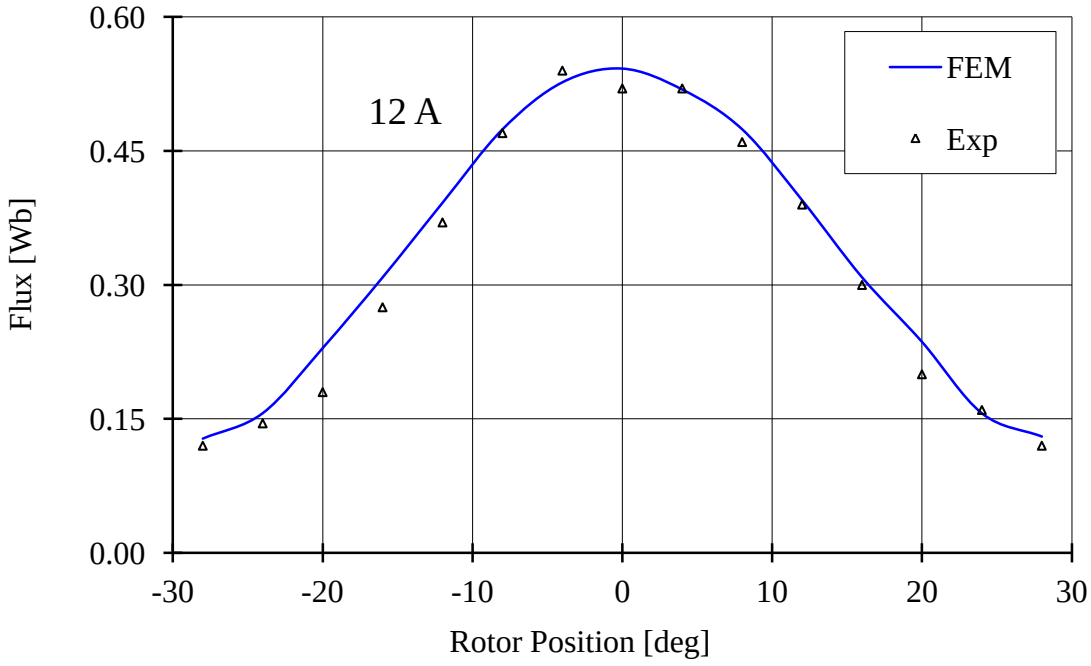

(b)

Figure. 3.7 Magnetic flux linkage in phase 1 as a function of the rotor position and excitation current obtained by the FEM and experiments. (a) 9 A. (b) 12 A.

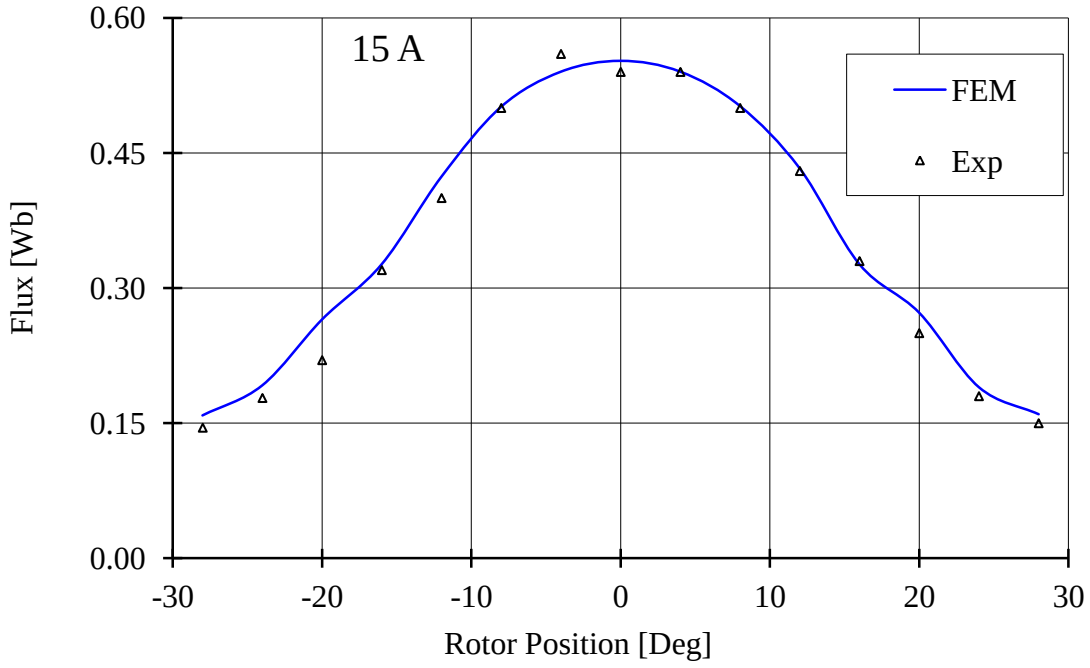

(a)

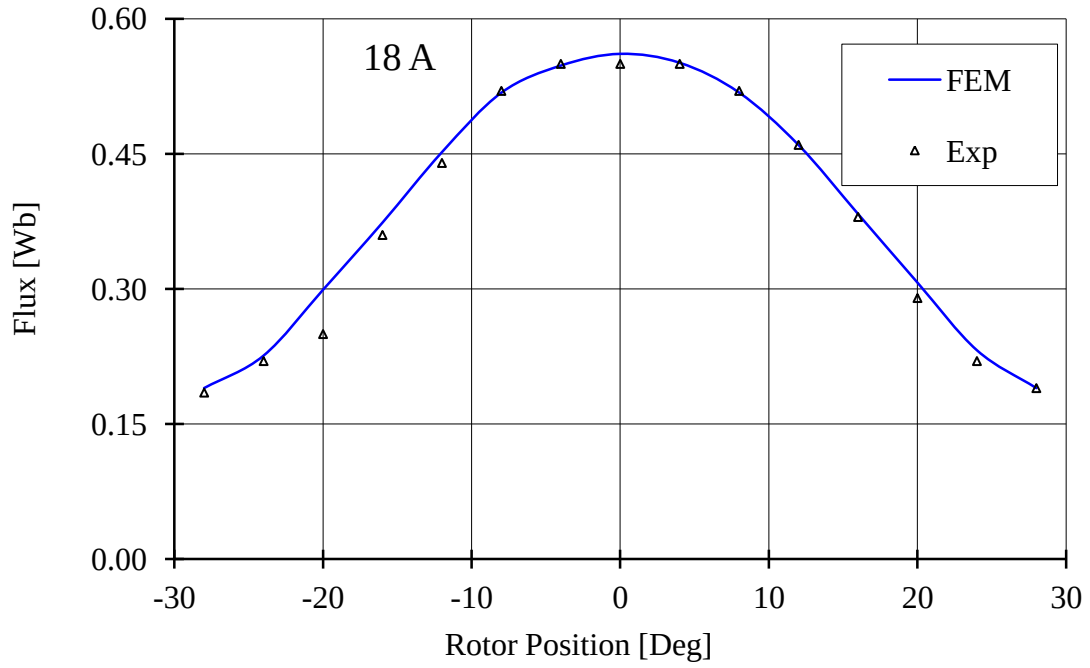

(b)

Figure. 3.8 Magnetic flux linkage in phase 1 as a function of the rotor position and excitation current obtained by the FEM and experiments. (a) 15 A. (b) 18 A.

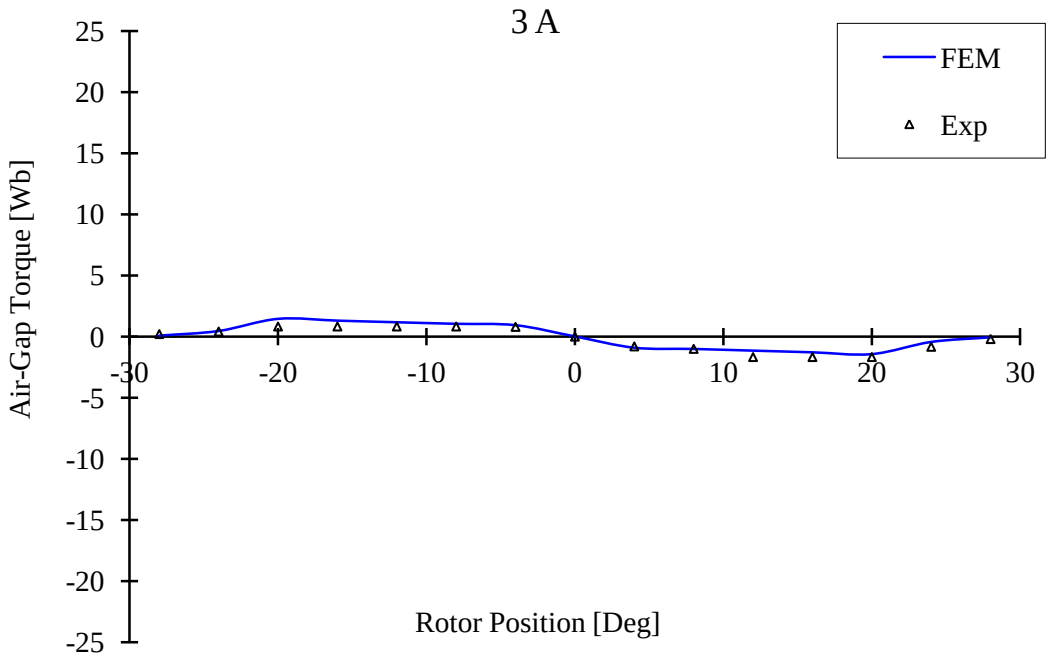

(a)

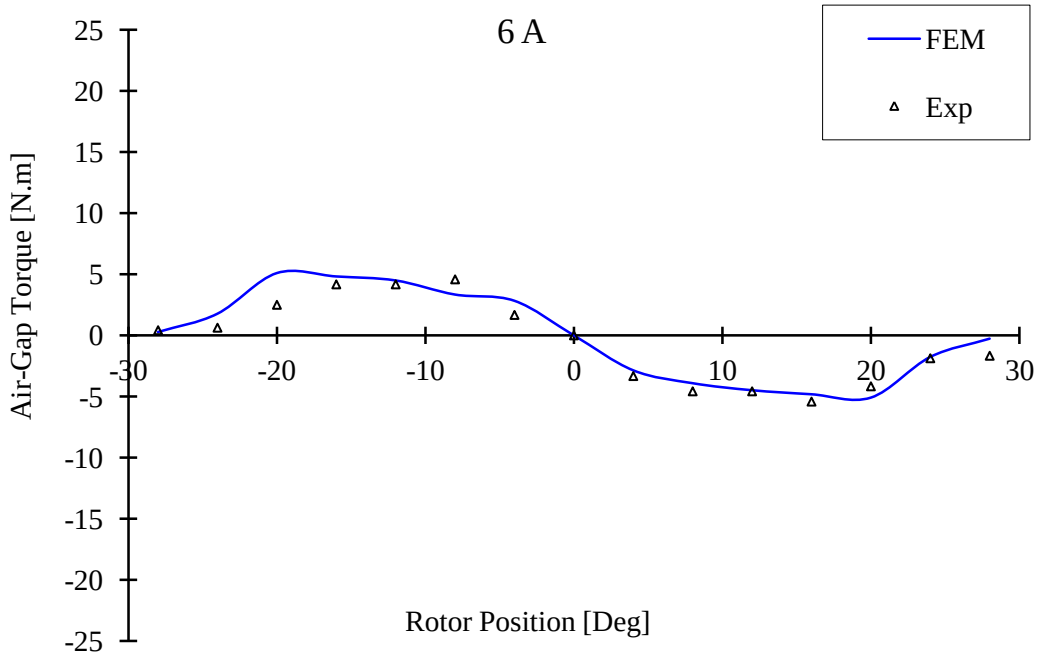

(b)

Figure 3.9 Air-gap torque produced on phase 1 as a function of the rotor position and excitation current obtained by the FEM and experiments. (a) 3 A. (b) 6 A..

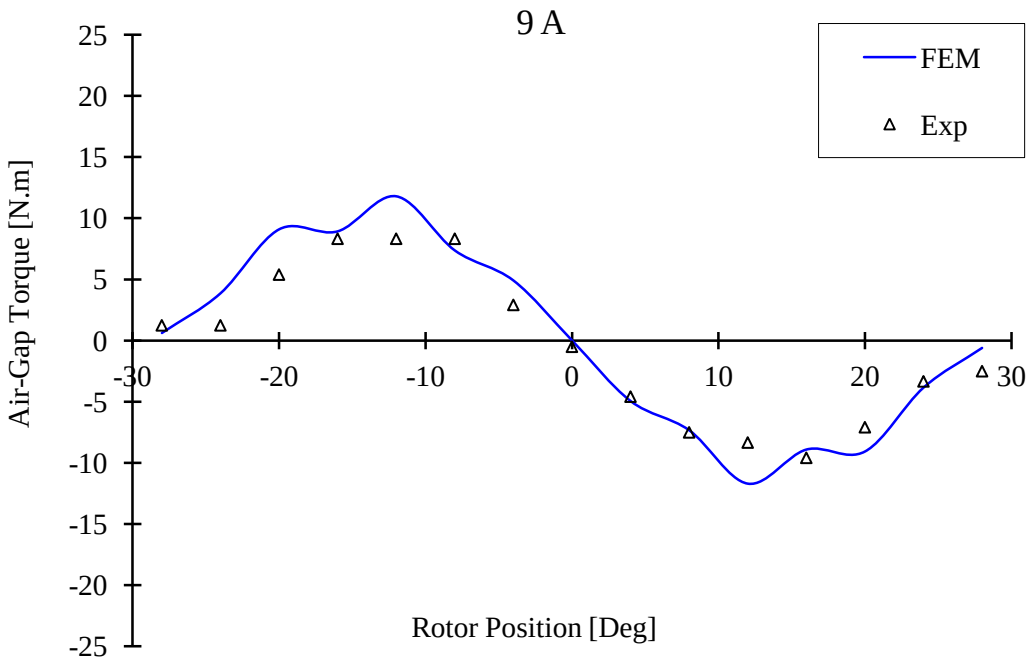

(a)

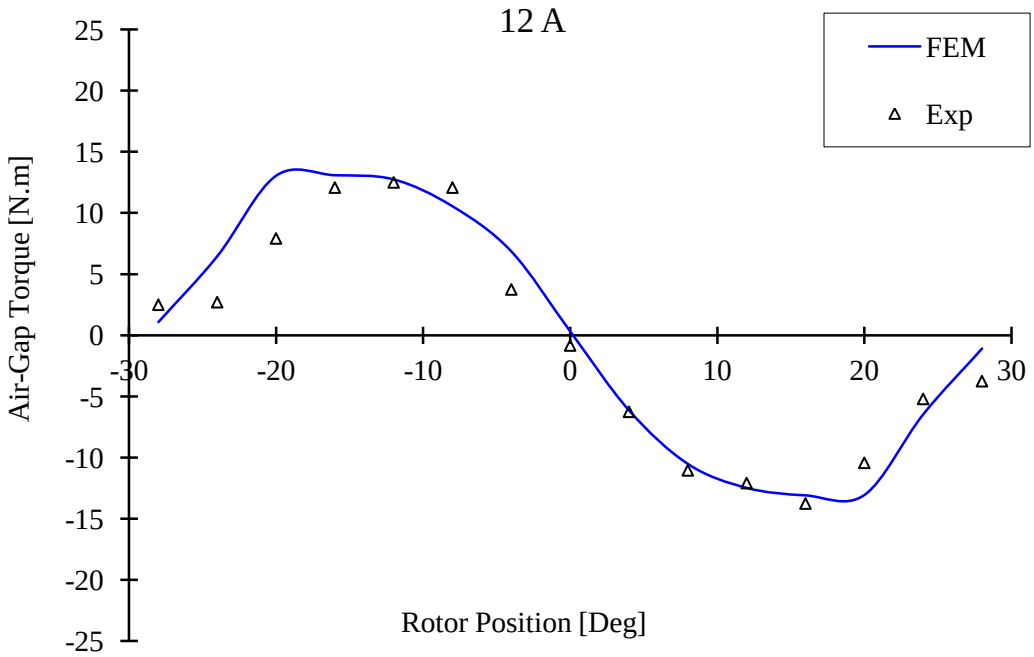

(b)

Figure 3.10 Air-gap torque produced on phase 1 as a function of the rotor position and excitation current obtained by the FEM and experiments. (a) 9 A. (b) 12 A.

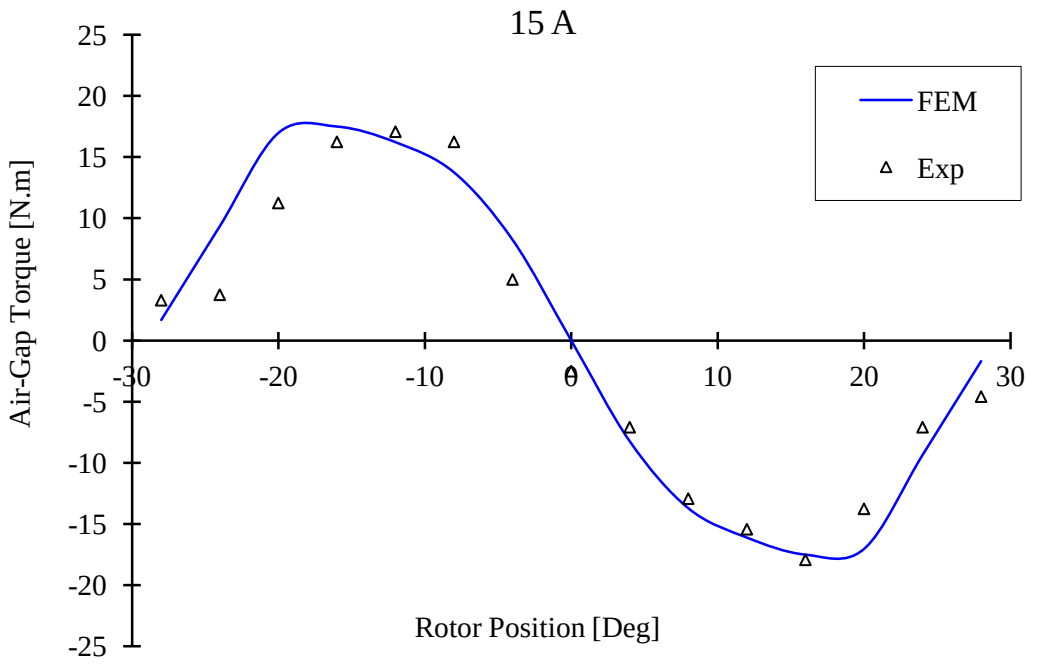

(a)

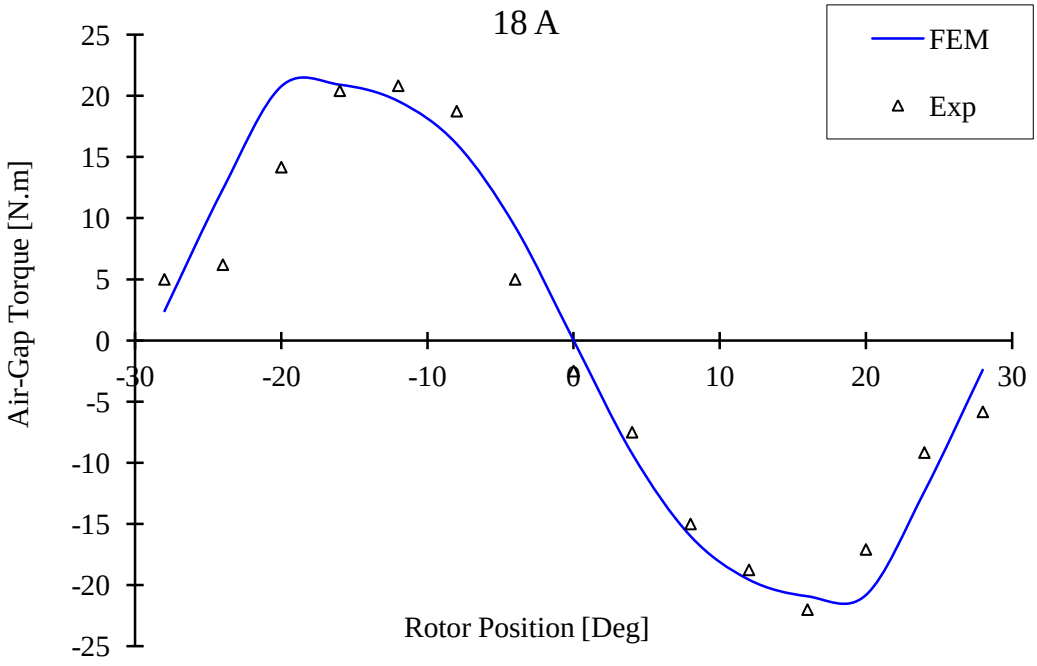

(b)

Figure 3.11 Air-gap torque produced on phase 1 as a function of the rotor position and excitation current obtained by the FEM and experiments. (a) 15 A. (b) 18 A.

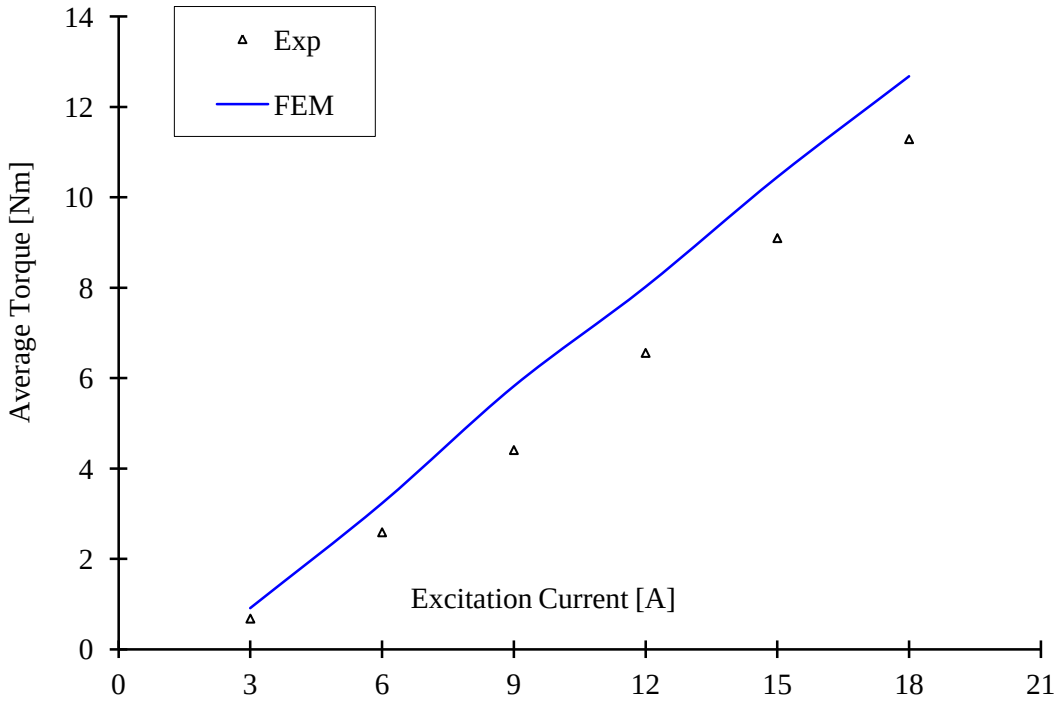

Figure 3.12 Average air-gap torque per phase vs. excitation current by the experimental and FEM model.

Chapter 4

INVESTIGATION OF EM FORCE DISTRIBUTION

4.1 Introduction

Recently, switched reluctance motor (SRM) drives have received more attention in the field of high performance drives because of their simple construction, variable speed operations, reliability, ruggedness and fault tolerance making it attractive for industrial and hybrid electric vehicle applications. However, significant acoustic noise and torque ripple are the two main drawbacks of SRM. Interaction of electromagnetic force and the mechanical structure produces these noise and vibrations [61].

Due to the absence of windings on the rotor, stored energy in the air gap of the SRM is almost entirely converted into the mechanical form except for the iron losses in the rotor. This magneto-mechanical energy conversion is manifested in Electromagnetic Force which is the sum of Lorenz force (LF) and the saliency force (SF) acting on rotor (Figure 4.1). As it can be seen in the Figure 4.1 Lorenz force is significantly smaller than the saliency force. The total force is distributed among the radial and tangential force components around the circular air gap. Tangential component of the force is acting on the rotor and stator poles resulting in generation of the electromagnetic torque on the rotor and tangential vibration of the stator poles. The radial component of the force, on the other hand, appears as a by-product and mainly contributes to the radial vibration of the stator which is known to be the main origin of acoustic noise in SRM drives [62].

It must also be noted that tangential and radial components of the force acting on the rotor can be partially transmitted to the stator via bearing and other mechanical parts

of the machine. Maxwell's Stress Tensor (MST) method has been applied to SRM and partial results on the distribution of the force components have been presented. It is an effective approach in selection of the contour and elements for securing high precision results from Maxwell stress computations. However, if the MST is used to calculate the forces from standard numerical solution for the field, it is difficult to obtain accurate results. The integral for the force or torque may be unreliable if it comprises terms which alternate in sign leading to an accumulation of numerical errors. It is also very sensitive to the numerical solution [62]. In the present work, finite element method (FEM) is used to calculate the flux densities at different rotor positions (from totally unaligned to fully aligned and then totally unaligned position) which constitutes a contour. The FEM model used for this study is described in detail in [60] including its physical dimensions and

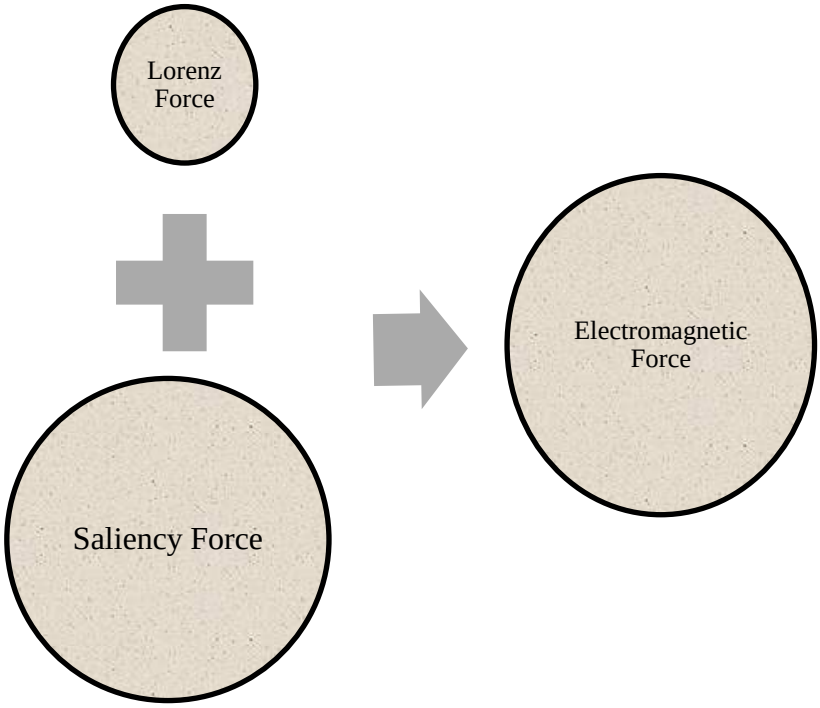

Figure 4.1 Types of electromagnetic force in SRM.

mechanical properties. Figure 4.2 shows the magnetic flux linkages as a function of the excitation current at different rotor positions of the investigated SRM. These flux densities are then used to generate the MST. However, in this research work, the above-mentioned difficulties with the conventional MST approach are avoided by implementing a tunable volume integration method. This method provides a generalized formulation for net magneto static force calculation combined with the surface and volume integration based on magnetic flux densities and an arbitrary scalar function [63]. It is simpler to implement the technique using the Cartesian co-ordinate system as compared to the polar co-ordinate system (radial and tangential directions). Therefore, the flux densities are resolved into B_x and B_y before implementation.

In this chapter, first, the conventional MST approach is applied to obtain the radial and tangential stresses from flux densities which were calculated by magneto static analysis. Then the Cartesian components of the flux density are used to predict the electromagnetic force using the tunable volume integration method. A dynamic analysis of the SRM employing in the case of single phase excitation has been performed and the results of the analysis are presented in the last section in terms of no-load torque and transient electromagnetic force.

4.2 Computation of Electromagnetic Forces

Virtual Work and Maxwell Stress Tensor methods are usually used to predict the electromagnetic forces acting on the SRM rotor. The advantages and disadvantages of both energy calculation methods are shown in Figure 4.2. The tuneable volume integration method combines the benefits of both methods. These two methods along

with the proposed tuneable Volume Integration Method are described in the following subsections.

4.3 The Virtual Wok Method

The Virtual Work method calculates the force by differentiating the co-energy *W'* of the system with respect to the displacement in *s*-direction as in (4.1),

$$F_s = \frac{\partial' W'}{\partial s} \approx \frac{\Delta W'}{\Delta s} \tag{4.1}$$

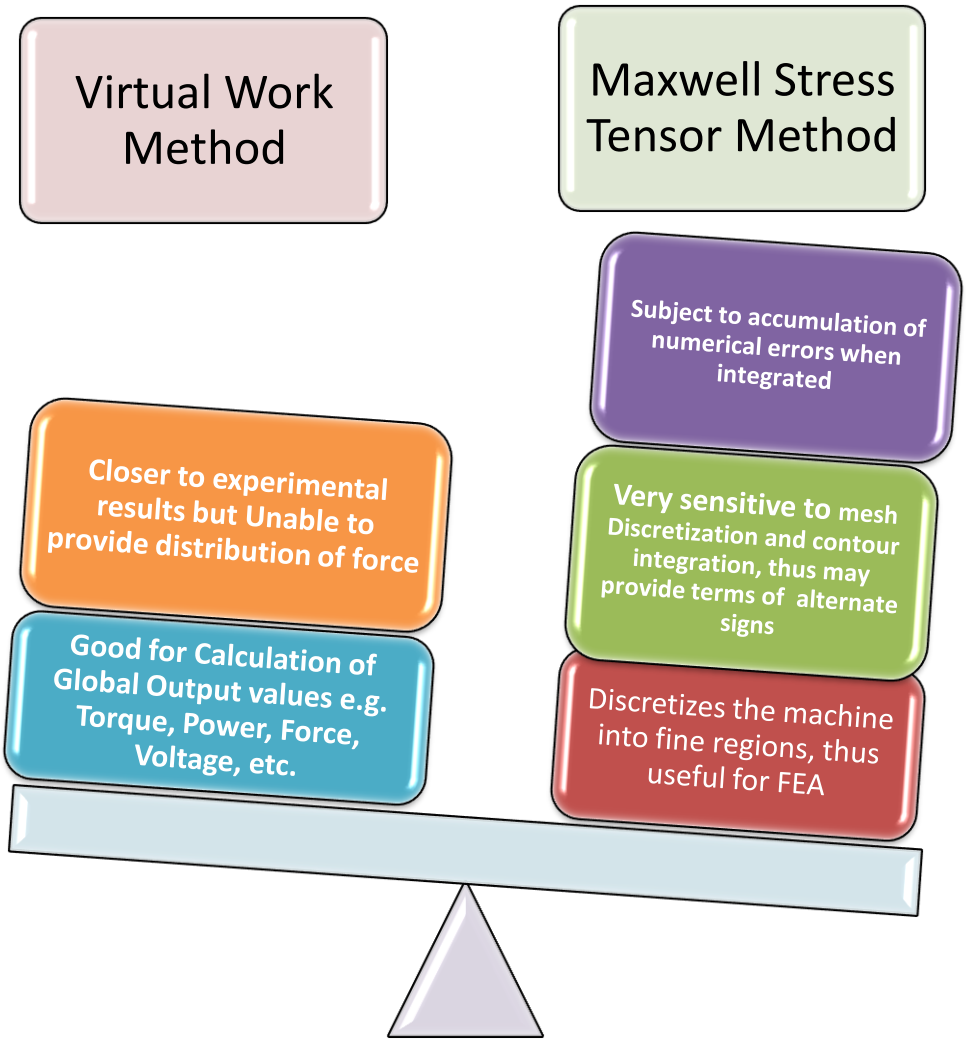

Figure 4.2 Comparisons of virtual work method and Maxwell stress tensor method.

4.4 Maxwell's Stress Method

MST is usually applied in FEA because it discretizes the closed surface of the body on which the force is acting into small elemental surfaces. The flux density at each element surface is then resolved into components parallel to coordinate planes. The corresponding stresses are calculated in those directions using (4.2) and (4.3).

$$\sigma_t = \left(\frac{1}{\mu_0}\right) B_r B_t \tag{4.2}$$

$$\sigma_r = \left(\frac{1}{2\mu_0}\right)\left(B_r^2 - B_t^2\right) \tag{4.3}$$

where σ_t and σ_t are the tangential and radial stresses and B_t and B_r are the tangential and normal flux densities respectively. μ_0 is the magnetic permeability in free space [62].

Figure 4.3 depicts the fingerprint characteristics to electromagnetic field from unaligned to aligned rotor position. At the midway position, the effects of local saturation are dominant and the overall magnitude of the flux in the stator pole and back iron is low. The maximum torque acting on the rotor occurs at or about this position. This indicates that maximum productivity of the SRM does not require storage of magnetic energy in the core which results in poor power quality.

4.5 Tuneable Volume Integration Method

The integral of MST can be unreliable due to the alternate signs leading to an accumulation of numerical errors when integrated by any standard numerical method as mentioned previously. Therefore, a flexible, non-iterative tunable volume integration method is suggested to balance this imperfection. This is based on the flux densities and arbitrary scalar function depending on the local field error as demonstrated below [6].

Considering Ω_a, be as an arbitrary isolated region within a magneto static system and Ω_b is the source-free vacuum region which immediately envelops Ω_a. *g* is the local field error-based function. With Ω_a free to contain both current and magnetizing material, the net magneto static loading force acting on Ω_a can be calculated as in equation (4.4)

$$F^{\Omega_a} = \left(\frac{1}{2\mu_0}\right)\int_{\Omega_a}\left[\frac{1}{2}B^2\nabla g - (B.\nabla g)B\right]dV \tag{4.4}$$

The error-based *g*-function, used to compute the component of the force in the *s*-direction can be generated by minimizing *W* in the following equation (4.5).

$$W(g) = \int_{\Omega_b}\left|w\left[\frac{1}{2}B^2\nabla g.s - (B.\nabla g)B.s\right]\right|^2 dV \tag{4.5}$$

W represents the weighted integration of the square of the *s*-directed component of the integrand of (4.4). Also *w* is the scalar weighting function based on local field error. *B* is the flux density, and *V* is the volume.

4.6 Radial Flux Densities and Stresses

The distribution of the flux density profiles in radial and tangential directions are presented in Figs. 4.4, 4.5 and 4.6. The maximum radial force exists at the aligned position. As the rotor moves from the fully aligned position, a negative repulsion force starts to appear. With the decrease in the overlap angle between rotor and stator poles, the amount of positive portion of the radial force acting on the stator pole decreases and magnitude of the negative portion of force increases. This distribution of the radial forces is recognized as a major contributor to acoustic noise in SRM drives.

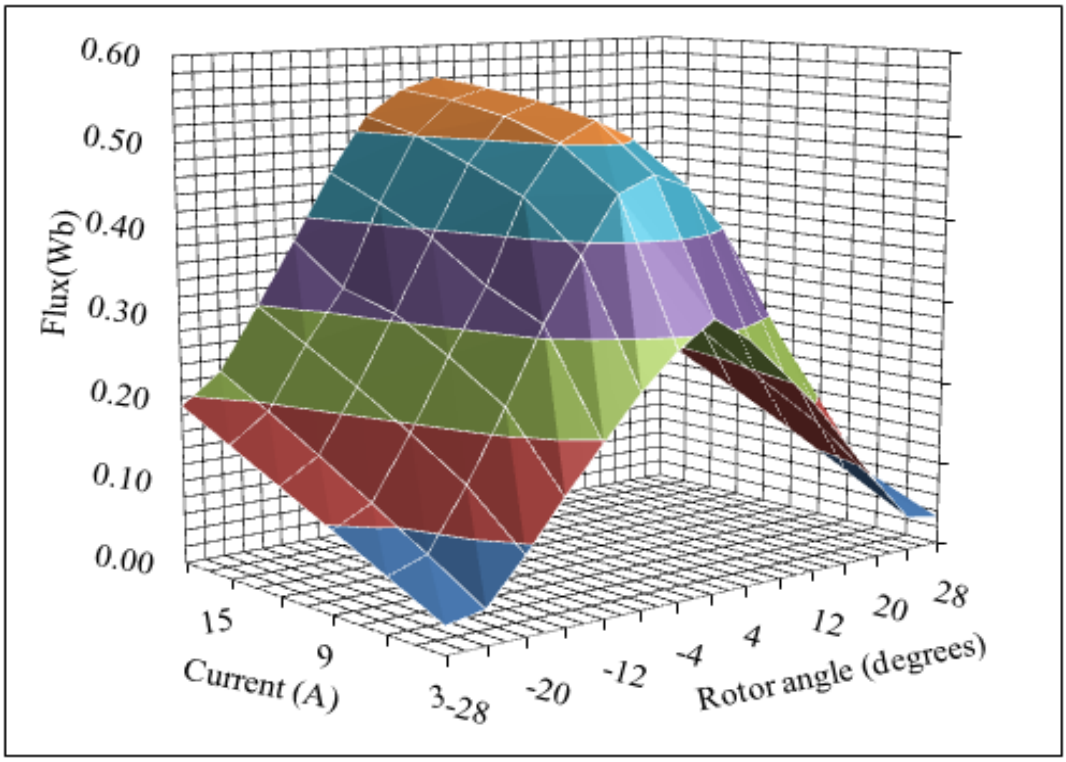

Figure 4.3 Magnetic flux versus the excitation current for different rotor positions.

Therefore, it is required to use the actual profile of the radial force acting on the stator pole arc. This becomes more necessary when the turn-off angle is sufficiently distant from the aligned position. Figure 4.7 shows that at aligned position there exists a substantial, square-shaped radial component across the entire stator pole arc. As the rotor moves from aligned position toward unaligned position the radial component of the field maintains its square shape. However, the width of the region within which the radial component exists decreases. The approximate width of the radial flux density can be approximated by the length of overlapped area between rotor and stator poles.

This approach is often neglected where the relationship between radial force and rotor position is obtained using an energy method. Energy method offers the area surrounded by the radial force profile and can be avoided. The distribution shown in

Figure 4.8 represents the radial forces in the middle of the air gap. As the shape of the radial component is closer to a square wave in the region of alignment, a design with similar shaped tangential component of the force can balance the radial component.

4.7 Tangential Flux Densities and Stresses

At the aligned rotor position, the tangential component of the field portrays an odd symmetry with respect to the midpoint of the stator/rotor arcs and pointing in opposite directions on both sides of the stator pole arc (Figure 4.9). Figure 4.10 shows that for the tangential component of the flux density, there remains no particular shape of the tangential flux density and sudden changes in shapes are observed within only a few degrees deviation from full alignment. Notably, the maximum tangential component appears at the respective corners of rotor and stator arcs that form the overlapped area. It is important to note that the effects of local saturation at these rotor and stator tips result in two local maxima in the tangential components of the flux density. Between these maxima, tangential component of the field are presented by a convex shape. Once the overlap between rotor and stator poles finishes, a sharp decrease in the tangential component of the field is observed. The tangential force offers a net zero area at aligned and unaligned positions which are the equilibrium states of the machine as shown in Figure 4.11. In addition, tangential force component have a convex profile with stationary local maxima at stator at an odd symmetry, similar to the one at aligned position at the unaligned position. The force acting on the rotor under locked rotor condition as a a function of rotor angle is presented in Figure 4.12 after integrating the stresses obtained

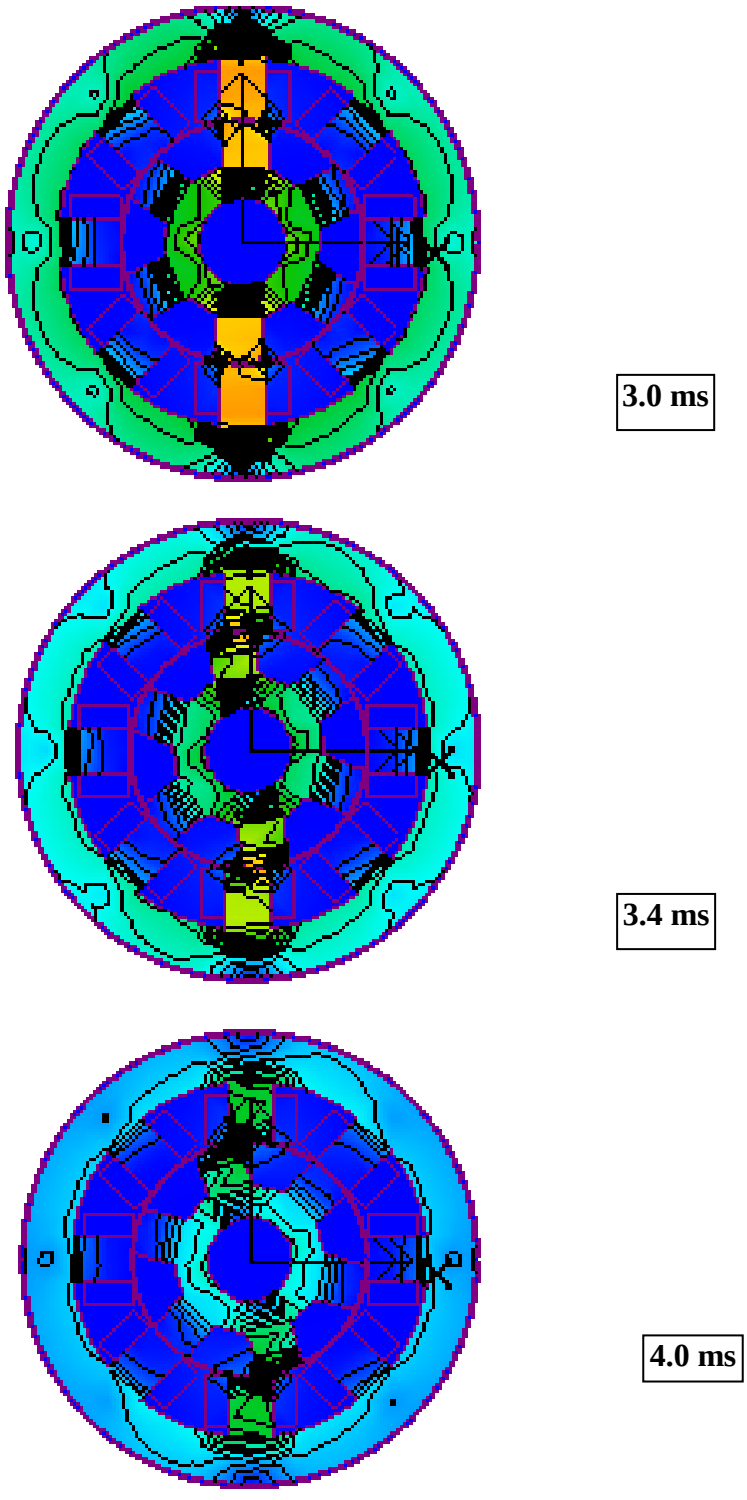

Figure 4.4 Distribution of magnetic flux density at different rotor positions at 3 ms, 3.4 ms, 4 ms (aligned to semi-aligned positions).

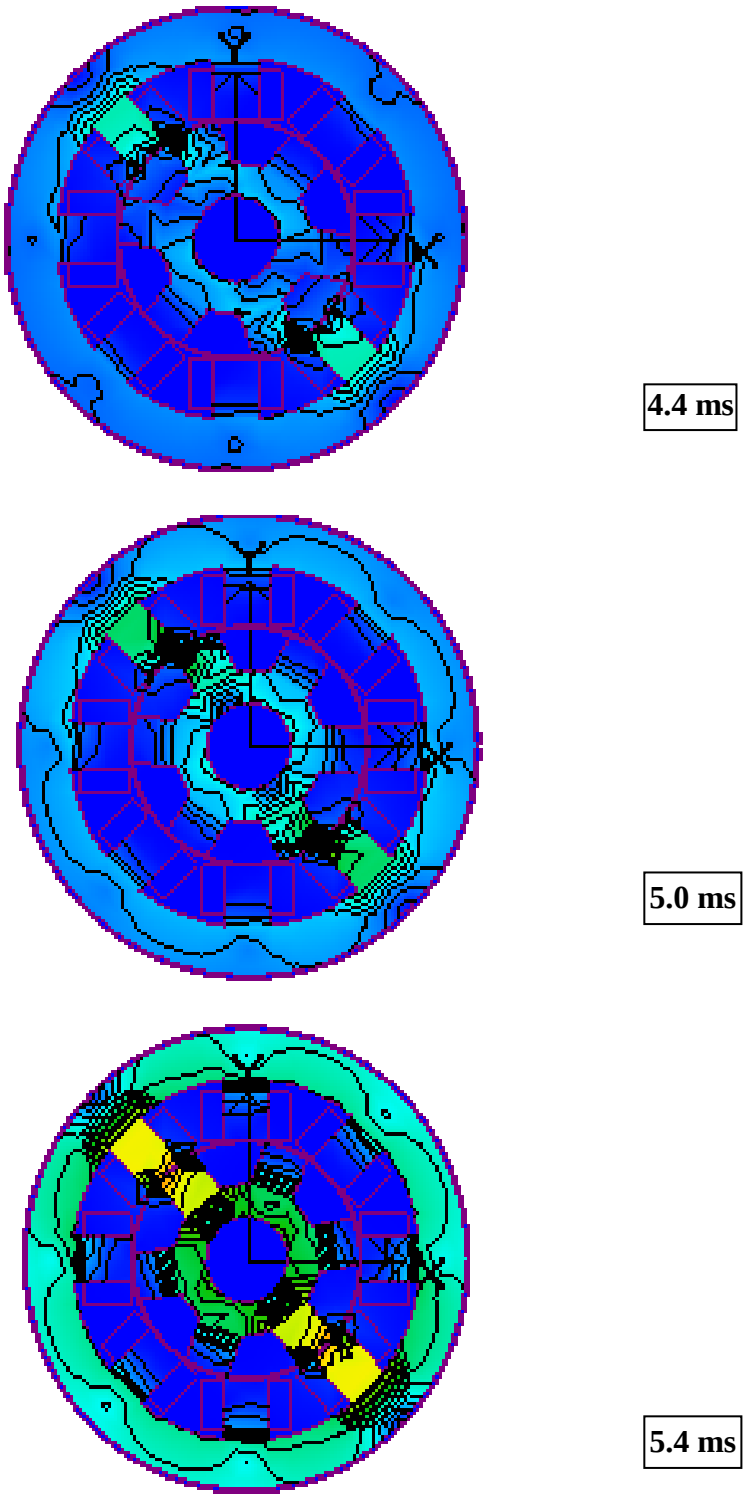

Figure 4.5 Distribution of magnetic flux density at different rotor positions at 4.4 ms, 5 ms and 5.4 ms (semi-aligned to aligned positions).

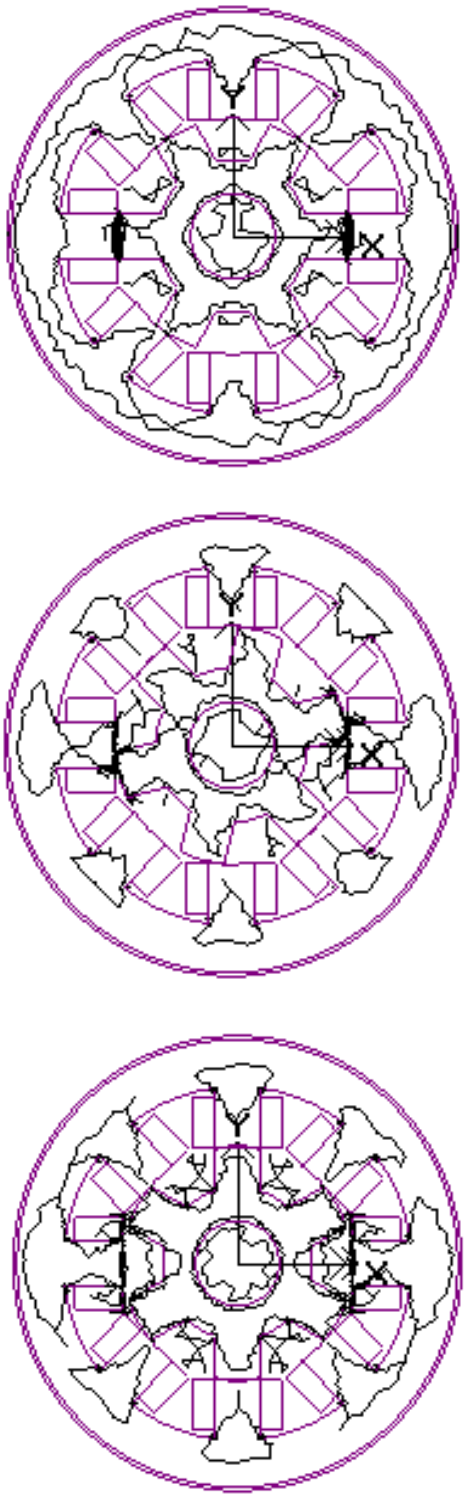

Figure 4.6 Radial flux density patterns for three different rotor positions (0, 15, 30 degrees).

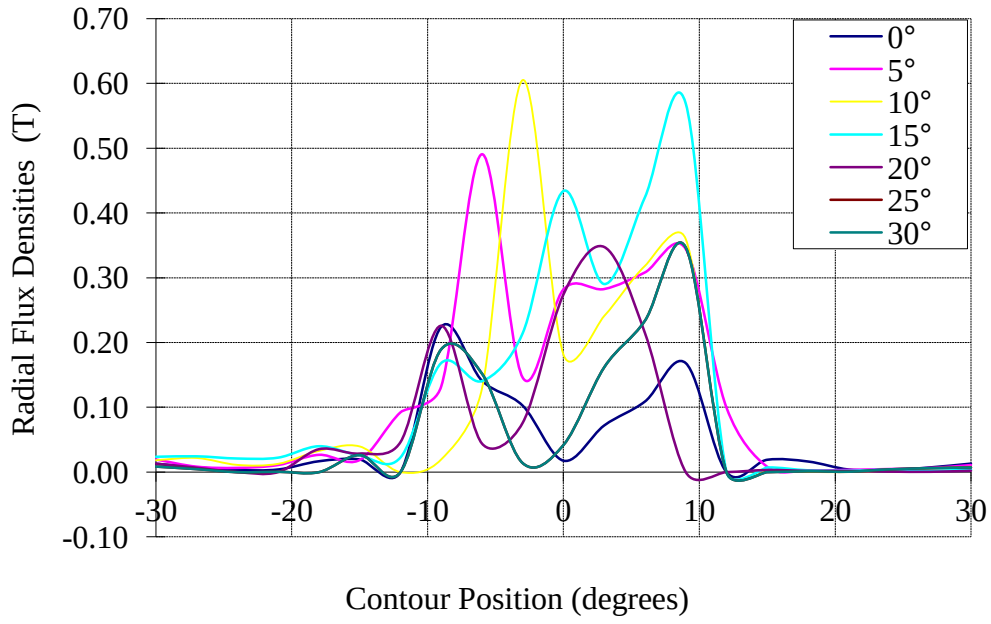

Figure 4.7 Radial components of flux densities vs. contour position (rotor position from aligned to unaligned).

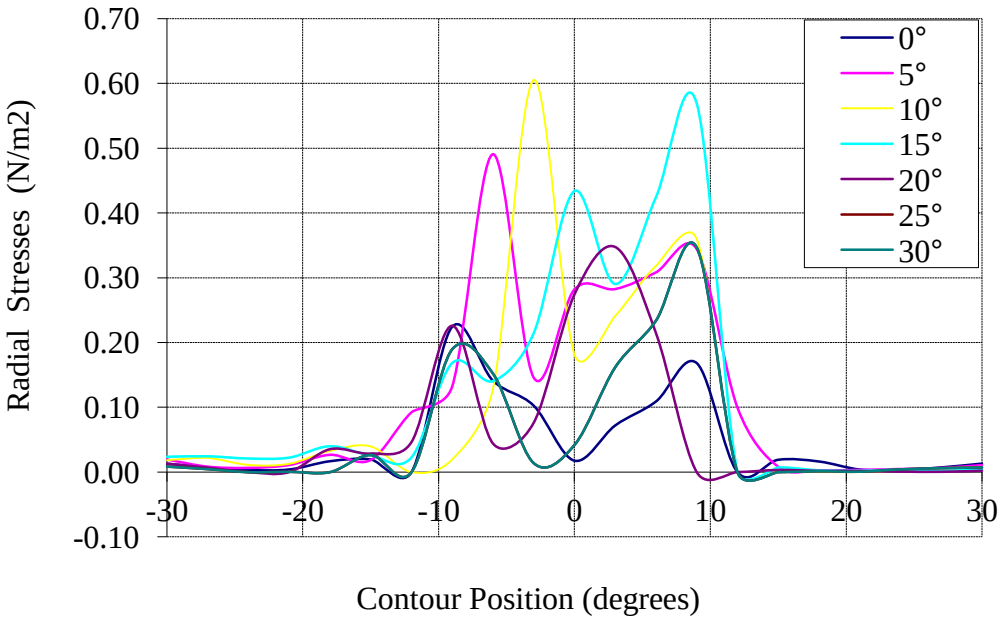

Figure 4.8 Radial components of electromagnetic stresses vs. contour position (rotor position from aligned to unaligned).

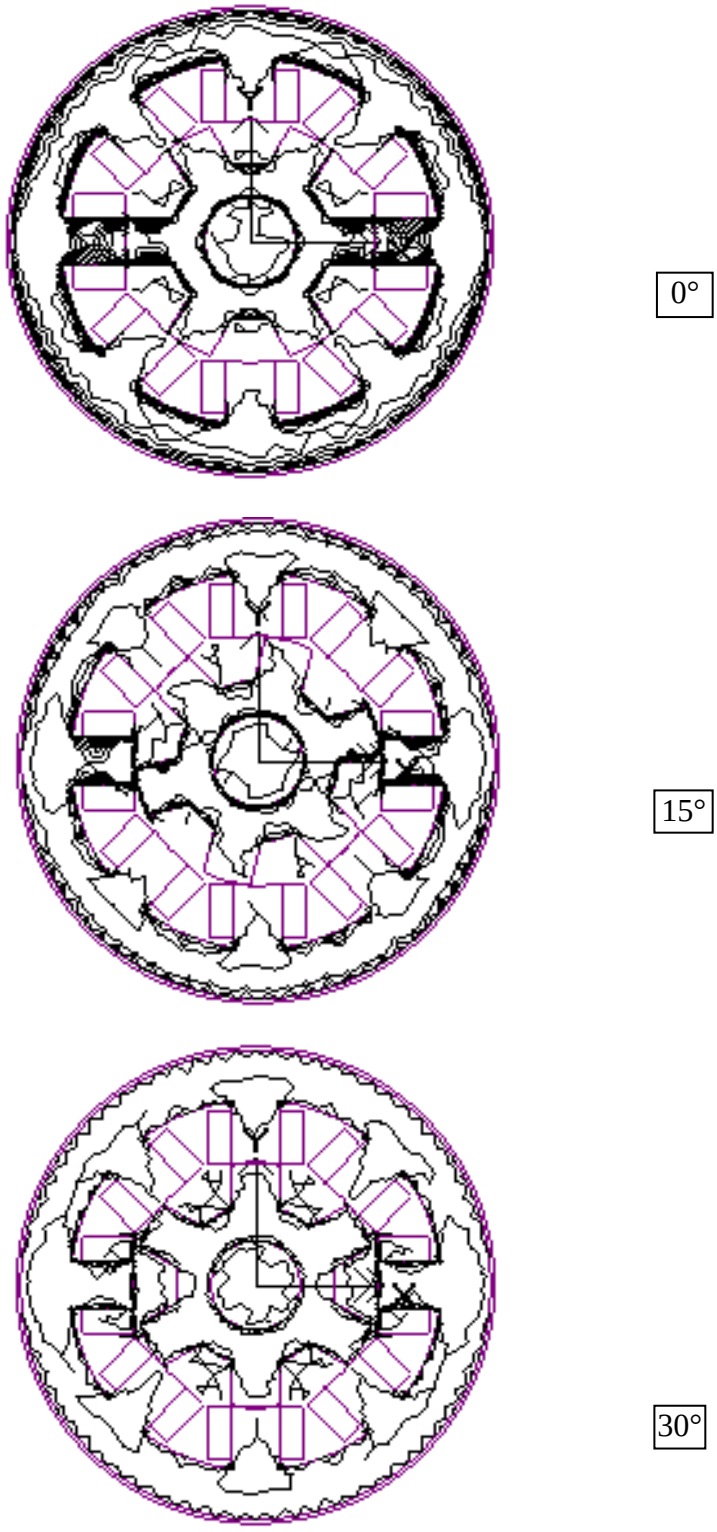

Figure 4.9 Tangential Flux density patterns for three different rotor positions (0°, 15°, 30°).

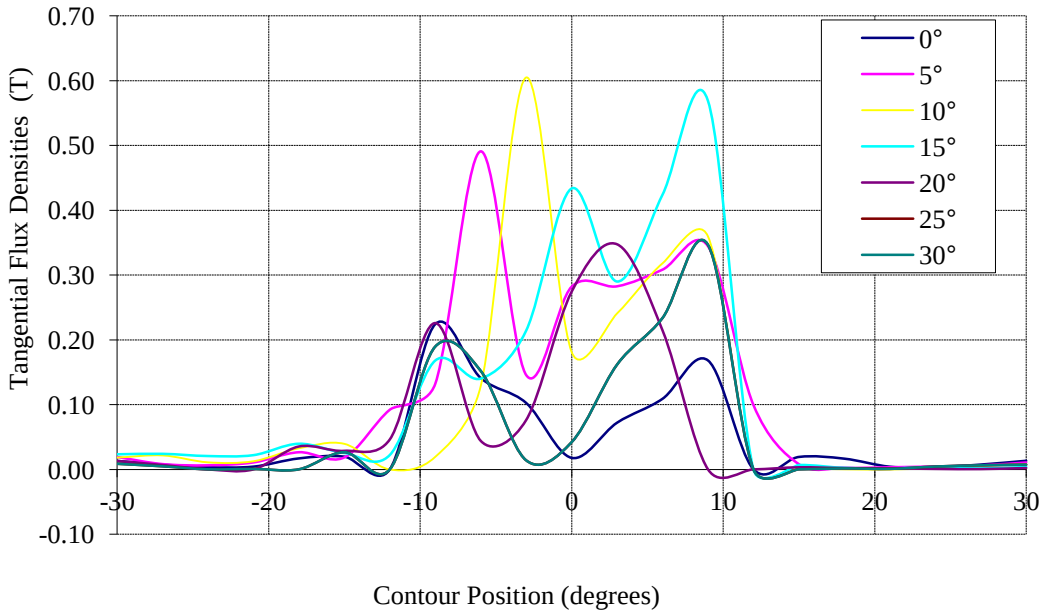

Figure 4.10 Tangential components of flux densities vs. contour position (rotor position from aligned to unaligned).

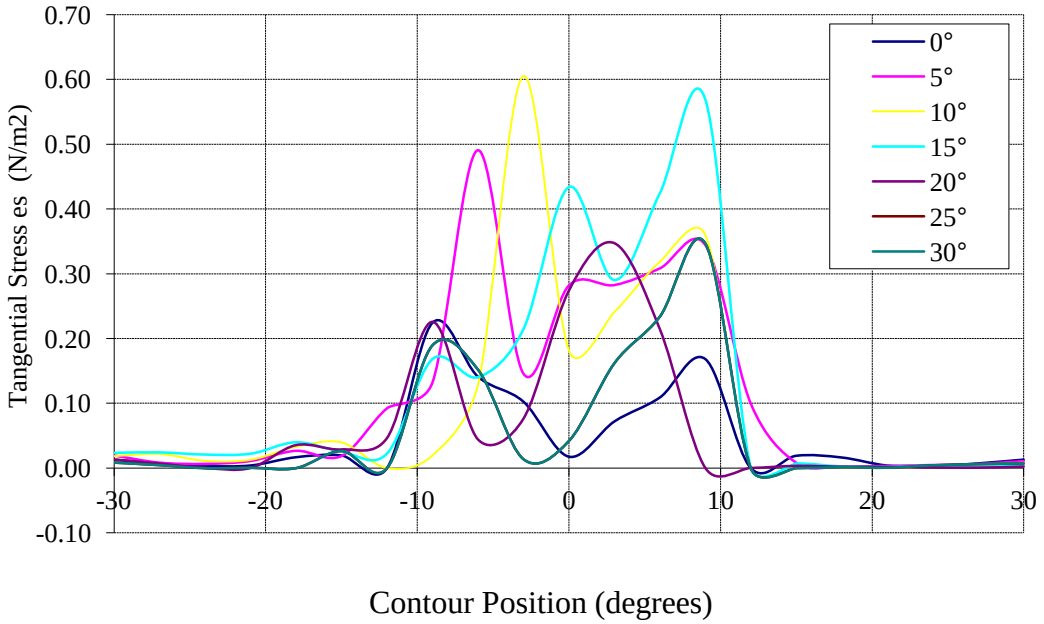

Figure 4.11 Tangential components of electromagnetic stresses vs. contour position (rotor position from aligned to unaligned).

in previous section by using a non-iterative, automatic, and efficient surface-volume combined integration, with an intelligent scalar function *g* based on local field error, which can be chosen in a way that can yield the solution according to MST or Coulomb's Virtual Works wherever required. It works in Cartesian co-ordinates.

4.8 Dynamic Analysis of Torque and EM Force

The performance of the machine can be assessed better on the basis of dynamic analysis of the parameters. Therefore, the stress components are integrated to obtain the value of electromagnetic force at different time instants under single the single phase excitation. In this simulation, the rotor was allowed to move contrary to the locked rotor condition. Figure 4.13 shows the results of this simulation in terms of the electromagnetic torque and corresponding EM force. It can be seen that the net electromagnetic torque is zero. It also shows the starting and steady state parameters of the machine as a result of dynamic analysis. Figure 4.14 shows the same output toque generated under the no-load condition whereas Figure 4.15 shows the electromagnetic force as a function of time.

A local minimum occurs almost at the midpoint from these two maxima. This can be explained by the significant drop of the tangential flux density at the midpoint location. The microscopic profile of the tangential force density has a substantial impact on explaining the nature of torque production and torque pulsation in the SRM drive. However, this results in the elimination of the local saturation at stator and rotor pole tips which can reduce the torque productivity of the machine.

4.9 Force Calculation Using Tuneable Volume Integration Method

Radial and tangential stresses are complex waveforms and cannot be integrated easily with any standard numerical solution. Secondly, due to sign alteration in values at

some points, the local field errors can dominate easily during integration and the solution optimization. Obtaining the integral over the cross-sectional area of the machine is also not easier due to the double saliency of the machine. Therefore, the radial and tangential stresses are commonly presented instead of the actual force.

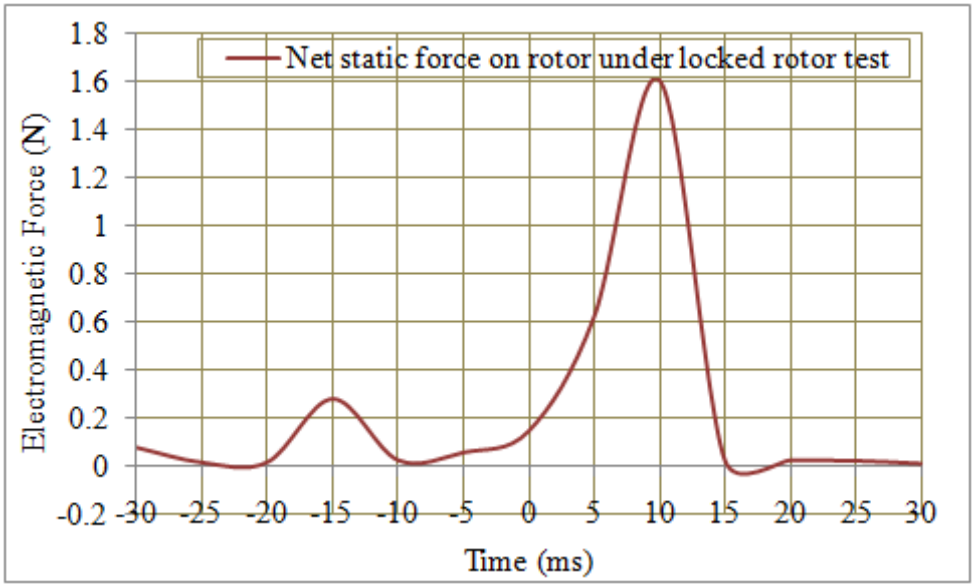

Figure 4.12 Net static electromagnetic force on rotor of the SRM.

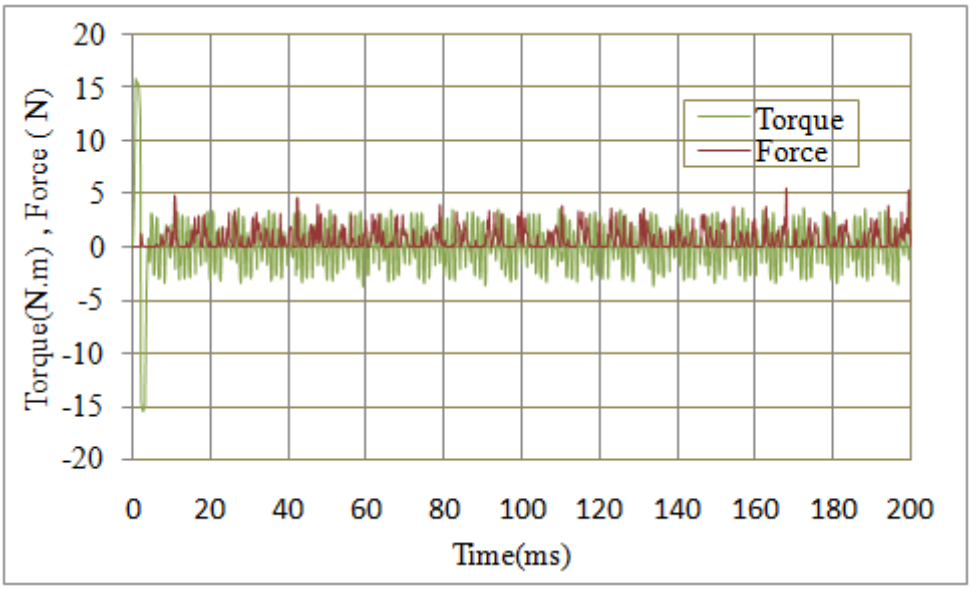

Figure 4.13 Dynamic electromagnetic force and torque on rotor of the SRM with single phase excitation.

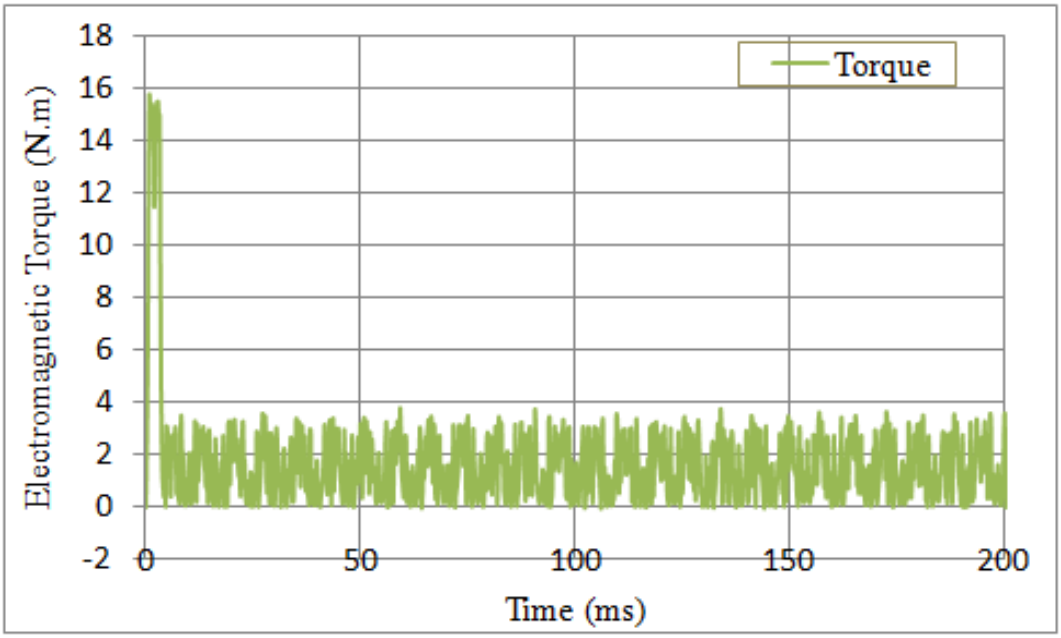

Figure 4.14 Dynamic behavior of the SRM with single phase excitation in terms of no-load torque.

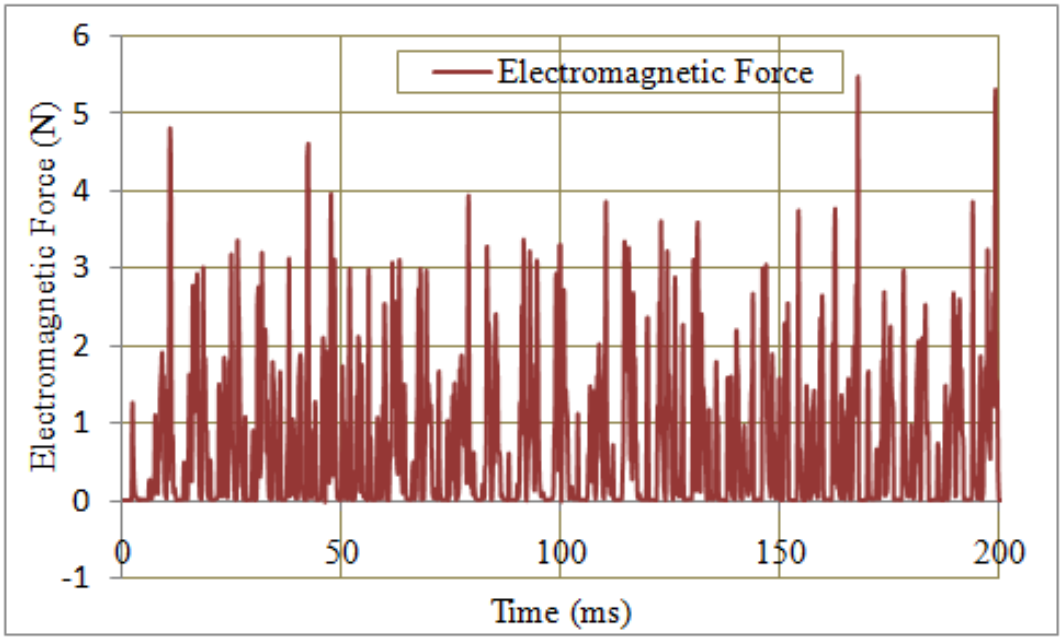

Figure 4.15 Electromagnetic force on rotor of the SRM with single phase excitation.

Chapter 5

INTEGRATION OF MULTI-LEVEL AND MULTIPHASE EXCITATION

5.1 Introduction

The reduction of torque ripple is the main target in research for designing a variable drive system with SRM for higher torque density and better efficiency. This ripple is due to the transition of excitation current between the adjacent phases. Precise control of turn-on and turn off angle is required to smooth the torque. In this paper, the effects of selecting the turn-on and turn-off angles are simulated in detail. It is observed that with the extended turn-on and turn off angles, the precise selection of turn-on and turn off angle can alter the shape of the excitation current in the stator coil and its point of overlapping with the adjacent coil. Therefore the transition between different phases can be smoothed out. The impact of this alteration on the excitation current and torque ripple as a function of different parameters of dwell angle is studied in detail in this paper. It is found that a sinusoidal current shape can also be obtained with the proper selection of these parameters.

There are many possible sources of torque ripple, vibration and acoustic noise in the SRM. The inherent vibration and acoustic noise are derived from the torque production mechanism, in which they are caused by the force between the excited stator teeth and the rotor. It contains a significant radial force component in addition to the required tangential component. A stator vibration is initiated when each time a phase winding was commuted. Not only magnetic and mechanical origin but also the control

algorithm and the inverter system are considered to overcome these problems. A multi-level switching technique has been used to reduce the radial attraction. A systematic approach to waveform design is introduced with switching angle variations. Design optimization of magnetic structure is also used to reduce resonance in the motor operation range. The winding topology and phase excitation methods were also considered. The full-pitched winding, which was used to utilize the mutual torque, however, is disadvantageous to drive efficiency. The symmetrical excitation technique in a conventional winding is also disadvantageous to the developed torque. A detailed comparison of various techniques has been presented.

5.2 Comparison with Experimental EM Characteristics

This chapter suggests an optimization of dwell angle parameters as a new method of current shape control and improving the torque ripple by using the continuously and non-linearly varying excitation current scheme without using multiple or variable voltage sources. It minimizes the acoustic noise and torque ripple by reducing the rapid change of radial magneto-motive force MMF. The electromagnetic structure of an ac motor has been designed so as to be suitable for operation with a sinusoidal wave source. However, an SRM has an electromagnetic structure suitable to be operated with current pulse. This multi-level excitation is achieved simply by controlling the dwell angle parameters to control the shape of the individual phase currents in nearly sinusoidal waveform instead of square waveform without using any variable voltage source or using many voltage sources or even without using the split voltage source. Therefore there will be no hardware complexity or limitations. This excitation method has an additional overlap of more than 2-phases excitation region, before one phase is off compared with

the conventional one-phase or two phase excitation method. In the overlapped excitation region, the rapid change of (MMF) from the previous phase off sequence is distributed by the other two adjacent phases.

In the first session, the pulsation in static torque characteristics is discussed in detail (Figure 5.1 and Figure 5.2). In the second section, the traditional mode of switching the phases is discussed with single level (constant value) excitation current with stator coils excited sequentially and one phase at a time. Later in the third section, the study of the machine with overlapping phases is presented i.e. adjacent poles are excited simultaneously, however the current levels are kept constant and the rise and fall time is kept negligible. It is found that although improved, the torque still has quite a significant amount of pulsation in it.

In the last section, the impact of varying the dwell angle parameters such as turn-on and turn-off angles are studied in detail. With the variation of these angles, the current shape is altered almost into a sinusoidal shape [64]-[66]. It is also noted that with the sinusoidal shape of the current, the current level in any of the two phases will never be same at the same time. Therefore, a current switching scheme is suggested which generates a multi-level and multi-phase multiphase excitation current without the complexity of the bipolar switching scheme.

5.3 Control Variables for Torque Profiling in SRM

Therefore, instantaneous torque level can be increased or decreased by varying these two key variables. Further in this chapter, two types of analysis are presented.

1. Comparative analysis of two major variations in current excitation schemes.

2. Integrated current profiling to address all major regions of operation.

5.4 Regions of Interests in EM Characteristics

- Region 1: slower rate of change of flux, smaller rotor angle (<15°), higher current (>3A)
- Region 2: rapid rate of change of flux, smaller rotor angle (<15°), lower current (<3A)
- Region 3: slower rate of change of flux, larger rotor angle (<15°), higher current (<3A)
- Region 4: rapid rate of change of flux, larger rotor angle (>15°), higher current (>3A)

The reason for dividing the EM characteristic curves into four regions are their distinctive torque range due to the salient structure and hence dependence on the corresponding excitation phase current values and rotor positions. Due to this saliency forces, non-linear problem (NLP) arises. They can have many local maxima. Therefore different approaches are required to reduce the torque ripple in the instantaneous torque profile. Before, suggesting any method, the torque requirement analysis in these regions are summarized as follows:

- Region 1 has acceptable torque ripple.
- Regions 2, 3 and 4 needs extra boost.
- Additional torque can be provided by two methods
  - ✓ Multi-level excitation (MLE):
  - ✓ Supplying extra excitation current

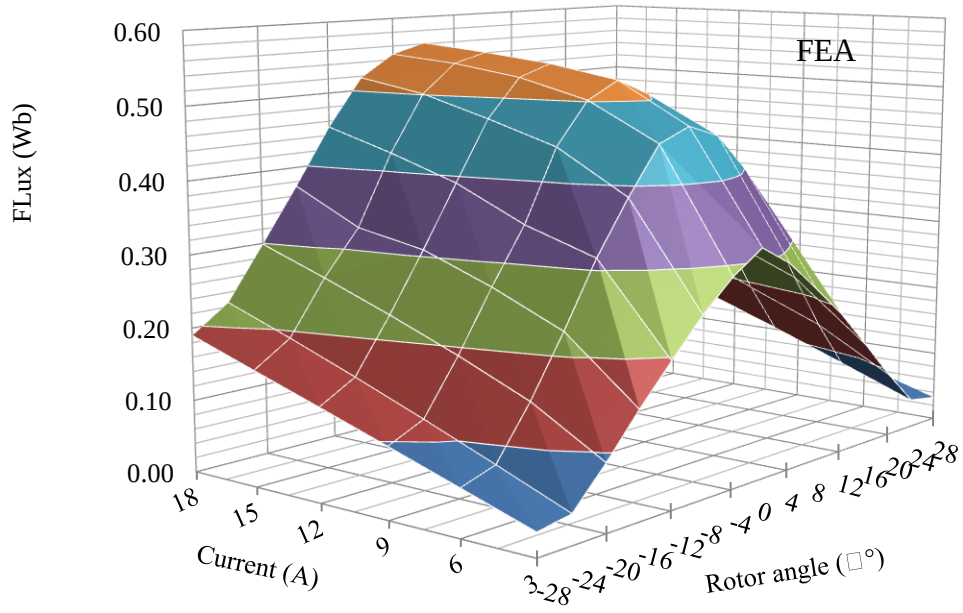

(a)

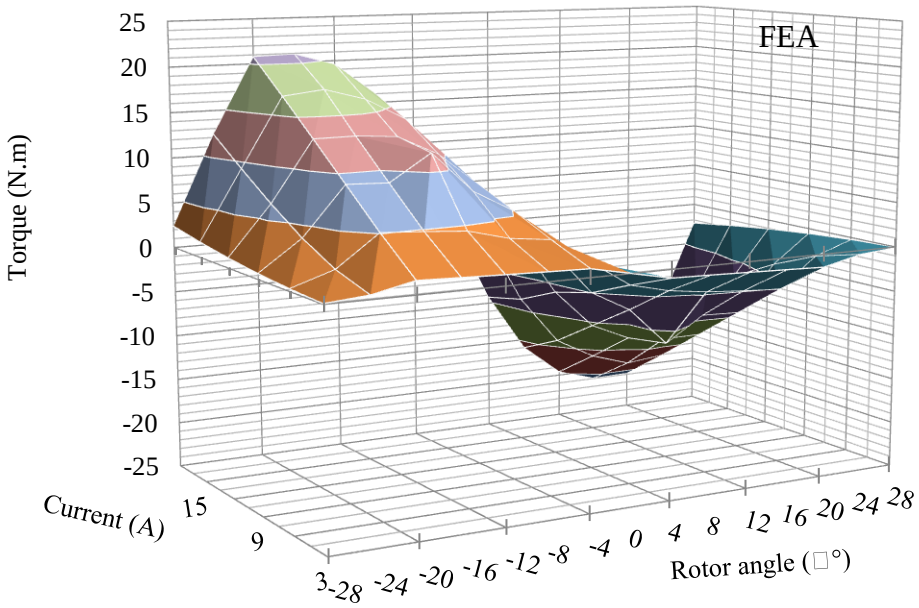

(b)

Figure 5.1 Electromagnetic characteristics of the SRM by FEA (a) flux profile. (b) torque profile.

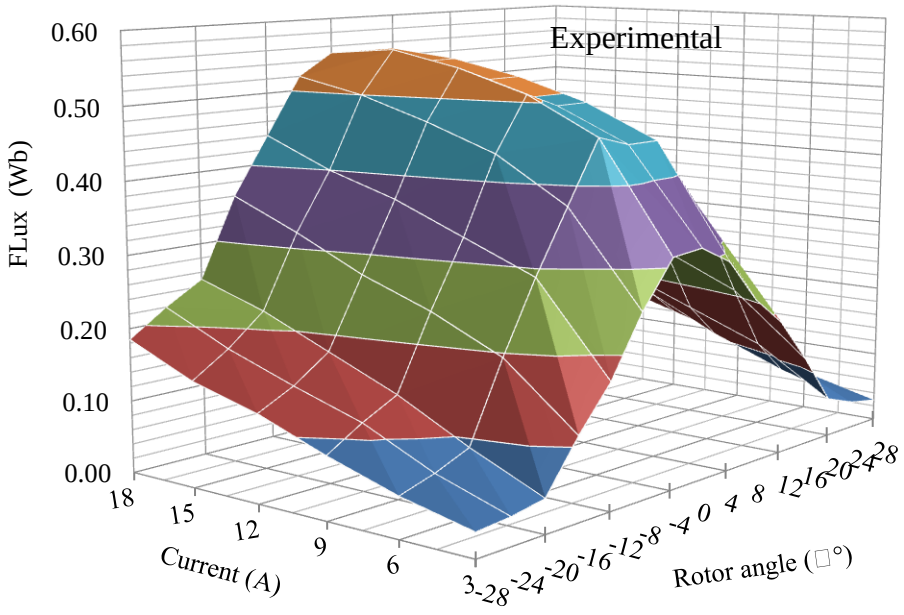

(a)

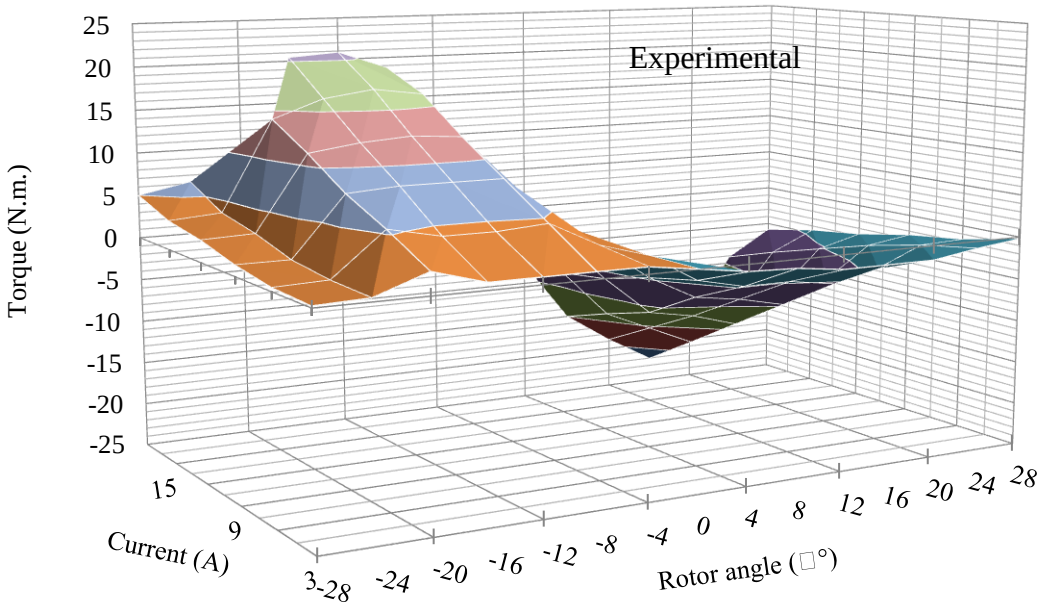

(b)

Figure 5.2 Electromagnetic characteristics of the laboratory SRM (a) flux profile. (b) torque profile.

(by using more than one supply or some storage element as capacitors).

1. Dwell angle parameter control (DAC):

(by controlling the position and duration of current conduction angle supplying mutual inductance from exciting adjacent poles).

In the next section, these techniques are simulated and the results of the two methods are discussed to compare the following aspects.

- Functional Differences
- Suitability and Limitations
- Conceptual Similarities.

5.5 Comparison of DAC and MLE

- EM force is a sum of saliency force (SF) and Lorenz force (LF).
- LF is extremely lower than SF but not negligible.
- SF is macroscopic while LF is microscopic in nature.
- Tangential force generates EM torque, thus desirable.
- Radial force generates acoustic noise and vibrations, therefore becomes unwanted. Also an increase in the ratio of tangential to radial force component is required to improve efficiency.
- Precise control of torque ripple depends on providing the additional tangential force component.

Mathematically, applying multi-level excitation current (with a multi-level converter or more than one input current source) reduces torque ripple significantly. Precise dwell angle switching control is not possible at higher speeds due to fast switching technique. Providing multi-level input values is theoretically have unlimited

degrees of freedom which is impossible practically. Dwell angle parameter control looks more practically applicable but even with limited number of degrees of freedom, It is usually uncontrollable where it is needed most. It becomes uncontrollable in rapidly flux increasing regions.

5.6 Region-wise Applicability

- **Region 1**:
  - ✓ MLE is better at higher speed
  - ✓ Precise timing not possible
  - ✓ Does not require numerous degrees of freedom.
- **Region 2:**
  - ✓ Both techniques can be implemented.
  - ✓ DAC is better due to cheaper and less speed
  - ✓ Precise control with continuously varying current.
  - ✓ MLE works with less number of degrees of freedom which is not significant.
- **Region 3:**
  - ✓ Both can be equally used.
- **Region 4:**
  - ✓ MLE is better at higher speed.

5.7 Analysis of Dwell Angle Parameters Control

Excitation current profiling has the following three key tunable parameters to shape the excitation current. The block diagram for the setup is shown in Figure 5.3. The simulation is performed with all three of them and at the last a combination of all three of

them with optimization objective of minimum torque ripple and secondary objective of higher average torque. The shapes of the current profiles are to be noted whereas the quantitative analysis not required understanding the effects on shape of current and torque waveforms.

In the later sections, the simulated effects of varying the dwell angle parameters on flux, excitation current shape and torque ripple are presented. Varying one parameter to study does not keep the other parameters constant.

- Percentage of overlapping.(torque sharing)
- Turn-on critical angle,
- Turn-off angle and
- Width of the dwell angle

5.8 Percentage of Overlapping

It is found that generally an over-lapping of two adjacent phases upto a certain limit reduces the ripple percentage in torque profile. If the overlap is increased too much, more than two of the phases can be conducted simultaneouly. However, when all of the phases are in conduction mode, the torque ripple will be reduced to very low. This is because some of the phases will provide negative torque due to the corresponding rotor position which can even sum up as a negative torque. On the other hand, if the neighbouring phasea are underlapped which means the next phase start rising gradually after the falling edge of the previous phase which is the usual case of traditional operation with single phase excitation. Precise control of turn-on and turn off angle is the key to a smoother torque profile in a multi-pulse switching. It is also found that the percentage of overlap between the two adjacent excited phases also affects the current shape.

5.9 Duration of the Dwell Angle

Figure 5.4 shows the effects of single phase excitation. This is the traditional operation of the SRM. The constant level of current i.e. 75% of the maximum value is only available in the primary phase with sharp rise and fall. Therefore there is no torque sharing. Only the primary phase is the major contributor of the torque. The torque profiles shows significant dips at the time of commutation.

Figure 5.5 shows an equal torque sharing between adjacent phases which is usually the 50% overlap by increasing the duration of conduction angle i.e. each phase keeping the current flowing into the stator coil more than its share of the mechanical cycle. This is also known as the multi-phase excitation. And more than one phase is fully conducting at each rotor position. This is expected to reduce the ripple by providing some additional torque near discontinuity to avoid dead beat in addition to the torque produced by the primary conducting phase. This is the most effective and popular method of reducing the torque ripple, so far. However, due to the constant current source and equal amount of current is flowing in each phase and resultant torque profile has some ripples not only due to the intrinsic behavior of the SRM but also due to the excessive or insufficient additional torque by the secondary phase. Torque sharing functions (TSF) between phases are usually employed to decide the timings of the firing angle so that the percentage of overlap can be controlled between the two phases.

5.10 Advanced Conduction Angle

Figure 5.6 shows the maximum advanced angle switching i.e. turning on the next phase before it reaches the fully aligned position by the previous phase excitation to avoid the torque discontinuity at the fully aligned position. In this switching scheme, if

the excitation current in the primary coil is not turned off before reaching the fully aligned position by the corresponding rotor poles, the reduction in torque ripple becomes insignificant because the average torque value is also reduced, and the percentage of ripple remains almost same. Therefore in advanced angle technique, the next phase is excited and primary phase conduction is stopped before the fully aligned position.

5.11 Delayed Tail Angle

Figure 5.7 shows the elongated conduction angle i.e. keeping the current flowing into the stator coil even after the next phase has been excited. This is expected to reduce the ripple by providing a counter torque or a kind of providing reluctance to the rotor pole to have a comparable reluctance during the rotor angle between non-aligned to semi-aligned position and from the semi aligned to fully aligned rotor position. Although, it reduces the amount of average torque but ripple percentage is improved.

5.12 An Optimized Combination of All Parameters

Figure 5.8 shows the combination of above to reduce as much ripple as much possible. Multi-phase excitation seems similar to the advanced turn-on angle method due to the conduction of next phase before fully aligned position. However, it is different due to the turned off angle of the primary phase in relation to fully aligned position. Similarly, the elongated tail-angle can be used as a type of multi-phase scheme if required. Figure 5.9 shows another example of an optimization of dwell angle in Simulink simulation and uncontrolled sharing of both dwell angle and multi-level excitation. This is actually the most effective local optimization to reduce the ripple by providing a adding some torque in addition to the torque produced by the primary conducting phase.

5.13 Position Dependent Multi-Level Current Excitation

This Study suggests the requirement of a new method of current shape control and the torque ripple reduction by using the continuously and non-linearly varying excitation current scheme Without using multiple or variable voltage sources. It minimizes the acoustic noise and torque ripple by reducing the rapid change of radial MMF in an energy-efficient manner in HEV applications. It is expected that the torque ripple can be minimized significantly by both DAC and MLE. MLE is more effective in saturated flux, higher current and high speed regions DAC is precisely effective only at lower speed applications and rapid flux change region. With the increase of number of possible current levels, MLE can be used for effectively in rapid flux change region. Therefore, intelligent integration of the two current profiling schemes is required to extremely minimize the torque ripple.

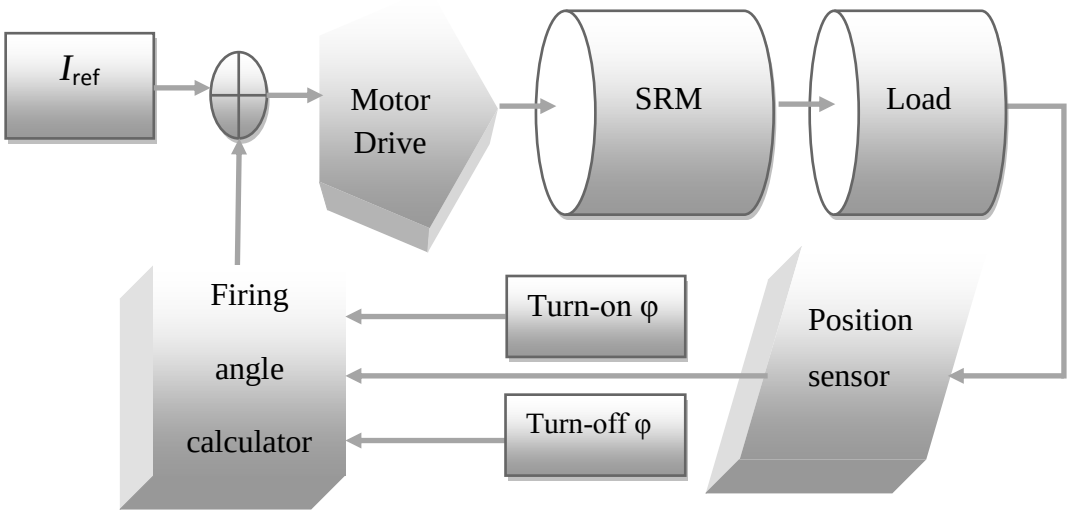

Figure 5.3 Block diagram of the feedback control system of the SRM drive.

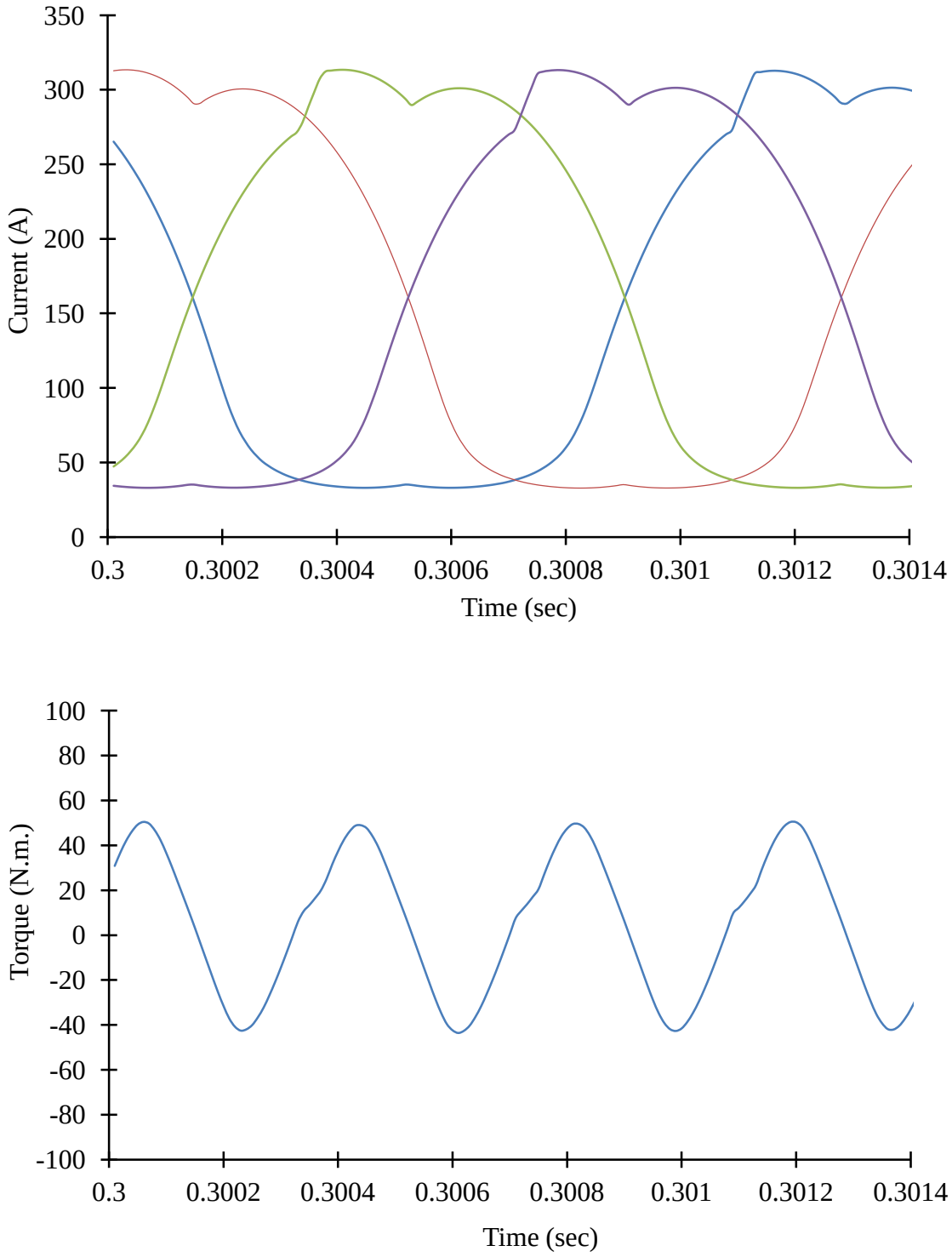

Figure 5.4 Impact of single phase excitation on current and torque profiles.

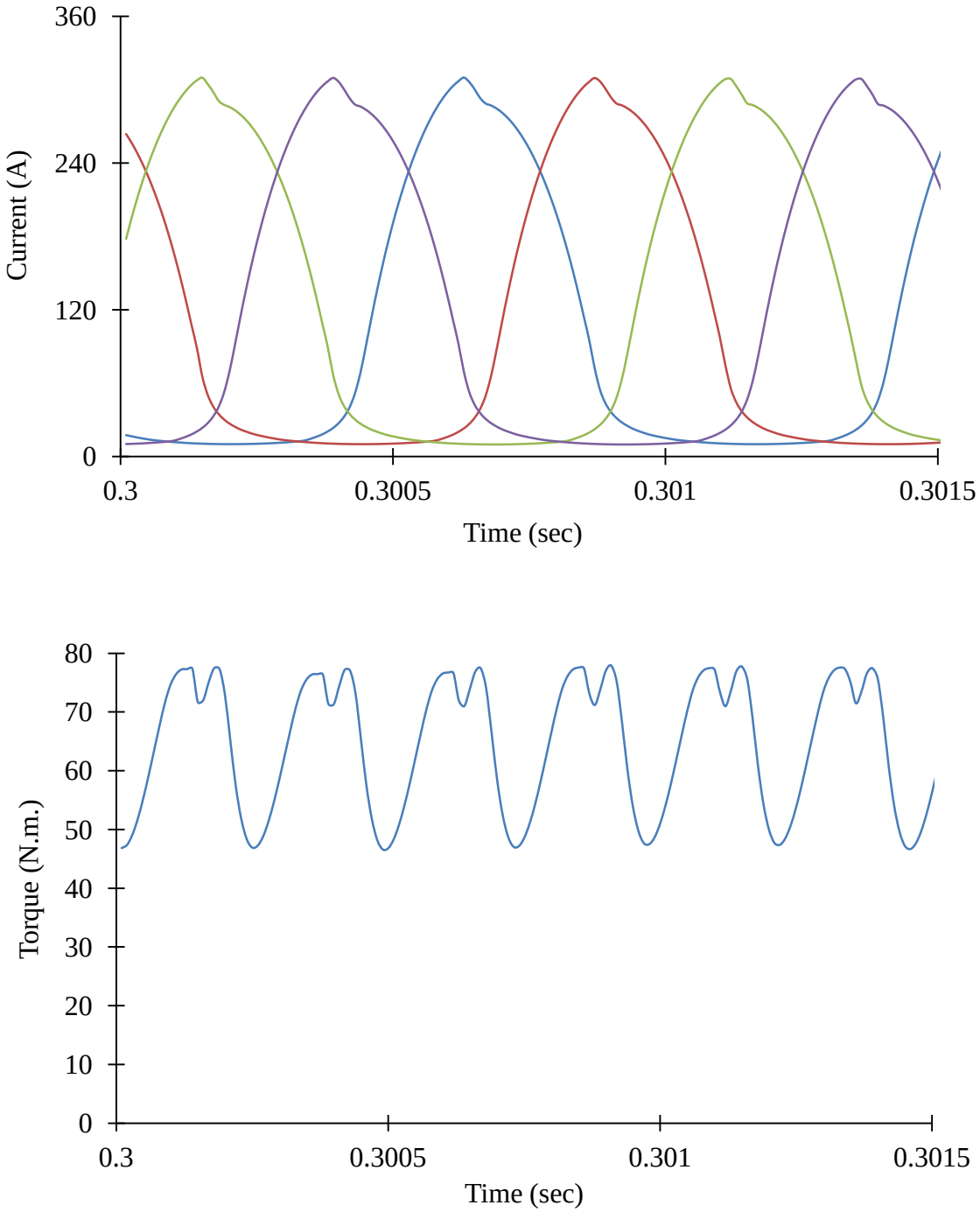

Figure 5.5 Simulated excitation current and torque profiles with one of the advanced angle method. (Also known as Multiphase Excitation with 50% overlap.)

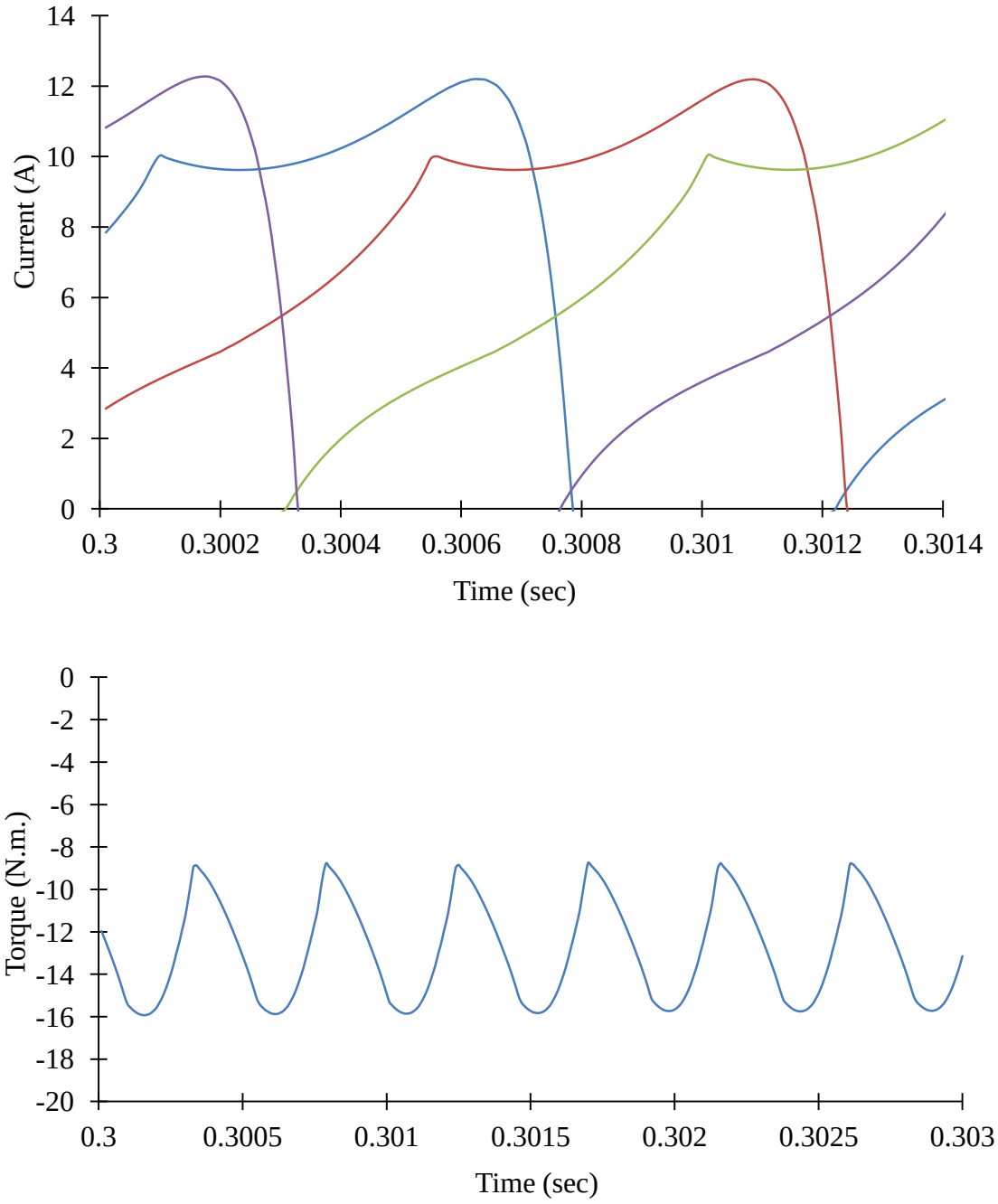

Figure 5.6 Simulated torque and current profiles with maximum advanced angle selection.

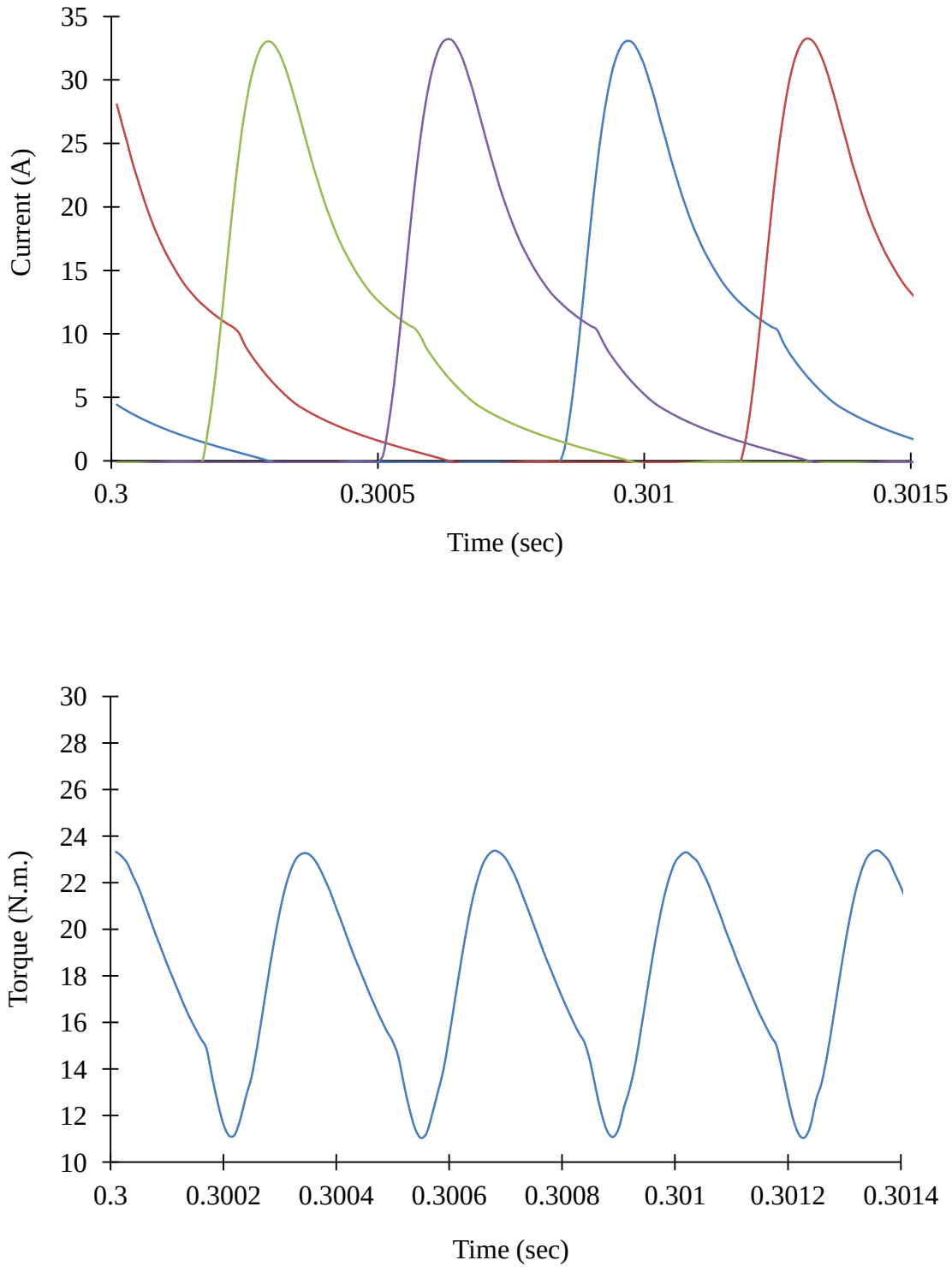

Figure 5.7 Variations in torque and current profiles by delayed turn-off angle selection.

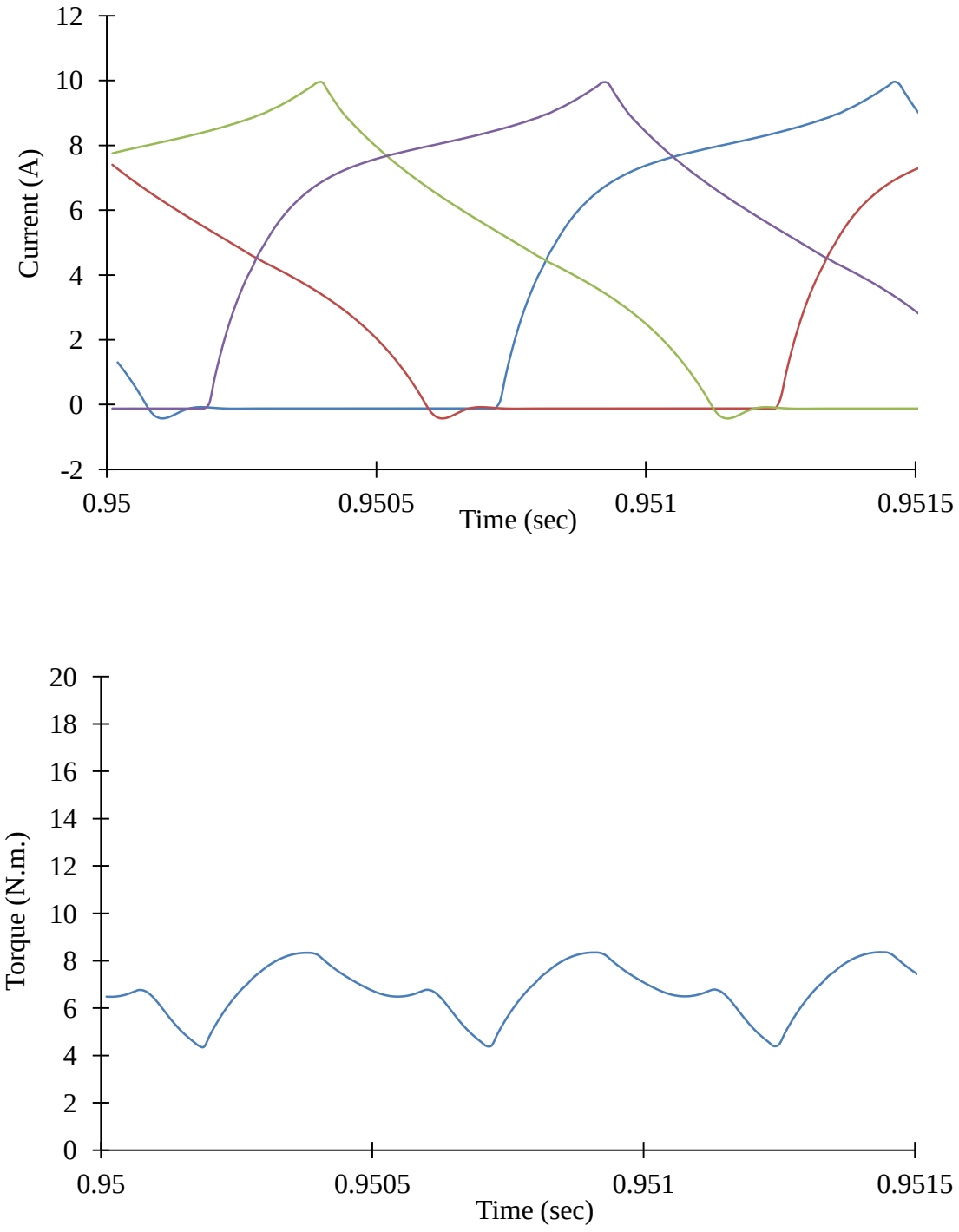

Figure 5.8 Simulated torque and current profiles by advanced turn-on and delayed turn-off angle selection.

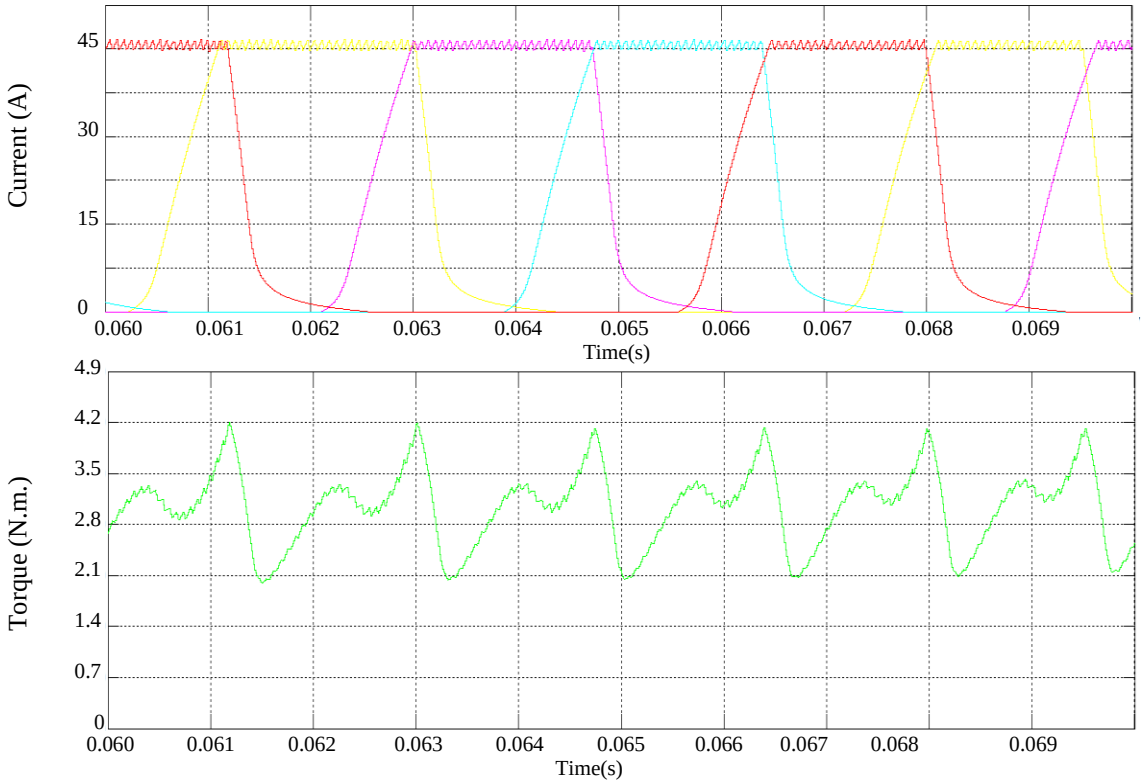

Figure 5.9 Sample simulation of excitation current (A) and torque profiles (N.m.) by uncontrolled integration of MLE and DAC.

Chapter 6

PROPOSED GLOBAL NLP OPTIMIZED TORQUE RIPPLE ELIMINATION METHOD

6.1 Introduction

The double saliency in the structure of a switched reluctance motor (SRM) produces significant ripple in instantaneous torque and degrades its performance [3], [4]. Switching time controls of the phase currents with torque sharing functions are more commonly used methods. A non-linear electronic control of the phase currents is needed to compensate for the unwanted radial EMF [45]-[48]. For the optimal multi-level excitation reference phase current generation, several methods have been proposed which are complicated, model dependent and/or energy-inefficient [67]-[77].

A global optimization method is proposed to balance out the crests and troughs of the torque ripples throughout the operation. Open loop simulations with precise drive model in the form of its fingerprints are studied. These fingerprints are actually the intrinsic electromagnetic characteristics of the machine. It is suggested that the proposed reference current waveforms will improve the performance by compensating for the intrinsic behavior of the machine which is the non-linear relationships of torque with phase currents and rotor positions.

A laboratory 1 hp SRM drive is used to carry out this optimization method for reduction of torque ripple in torque profile and generation of reference phase currents. The electromagnetic behavior of this laboratory SRM is taken as the experimental data required for global optimization of non-linear problems (NLP). The machine performance

is investigated through 3D finite-element analysis (FEA) and the optimized torque and current profiles are verified on the FEA model.

In the next section, the global optimization technique for NLP is introduced. It also includes the discussion on reasons for considering the torque ripple minimization as a non-linear problem and why adopting the global optimization method is the most accurate solution. The practical implementation procedures required for employing the fast-filled algorithm on initial torque profile and constant phase current waveforms are presented in the next section. Therefore, the torque and phase current profiles transformation through the proposed method are discussed into details. After that, the impact of these optimized torque and the resultant generated phase current profiles on dwell angle parametric design in terms of switching time variations are analyzed.

In the last section, a comparative quantitative analysis of the torque and current profiles obtained by proposed method is performed in terms of the torque ripple percentage and the shape of the exact reference current waveforms in comparison with the traditional operation and the dwell angle control approach such as advanced turn-on angle method. Providing slightly additional current in the saturation region can flatten the saturation characteristics without fully exciting the adjacent phase and is therefore very energy efficient. However this method is limited to a region otherwise needs an extra power supply and thus becomes energy inefficient. This method is very effective in the elimination of small ripples in the torque. In this paper, the two methods are integrated with need-based contribution of both, which are also simulated individually for comparison.

Optimization procedure is designed to reach an optimal value of a specified objective function while keeping other technical indices within acceptable ranges. The explicit methods of optimization to make a gradient equal to zero are infeasible for electrical machine design due to saturation. Therefore, practical optimization needs NLP techniques. Traditional optimization techniques usually are only effective to find the local optima whereas this non-linear problem is actually a multivariable problem since the exact torque is non-linearly dependent on two variables which are inductance and current. The inductance also non-linearly depends on phase current and rotor position. Therefore, this nonlinear problem cannot be represented as a single function. Its solution will be non-convex, and the function is to be plotted to observe the behavior in the whole domain. However, a multivariable problem cannot be plotted in terms of the two variables. Therefore, a procedure to obtain a matrix of experimental data defined as unique fingerprints of the machine describing the behavior is needed to find parameters by reducing the error between the experimental and calculated values. In such situations, implementation of a global optimization technique is the only choice. Therefore, this technique is applied on torque ripple minimization to profile current in each coil. Many combinations of adjacent coil current pairs are possible in an electrical cycle to reach the constant torque level making it a multi-dimensional optimization problem as in (6.1).

$$T_\theta = g\left(i_{i,\theta}, i_{j,\theta}\right) = Const = T_D \tag{6.1}$$

In the single phase operation, current is flowing only in primary stator windings. The difference at each rotor position between the instantaneous and desired torque is shown in (6.2). All possible supplementary torque components which can be added in the instantaneous torque to keep it constant are shown in equations (6.3), (6.4) and (6.5).

$$T_D - T_i = \Delta T_i \tag{6.2}$$

$$\Delta T_i = T(\Delta i, \theta_i) + \sum_{n=i+1}^{m} T(i_i, \Delta\theta_n) \tag{6.3}$$

$$T_D(i_1,...i_m, \theta_1,..., \theta_m) = T[i_1(\theta_1), \theta_1] + T(\Delta i, \theta_i) + \sum_{n=i+1}^{m} T(i_i, \Delta\theta_n) \tag{6.4}$$

$$T_D(i_1,...i_m, \theta_1,..., \theta_k) = T_i(i_1(\theta_1), \theta_1) + \sum_{n=1}^{m} \Delta T_{i,n} \tag{6.5}$$

The torque ripple factor is calculated using (6.6),

$$R_t(\theta) = \frac{T_i(\theta) - T_D}{T_D} \tag{6.6}$$

The test condition for the ripple elimination is defined in (6.7).

$$\frac{\partial^m T(i_1,...i_m, \theta_1,...\theta_m)}{\partial\theta_1,..., \partial\theta_m} = 0 \tag{6.7}$$

6.2 Electromagnetic Torque Profile Measurements

This concept employs a modified version of flood-fill algorithm to keep the torque level constant at each rotor position. As discussed before, a matrix of experimental data, in this case, the electromagnetic characteristics of the SRM as a unique fingerprint of the machine is needed for NLP optimization. A laboratory 1 hp SRM drive is setup to obtain the machine characteristics experimentally. A locked rotor test of the SRM drive as shown in the experimental setup of Figure 6.1 is conducted to obtain the electromagnetic characteristics in terms of flux vs. rotor angle and phase current.

A 3D FEA model of the laboratory SRM is built with exactly same material and size of the interior and exterior and physical, mechanical, electrical and electromagnetic characteristics. The internal geometry of the in-house SRM is presented in Figures 2.1

and 2.2 and virtual machines by FEA in Figure 6.2. A similar locked rotor test is conducted on the 3D FEA model. The experimental and FEA flux profiles verified that the two machines provide the same flux profile, therefore, same intrinsic behavior of the SRM precisely match with each other as shown in Figure 6.3.

In the last phase, the corresponding rotor angles for all other phases are calculated. Torque and the excitation current values for all coils are then calculated in accordance with the primary phase in the form of a 4D look-up table. The initial torque profile for traditional SRM operation is thus obtained and used as the experimental database. The study of force distribution provides the weaker and discontinuous points in torque profile in terms of rotor angle and helps in choosing the method of obtaining additional torque for optimization.

The highest crest value is chosen as the desired value of torque at each rotor position for each value of current in the primary phase. The choice of the highest value is to increase the torque to current ratio which is one of the best characteristics of SRM and to avoid the need for generating negative torque by any of the secondary phase to balance at this rotor position which in turn keeps the operation energy-efficient.

For less fluctuation in the excitation current profile, firstly the advanced critical angle technique is employed and then to make the torque further smoother, the search and swapping algorithm is applied for additional boost. The direction of search is kept in the primary phase for higher current values and then if required moves to the secondary phase current options. Hence a current profile is generated as a reference waveform for feed-forward torque control scheme for open-loop as well as closed loop strategies.

For comparison, torque and current profiles using other popular techniques are

also used such as advanced critical angle, multi-phase and multi-level excitation methods. Advanced angle method is applied by varying the turn-on and off angles before the fully-aligned position i.e. choosing the best active rotor positions. A precise multi-level technique is implemented by applying this proposed algorithm on the single phase data. The two locally optimized solutions are used for comparison. The cold test runs for verifications are performed on 3D electromagnetic FEA model. Quantitative analysis of torque ripple in each technique is performed in terms of parameters such as average torque and percentage torque ripple.

6.3 Parametric Analysis of Torque and Phase Current Profiles

The objective of the proposed method is to keep the desired torque at each individual rotor position alone and does not rely on the entire waveform. In single phase excitation commutation is instantaneous and the optimization of the phase torque is at the critical rotor positions θ^i_c when (6.8) is satisfied.

$$i\left(T_D, \theta^i_c\right) = i\left(T_D, \theta^i_c + \theta_{pitch}\right) \tag{6.8}$$

At speed, adjacent phases commute under the condition (6.9) when both phases produce half the required torque ($T_D/2$):

$$i\left(T_D \big/ 2, \theta^i_c\right) = i\left(T_D \big/ 2, \theta^i_c + \theta_{pitch}\right) \tag{6.9}$$

The on-coming phase j is fully excited before θ approaches θ^i_c in advanced angle method so that it reaches the required torque level at $T_D/2$ exactly at θ^i_c. However, in the proposed method, it rises gradually. As θ passes θ^i_c the flux in the phase j-1 is adjusted to keep the total torque constant while the current in phase j is constant. The saturation region has a phase torque proportional to the current. The torque constant ratios in a

Controller SRM Dyno

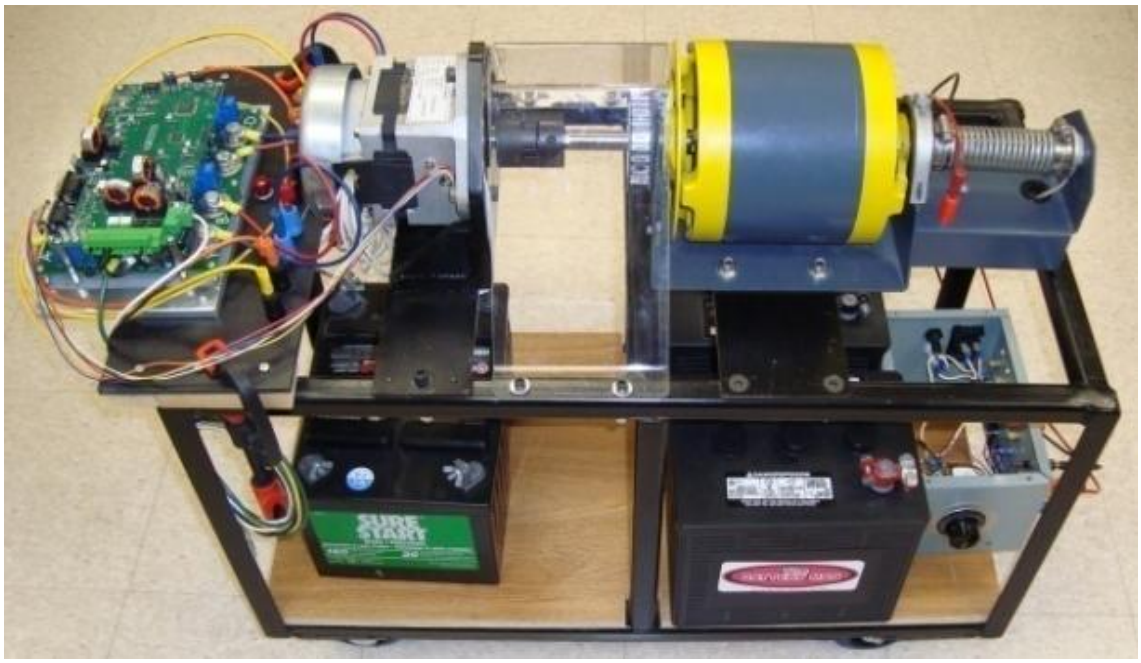

Figure 6.1 Experimental setup of SRM for locked rotor test with In-house SRM.

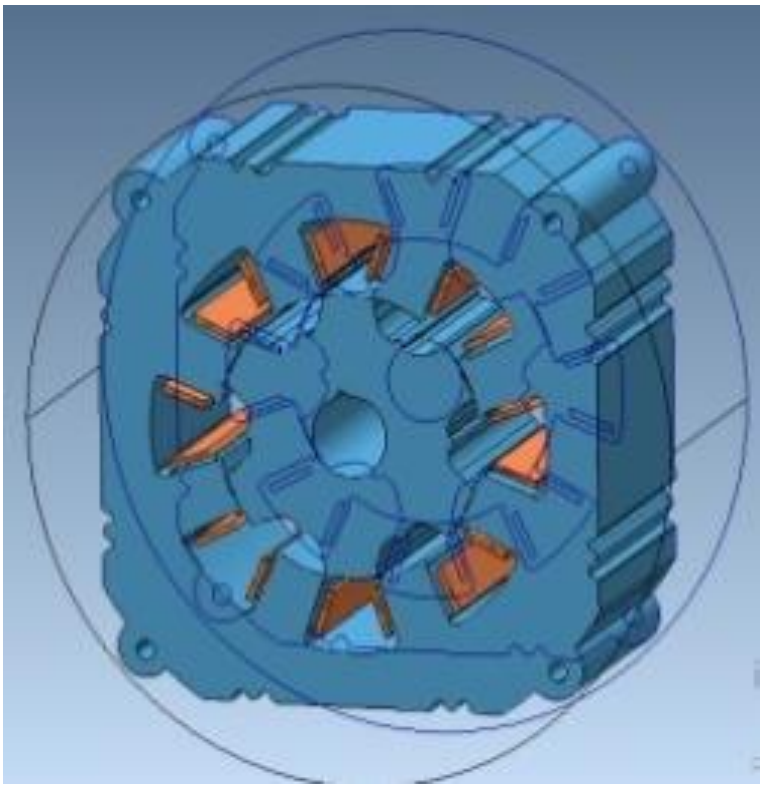

Figure 6.2 3D FEA model of the In-house SRM used in the investigations.

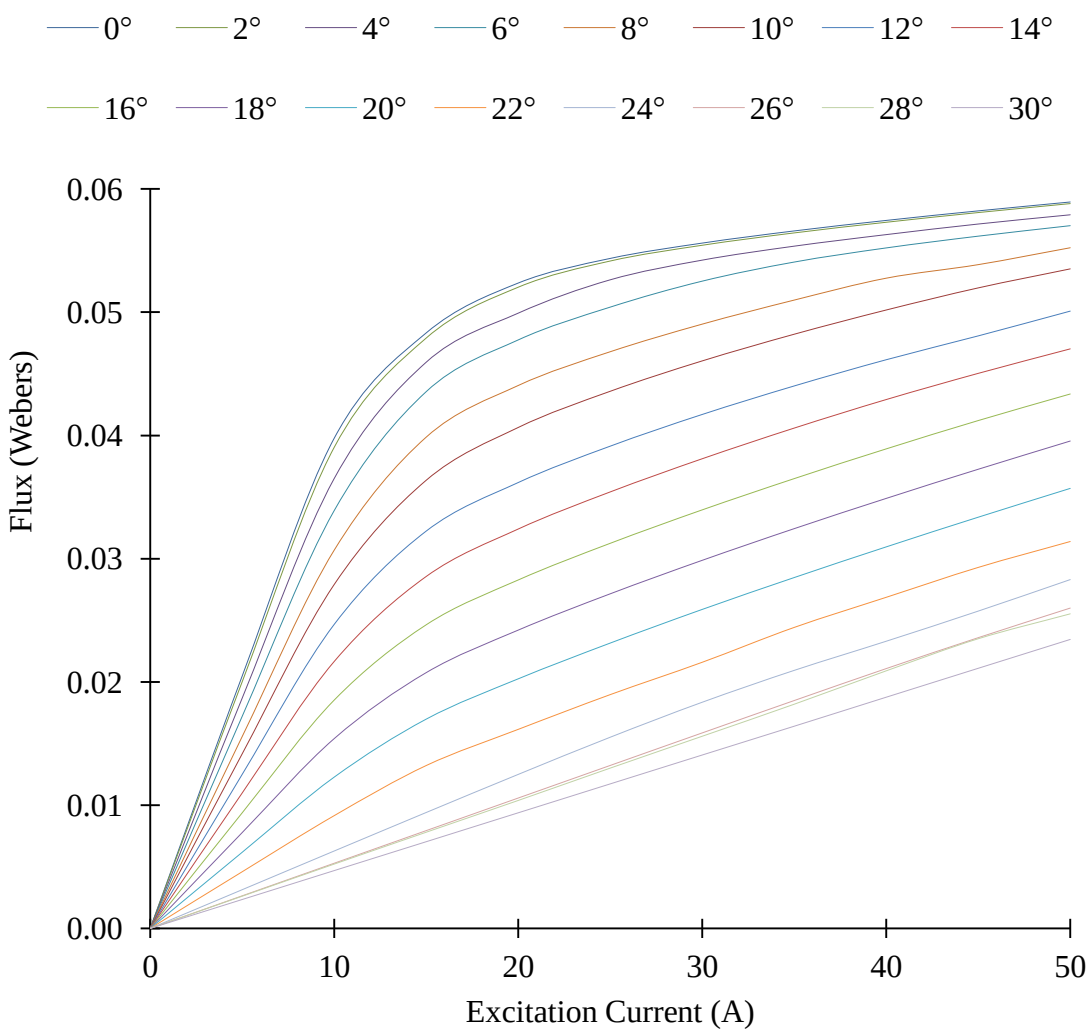

Figure 6.3 Electromagnetic characteristics of the in-house SRM used.

phase and with adjacent phases are defined in (6.10).

$$T_j = k_{T,j}.i_j,\ k_0 = k_{T,j} / k_{T,j+1} \tag{6.10}$$

When the two phases produce equal torques at equal currents (k_0=1), then the torques can be shared equally. If the torque constant ratio between the two phases, $k_0 \geq 1$, then the smooth torque requirement is shown in (6.11) and (6.12),

$$i\left(T_D/2, \theta_c^{\Psi}\right) > i\left(T_D/2, \theta_c^{\Psi} + \theta_{pitch}\right) \tag{6.11}$$

$$T_D = T_j(\theta) + T_{j+1}(\theta) \tag{6.12}$$

Therefore the boundaries for the operation with maximum torque per ampere and reduced torque ripple with minimum additional boosts from neighboring phase are detected. The torque sharing waveform can be divided into 3 regions. In the magnetization region the on-coming phase is turned on at θ_{on} as in (6.13) before θ_c where phase (j-1) is the major contributor.

$$\theta_{on} = \theta_c - \frac{\omega\Psi\left(T_D/2, \theta_c\right)}{V_{DC}} \tag{6.13}$$

A phase is a major contributor from θ_c to $\theta_c+\theta_{pitch}$. In this central region, the current level and angular width remains constant even if it is multiphase. The torque is shown in (6.14).

$$T_j(\theta) = T_D - T_{j-1}(\theta) - T_{j+1}(\theta) \tag{6.14}$$

In demagnetization region, after $\theta_c+\theta_{pitch}$, the phase current requires to decrease linearly. (6.15) determines the precise θ_{off} position. Equation (6.16) explains the conditions required for the angular width proportion of magnetization and demagnetization time period in case of either energy efficient or least input variation chosen as the second objective of optimization.

$$\theta_{off} = \theta_c + \frac{\omega\Psi\left(T_D/2, \theta_c\right)}{V_{DC}} + \theta_{pitch} \tag{6.15}$$

$$\left.\begin{array}{l}\left(\theta_c^i - \theta_{on}\right) < \left(\theta_{off} - \theta_c^i - \theta_{pitch}\right) \\ \left(\theta_c^{\Psi} - \theta_{on}\right) = \left(\theta_{off} - \theta_c^{\Psi} - \theta_{pitch}\right)\end{array}\right\} \tag{6.16}$$

For lower or medium speeds, two neighboring phases shares the torque for

desired level. However, when only two adjacent phases are conducting simultaneously, the reference current waveforms can only hold up to a certain speed as in (6.17) because at higher speeds, the current will not be able to reach the maximum value in the shorter period of time.

$$\left(\theta_c - \theta_{on}\right) \le \theta_{pitch},\ \left(\theta_{off} - \theta_c - \theta_{pitch}\right) \le \theta_{pitch} \tag{6.17}$$

At higher speed operations, more than two or all four phases are required to conduct simultaneously, the satisfactory conditions is presented in (6.18).

$$\left(\theta_c - \theta_{on}\right) + \left(\theta_{off} - \theta_c - \theta_{pitch}\right) \ge \theta_{pitch} \tag{6.18}$$

6.4 Quantitative Analysis of Torque and Current Profiles

The torque profile optimization procedure is performed in all regions of the electromagnetic characteristics. The torque profiles for the proposed method, traditional method, the advanced turn-on angle method and the additional boost method are quantitatively compared and are presented in Figures 6.4, 6.5 and 6.6 for phase currents of all regions.

The dwell angle parameter control using advanced critical angle and longer tail angle method are the most accurate ones for avoiding the discontinuity at the fully aligned position and other rotor positions near it. Due to the advanced critical angle, the commutation between the adjacent phases can occur long before the radial force becomes significant. Even though the equal torque share is not required and the position is not necessarily the equal torque producing, the excitation current levels in both phases are same and constant. Therefore, the torque values in both phases add up and increase the torque level at certain rotor positions. Although, this increase in the torque is very good and it improves the average torque. This improvement however, brings a new reason for

ripple generation. Figures 6.7, 6.8, 6.9 and 6.10 are the phase current profiles of all three methods employed.

Additional boost method is very accurate in removing the ripples in the saturated region. However, the discontinuity or bigger ripples cannot be avoided with the increase in current at the fully aligned position or the positions near it. Therefore the usability of this method is limited to a particular region. If the performance is measured in the saturated region only, it makes the torque level constant and slightly extends the width of that region. When integrated with the advanced angle method in the proposed method, the requirement of keeping the torque generation continuous is provided by advanced angle. Therefore, the small ripples and the ripple due to advanced angle method are both compensated to have the desired torque level. The proposed method determines the need and location of the additional boost method at some specific rotor positions. It is more successful because it combines the benefit of both methods and thus eliminates the ripple with the accuracy of the additional boost approach in the saturation region only. The results become better than the additional boost method because the discontinuity is removed from the torque profile at the fully aligned position by using advanced angle approach. The proposed method is proved to be better than the advanced angle method by removing the limitation of constant phase current values [77]. The advanced turn-on and delayed turn-off angles with gradual rise and fall significantly eliminate the torque ripple. Table 6.1 presents the period-wise quantitative torque ripple analysis of the three methods in comparison with traditional operation of SRM for 15 A, 30 A and 45 A in primary phase currents. It is obvious that the proposed method produces ripple in all regions less than 1%.

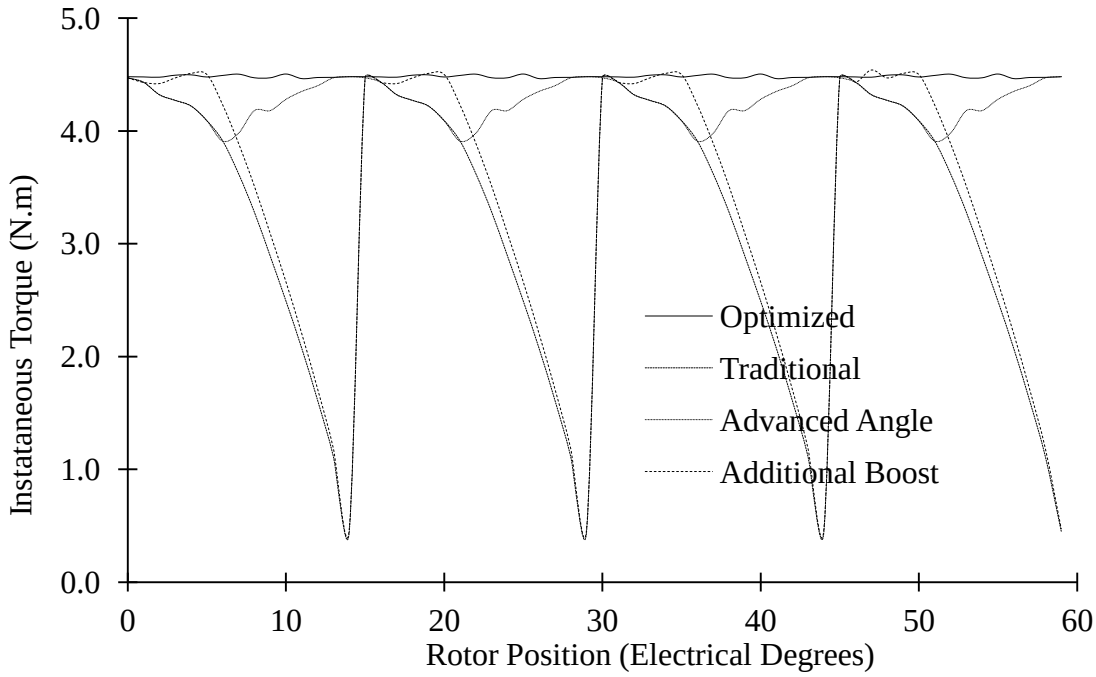

Figure 6.4 Instantaneous torque profile by the proposed method, traditional, advanced angle and additional boost method with primary phase current at 45 A.

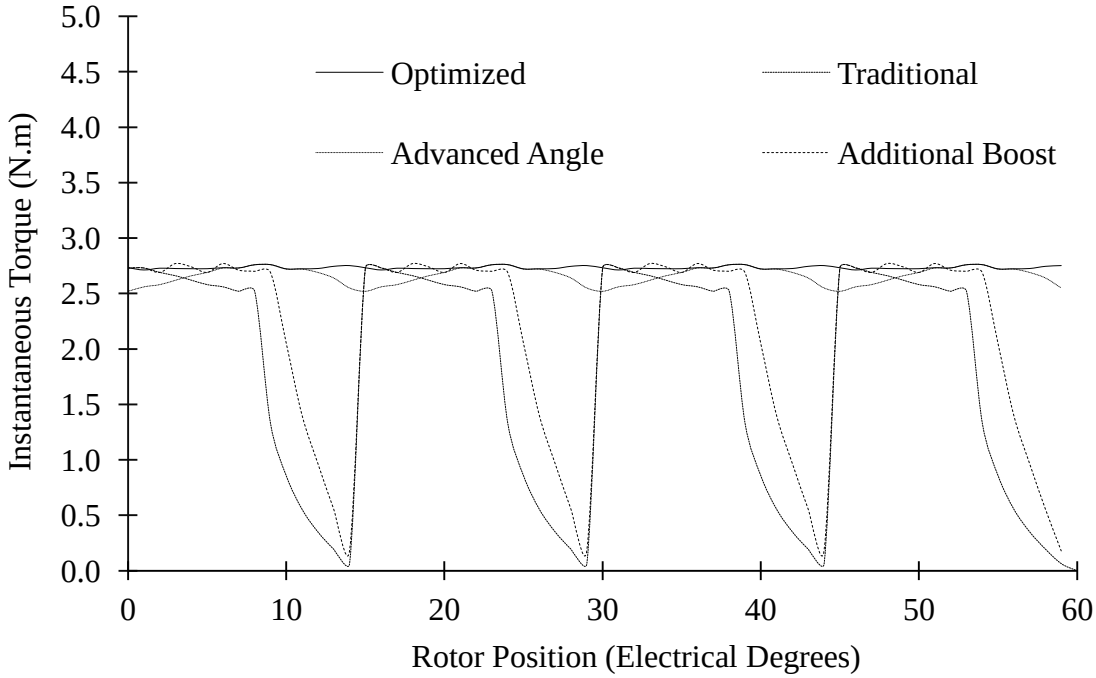

Figure 6.5 Instantaneous torque profile by the proposed method, traditional, advanced angle and additional boost method with primary phase current at 30 A.

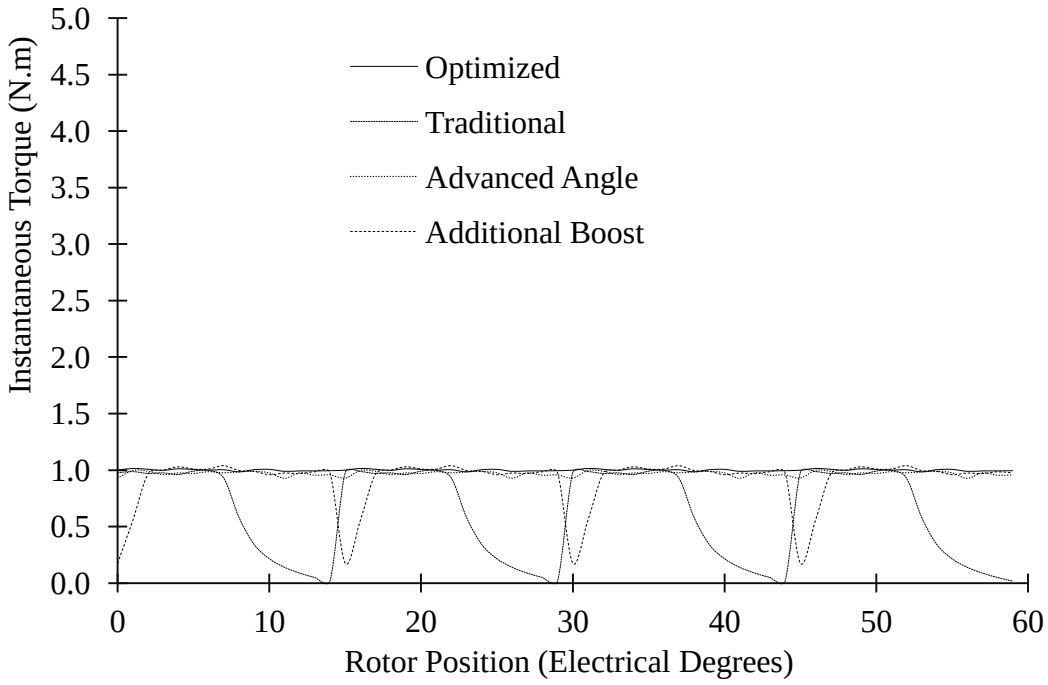

Figure 6.6 Instantaneous torque profile by the proposed method, traditional, advanced angle and additional boost method with primary phase current at 15 A.

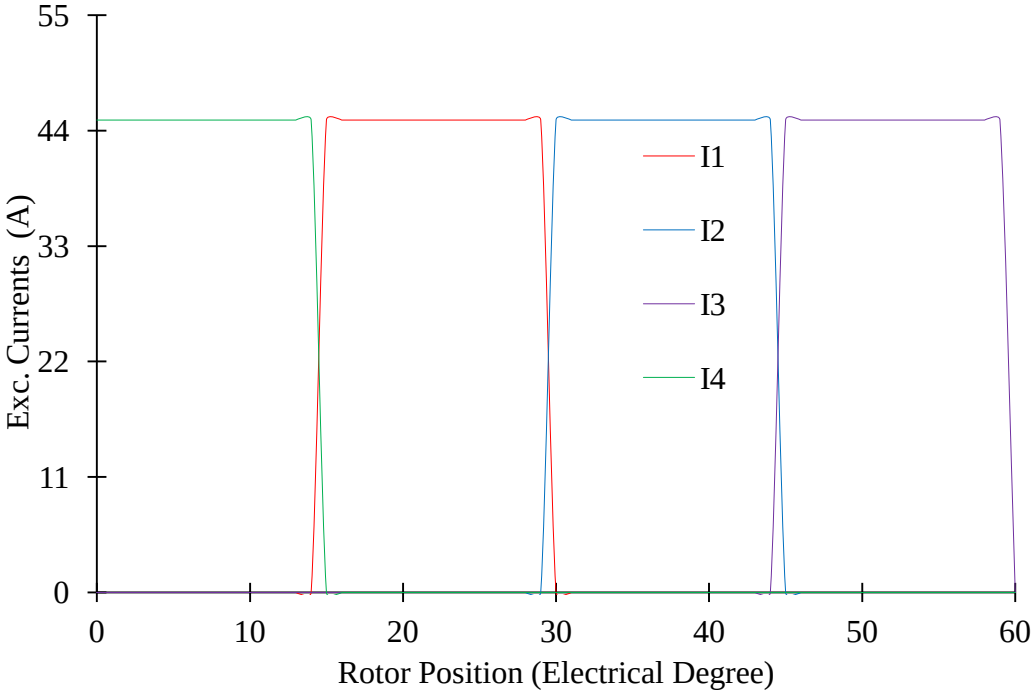

Figure 6.7. Traditional single-phase excitation current profiles at 45 A (I1: phase 1, I2: phase 2, I3: phase 3, and I4: phase 4).

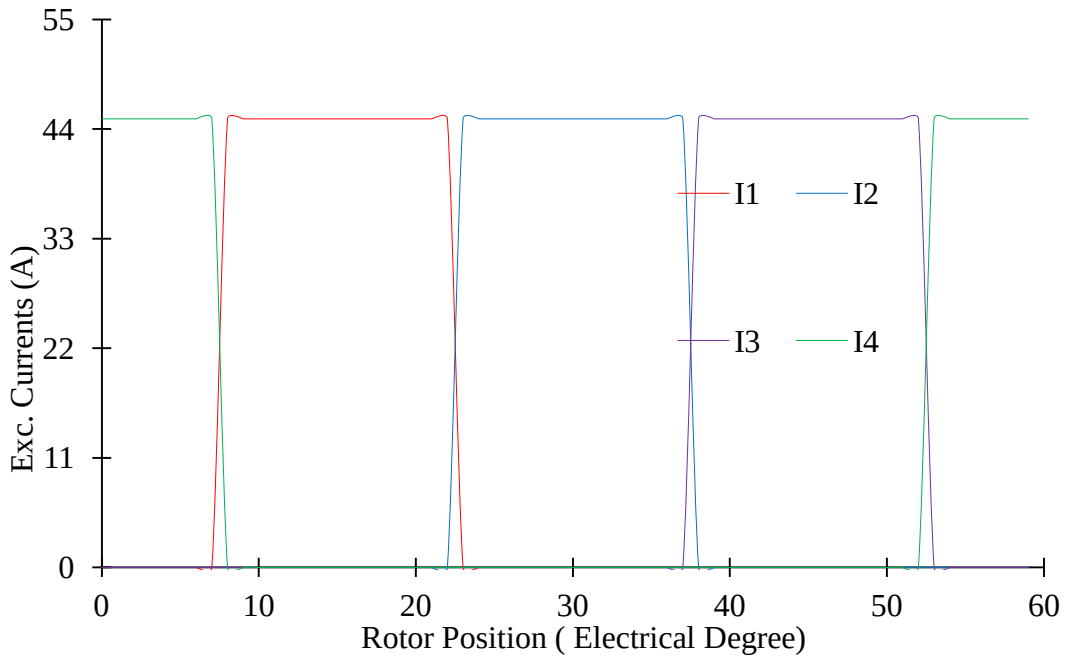

Figure 6.8 Advanced critical angle excitation current profiles at 45 A

(I1: phase 1, I2: phase 2, I3: phase 3, and I4: phase 4).

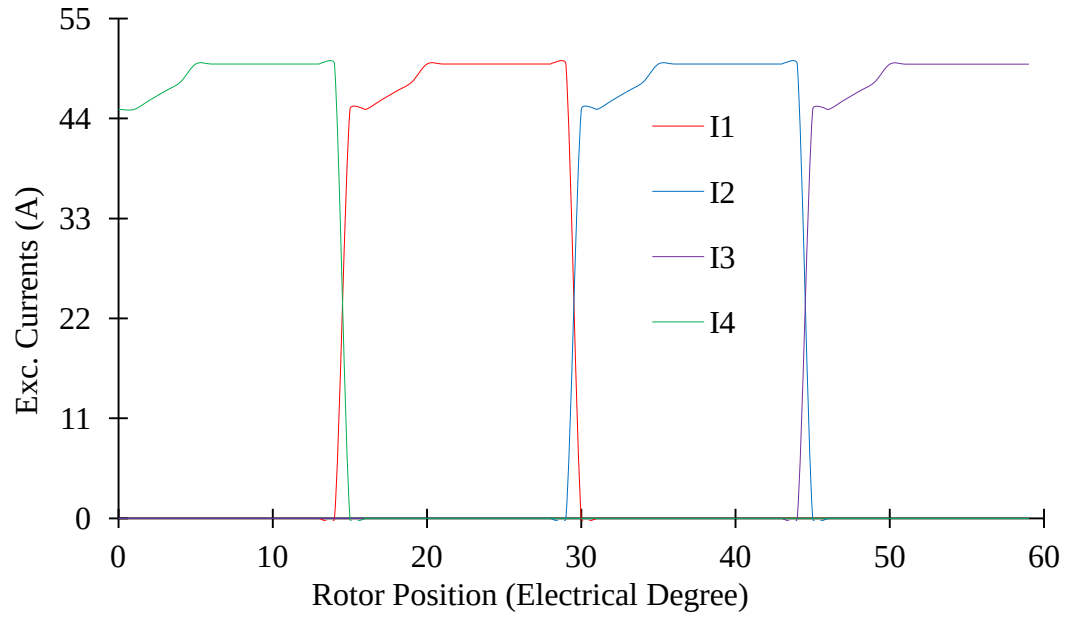

Figure 6.9 Additional boost multi-level excitation current profiles at 45 A

(I1: phase 1, I2: phase 2, I3: phase 3, and I4: phase 4).

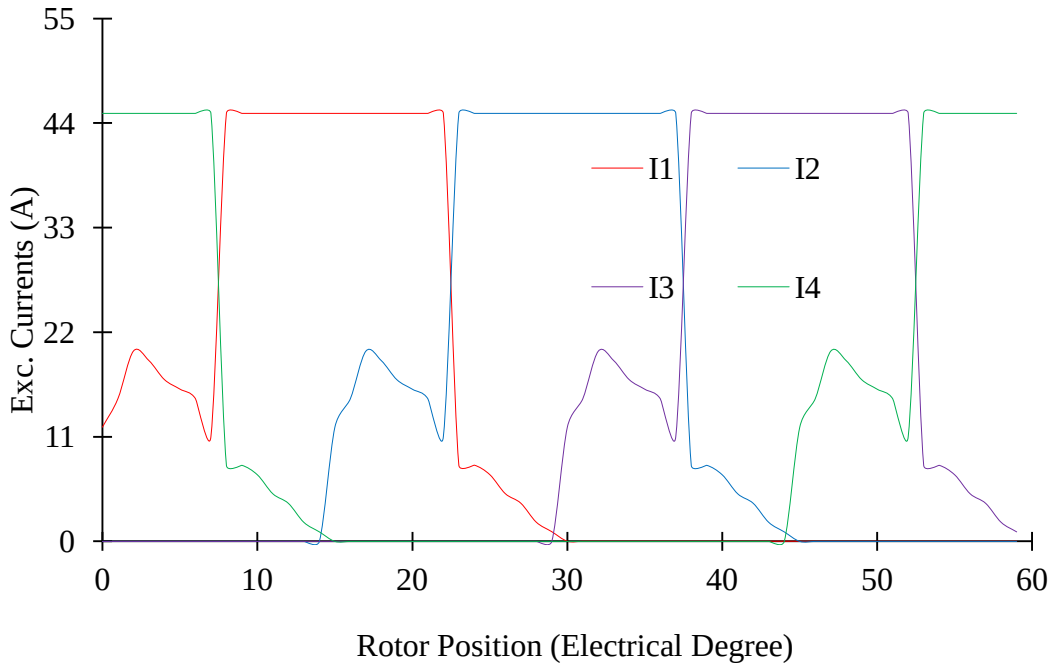

Figure 6.10 Proposed optimized excitation current profiles at 45 A (I1: phase 1, I2: phase 2, I3: phase 3, and I4: phase 4).

Table 6.1 Comparative Torque Analysis of the Proposed Optimization Method.

Torque (N.m)	I_{ph} **(A)**	**Traditional**	**Advanced Angle, θ**	**Additional Boost**	**Proposed Method**
Maximum torque	15	1.00	1.04	1.00	1.0
	30	2.73	2.77	2.76	2.80
	45	4.4	4.51	4.48	4.50
Minimum torque	15	0.02	0.91	0.18	0.99
	30	0.06	2.52	0.18	2.76
	45	0.14	3.91	0.18	4.46
Average torque	15	0.61	0.97	0.59	1.00
	30	1.76	2.65	1.47	2.77
	45	2.88	4.21	2.33	4.48
Torque ripple	15	0.39	0.065	0.41	0.005
	30	1.34	0.125	1.29	0.02
	45	2.13	0.3	2.15	0.02
Torque ripple (%)	15	49	6.0	41	0.50
	30	49	4.5	46.7	0.71
	45	65.5	6.0	52	0.44

Chapter 7

IMPLEMENTATION THROUGH A NON-SINUSOIDAL MATRIX CONVERTER

7.1 Introduction

However, SRM drives have still not yet found broad industry acceptance, they continue to attract research interest, stimulated mainly by the promise of simple and rugged motor construction, the possibility of high motor speeds, high torque-to-inertia ratio, an inverter with a reduced number of power switches, and an overall robust drive. This research activity has resulted in a number of inverter topologies, some of which have been described in the literature [78]-[80].

For SRM drives, the suitability of a particular inverter circuit changes with the motor geometry. It is in contrast to the drives operating with sinusoidal voltages and currents. where the inverter topology is independent of the motor design. Specifically, in the case of SRM, the number of the stator/rotor poles and the related issues of the dwell angle and current overlap parameters affect the inverter choice. The multilevel power converters open up a great deal of possibilities in control and can be used to achieve flexible current profiling but with the added benefit of lower switching frequencies and hence less converter losses.

Among the popular SRM drive converter choices, if the current overlap can be restricted to speeds where the motor-magnetizing voltage is below approximately one half the dc-link voltages, the most advantageous circuit is Miller Circuit. However, since the majority of SRMs operate with a current overlap over most of their speed range, the

classic inverter becomes most attractive topology in that case. Also the SRM starting torque very much influences the inverter rating. In order to provide a rated torque starting for any rotor position, the inverter rating may have to be increased several times over the value required by the motor-rated power. Conversely, if the starting currents are limited to their rated value, the starting torque is severely reduced for worst-case rotor initial position. To achieve operation at higher dc-linkvoltages, a multiple voltage level approach needs to be adopted where a power converter can be realised using lower voltage rated power switches. This approach also allows operation at higher switching frequencies than would otherwise be possible with much high voltage power switches.

The need for a high PWM frequency is not as strong in SRM drives as in IM drives because the total phase inductance is important than just the leak inductance like in IM. Freewheeling inverter states also permit reduced PWM frequency for the same current ripple. Therefore, in order to make SRM popular on industrial and manufacturing level, the need for improvement in SRM converter drives is direly needed where extremely close design coordination between the motor, the control and the inverter is possible. That coordination has to be much closer than in the case of brushless drives

Therefore, a novel idea of non-sinusoidal multilevel matrix converter (MC) is presented in this chapter. In order to prove the validity of the proposed topology, a simple output voltage control strategy is described and utilized in the next section of a classical ac-ac sparse matrix converter.. Operation principles and current commutation strategies are analyzed in detail. The non-sinusoidal simulation model is developed in Matlab/ Simulink and interfaced with FEA model of the 1*hp* in-house switched reluctance motor for validation. The DC current levels varying at each step size in switching sequence are

generated through the proposed non-sinusoidal MC which are quiet close to the DC levels required by the proposed method of global optimization for ripple free instantaneous torque profile.

7.2 Classical SRM Multilevel Converter Topologies

Multilevel converters as shown in Fig. 7.1 are finding increased attention in industry and academia as one of the preferred choices of electronic power conversion for high-power applications. Although it is an enabling and already proven technology, multilevel converters present a great deal of challenges, and even more importantly, they offer such a wide range of possibilities that their research and development is still growing in depth and width. Researchers all over the world are not only contributing to further improve energy efficiency, reliability, power density, simplicity, and cost of multilevel converters, but also broaden their application field as they become more attractive and competitive than classic topologies.

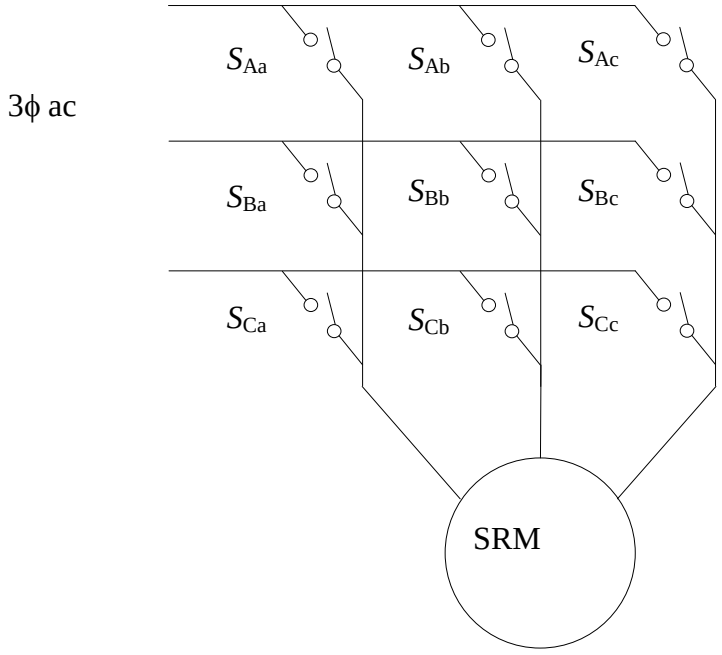

Figure 7.1 A classical ac-ac matrix converter circuit.

The matrix converter belongs to the direct conversion family since it directly connects the input ac lines to the output ac lines through bidirectional switches and without need of energy storage devices, such as capacitors or inductors. As a consequence, their strengths are important weight/volume reduction and inherent four-quadrant operation, which are desirable features for transportation systems (electric vehicles, more electric aircraft, military vehicles, etc.). The lack of energy storage devices does not favor the possibility to arrange semiconductors in such a way that higher voltages and more voltage levels can be reached. This is why this topology was limited to low power and a small application scope. However, recently several multilevel matrix converter topologies have been reported. Most of them are actually based on the three classic multilevel topologies: the classical Matrix Converter, the Indirect Matrix and the Frequency converter matrix converter.

The inherently bi-directional matrix converter regenerates energy, which is very desirable in EV applications. It draws sinusoidal input current and depending on the modulation technique, it can be arranged that unity displacement factor is seen at the supply side irrespective of the type of load. The size can be greatly reduced compared to conventional technologies since there are no large capacitors or inductors to store energy. Recently there has been considerable interest in the potential benefits of matrix converter technology, especially for applications where size, weight and long term reliability are important factors such as electric power trains [84].

Number of phases is not limited. By using nine bidirectional switches, the matrix converter is able to create a variable output voltage system of a desired frequency and magnitude. Normally, a BDS is built by two collector– or emitter-connected insulated

gate bipolar transistors (IGBTs). This enables a high switching frequency which is necessary to decouple input and output systems of the matrix converter. Altogether, 18 IGBTs for the BDS are more than 12 IGBTs needed for a dc-voltage link converter with power regeneration. However, it is a fact that the size of IGBT chips needed to build up a comparable matrix converter in power, is reduced [82]. A further aspect is the reduction of unit volume by renunciation of a chopper resistor and a live time limiting dc-link reactance. The input power factor can be adjusted with little reduction to the active power transfer ratio. The sinusoidal voltage transfer ratio is limited to 0.86 on principle. To handle concerning the commutation behaviour and at pulse-off, a reliable protection at pulse-off is required. Multilevel technology is a good solution in medium or high voltage power conversion. However, the existing multilevel converters have their limitations such as cascaded cell multilevel converter requires two split DC supplies while the capacitor clamping converter has to balance the capacitors while diode clamping uses half the DC-link voltage and many of the switching states cannot be used

7.3 Proposed Non-sinusoidal Matrix Converter

For more than 20 years, the matrix converter has been discussed academically. The traditional matrix converter offers an all silicon solution for ac-ac power conversion. The Sparse Matrix Converter is used to simplify when all of the switching states are not required for supplying loads in which only one current direction is required. The focus of matrix converter drives research has largely been on sinusoidal motors (induction, permanent magnet synchronous and the like) [81]. However, it is also possible to use the matrix converter to drive non-sinusoidal output currents, typically with nearly rectangular output current waveforms [82]. Such non-sinusoidal excitation waveforms can also lead

to increased torque per ampere realizations with particular motor designs. For EV applications, the converter can be designed to be operated with n- level DC V [83]. Such a design is proposed and implemented as in Figure 7.2 in this chapter.

7.4 Mathematical Model and Design of MC

This chapter demonstrates a technique to drive an open loop 8/6 four-phase finite element model of the SRM using a quasi multi-level sparse matrix converter using RB-IGBTs. A simple modulation strategy has been developed to produce the step multi-level output currents for each phase independent of each other keeping the fault-tolerant characteristics of SRM [85]-[87]. The configuration of the proposed multilevel matrix converter is shown in Figure 7.3. Since the inputs of multilevel converter is connected to voltage sources, the input lines must not be short circuit, and due to the inductive nature of the load, the output loops must not left opened. The switching functions of switches are defined as equation (7.1). The general direct forms of voltage and current equations of matrix converters are given by equations (7.1)-(7.3). With these constraints, the proposed multilevel matrix converter finds 729 available switching modes. The switching schemes can generate the state tables which depicts the options for each phase.

$$\underbrace{\begin{bmatrix} u \\ v \\ w \end{bmatrix}}_{v_o} = \begin{bmatrix} u^* + v_z \\ v^* + v_z \\ w^* + v_z \end{bmatrix} = \underbrace{\begin{bmatrix} m_{11} & m_{12} & m_{13} \\ m_{21} & m_{22} & m_{23} \\ m_{31} & m_{23} & m_{33} \end{bmatrix}}_{M} \underbrace{\begin{bmatrix} R \\ S \\ T \end{bmatrix}}_{v_i} \equiv v_o = M v_i \tag{7.1}$$

$$\underbrace{\begin{bmatrix} i_R \\ i_S \\ i_T \end{bmatrix}}_{i_i} = \underbrace{\begin{bmatrix} m_{11} & m_{12} & m_{13} \\ m_{21} & m_{22} & m_{23} \\ m_{31} & m_{32} & m_{33} \end{bmatrix}^T}_{M^T} \underbrace{\begin{bmatrix} i_u \\ i_v \\ i_w \end{bmatrix}}_{v_i} \equiv i_i = M^T i_o \tag{7.2}$$

$$where \quad 0 \le m_j \le 1, \quad \sum_{j=i}^{3} m_j \quad i = \{1 \quad 2 \quad 3\} \; j = \{1 \quad 2 \quad 3\} \tag{7.3}$$

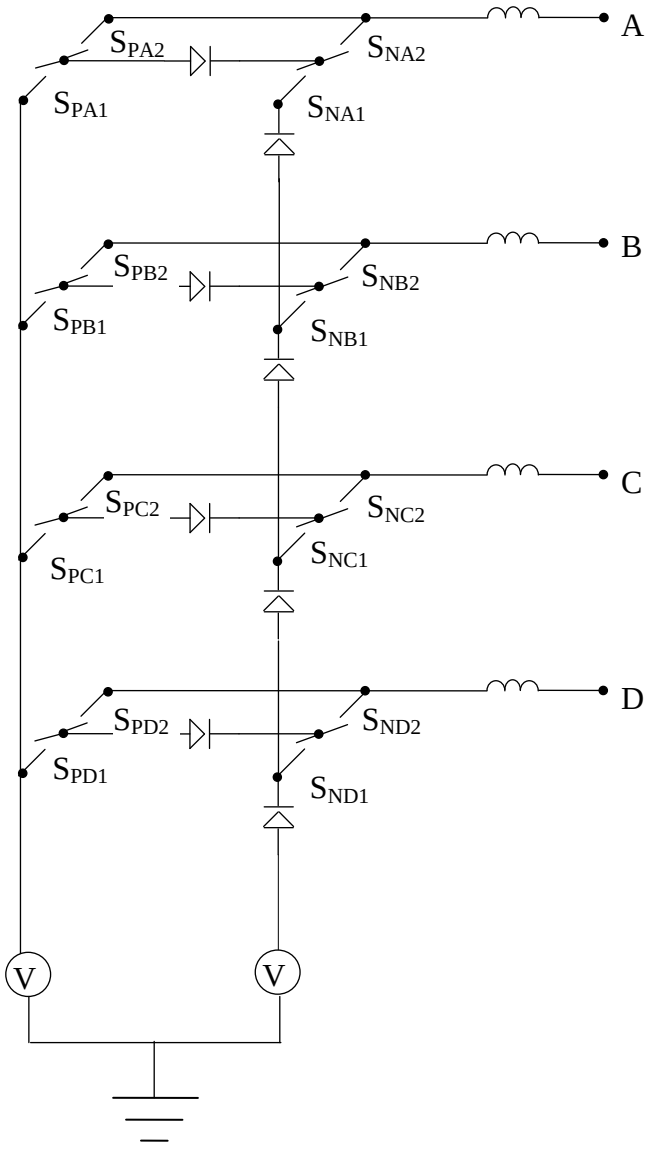

Figure 7.2 Possible configuration of a sparse matrix converter for SRM with dc voltage.

At any instant, the input voltages can be sorted into at least the maximum, median and minimum voltage levels if three voltage levels are required. There could be configurations for 2 or more middle voltage levels if required. In the discussion below, a particular combination of enabled switch connections between input lines and the output legs is called a switch state. During a given switching period, all the voltage levels may be assumed to be invariant. Clearly, at any instant, each of the two legs must be connected to any one of the input lines because they are inductive in nature. There can be

many allowed switch states determined by the Boolean table i.e. (x, y) = (0, 0), (0, 1), (1, 1) and (1, 0). In case of more legs and switching combinations, the possible switching states can be increased for each phase. During a switching cycle, the converter can go through all required states.

7.5 Analysis of Commutation Strategies for Allowed Switching States

The knowledge of matrix converter commutation is fundamental in understanding the difficulties of the converter. In contrast to the well-known dc-voltage link converter, a commutation cannot be initiated without any knowledge of the commutation conditions. To perform a commutation, the voltage between the involved BDS or the load current must be measured. For a commutation, only the sign of one of the two quantities is important, as the sign determines the commutation sequence. A well-selected sequence enables a commutation without short circuiting the input voltages or breaking the load current. Before a commutation, a whole Bidirectional switch in an output phase is switched on. After a commutation has passed, this BDS is off and a BDS connected to a different input phase is switched on. There are 12 ways to perform a commutation. The paths from a starting situation can be decided according to the requirement of the output waveform. In order to deal with the delay times of the IGBTs, a little dead time is kept between each commutation step. The two sequences on the axis only need the evaluation of the sign of the load current and are named “current commutation”.

The remaining sequences need the evaluation of both signs. This fact makes them harder to handle. As a result, voltage or current commutation should be used. Another idea to achieve a commutation is the “two-step commutation”. The basic idea is

to switch only the IGBT in a BDS which will lead the load current. In addition, all IGBTs in the matrix which will not conduct are switched on. This will reduce the total time of the commutation and opens additional free-wheeling paths for the load current in case of error. The two-step commutation can be voltage controlled or current controlled. The commutation logic deals only with the switching commands of the PWM generator and the utilized sign of commutation.

The matrix converter should mimic a classical four phase inverter while driving an SRM motor. In a rotation through 360 electrical degrees, each phase of the motor goes through four distinct back-emf regions. These regions determine the conduction mode of the phase leg X (= *u*, *v* or *w*). Let the variable *x* denote the switch position of the positive leg; $x = 0$ denotes a connection to the median voltage and $x = 1$ denotes a connection to the maximum voltage as per the switching rule above. Similarly, let *y* denote the switch position of the negative leg; $y = 0$ denotes a connection to the median voltage and $y = 1$ denotes a connection to the minimum voltage as per the switching rule above. For example, there are four allowed switch states denoted by $(x, y) = (0, 0), (0, 1), (1, 1)$ and $(1, 0)$. If *xy* be the duty cycle of the state with the positive leg at x and the negative leg at *y*. During a switching cycle, the converter goes through all allowed states.

In order to get a leg-leg output of twice to thrice of the base value of increment in input, or, the duty ratios have to be suitably chosen. Kirchhoff's law is averaged over one switching cycle. These duty ratios ensure that the average of the output is a fixed DC value. This is actually a carrier-based scheme similar to elementary PWM schemes for inverters.

7.6 Sample Configuration for Testing

The desired excitation phase current waveforms generated by the global optimization of the instantaneous electromagnetic torque are not very simple. It is neither sinusoidal nor a constant current source. It has many DC- current levels depending on the rotor position. One of the reasons for not using multi-level current source for improving the instantaneous torque profile is to avoid multiple input sources. Therefore, a non-sinusoidal with DC voltage source sparse matrix converter is simulated in Simulink to obtain these waveforms. Figure 7.3 presents the comparison of instantaneous torque profiles generated by selecting 3 different switching sequence with the ripple free instantaneous torque profile generated by the implementation of the global optimization method for torque ripple elimination. Figure 7.4 presents the comparison of instantaneous torque profiles generated by selecting 3 different switching sequence with the ripple free instantaneous torque profile generated by the conventional methods for torque ripple elimination.Deciding the switching sequence and the number of switches is the key factor in selecting a matrix converter. (The fractions 1/3, ½ and ¼ shows the chopping technique of possible DC-current levels to decrease the number of DC levels. Therefore 1/3 represents the 9 DC-Levels, ½ shows the 11 DC levels while the ¼ shows the 7DC level output cases). There are 22 DC levels required for 45A reference current waveform generation i.e. from 0 A to 21 A with an increment of 1A as the secondary phase currents and 45A when excited as the primary phase current. Three case studies are performed with higher increment levels to minimize the DC levels and number of active switches. Figure 7.5, Figure 7.6 and Figure 7.7 shows the generated excitation phase current

waveforms. Table 7.1 compares the results of the three cases with the optimized current waveform results. Therefore, the three case studies selected are as follows.

1. An increment level of 4 A i.e. in between 0 to 20 A in addition to the primary phase current i.e. 45 A. A total of 7 DC-Levels (1/4 chopping).
2. An increment level of 3 A i.e. from 0 to 21 A in addition to the primary phase current level i.e. 45 A. A total of 9 DC-Levels (1/3 chopping).
3. An increment level of 2 A i.e. from 0 to 20 A in addition to the primary phase current i.e. 45 A. A total of 12 DC-Levels (1/2 chopping)

All of them have the torque ripple only up to the 2%. However, the torque ripple with 12-DC levels is less than 1% which is the target level for global optimization method. Therefore, the non-sinusoidal matrix converter provides the means to implement the proposed method.

Table 7.1 Comparative Torque Analyses of the Matrix Converter Configurations. (at 45 A)

Torque (N.m)	Optimized (22-DC Levels)	7-DC Levels	9-DC Levels	12-DC-Level
Maximum torque	4.50	4.60	4.60	4.49
Minimum torque	4.46	4.42	4.45	4.41
Average Torque	4.48	4.50	4.52	4.46
Crest	0.02	0.10	0.09	0.03
Trough	0.02	0.08	0.06	0.05
Ripple	0.02	0.09	0.075	0.04
Ripple (%)	0.45%	2.00%	1.66%	0.90%

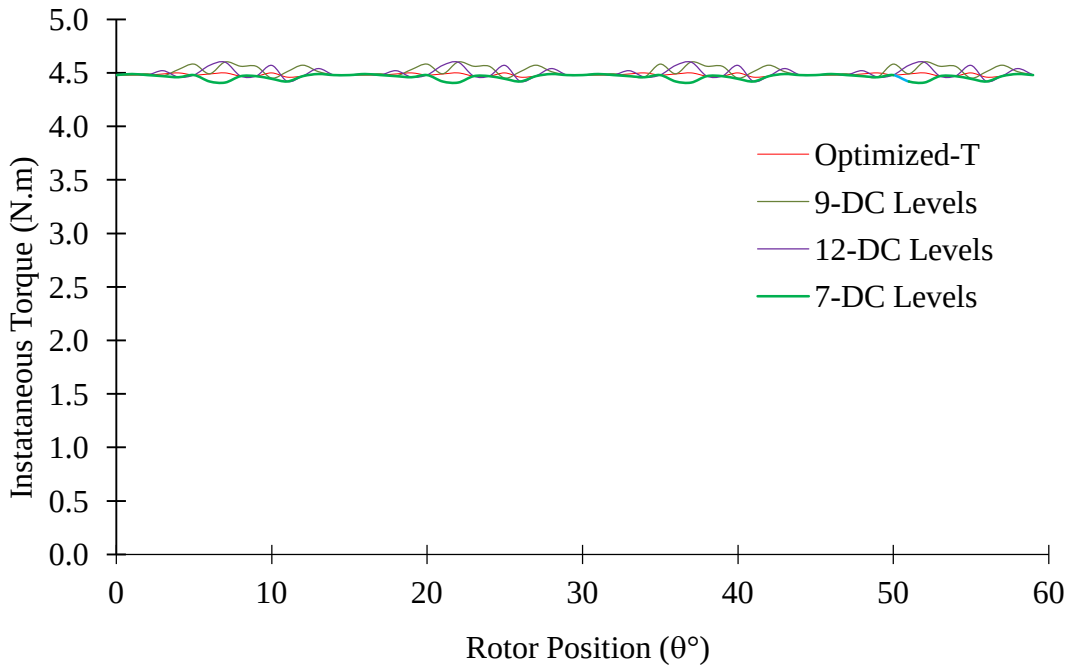

(a)

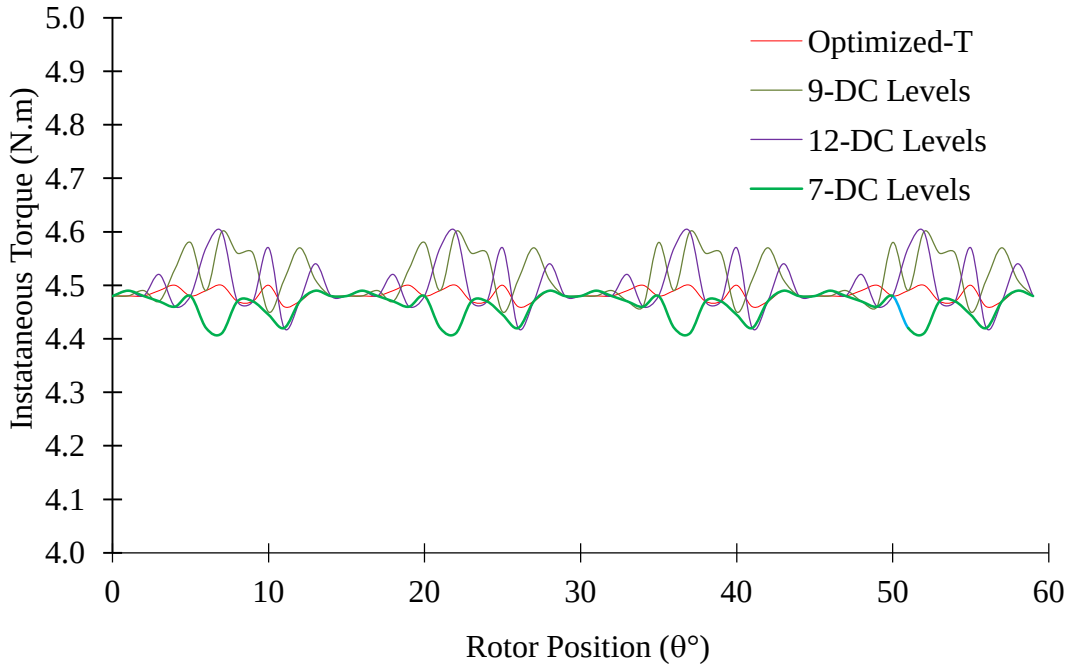

(b)

Figure 7.3 Comparisons of instantaneous torque profiles by the implementation of proposed method using Matrix Converter at 45 A with the proposed method.

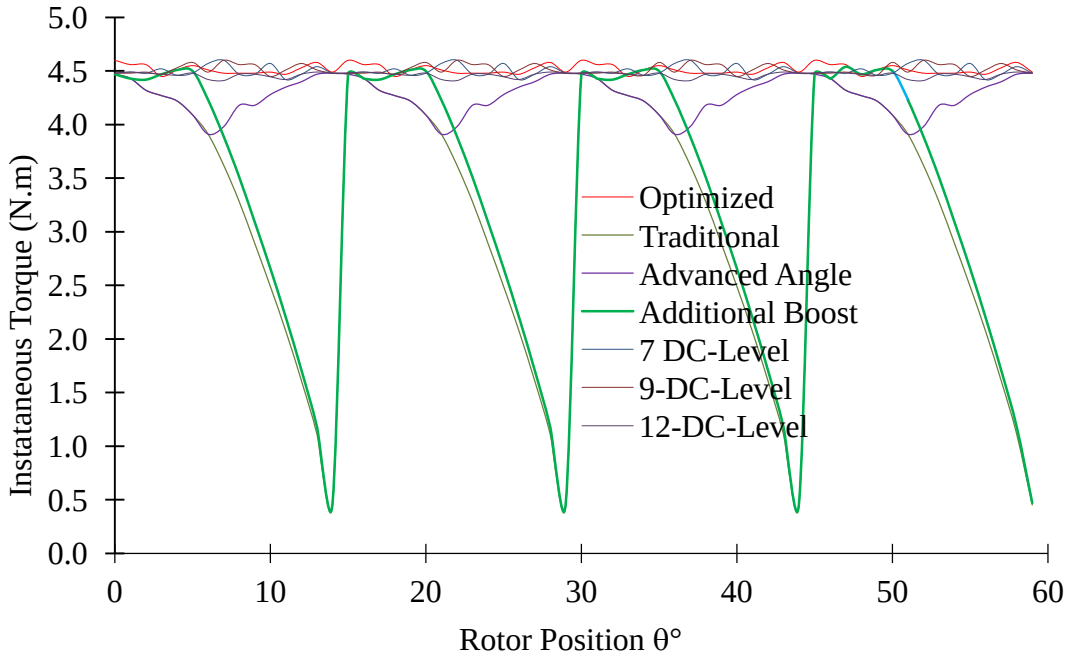

Figure 7.4 Comparison of torque profiles by the implementation through matrix converter at 45 A with the proposed method and conventional methods.

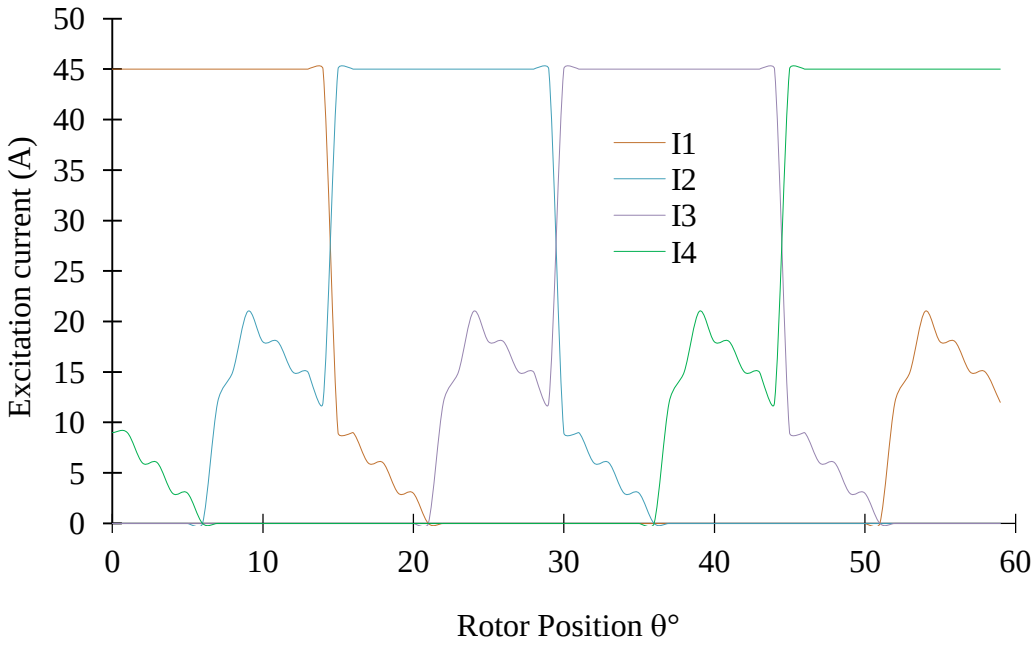

Figure 7.5 Excitation current profiles at 45 A using matrix converter with 9 DC levels. (I1: phase 1, I2: phase 2, I3: phase 3, and I4: phase 4).

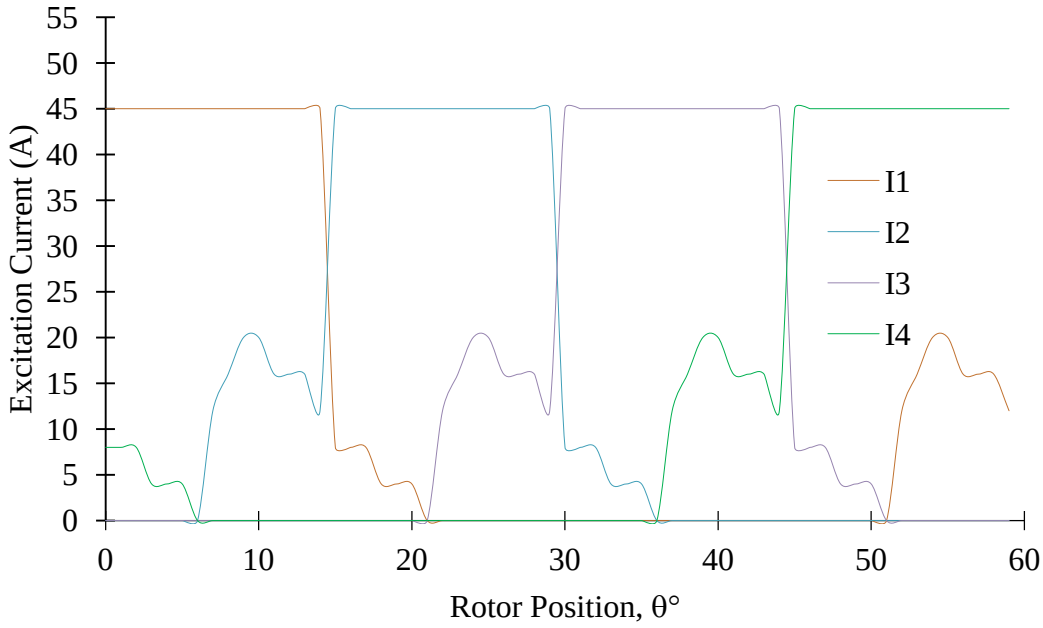

Figure 7.6 Excitation current profiles at 45 A using matrix converter with 7 dc levels. (I1: phase 1, I2: phase 2, I3: phase 3, and I4: phase 4).

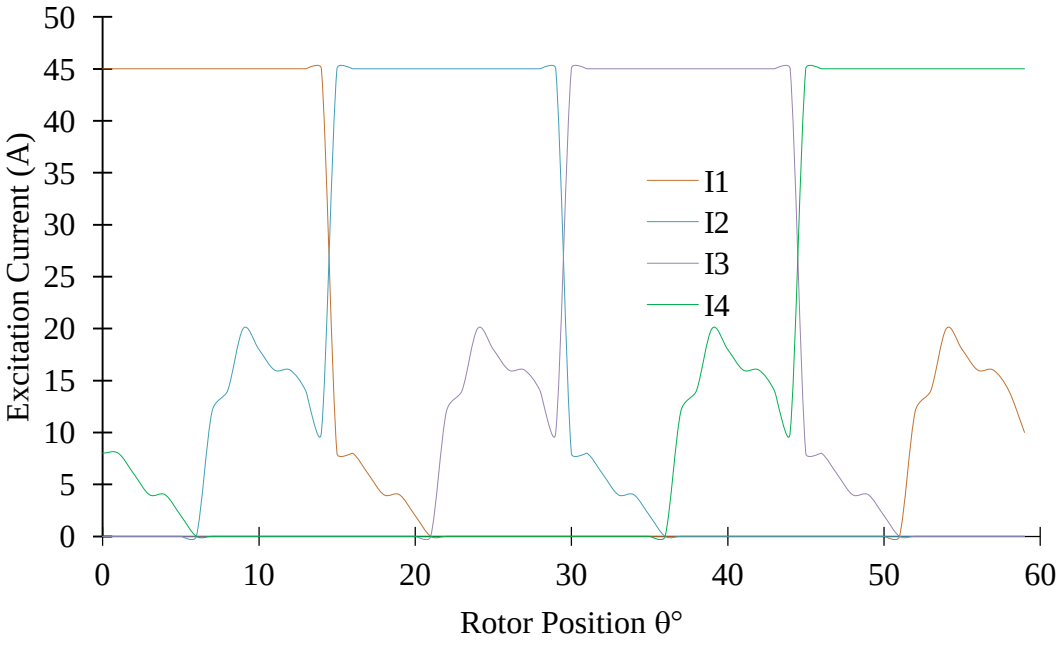

Figure 7.7 Excitation current profiles at 45 A using matrix converter with 12 dc levels. (I1: phase 1, I2: phase 2, I3: phase 3, and I4: phase 4).

Chapter 8

CONCLUSIONS

This dissertation proposes a novel method of eliminating the torque ripple in the instantaneous torque profile of SRM and a method to generate the precise reference phase current waveforms for even open loop operational design. For the purpose for implementation of global optimization technique, a non-sinusoidal DC matrix converter is also proposed to be able to generate such waveforms without using multiple source voltages and to be able to use the drive in electric vehicle applications where a battery system is available for DC voltage sources.

The first stage was to determine the static performance of an 8/6 switched reluctance machine through experiments on a in-house SRM as unique and exact machine characteristics to be used instead of a mathematical or analytical model which is never precise enough. Finite Element Analysis is used to implement and verify the results. Therefore, an FEA model is developed and compared with experimental characteristics. The flux and air-gap torque as determined by the FEA are found to be in a good agreement with the experimental ones in the case of single-phase excitation.

In the second stage, a series of static force investigations are performed to characterize the electromagnetic force distribution as a function of instantaneous rotor positions and excitation current using FEA. These results are obtained by integrating the radial and tangential components of the flux densities using tunable volume integration method. The results are validated with finite element results for flux path for single phase

excitation. The results are then extended to quantify the radial and tangential force components for multiphase excitation.

Hence, it is concluded that a precise solution for this non-linear problem can only be attained with a global optimization method. Therefore a modified fast-filled method is proposed to balance out the crests and troughs of the torque ripples throughout the operation of SRMs. A set of novel reference current waveforms are generated for feed-forward torque control. For comparison, torque and current profiles of other control schemes are also obtained. The torque characteristics calculated by the proposed method is quantitatively compared with other existing methods. It is observed that the proposed method produces torque with less than 1% ripple. Therefore, it is concluded that the advanced turn-on and delayed turn-off angles with gradual rise and fall significantly eliminate the ripple.

At the end, a non-conventional non-sinusoidal DC matrix converter is proposed to generate a multi-level excitation phase current from a single DC source which is very effectively designed for a hybrid machine i.e. SRM converter design because it is flexible to accommodate the variations in the requirement of SRM drives accurately. The use of SRM with matrix converter topology for EV applications suggests a motivation to investigate further to eliminate the DC-link energy storage elements from the battery bank and improves the power factor.

Therefore, it is concluded that using the global optimization scheme of torque ripple elimination implement through a matrix converter will eliminate a lot of limitations associated with accurate SRM control design and hence its industrial acceptance.

REFERENCES

[1] Y. Tang, "Characterization, numerical analysis, and design of switched reluctance motors," *IEEE Transactions on Industry Applications*, vol. 33, no. 6, pp. 1544-1552, 1997.

[2] X. Xue, K. W. E. Cheng, S. L. Ho and J. K. Lin, "A drive train scheme of electric vehicles using switched reluctance motors with torque ripple reduction," in *Proc. of the 8th International Conference on Advances in Power System Control, Operation and Management*, pp. 1-6, 1999.

[3] K. N. Srinivas and R. Arumugam, "Analysis and characterization of switched reluctance motors: Part I dynamic, static, and frequency spectrum analyses," *IEEE Transactions on Magnetics*, vol. 41, no. 4, pp. 1306-1320, 2005.

[4] K. N. Srinivas and R. Arumugam, "Analysis and characterization of switched reluctance motors: Part II. flow, thermal, and vibration analyses," *IEEE Transactions on Magnetics*, vol. 41, no. 4, pp. 1321-1332, 2005.

[5] T. J. E. Miller, "Optimal design of switched reluctance motors," *IEEE Transactions on Industrial Electronics*, vol. 49, no. 1, pp. 15-27, 2002.

[6] Z. Zhuo, C. Changqing and L. Wenzhou, "Study on reduction of running noise from a switched reluctance motor," in *Proc. of the 5th International Conference on Computer Science and Education*, pp. 1204-1027, 2010.

[7] S. M. Jang, D. You, Y. H. Han and J. P. Lee, "Analytical design and dynamic characteristics of switched reluctance motor with minimum torque ripple," in *Proc. of the International Conference on Electrical Machines and Systems*, pp. 1236-1239, 2007.

[8] B. Parreira, S. Rafael, A. J. Pires and P. J. C. Branco, "Obtaining the magnetic characteristics of an 8/6 switched reluctance machine: From FEM analysis to the experimental tests," *IEEE Transactions on Industrial Electronics*, vol. 52, no. 6, pp. 1635-1643, 2005.

[9] S. K. Sahoo, S. Dasgupta, S. K. Panda and J. X. Xu, "A lyapunov function-based robust direct torque controller for a switched reluctance motor drive system," *IEEE Transactions on Power Electronics*, vol. 27, no. 2, pp. 555-564, 2012.

[10] A. Khalil and I. Husain, "A fourier series generalized geometry-based analytical model of switched reluctance machines," *IEEE Transactions on Industry Applications*, vol. 43, no. 3, pp. 673-684, 2007.

[11] V. P. Vujičić, "Minimization of torque ripple and copper losses in switched reluctance drive," *IEEE Transactions on Power Electronics*, vol. 27, no. 1, pp. 388-399, 2012.

[12] K. H. Ha, J. P. Hong, G. T. Kim, K. C. Chang and J. Lee, "Orbital analysis of rotor due to electromagnetic force for switched reluctance motor," *IEEE Transactions on Magnetics*, vol. 36, no. 4, pp. 1407-1411, 2000.

[13] E. Bizkevelci, H. B. Ertan and K. Leblebicioglu, "A novel noise reduction technology for switched reluctance motors," in *Proc. of the IEEE 21st Century Power and Energy Society General Meeting - Conversion and Delivery of Electrical Energy*, pp. 1-4, 2008.

[14] J. Y. Chai, Y. W. Lin and C. M. Liaw, "Comparative study of switching controls in vibration and acoustic noise reductions for switched reluctance motor," *IEE Proceedings- Electric Power Applications*, vol. 153, no. 3, pp. 348-360, 2006.

[15] C. Lin and B. Fahimi, "Reduction of torque ripple in Switched Reluctance Motor drives using Field Reconstruction Method," in *Proc. of the IEEE Vehicle Power and Propulsion Conference*, pp. 1-5, 2011.

[16] X. D. Xue, K. W. E. Cheng, J. K. Lin, Z. Zhang, K. F. Luk, T. W. Ng and N. C. Cheung, "Optimal control method of motoring operation for SRM drives in electric vehicles," *IEEE Transactions on Vehicular Technology*, vol. 59, no. 3, pp. 1191-1204, 2010.

[17] H. Ishikawa, Y. Kobayashi and H. Naitoh, "A novel position control system with torque ripple reduction for SRMs," in *Proc. of the 37th IEEE Annual Conference on Industrial Electronics*, pp. 1716-1721, 2011.

[18] R. Zaimeddine and T. Undeland, "DTC control schemes for induction motor fed by three-level NPC-VSI using Space Vector Modulation," in *Proc. of the International Symposium on Power Electronics Electrical Drives Automation and Motion*, pp. 966-971, 2010.

[19] Y. B. Wang, Y. Z. Xu, R. Zhong and S. L. Lu, "Improved dual-SRM synchronization control based on fast torque computation," in *Proc. of the International Conference on Computer, Mechatronics, Control and Electronic Engineering*, pp. 308-311, 2010.

[20] Y. Saleem and T. Izhar, "Control of torque in switched reluctance motor," *in Proc. of the 2nd International Conference on Electrical Engineering*,. pp. 1-4, 2008.

[21] H. M. Amreiz, "A comparison between transverse flux and conventional switched reluctance machines," in *Proc. of the XIX International Conference on Electrical Machines*, pp. 1-8, 2010.

[22] T. Higuchi, K. Suenaga and T. Abe, "Torque ripple reduction of novel segment type Switched reluctance motor by increasing phase number," in *Proc. of the International Conf. on Electrical Machines and Systems*, pp. 1-4, 2009.

[23] A. Siadatan, M. Asgar, V. Najmi and E. Afjei, "A novel method for torque ripple reduction in 6/4 two rotor stack switched reluctance motor," in *Proceedings of the 14th European Conference on Power Electronics and Applications*, pp. 1-10, 2011.

[24] P. T. Hieu, D. H. Lee and J. W. Ahn, "Design of 2-phase 4/2 SRM for torque ripple reduction," in *Proc. of the 15th International Conference on Electrical Machines and Systems*, pp. 1-6, 2012.

[25] M. Jahanmahin, A. Hajihosseinlu, E. Afjei, A. Siadatan and A. Tavakoli, "A novel multilayer 8/4 switch reluctance machine with ripple reduction," in *Proc. of the International Symposium on Power Electronics, Electrical Drives, Automation and Motion*, pp. 536-540, 2012.

[26] A. Hajihosseinlu, M. Jahanmahin, E. Afjei and S. Tajik, "A novel four layer switch reluctance motor with high torque and ripple reduction," in *Proc. of the Power Electronics and Drive Systems Technology*, pp. 62-67, 2012.

[27] M. A. Tavakkoli and M. Moallem, "Torque ripple mitigation of double stator switched reluctance motor (DSSRM) using a novel rotor shape optimization," in *Proc. of the IEEE Energy Conversion Congress and Exposition*, pp. 848-852, 2012.

[28] S. Balathandayuthapani, F. Fleming, C. Edrington and E. El-Kharashi, "Impact of modifying the stator tooth tip on electromagnetic torque production for an 8/6 switched reluctance machine," in *Proc. of the IEEE Intl. Electric Machines & Drives Conference*, pp. 1386-1390, 2011.

[29] C. Sahin, A. E. Amac, M. Karacor and A. Emadi, "Reducing torque ripple of switched reluctance machines by relocation of rotor moulding clinches," *IET-Electric Power Applications*, vol. 6, no. 9, pp. 753-760, 2012.

[30] J. Li, B. Sun, S. Fan and L. He, "Harmony Optimization of Physical Design and Control Strategy of Switched Reluctance Motor," in *Proc. of the 2nd International Conference on Intelligent Networks and Intelligent Systems*, pp. 130-133, 2009.

[31] D. H. Lee, H. K. M. Khoi and J. W. Ahn, "The performance of 2-phase high speed SRM with variable air-gap rotor poles for blower system," in *Proc. of the International Conference on Electrical Machines and Systems*, pp. 1595-1598, 2010.

[32] Y. K. Choi, H. S. Yoon and C. S. Koh, "Pole-shape optimization of a switched-reluctance motor for torque ripple reduction," *IEEE Transactions on Magnetics*, vol. 43, no. 4, pp. 1797-1800, 2007.

[33] T. Higuchi, T. Ueda and T. Abe, "Torque ripple reduction control of a novel segment type SRM with 2-steps slide rotor," in *Proc. of the International Power Electronics Conference*, pp. 2175-2180, 2010.

[34] J. Sun, S. Wang, Z. Kuang and H. Wu, "Torque ripple comparison of short-pitched and fully-pitched winding switched reluctance machine," in *Proc. of the 15th International Conference on Electrical Machines and Systems*, pp. 1-6, 2012.

[35] J. D. Widmer, R. Martin, C. M. Spargo, B. C. Mecrow and T. Celik, "Winding configurations for a six phase switched reluctance machine," in *Proc. of the XXth International Conference on Electrical Machines*, pp. 532-538, 2012.

[36] M. C. Ta and C. Dufour, "Real-time simulation and control of reluctance motor drives for high speed operation with reduced torque ripple," in *Proc. of the 37th Annual Conference on IEEE Industrial Electronics Society* pp. 4176-4181, 2011.

[37] D. H. Lee, Z. G. Lee, J. Liang and J. W. Ahn, "Single-phase SRM drive with torque ripple reduction and power factor correction," *IEEE Transactions on Industry Applications*, vol. 43, no. 6, pp. 1578-1587, 2007.

[38] H. S. Lim and R. Krishnan, "Novel Measurement Disturbance Rejection Current Control for Linear Switched Reluctance Motor Drives," in *Proc. of the 42nd IEEE/IAS Annual Meeting Conference on Industry Applications*, pp. 2226-2233, 2007.

[39] M. M. N. Isfahani, S. M. S. Nejad, A. Rashidi and H.A. Zarchi, "Passivity-based adaptive sliding Mode speed control of switched reluctance motor

drive considering torque ripple reduction," in *Proc. of the IEEE Intl. Electric Machines & Drives Conference*, pp. 1480-1485, 2011.

[40] N. C. Sahoo, I. Elamvazuthi, R. A. Shaikh and N. M. Nor, "A comparative study of single pulse voltage and hysteresis current control methods for switched reluctance motors," in *Proc. of the International Conference on Energy, Automation, and Signal*, pp. 1-6, 2011.

[41] H. Wen and Z. Pan, "A novel dead-beat torque control of switched reluctance machines," in *Proc. of the International Conference on Electrical Machines and Systems*, pp. 1-5, 2011.

[42] C. S. Edrington, M. Krishnamurthy and B. Fahimi, "Bipolar switched reluctance machines: A novel solution for automotive applications," *IEEE Trans. on Vehicular Technology*, vol. 54, no. 3, pp. 795-80, 2005.

[43] N. S. Gameiro and A. J. M. Cardoso, "Fault tolerant control strategy of SRM drives," in *Proc. of the International Symposium on Power Electronics, Electrical Drives, Automation and Motion*, pp. 301-306, 2008.

[44] B. Qu, J. Song, T. Liang and H. Zhang, "Mutual coupling and its effect on torque waveform of even number phase switched reluctance motor," in *Proc. of the International Conference on Electrical Machines and Systems*, pp. 3405-3410, 2008.

[45] D. H. Lee, J. Liang, Z. G. Lee and J. W. Ahn, "A simple nonlinear logical torque sharing function for low-torque ripple SR drive," *IEEE Transactions on Industrial Electronics*, vol. 56, no. 8, pp. 3021-3028, 2009.

[46] D. H. Lee, S. Y. Ahn, J. W. Ahn and J. M. Kim, "Modified TSF for the high speed Switched Reluctance Motor," in *Proc. of the IEEE International Symposium on Industrial Electronics*, pp. 655-660, 2011.

[47] T. H. Kim, D. H. Lee and J. W. Ahn, "Advanced non-linear logic torque sharing function of SRM for torque ripple reduction," in *Proc. of the 31st International Telecommunications Energy Conference*, pp. 1-4, 2009.

[48] A. K. Jain and N. Mohan, "Dynamic modeling, experimental characterization, and verification for SRM operation with simultaneous two-phase excitation," *IEEE Transactions on Industrial Electronics*, vol. 53, no. 4, pp. 1238-1249, 2006.

[49] H. Hannoun, M. Hilairet and C. Marchand, "Experimental validation of a switched reluctance machine operating in continuous-conduction mode," *IEEE Transactions on Vehicular Technology*, vol. 60, no. 4, pp. 1453-1460, 2011.

[50] F. Kucuk, H. Goto, H. J. Guo and O. Ichinokura, "Artificial neural networks and inductance vector based sensorless torque estimation in switched reluctance motor drive," in *Proc. of the International Conference on Electrical Machines and Systems*, pp. 503-507, 2007.

[51] Y. A. Beromi, Z. Moravej and S. Darabi, "Torque ripple reduction of switched reluctance motor using PID fuzzy logic controller," in *Proc. of the International Conference and Exposition on Electrical and Power Engineering*, pp. 456-459, 2012.

[52] L. Yi, W. GenPing, H. Peng, W. Li and Z. Huang, "Research of restraining torque ripple reduction by fuzzy logic controller in SRM based on the nonlinear model," in *Proc. of the World Automation Congress*, pp. 1-4, 2008.

[53] C. H. Lin, "An Adaptive FNN Control for Torque-Ripple Reduction of SR Motor Drive," in *Proc. of the* IEEE *Power Conversion Conference* - Nagoya, pp. 253-258, 2007.

[54] M. Divandari, R. Brazamini, A. Dadpour and M. Jazaeri, "A novel dynamic observer and torque ripple minimization via fuzzy logic for SRM drives," in *Proc. of the IEEE International Symposium on Industrial Electronics*, pp. 847-852, 2009.

[55] C. Pavlitov, H. Chen, Y. Gorbounov, T. Georgiev, W. Xing and X. Zan, "Neural network torque estimator for switched reluctance motor," in *Proc.*

of the 13th European Conference on Power Electronics and Applications, pp. 1-9, 2009.

[56] E. Daryabeigi, A. Emanian, M.M. Namazi, A. Rashidi and S.M. S. Nejad, "Torque ripple reduction of switched reluctance motor (SRM) drives, with emotional controller (BELBIC)," in *Proc. of the 27th Annual IEEE Applied Power Electronics Conf. and Exposition*, pp. 1528-1535, 2012.

[57] E. Daryabeigi, G. A. Markadeh, C. Lucas and A. Askari, "Switched reluctance motor (SRM) control, with the developed brain emotional learning based intelligent controller (BELBIC), considering torque ripple reduction," in *Proc. of the IEEE International Electric Machines and Drives Conference*, pp. 979-986, 2009.

[58] T. Nobels, T. Gheysen, M. Vanhove and S. Stevens, "Design considerations for a plug-in hybrid car electrical motor," in *Proc. of the International Conference on Clean Electrical Power*, pp. 755-759, 2009.

[59] D. H. Lee, J. H. Lee and J. W. Ahn, "Current control of a high speed SRM with an advanced 4-level converter," in *Proc. of the IEEE 8th International Conference on Power Electronics and ECCE Asia*, pp. 109-114, 2011.

[60] S. F. Ghousia and N. C. Kar, "Performance Analysis of an 8/6 Switched Reluctance Machine Using Finite-Element Method," in *Proc. of the IEEE Power Engineering Society General Meeting*, pp. 24-28, June, 2007.

[61] M. Divandari and A. Dadpour, "Radial force and torque ripple optimization for acoustic noise reduction of SRM drives via fuzzy logic control," in *Proc. of the 9th IEEE/IAS International Conference on Industry Applications*, pp. 1-6, 2010.

[62] S. McFee, J. P. Webb and D. A. Lowther, "A tunable volume integration formulation for force calculation in finite-element based computational magnetostatics," *IEEE Transactions on Magnetics*, vol. 24, no. 1, pp. 439-442, 1988.

[63] S. F. Ghousia and N. C. Kar, “Investigation of Electromagnetic Force Using Tunable Volume Integration Method in a Switched Reluctance Motor,” in *Proc. of the Electrimacs International Conference on Theory and Application of Modeling and Simulation in Electrical Power Engineering*, Quebec, June 8-11, 2008.

[64] F. C. Lin and S. M. Yang, "Instantaneous shaft radial force control with sinusoidal excitations for switched reluctance motors," *IEEE Transactions on Energy Conversion*, vol. 22, no. 3, pp. 629-636, 2007.

[65] M. Rafiee, H. Moradi, A. Siadatan and E. Afjei, "Improving the torque ripple in SRMs utilizing RST," in *Proc. of the International Symposium on Power Electronics, Electrical Drives, Automation and Motion*, pp. 517-521, 2012.

[66] F. C. Lin and S. M. Yang, "Self-bearing control of a switched reluctance motor using sinusoidal currents," *IEEE Transactions on Power Electronics*, vol. 22, no. 6, pp. 2518-2526, 2007.

[67] R. Gobbi and K. Ramar, "Practical current control techniques for torque ripple minimization in SR motors," in *Proc. of the IEEE 2nd International Power and Energy Conference*,. pp. 743-748, 2008.

[68] M. Shirahase, S. Morimoto and M. Sanada, "Torque ripple reduction of SRM by optimization of current reference," in *International Power Electronics Conference (IPEC)*, 2010, pp. 2501-2507.

[69] S. Y. Ahn, J. W. Ahn and D. H. Lee, "A novel torque controller design for high speed SRM using negative torque compensator," in *Proc. of the 8th IEEE International Conference on Power Electronics and ECCE Asia*, pp. 937-944, 2011.

[70] J. Liang, G. Xu, L. Jian, D. H. Lee and J. W. Ahn, "Zero-torque control of switched reluctance motor drive system with on-board charger," in *Proc. of the International Conference on Electrical Machines and Systems*, pp. 1-6, 2011.

[71] F. Fleming, F. Akar and C.S. Edrington, "An optimal maximum torque per ampere strategy for switched reluctance machines," in *Proc. of the IEEE Transportation Electrification Conference and Expo*, pp. 1-6, 2012.

[72] F. Akar, F. Fleming and C.S. Edrington, "A computationally intelligent maximum torque per ampere control strategy for switched reluctance machines," in *Proc. of the IEEE Intl. Electric Vehicle Conference*, pp. 1-6, 2012.

[73] W. M. Hua and W. G. Zhou, "Analysis in start-up performance of SRM based on direct instantaneous torque control," in *Proc. of the International Conference on Electrical and Control Engineering*, pp. 4721-4724, 2011.

[74] H. Wang, D. H. Lee and J. W. Ahn, "Torque ripple reduction of SRM using advanced direct instantaneous torque control scheme," in *Proc. of the Intl. Conference on in Electrical Machines and Systems*,. pp. 492-496, 2007.

[75] M. M. Bosra, M. Saniei and R. Kianinezhad, "Direct Instantaneous Torque Control of Switched Reluctance Motors Using Five Level Converter," in *Proc. of the* 46th International *Universities' Power Engineering Conference*, pp. 1-6, 2011.

[76] S. F. Ghousia, N. C. Kar, "A Novel Optimized Instantaneous Torque Ripple Minimization Method with Current Profiling in Switched Reluctance Motors", in *Proc. of The 12th Joint MMM/Intermag Conference*, Chicago, IL, Jan 14-18, 2013.

[77] J. Y. Chai and C. M. Liaw, "Reduction of speed ripple and vibration for switched reluctance motor drive via intelligent current profiling," *IET-Electric Power Applications*, vol. 4, no. 5, pp. 380-396, 2010.

[78] C. Pavlitov, H. Chen, Y. Gorbounov, T. Tashev, T. Georgiev and W. Xing, "Switched Reluctance Motor Torque Ripples Reduction by the Aid Of Adaptive Reference Model," in *Proc. of the Intl. Symposium on Power*

Electronics Electrical Drives Automation and Motion, pp. 1276-1279, 2010.

[79] A. Nishimiya, H. Goto, H. J. Guo and O. Ichinokura, "Control of SR motor EV by instantaneous torque control using flux based commutation and phase torque distribution technique," in *Proc. of the 13th Power Electronics and Motion Control Conference*, pp. 1163-1167, 2008.

[80] J. D. Widmer, B. C. Mecrow, C. M. Spargo, R. Martin and T. Celik, "Use of a 3 phase full bridge converter to drive a 6 phase switched reluctance machine," in *Proc. of the 6th IET International Conference on Power Electronics, Machines and Drives*, pp. 1-6, 2012.

[81] J. Fort, B. Skala and V. Kus, "The torque ripple reduction at the drive with the switched reluctance motor," *in the Proc. of 15th International Power Electronics and Motion Control Conference*, pp. DS2a.16-1-DS2a.16-4, 2012.

[82] D. Zhou, K. P. Phillips, G.L. Skibinski, J. L. McCarty, M. W. Loth, B. R. Buchholz, D. H. Braun and R. A. Lukaszweski, "Evaluation of AC-AC matrix converter, a manufacturer's perspective," in *Proc. of the 37th IAS Annual Meeting. Conference*, vol.3, pp. 1558-1563, 2002.

[83] R. Bucknall and K. M. Ciaramella, "On the conceptual design and performance of a matrix converter for marine electric propulsion," *IEEE Transactions on Power Electronics*, vol. 25, no. 6, pp. 1497-1508, 2010.

[84] S. Bala and G. Venkataramanan, "Matrix converter BLDC drive using reverse-blocking IGBTs," in *Proc. of the 21st Annual IEEE Applied Power Electronics Conference and Exposition*, 2006.

[85] Chunmei Hong and Bo Zhou, "Over-modulation strategy of matrix converter driving Brushless DC motor systems," in *Proc. of the IEEE 6th International Power Electronics and Motion Control Conference*, pp. 1906-1912, 2009.

[86] J. K. Seok, J. S. Kim and S. K. Sul, "Overmodulation strategy for high-performance torque control," *IEEE Transactions on Power Electronics*, vol. 13, no. 4, pp. 786-792, 1998.

[87] P. Kiatsookkanatorn and S. Sangwongwanich, "A unified PWM method for matrix converters and its carrier-based realization using dipolar modulation technique," *IEEE Transactions on Industrial Electronics*, vol. 59, no. 1, pp. 80-92, 2012.

APPENDIX A: LAB SRM EXPERIMENTAL DATA

This is the experimental data set is obtained under the locked rotor test to develop model-free solution for precision. The graphical forms hav been presentd and discussed in chapter 6. The data points can be extracted from those graphs. However, the graphs can only give approximate values. For any future work on the basis of this dissertation will require accurate data and exact machine characteristics for the proposed data-driven, model-free global optimzation method of torque ripple elimination. Therefore, data matrix constructed on the experimental values are presented in the tabular form (individual data points) in all the apendices for precision and accuracy. Data set is transformed to $\theta = 0°$ to $60°$ instead of $\theta = -30°$ to $30°$ to generate this table and the rest of the matrix data construction for convenience. Therefore, the fully aligned position is 30° instead of 0° and 0° and 60° are fully unaligned positions.

Table A.1 2D-Flux Characteristics of the In-house 1 hp SRM.

Angle (θ°) /Current (A)	0	5	10	15	20	25	30	35	40	45	50
0	0.0000	0.0023	0.0047	0.0070	0.0094	0.0117	0.0141	0.0164	0.0188	0.0211	0.0235
2	0.0000	0.0026	0.0052	0.0078	0.0104	0.0130	0.0156	0.0182	0.0209	0.0235	0.0255
4	0.0000	0.0026	0.0053	0.0079	0.0106	0.0132	0.0159	0.0185	0.0211	0.0236	0.0260
6	0.0000	0.0031	0.0063	0.0094	0.0125	0.0155	0.0184	0.0209	0.0233	0.0258	0.0283
8	0.0000	0.0046	0.0092	0.0132	0.0161	0.0190	0.0216	0.0244	0.0269	0.0293	0.0314
10	0.0000	0.0062	0.0123	0.0170	0.0203	0.0232	0.0259	0.0285	0.0310	0.0334	0.0357
12	0.0000	0.0078	0.0154	0.0208	0.0242	0.0271	0.0299	0.0324	0.0349	0.0372	0.0395
14	0.0000	0.0094	0.0185	0.0246	0.0283	0.0313	0.0340	0.0365	0.0389	0.0412	0.0434
16	0.0000	0.0110	0.0217	0.0286	0.0324	0.0354	0.0381	0.0406	0.0429	0.0450	0.0470
18	0.0000	0.0125	0.0247	0.0322	0.0362	0.0391	0.0417	0.0440	0.0461	0.0481	0.0501
20	0.0000	0.0142	0.0279	0.0364	0.0406	0.0436	0.0461	0.0482	0.0502	0.0520	0.0535
22	0.0000	0.0156	0.0307	0.0399	0.0440	0.0468	0.0490	0.0510	0.0528	0.0539	0.0552
24	0.0000	0.0172	0.0339	0.0436	0.0478	0.0504	0.0525	0.0541	0.0552	0.0562	0.0570
26	0.0000	0.0187	0.0365	0.0460	0.0499	0.0526	0.0542	0.0554	0.0563	0.0572	0.0579
28	0.0000	0.0200	0.0390	0.0479	0.0520	0.0541	0.0554	0.0564	0.0573	0.0581	0.0588
30	0.0000	0.0205	0.0398	0.0483	0.0524	0.0544	0.0556	0.0566	0.0574	0.0582	0.0589
32	0.0000	0.0200	0.0390	0.0479	0.0520	0.0541	0.0554	0.0564	0.0573	0.0581	0.0588
34	0.0000	0.0187	0.0365	0.0460	0.0499	0.0526	0.0542	0.0554	0.0563	0.0572	0.0579
36	0.0000	0.0172	0.0339	0.0436	0.0478	0.0504	0.0525	0.0541	0.0552	0.0562	0.0570
38	0.0000	0.0156	0.0307	0.0399	0.0440	0.0468	0.0490	0.0510	0.0528	0.0539	0.0552
40	0.0000	0.0142	0.0279	0.0364	0.0406	0.0436	0.0461	0.0482	0.0502	0.0520	0.0535
42	0.0000	0.0125	0.0247	0.0322	0.0362	0.0391	0.0417	0.0440	0.0461	0.0481	0.0501
44	0.0000	0.0110	0.0217	0.0286	0.0324	0.0354	0.0381	0.0406	0.0429	0.0450	0.0470
46	0.0000	0.0094	0.0185	0.0246	0.0283	0.0313	0.0340	0.0365	0.0389	0.0412	0.0434
48	0.0000	0.0078	0.0154	0.0208	0.0242	0.0271	0.0299	0.0324	0.0349	0.0372	0.0395
50	0.0000	0.0062	0.0123	0.0170	0.0203	0.0232	0.0259	0.0285	0.0310	0.0334	0.0357
52	0.0000	0.0046	0.0092	0.0132	0.0161	0.0190	0.0216	0.0244	0.0269	0.0293	0.0314
54	0.0000	0.0031	0.0063	0.0094	0.0125	0.0155	0.0184	0.0209	0.0233	0.0258	0.0283
56	0.0000	0.0026	0.0053	0.0079	0.0106	0.0132	0.0159	0.0185	0.0211	0.0236	0.0260
58	0.0000	0.0026	0.0052	0.0078	0.0104	0.0130	0.0156	0.0182	0.0209	0.0235	0.0255
60	0.0000	0.0023	0.0047	0.0070	0.0094	0.0117	0.0141	0.0164	0.0188	0.0211	0.0235

APPENDIX B: EXPERIMENTAL DATA MATRIX CONSTRUCTION

Table B.1 4D Primary Phase Matrix Constructed from the Experimental Results for Global Optimization Method (0-16 A).

This is the experimental data matrix set developed using the raw machine data for the low current region of the electromagnetic characteristics in terms of torque vs. excitation current (A) and rotor angle (θ°) from the primary phase stator.

Angle (θ°) / Current(A)	0	1	2	3	4	5	6	7	8	9	10	11	12	13	14	15	16
0	0.00	0.00	0.00	0.00	0.00	0.00	0.00	0.00	0.00	0.01	0.01	0.01	0.01	0.01	0.01	0.02	0.02
1	0.00	0.00	0.00	0.00	0.00	0.01	0.01	0.01	0.01	0.02	0.02	0.03	0.03	0.04	0.04	0.05	0.06
2	0.00	0.00	0.00	0.00	0.01	0.01	0.01	0.02	0.02	0.03	0.04	0.05	0.06	0.07	0.08	0.09	0.10
3	0.00	0.00	0.00	0.01	0.01	0.02	0.02	0.03	0.04	0.05	0.06	0.07	0.09	0.10	0.12	0.14	0.16
4	0.00	0.00	0.00	0.01	0.02	0.02	0.03	0.05	0.06	0.08	0.10	0.12	0.14	0.16	0.19	0.22	0.24
5	0.00	0.00	0.01	0.01	0.02	0.04	0.05	0.07	0.10	0.13	0.15	0.18	0.22	0.26	0.30	0.34	0.39
6	0.00	0.00	0.01	0.02	0.04	0.06	0.09	0.13	0.17	0.22	0.26	0.31	0.37	0.44	0.51	0.58	0.66
7	0.00	0.00	0.02	0.04	0.07	0.11	0.16	0.21	0.28	0.36	0.43	0.52	0.62	0.72	0.82	0.93	1.04
8	0.00	0.00	0.02	0.04	0.073	0.11	0.16	0.22	0.29	0.38	0.45	0.55	0.65	0.76	0.87	1.00	1.12
9	0.00	0.00	0.02	0.04	0.07	0.11	0.16	0.22	0.29	0.38	0.46	0.55	0.65	0.76	0.86	0.99	1.11
10	0.00	0.00	0.02	0.04	0.07	0.11	0.16	0.22	0.29	0.38	0.46	0.55	0.65	0.76	0.87	0.96	1.07
11	0.00	0.00	0.02	0.04	0.07	0.11	0.17	0.22	0.29	0.37	0.46	0.55	0.65	0.75	0.87	0.98	1.08
12	0.00	0.00	0.02	0.04	0.07	0.12	0.17	0.23	0.29	0.37	0.46	0.56	0.65	0.76	0.86	0.97	1.09
13	0.00	0.00	0.02	0.04	0.07	0.12	0.17	0.23	0.30	0.38	0.46	0.56	0.66	0.77	0.87	0.99	1.11
14	0.00	0.00	0.02	0.04	0.07	0.11	0.16	0.22	0.29	0.37	0.46	0.56	0.65	0.77	0.86	0.98	1.09
15	0.00	0.00	0.02	0.04	0.07	0.12	0.17	0.23	0.29	0.37	0.46	0.55	0.66	0.77	0.87	0.98	1.11
16	0.00	0.00	0.02	0.04	0.07	0.12	0.17	0.23	0.29	0.37	0.46	0.55	0.65	0.77	0.86	0.99	1.10
17	0.00	0.00	0.02	0.04	0.07	0.12	0.17	0.23	0.29	0.37	0.46	0.55	0.66	0.77	0.87	0.98	1.13
18	0.00	0.00	0.02	0.04	0.07	0.11	0.15	0.21	0.27	0.34	0.45	0.51	0.61	0.72	0.82	0.93	1.10
19	0.00	0.00	0.02	0.04	0.07	0.11	0.16	0.22	0.29	0.37	0.46	0.55	0.66	0.77	0.86	0.98	1.09
20	0.00	0.00	0.02	0.04	0.07	0.11	0.16	0.22	0.28	0.36	0.45	0.54	0.65	0.76	0.85	0.96	1.07
21	0.00	0.00	0.02	0.04	0.07	0.11	0.16	0.22	0.29	0.37	0.45	0.54	0.65	0.76	0.85	0.96	1.07
22	0.00	0.00	0.02	0.04	0.07	0.11	0.16	0.21	0.28	0.35	0.44	0.53	0.63	0.76	0.84	0.94	1.04
23	0.00	0.00	0.02	0.04	0.07	0.11	0.15	0.21	0.27	0.35	0.43	0.52	0.61	0.73	0.83	0.93	1.06
24	0.00	0.00	0.02	0.04	0.07	0.10	0.15	0.20	0.27	0.34	0.42	0.50	0.61	0.71	0.78	0.90	1.00
25	0.00	0.00	0.02	0.04	0.07	0.11	0.15	0.20	0.27	0.33	0.41	0.50	0.58	0.68	0.76	0.82	1.01
26	0.00	0.00	0.02	0.04	0.06	0.10	0.15	0.20	0.26	0.33	0.40	0.48	0.55	0.65	0.70	0.77	0.79
27	0.00	0.00	0.02	0.03	0.06	0.10	0.14	0.19	0.25	0.31	0.38	0.45	0.51	0.62	0.66	0.68	0.81
28	0.00	0.00	0.01	0.03	0.05	0.08	0.12	0.16	0.21	0.27	0.33	0.39	0.44	0.53	0.50	0.56	0.58
29	0.00	0.00	0.01	0.01	0.03	0.04	0.06	0.08	0.11	0.13	0.16	0.19	0.22	0.26	0.25	0.26	0.28
30	0.00	0.00	0.00	0.00	0.00	0.00	0.00	0.00	0.00	0.00	0.00	0.00	0.00	0.00	0.00	0.00	0.00
31	0.00	0.00	-0.01	-0.01	-0.03	-0.04	-0.06	-0.08	-0.11	-0.13	-0.16	-0.19	-0.22	-0.26	-0.25	-0.26	-0.28
32	0.00	0.00	-0.01	-0.03	-0.05	-0.08	-0.12	-0.16	-0.21	-0.27	-0.33	-0.39	-0.44	-0.53	-0.50	-0.56	-0.58
33	0.00	0.00	-0.02	-0.03	-0.06	-0.10	-0.14	-0.19	-0.25	-0.31	-0.38	-0.45	-0.51	-0.62	-0.66	-0.68	-0.81
34	0.00	0.00	-0.02	-0.04	-0.06	-0.10	-0.15	-0.20	-0.26	-0.33	-0.40	-0.48	-0.55	-0.65	-0.70	-0.77	-0.79
35	0.00	0.00	-0.02	-0.04	-0.07	-0.11	-0.15	-0.20	-0.27	-0.33	-0.41	-0.50	-0.58	-0.68	-0.76	-0.82	-1.01
36	0.00	0.00	-0.02	-0.04	-0.07	-0.10	-0.15	-0.20	-0.27	-0.34	-0.42	-0.50	-0.61	-0.71	-0.78	-0.90	-1.00
37	0.00	0.00	-0.02	-0.04	-0.07	-0.11	-0.15	-0.21	-0.27	-0.35	-0.43	-0.52	-0.61	-0.73	-0.83	-0.93	-1.06

38	0.00	0.00	-0.02	-0.04	-0.07	-0.11	-0.16	-0.21	-0.28	-0.35	-0.44	-0.53	-0.63	-0.76	-0.84	-0.94	-1.04
39	0.00	0.00	-0.02	-0.04	-0.07	-0.11	-0.16	-0.22	-0.29	-0.37	-0.45	-0.54	-0.65	-0.76	-0.85	-0.96	-1.07
40	0.00	0.00	-0.02	-0.04	-0.07	-0.11	-0.16	-0.22	-0.28	-0.36	-0.45	-0.54	-0.65	-0.76	-0.85	-0.96	-1.07
41	0.00	0.00	-0.02	-0.04	-0.07	-0.11	-0.16	-0.22	-0.29	-0.37	-0.46	-0.55	-0.66	-0.77	-0.86	-0.98	-1.09
42	0.00	0.00	-0.02	-0.04	-0.07	-0.12	-0.17	-0.23	-0.29	-0.37	-0.46	-0.55	-0.66	-0.77	-0.87	-0.98	-1.13
43	0.00	0.00	-0.02	-0.04	-0.07	-0.11	-0.15	-0.21	-0.27	-0.34	-0.45	-0.51	-0.61	-0.72	-0.82	-0.93	-1.10
44	0.00	0.00	-0.02	-0.04	-0.07	-0.12	-0.17	-0.23	-0.29	-0.37	-0.46	-0.55	-0.65	-0.77	-0.86	-0.99	-1.10
45	0.00	0.00	-0.02	-0.04	-0.07	-0.12	-0.17	-0.23	-0.29	-0.37	-0.46	-0.55	-0.66	-0.77	-0.87	-0.98	-1.11
46	0.00	0.00	-0.02	-0.04	-0.07	-0.11	-0.16	-0.22	-0.29	-0.37	-0.46	-0.56	-0.65	-0.77	-0.86	-0.98	-1.09
47	0.00	0.00	-0.02	-0.04	-0.07	-0.12	-0.17	-0.23	-0.30	-0.38	-0.46	-0.56	-0.66	-0.77	-0.87	-0.99	-1.11
48	0.00	0.00	-0.02	-0.04	-0.07	-0.12	-0.17	-0.23	-0.29	-0.37	-0.46	-0.56	-0.65	-0.76	-0.86	-0.97	-1.09
49	0.00	0.00	-0.02	-0.04	-0.07	-0.11	-0.17	-0.22	-0.29	-0.37	-0.46	-0.55	-0.65	-0.75	-0.87	-0.98	-1.08
50	0.00	0.00	-0.02	-0.04	-0.07	-0.11	-0.16	-0.22	-0.29	-0.38	-0.46	-0.55	-0.65	-0.76	-0.87	-0.96	-1.07
51	0.00	0.00	-0.02	-0.04	-0.07	-0.11	-0.16	-0.22	-0.29	-0.38	-0.46	-0.55	-0.65	-0.76	-0.86	-0.99	-1.11
52	0.00	0.00	-0.02	-0.04	-0.07	-0.11	-0.16	-0.22	-0.29	-0.38	-0.45	-0.55	-0.65	-0.76	-0.87	-1.00	-1.12
53	0.00	0.00	-0.02	-0.04	-0.07	-0.11	-0.16	-0.21	-0.28	-0.36	-0.43	-0.52	-0.62	-0.72	-0.82	-0.93	-1.04
54	0.00	0.00	-0.01	-0.02	-0.04	-0.06	-0.09	-0.13	-0.17	-0.22	-0.26	-0.31	-0.37	-0.44	-0.51	-0.58	-0.66
55	0.00	0.00	-0.01	-0.01	-0.02	-0.04	-0.05	-0.07	-0.10	-0.13	-0.15	-0.18	-0.22	-0.26	-0.30	-0.34	-0.39
56	0.00	0.00	0.00	-0.01	-0.02	-0.02	-0.03	-0.05	-0.06	-0.08	-0.10	-0.12	-0.14	-0.16	-0.19	-0.22	-0.24
57	0.00	0.00	0.00	-0.01	-0.01	-0.02	-0.02	-0.03	-0.04	-0.05	-0.06	-0.07	-0.09	-0.10	-0.12	-0.14	-0.16
58	0.00	0.00	0.00	0.00	-0.01	-0.01	-0.01	-0.02	-0.02	-0.03	-0.04	-0.05	-0.06	-0.07	-0.08	-0.09	-0.10
59	0.00	0.00	0.00	0.00	0.00	-0.01	-0.01	-0.01	-0.01	-0.02	-0.02	-0.03	-0.03	-0.04	-0.04	-0.05	-0.06

Table B.2 4D Primary Phase Matrix Constructed from the Experimental Results for Global Optimization Method (17-33 A).

This is the experimental data matrix set developed using the raw machine data for the unsaturated region of the electromagnetic characteristics in terms of torque vs. excitation current (A) and rotor angle (θ°) from the primary phase stator.

Angle (θ°)/ Current (A)	17	18	19	20	21	22	23	24	25	26	27	28	29	30	31	32	33
0	0.02	0.02	0.03	0.03	0.03	0.03	0.04	0.04	0.04	0.05	0.05	0.06	0.06	0.06	0.07	0.07	0.08
1	0.06	0.07	0.08	0.09	0.09	0.10	0.11	0.12	0.13	0.15	0.16	0.17	0.18	0.19	0.21	0.22	0.23
2	0.11	0.13	0.14	0.16	0.17	0.19	0.21	0.22	0.24	0.26	0.28	0.31	0.33	0.35	0.37	0.40	0.42
3	0.18	0.20	0.22	0.25	0.27	0.30	0.33	0.36	0.39	0.42	0.45	0.48	0.52	0.55	0.59	0.63	0.67
4	0.28	0.31	0.35	0.38	0.42	0.46	0.51	0.55	0.59	0.64	0.69	0.74	0.80	0.86	0.91	0.97	1.03
5	0.44	0.49	0.55	0.60	0.67	0.73	0.79	0.87	0.94	1.01	1.09	1.17	1.25	1.33	1.42	1.50	1.59
6	0.74	0.83	0.92	1.01	1.11	1.21	1.32	1.41	1.51	1.62	1.72	1.83	1.93	2.03	2.12	2.22	2.31
7	1.16	1.28	1.40	1.52	1.64	1.78	1.88	1.92	2.02	2.12	2.22	2.32	2.42	2.52	2.61	2.71	2.81
8	1.25	1.38	1.43	1.54	1.64	1.75	1.86	1.94	2.04	2.15	2.25	2.35	2.46	2.56	2.66	2.77	2.87
9	1.18	1.30	1.41	1.52	1.61	1.75	1.84	1.93	2.04	2.15	2.26	2.36	2.47	2.58	2.69	2.80	2.91
10	1.19	1.28	1.42	1.51	1.62	1.73	1.86	1.95	2.07	2.18	2.29	2.40	2.51	2.62	2.74	2.85	2.96
11	1.19	1.32	1.41	1.52	1.64	1.75	1.86	1.98	2.10	2.22	2.31	2.44	2.54	2.66	2.77	2.89	3.00
12	1.21	1.33	1.46	1.54	1.65	1.77	1.88	1.99	2.11	2.26	2.34	2.45	2.57	2.69	2.80	2.92	3.03
13	1.21	1.32	1.44	1.56	1.67	1.82	1.91	2.02	2.16	2.26	2.38	2.49	2.61	2.73	2.85	2.96	3.08
14	1.20	1.31	1.44	1.57	1.66	1.77	1.90	2.02	2.14	2.26	2.38	2.48	2.62	2.73	2.85	2.97	3.09
15	1.21	1.34	1.45	1.56	1.67	1.79	1.91	2.03	2.15	2.29	2.39	2.50	2.63	2.76	2.87	2.98	3.11
16	1.21	1.33	1.46	1.56	1.67	1.78	1.92	2.04	2.15	2.27	2.40	2.51	2.63	2.76	2.87	2.99	3.11
17	1.20	1.32	1.48	1.55	1.67	1.79	1.90	2.02	2.15	2.27	2.39	2.49	2.61	2.72	2.83	2.94	3.06
18	1.20	1.32	1.40	1.52	1.64	1.76	1.88	2.00	2.12	2.24	2.36	2.50	2.59	2.72	2.83	2.94	3.06
19	1.24	1.31	1.42	1.54	1.66	1.80	1.91	2.02	2.13	2.25	2.36	2.46	2.58	2.69	2.80	2.91	3.01
20	1.18	1.29	1.41	1.54	1.63	1.76	1.87	1.98	2.10	2.20	2.30	2.41	2.52	2.64	2.73	2.82	2.92
21	1.18	1.32	1.49	1.52	1.61	1.72	1.86	1.95	2.07	2.14	2.25	2.35	2.45	2.55	2.65	2.74	2.84
22	1.14	1.25	1.38	1.47	1.57	1.68	1.79	1.86	1.99	2.07	2.15	2.25	2.34	2.44	2.53	2.62	2.71
23	1.15	1.24	1.37	1.41	1.57	1.60	1.69	1.78	1.87	1.98	2.02	2.11	2.20	2.30	2.37	2.46	2.55
24	1.10	1.16	1.31	1.34	1.38	1.47	1.57	1.70	1.74	1.79	1.88	1.95	2.03	2.13	2.18	2.25	2.31
25	1.10	1.15	1.22	1.31	1.27	1.35	1.44	1.56	1.56	1.63	1.70	1.76	1.83	1.88	1.93	1.98	2.03
26	0.90	0.93	1.13	1.08	1.14	1.21	1.42	1.30	1.35	1.41	1.45	1.50	1.54	1.59	1.62	1.66	1.70
27	0.81	0.88	0.95	0.99	0.97	1.08	1.01	1.07	1.12	1.13	1.18	1.20	1.23	1.26	1.28	1.31	1.33
28	0.67	0.69	0.80	0.74	0.77	0.75	0.77	0.79	0.81	0.82	0.85	0.86	0.88	0.89	0.91	0.93	0.94
29	0.30	0.32	0.33	0.33	0.32	0.33	0.33	0.34	0.35	0.36	0.36	0.36	0.37	0.38	0.38	0.39	0.39
30	0.00	0.00	0.00	0.00	0.00	0.00	0.00	0.00	0.00	0.00	0.00	0.00	0.00	0.00	0.00	0.00	0.00
31	-0.30	-0.32	-0.33	-0.33	-0.32	-0.33	-0.33	-0.34	-0.35	-0.36	-0.36	-0.36	-0.37	-0.38	-0.38	-0.39	-0.39
32	-0.67	-0.69	-0.80	-0.74	-0.77	-0.75	-0.77	-0.79	-0.81	-0.82	-0.85	-0.86	-0.88	-0.89	-0.91	-0.93	-0.94
33	-0.81	-0.88	-0.95	-0.99	-0.97	-1.08	-1.01	-1.07	-1.12	-1.13	-1.18	-1.20	-1.23	-1.26	-1.28	-1.31	-1.33
34	-0.90	-0.93	-1.13	-1.08	-1.14	-1.21	-1.42	-1.30	-1.35	-1.41	-1.45	-1.50	-1.54	-1.59	-1.62	-1.66	-1.70
35	-1.10	-1.15	-1.22	-1.31	-1.27	-1.35	-1.44	-1.56	-1.56	-1.63	-1.70	-1.76	-1.83	-1.88	-1.93	-1.98	-2.03
36	-1.10	-1.16	-1.31	-1.34	-1.38	-1.47	-1.57	-1.70	-1.74	-1.79	-1.88	-1.95	-2.03	-2.13	-2.18	-2.25	-2.31
37	-1.15	-1.24	-1.37	-1.41	-1.57	-1.60	-1.69	-1.78	-1.87	-1.98	-2.02	-2.11	-2.20	-2.30	-2.37	-2.46	-2.55

38	-1.14	-1.25	-1.38	-1.47	-1.57	-1.68	-1.79	-1.86	-1.99	-2.07	-2.15	-2.25	-2.34	-2.44	-2.53	-2.62	-2.71
39	-1.18	-1.32	-1.49	-1.52	-1.61	-1.72	-1.86	-1.95	-2.07	-2.14	-2.25	-2.35	-2.45	-2.55	-2.65	-2.74	-2.84
40	-1.18	-1.29	-1.41	-1.54	-1.63	-1.76	-1.87	-1.98	-2.10	-2.20	-2.30	-2.41	-2.52	-2.64	-2.73	-2.82	-2.92
41	-1.24	-1.31	-1.42	-1.54	-1.66	-1.80	-1.91	-2.02	-2.13	-2.25	-2.36	-2.46	-2.58	-2.69	-2.80	-2.91	-3.01
42	-1.20	-1.32	-1.48	-1.55	-1.67	-1.79	-1.90	-2.02	-2.15	-2.27	-2.39	-2.49	-2.61	-2.72	-2.83	-2.94	-3.06
43	-1.20	-1.32	-1.40	-1.52	-1.64	-1.76	-1.88	-2.00	-2.12	-2.24	-2.36	-2.50	-2.59	-2.72	-2.83	-2.94	-3.06
44	-1.21	-1.33	-1.46	-1.56	-1.67	-1.78	-1.92	-2.04	-2.15	-2.27	-2.40	-2.51	-2.63	-2.76	-2.87	-2.99	-3.11
45	-1.21	-1.34	-1.45	-1.56	-1.67	-1.79	-1.91	-2.03	-2.15	-2.29	-2.39	-2.50	-2.63	-2.76	-2.87	-2.98	-3.11
46	-1.20	-1.31	-1.44	-1.57	-1.66	-1.77	-1.90	-2.02	-2.14	-2.26	-2.38	-2.48	-2.62	-2.73	-2.85	-2.97	-3.09
47	-1.21	-1.32	-1.44	-1.56	-1.67	-1.82	-1.91	-2.02	-2.16	-2.26	-2.38	-2.49	-2.61	-2.73	-2.85	-2.96	-3.08
48	-1.21	-1.33	-1.46	-1.54	-1.65	-1.77	-1.88	-1.99	-2.11	-2.26	-2.34	-2.45	-2.57	-2.69	-2.80	-2.92	-3.03
49	-1.19	-1.32	-1.41	-1.52	-1.64	-1.75	-1.86	-1.98	-2.10	-2.22	-2.31	-2.44	-2.54	-2.66	-2.77	-2.89	-3.00
50	-1.19	-1.28	-1.42	-1.51	-1.62	-1.73	-1.86	-1.95	-2.07	-2.18	-2.29	-2.40	-2.51	-2.62	-2.74	-2.85	-2.96
51	-1.18	-1.30	-1.41	-1.52	-1.61	-1.75	-1.84	-1.93	-2.04	-2.15	-2.26	-2.36	-2.47	-2.58	-2.69	-2.80	-2.91
52	-1.25	-1.38	-1.43	-1.54	-1.64	-1.75	-1.86	-1.94	-2.04	-2.15	-2.25	-2.35	-2.46	-2.56	-2.66	-2.77	-2.87
53	-1.16	-1.28	-1.40	-1.52	-1.64	-1.78	-1.88	-1.92	-2.02	-2.12	-2.22	-2.32	-2.42	-2.52	-2.61	-2.71	-2.81
54	-0.74	-0.83	-0.92	-1.01	-1.11	-1.21	-1.32	-1.41	-1.51	-1.62	-1.72	-1.83	-1.93	-2.03	-2.12	-2.22	-2.31
55	-0.44	-0.49	-0.55	-0.60	-0.67	-0.73	-0.79	-0.87	-0.94	-1.01	-1.09	-1.17	-1.25	-1.33	-1.42	-1.50	-1.59
56	-0.28	-0.31	-0.35	-0.38	-0.42	-0.46	-0.51	-0.55	-0.59	-0.64	-0.69	-0.74	-0.80	-0.86	-0.91	-0.97	-1.03
57	-0.18	-0.20	-0.22	-0.25	-0.27	-0.30	-0.33	-0.36	-0.39	-0.42	-0.45	-0.48	-0.52	-0.55	-0.59	-0.63	-0.67
58	-0.11	-0.13	-0.14	-0.16	-0.17	-0.19	-0.21	-0.22	-0.24	-0.26	-0.28	-0.31	-0.33	-0.35	-0.37	-0.40	-0.42
59	-0.06	-0.07	-0.08	-0.09	-0.09	-0.10	-0.11	-0.12	-0.13	-0.15	-0.16	-0.17	-0.18	-0.19	-0.21	-0.22	-0.23

Table B.3 4D Primary Phase Matrix Constructed from the Experimental Results for Global Optimization Method (34-50 A).

This is the experimental data matrix set developed using the raw machine data for the saturated region of the electromagnetic characteristics in terms of torque vs. excitation current(A) and rotor angle (θ°) from the primary phase stator.

Angle (θ°)/ Current (A)	34	35	36	37	38	39	40	41	42	43	44	45	46	47	48	49	50
0	0.08	0.09	0.09	0.10	0.10	0.11	0.11	0.12	0.13	0.13	0.14	0.14	0.15	0.16	0.16	0.17	0.18
1	0.25	0.26	0.28	0.29	0.31	0.33	0.34	0.36	0.38	0.40	0.42	0.44	0.46	0.48	0.50	0.52	0.55
2	0.45	0.48	0.50	0.53	0.56	0.57	0.62	0.65	0.67	0.72	0.75	0.76	0.80	0.83	0.89	0.93	0.97
3	0.71	0.75	0.74	0.78	0.82	0.86	0.96	1.01	1.00	1.05	1.10	1.15	1.20	1.25	1.30	1.35	1.40
4	1.10	1.16	1.23	1.29	1.33	1.43	1.47	1.57	1.61	1.69	1.75	1.82	1.88	1.95	1.93	1.98	2.05
5	1.68	1.76	1.85	1.89	1.98	1.87	1.95	2.02	2.10	2.18	2.27	2.34	2.42	2.69	2.58	2.86	2.93
6	2.40	2.49	2.61	2.70	2.76	3.00	2.96	3.05	3.14	3.24	3.32	3.41	3.50	3.60	3.69	3.77	3.86
7	2.91	3.01	3.10	3.23	3.33	3.43	3.53	3.63	3.74	3.79	3.88	3.98	4.08	4.18	4.28	4.37	4.46
8	2.97	3.08	3.19	3.31	3.40	3.50	3.63	3.73	3.80	3.93	4.01	4.18	4.22	4.32	4.42	4.57	4.62
9	3.01	3.12	3.22	3.33	3.45	3.55	3.65	3.76	3.87	3.98	4.08	4.18	4.29	4.40	4.50	4.61	4.72
10	3.07	3.18	3.29	3.39	3.51	3.62	3.73	3.84	3.95	4.06	4.17	4.28	4.38	4.49	4.60	4.72	4.82
11	3.11	3.23	3.34	3.45	3.56	3.68	3.79	3.90	4.02	4.13	4.24	4.35	4.46	4.57	4.68	4.79	4.90
12	3.15	3.26	3.38	3.49	3.61	3.72	3.84	3.95	4.06	4.18	4.29	4.40	4.51	4.64	4.74	4.85	4.96
13	3.20	3.31	3.43	3.55	3.67	3.78	3.89	4.02	4.13	4.24	4.36	4.47	4.59	4.70	4.81	4.92	5.03
14	3.21	3.32	3.44	3.56	3.68	3.79	3.91	4.03	4.14	4.25	4.38	4.48	4.59	4.71	4.82	4.93	5.04
15	3.22	3.34	3.46	3.57	3.69	3.81	3.92	4.03	4.15	4.26	4.36	4.47	4.59	4.69	4.80	4.90	5.01
16	3.24	3.34	3.45	3.56	3.68	3.78	3.89	4.01	4.12	4.21	4.33	4.43	4.54	4.65	4.75	4.85	4.96
17	3.18	3.28	3.38	3.49	3.60	3.70	3.81	3.91	4.01	4.12	4.22	4.32	4.42	4.51	4.61	4.71	4.80
18	3.17	3.28	3.39	3.47	3.58	3.70	3.79	3.90	4.01	4.06	4.16	4.27	4.37	4.47	4.57	4.66	4.76
19	3.12	3.22	3.33	3.45	3.53	3.64	3.74	3.84	3.94	4.03	4.13	4.22	4.32	4.41	4.51	4.60	4.69
20	3.04	3.13	3.23	3.33	3.43	3.53	3.62	3.72	3.81	3.90	4.00	4.09	4.18	4.26	4.34	4.42	4.50
21	2.95	3.03	3.13	3.22	3.32	3.41	3.50	3.58	3.67	3.75	3.83	3.91	3.98	4.04	4.11	4.17	4.23
22	2.80	2.89	2.98	3.06	3.15	3.23	3.31	3.37	3.44	3.51	3.57	3.62	3.68	3.74	3.79	3.84	3.89
23	2.63	2.70	2.78	2.84	2.91	2.97	3.02	3.08	3.13	3.18	3.24	3.28	3.33	3.38	3.42	3.47	3.51
24	2.38	2.43	2.49	2.54	2.59	2.64	2.68	2.73	2.77	2.81	2.85	2.89	2.93	2.97	3.01	3.05	3.09
25	2.08	2.12	2.16	2.20	2.24	2.28	2.32	2.35	2.39	2.42	2.46	2.49	2.53	2.56	2.59	2.62	2.66
26	1.73	1.77	1.80	1.83	1.86	1.89	1.92	1.95	1.98	2.01	2.04	2.07	2.09	2.12	2.15	2.17	2.20
27	1.36	1.38	1.41	1.43	1.45	1.48	1.50	1.52	1.54	1.56	1.59	1.61	1.63	1.65	1.67	1.69	1.71
28	0.96	0.97	0.99	1.00	1.02	1.03	1.05	1.06	1.07	1.09	1.10	1.11	1.13	1.14	1.15	1.16	1.18
29	0.40	0.40	0.41	0.41	0.42	0.42	0.43	0.43	0.44	0.44	0.45	0.45	0.46	0.46	0.46	0.47	0.47

30	0.00	0.00	0.00	0.00	0.00	0.00	0.00	0.00	0.00	0.00	0.00	0.00	0.00	0.00	0.00	0.00	0.00
31	-0.40	-0.40	-0.41	-0.41	-0.42	-0.42	-0.43	-0.43	-0.44	-0.44	-0.45	-0.45	-0.46	-0.46	-0.46	-0.47	-0.47
32	-0.96	-0.97	-0.99	-1.00	-1.02	-1.03	-1.05	-1.06	-1.07	-1.09	-1.10	-1.11	-1.13	-1.14	-1.15	-1.16	-1.18
33	-1.36	-1.38	-1.41	-1.43	-1.45	-1.48	-1.50	-1.52	-1.54	-1.56	-1.59	-1.61	-1.63	-1.65	-1.67	-1.69	-1.71
34	-1.73	-1.77	-1.80	-1.83	-1.86	-1.89	-1.92	-1.95	-1.98	-2.01	-2.04	-2.07	-2.09	-2.12	-2.15	-2.17	-2.20
35	-2.08	-2.12	-2.16	-2.20	-2.24	-2.28	-2.32	-2.35	-2.39	-2.42	-2.46	-2.49	-2.53	-2.56	-2.59	-2.62	-2.66
36	-2.38	-2.43	-2.49	-2.54	-2.59	-2.64	-2.68	-2.73	-2.77	-2.81	-2.85	-2.89	-2.93	-2.97	-3.01	-3.05	-3.09
37	-2.63	-2.70	-2.78	-2.84	-2.91	-2.97	-3.02	-3.08	-3.13	-3.18	-3.24	-3.28	-3.33	-3.38	-3.42	-3.47	-3.51
38	-2.80	-2.89	-2.98	-3.06	-3.15	-3.23	-3.31	-3.37	-3.44	-3.51	-3.57	-3.62	-3.68	-3.74	-3.79	-3.84	-3.89
39	-2.95	-3.03	-3.13	-3.22	-3.32	-3.41	-3.50	-3.58	-3.67	-3.75	-3.83	-3.91	-3.98	-4.04	-4.11	-4.17	-4.23
40	-3.04	-3.13	-3.23	-3.33	-3.43	-3.53	-3.62	-3.72	-3.81	-3.90	-4.00	-4.09	-4.18	-4.26	-4.34	-4.42	-4.50
41	-3.12	-3.22	-3.33	-3.45	-3.53	-3.64	-3.74	-3.84	-3.94	-4.03	-4.13	-4.22	-4.32	-4.41	-4.51	-4.60	-4.69
42	-3.18	-3.28	-3.38	-3.49	-3.60	-3.70	-3.81	-3.91	-4.01	-4.12	-4.22	-4.32	-4.42	-4.51	-4.61	-4.71	-4.81
43	-3.17	-3.28	-3.39	-3.47	-3.58	-3.70	-3.79	-3.90	-4.01	-4.06	-4.16	-4.27	-4.37	-4.47	-4.57	-4.66	-4.76
44	-3.24	-3.34	-3.45	-3.56	-3.68	-3.78	-3.89	-4.01	-4.12	-4.21	-4.33	-4.43	-4.54	-4.65	-4.75	-4.85	-4.98
45	-3.22	-3.34	-3.46	-3.57	-3.69	-3.81	-3.92	-4.03	-4.15	-4.26	-4.36	-4.47	-4.59	-4.69	-4.80	-4.90	-5.01
46	-3.21	-3.32	-3.44	-3.56	-3.68	-3.79	-3.91	-4.03	-4.14	-4.25	-4.38	-4.48	-4.59	-4.71	-4.82	-4.93	-5.04
47	-3.20	-3.31	-3.43	-3.55	-3.67	-3.78	-3.89	-4.02	-4.13	-4.24	-4.36	-4.47	-4.59	-4.70	-4.81	-4.92	-5.03
48	-3.15	-3.26	-3.38	-3.49	-3.61	-3.72	-3.84	-3.95	-4.06	-4.18	-4.29	-4.40	-4.51	-4.64	-4.74	-4.85	-4.96
49	-3.11	-3.23	-3.34	-3.45	-3.56	-3.68	-3.79	-3.90	-4.02	-4.13	-4.24	-4.35	-4.46	-4.57	-4.68	-4.92	-4.90
50	-3.07	-3.18	-3.29	-3.39	-3.51	-3.62	-3.73	-3.84	-3.95	-4.06	-4.17	-4.28	-4.38	-4.49	-4.60	-4.72	-4.82
51	-3.01	-3.12	-3.22	-3.33	-3.45	-3.55	-3.65	-3.76	-3.87	-3.98	-4.08	-4.18	-4.29	-4.40	-4.50	-4.61	-4.72
52	-2.97	-3.08	-3.19	-3.31	-3.40	-3.50	-3.63	-3.73	-3.80	-3.93	-4.01	-4.18	-4.22	-4.32	-4.42	-4.57	-4.62
53	-2.91	-3.01	-3.10	-3.23	-3.33	-3.43	-3.53	-3.63	-3.74	-3.79	-3.88	-3.98	-4.08	-4.18	-4.28	-4.37	-4.46
54	-2.40	-2.49	-2.61	-2.70	-2.76	-3.00	-2.96	-3.05	-3.14	-3.24	-3.32	-3.41	-3.50	-3.60	-3.69	-3.77	-3.86
55	-1.68	-1.76	-1.85	-1.89	-1.98	-1.87	-1.95	-2.02	-2.10	-2.18	-2.27	-2.34	-2.42	-2.69	-2.89	-2.86	-2.93
56	-1.10	-1.16	-1.23	-1.29	-1.33	-1.43	-1.47	-1.57	-1.61	-1.69	-1.75	-1.82	-1.88	-1.95	-1.93	-1.98	-2.05
57	-0.71	-0.75	-0.74	-0.78	-0.82	-0.86	-0.96	-1.01	-1.00	-1.05	-1.10	-1.15	-1.20	-1.25	-1.30	-1.35	-1.40
58	-0.45	-0.48	-0.50	-0.53	-0.56	-0.57	-0.62	-0.65	-0.67	-0.72	-0.75	-0.76	-0.80	-0.83	-0.89	-0.93	-0.97
59	-0.25	-0.26	-0.28	-0.29	-0.31	-0.33	-0.34	-0.36	-0.38	-0.40	-0.42	-0.44	-0.46	-0.48	-0.50	-0.52	-0.55

Table B.4 4D Secondary Phase (#1) Matrix Constructed from the Experimental Results for Global Optimization Method (0-16 A).

This is the experimental data matrix set developed using the raw machine data for the low current region of the electromagnetic characteristics in terms of torque contribution of the up-coming phase (secondary phase # 1) vs. excitation current(A) in the secondary phase and the active position (θ°) of the rotor close to the primary phase stator. The position of the upcoming secondary rotor with respect to the secondary phase stator, $\left(\phi_1 = \theta - 15^{o}\right)$.

Angle (θ°) / Current(A)	0	1	2	3	4	5	6	7	8	9	10	11	12	13	14	15	16
0	0.00	0.00	0.02	0.04	0.07	0.12	0.17	0.23	0.29	0.37	0.46	0.55	0.66	0.77	0.87	0.98	1.11
1	0.00	0.00	0.02	0.04	0.07	0.12	0.17	0.23	0.29	0.37	0.46	0.55	0.65	0.77	0.86	0.99	1.10
2	0.00	0.00	0.02	0.04	0.07	0.12	0.17	0.23	0.29	0.37	0.46	0.55	0.66	0.77	0.87	0.98	1.13
3	0.00	0.00	0.02	0.04	0.07	0.11	0.15	0.21	0.27	0.34	0.45	0.51	0.61	0.72	0.82	0.93	1.10
4	0.00	0.00	0.02	0.04	0.07	0.11	0.16	0.22	0.29	0.37	0.46	0.55	0.66	0.77	0.86	0.98	1.09
5	0.00	0.00	0.02	0.04	0.07	0.11	0.16	0.22	0.28	0.36	0.45	0.54	0.65	0.76	0.85	0.96	1.07
6	0.00	0.00	0.02	0.04	0.07	0.11	0.16	0.22	0.29	0.37	0.45	0.54	0.65	0.76	0.85	0.96	1.07
7	0.00	0.00	0.02	0.04	0.07	0.11	0.16	0.21	0.28	0.35	0.44	0.53	0.63	0.76	0.84	0.94	1.04
8	0.00	0.00	0.02	0.04	0.07	0.11	0.15	0.21	0.27	0.35	0.43	0.52	0.61	0.73	0.83	0.93	1.06
9	0.00	0.00	0.02	0.04	0.07	0.10	0.15	0.20	0.27	0.34	0.42	0.50	0.61	0.71	0.78	0.90	1.00
10	0.00	0.00	0.02	0.04	0.07	0.11	0.15	0.20	0.27	0.33	0.41	0.50	0.58	0.68	0.76	0.82	1.01
11	0.00	0.00	0.02	0.04	0.06	0.10	0.15	0.20	0.26	0.33	0.40	0.48	0.55	0.65	0.70	0.77	0.79
12	0.00	0.00	0.02	0.03	0.06	0.10	0.14	0.19	0.25	0.31	0.38	0.45	0.51	0.62	0.66	0.68	0.81
13	0.00	0.00	0.01	0.03	0.05	0.08	0.12	0.16	0.21	0.27	0.33	0.39	0.44	0.53	0.50	0.56	0.58
14	0.00	0.00	0.01	0.01	0.03	0.04	0.06	0.08	0.11	0.13	0.16	0.19	0.22	0.26	0.25	0.26	0.28
15	0.00	0.00	0.00	0.00	0.00	0.00	0.00	0.00	0.00	0.00	0.00	0.00	0.00	0.00	0.00	0.00	0.00
16	0.00	0.00	-0.01	-0.01	-0.03	-0.04	-0.06	-0.08	-0.11	-0.13	-0.16	-0.19	-0.22	-0.26	-0.25	-0.26	-0.28
17	0.00	0.00	-0.01	-0.03	-0.05	-0.08	-0.12	-0.16	-0.21	-0.27	-0.33	-0.39	-0.44	-0.53	-0.50	-0.56	-0.58
18	0.00	0.00	-0.02	-0.03	-0.06	-0.10	-0.14	-0.19	-0.25	-0.31	-0.38	-0.45	-0.51	-0.62	-0.66	-0.68	-0.81
19	0.00	0.00	-0.02	-0.04	-0.06	-0.10	-0.15	-0.20	-0.26	-0.33	-0.40	-0.48	-0.55	-0.65	-0.70	-0.77	-0.79
20	0.00	0.00	-0.02	-0.04	-0.07	-0.11	-0.15	-0.20	-0.27	-0.33	-0.41	-0.50	-0.58	-0.68	-0.76	-0.82	-1.01
21	0.00	0.00	-0.02	-0.04	-0.07	-0.10	-0.15	-0.20	-0.27	-0.34	-0.42	-0.50	-0.61	-0.71	-0.78	-0.90	-1.00
22	0.00	0.00	-0.02	-0.04	-0.07	-0.11	-0.15	-0.21	-0.27	-0.35	-0.43	-0.52	-0.61	-0.73	-0.83	-0.93	-1.06
23	0.00	0.00	-0.02	-0.04	-0.07	-0.11	-0.16	-0.21	-0.28	-0.35	-0.44	-0.53	-0.63	-0.76	-0.84	-0.94	-1.04
24	0.00	0.00	-0.02	-0.04	-0.07	-0.11	-0.16	-0.22	-0.29	-0.37	-0.45	-0.54	-0.65	-0.76	-0.85	-0.96	-1.07
25	0.00	0.00	-0.02	-0.04	-0.07	-0.11	-0.16	-0.22	-0.28	-0.36	-0.45	-0.54	-0.65	-0.76	-0.85	-0.96	-1.07
26	0.00	0.00	-0.02	-0.04	-0.07	-0.11	-0.16	-0.22	-0.29	-0.37	-0.46	-0.55	-0.66	-0.77	-0.86	-0.98	-1.09
27	0.00	0.00	-0.02	-0.04	-0.07	-0.12	-0.17	-0.23	-0.29	-0.37	-0.46	-0.55	-0.66	-0.77	-0.87	-0.98	-1.13
28	0.00	0.00	-0.02	-0.04	-0.07	-0.11	-0.15	-0.21	-0.27	-0.34	-0.45	-0.51	-0.61	-0.72	-0.82	-0.93	-1.10
29	0.00	0.00	-0.02	-0.04	-0.07	-0.12	-0.17	-0.23	-0.29	-0.37	-0.46	-0.55	-0.65	-0.77	-0.86	-0.99	-1.10
30	0.00	0.00	-0.02	-0.04	-0.07	-0.12	-0.17	-0.23	-0.29	-0.37	-0.46	-0.55	-0.66	-0.77	-0.87	-0.98	-1.11
31	0.00	0.00	-0.02	-0.04	-0.07	-0.11	-0.16	-0.22	-0.29	-0.37	-0.46	-0.56	-0.65	-0.77	-0.86	-0.98	-1.09
32	0.00	0.00	-0.02	-0.04	-0.07	-0.12	-0.17	-0.23	-0.30	-0.38	-0.46	-0.56	-0.66	-0.77	-0.87	-0.99	-1.11
33	0.00	0.00	-0.02	-0.04	-0.07	-0.12	-0.17	-0.23	-0.29	-0.37	-0.46	-0.56	-0.65	-0.76	-0.86	-0.97	-1.09
34	0.00	0.00	-0.02	-0.04	-0.07	-0.11	-0.17	-0.22	-0.29	-0.37	-0.46	-0.55	-0.65	-0.75	-0.87	-0.98	-1.08
35	0.00	0.00	-0.02	-0.04	-0.07	-0.11	-0.16	-0.22	-0.29	-0.38	-0.46	-0.55	-0.65	-0.76	-0.87	-0.96	-1.07

36	0.00	0.00	-0.02	-0.04	-0.07	-0.11	-0.16	-0.22	-0.29	-0.38	-0.46	-0.55	-0.65	-0.76	-0.86	-0.99	-1.11
37	0.00	0.00	-0.02	-0.04	-0.07	-0.11	-0.16	-0.22	-0.29	-0.38	-0.45	-0.55	-0.65	-0.76	-0.87	-1.00	-1.12
38	0.00	0.00	-0.02	-0.04	-0.07	-0.11	-0.16	-0.21	-0.28	-0.36	-0.43	-0.52	-0.62	-0.72	-0.82	-0.93	-1.04
39	0.00	0.00	-0.01	-0.02	-0.04	-0.06	-0.09	-0.13	-0.17	-0.22	-0.26	-0.31	-0.37	-0.44	-0.51	-0.58	-0.66
40	0.00	0.00	-0.01	-0.01	-0.02	-0.04	-0.05	-0.07	-0.10	-0.13	-0.15	-0.18	-0.22	-0.26	-0.30	-0.34	-0.39
41	0.00	0.00	0.00	-0.01	-0.02	-0.02	-0.03	-0.05	-0.06	-0.08	-0.10	-0.12	-0.14	-0.16	-0.19	-0.22	-0.24
42	0.00	0.00	0.00	-0.01	-0.01	-0.02	-0.02	-0.03	-0.04	-0.05	-0.06	-0.07	-0.09	-0.10	-0.12	-0.14	-0.16
43	0.00	0.00	0.00	0.00	-0.01	-0.01	-0.01	-0.02	-0.02	-0.03	-0.04	-0.05	-0.06	-0.07	-0.08	-0.09	-0.10
44	0.00	0.00	0.00	0.00	0.00	-0.01	-0.01	-0.01	-0.01	-0.02	-0.02	-0.03	-0.03	-0.04	-0.04	-0.05	-0.06
45	0.00	0.00	0.00	0.00	0.00	0.00	0.00	0.00	0.00	0.01	0.01	0.01	0.01	0.01	0.01	0.02	0.02
46	0.00	0.00	0.00	0.00	0.00	0.01	0.01	0.01	0.01	0.02	0.02	0.03	0.03	0.04	0.04	0.05	0.06
47	0.00	0.00	0.00	0.00	0.01	0.01	0.01	0.02	0.02	0.03	0.04	0.05	0.06	0.07	0.08	0.09	0.10
48	0.00	0.00	0.00	0.01	0.01	0.02	0.02	0.03	0.04	0.05	0.06	0.07	0.09	0.10	0.12	0.14	0.16
49	0.00	0.00	0.00	0.01	0.02	0.02	0.03	0.05	0.06	0.08	0.10	0.12	0.14	0.16	0.19	0.22	0.24
50	0.00	0.00	0.01	0.01	0.02	0.04	0.05	0.07	0.10	0.13	0.15	0.18	0.22	0.26	0.30	0.34	0.39
51	0.00	0.00	0.01	0.02	0.04	0.06	0.09	0.13	0.17	0.22	0.26	0.31	0.37	0.44	0.51	0.58	0.66
52	0.00	0.00	0.02	0.04	0.07	0.11	0.16	0.21	0.28	0.36	0.43	0.52	0.62	0.72	0.82	0.93	1.04
53	0.00	0.00	0.02	0.04	0.073	0.11	0.16	0.22	0.29	0.38	0.45	0.55	0.65	0.76	0.87	1.00	1.12
54	0.00	0.00	0.02	0.04	0.07	0.11	0.16	0.22	0.29	0.38	0.46	0.55	0.65	0.76	0.86	0.99	1.11
55	0.00	0.00	0.02	0.04	0.07	0.11	0.16	0.22	0.29	0.38	0.46	0.55	0.65	0.76	0.87	0.96	1.07
56	0.00	0.00	0.02	0.04	0.07	0.11	0.17	0.22	0.29	0.37	0.46	0.55	0.65	0.75	0.87	0.98	1.08
57	0.00	0.00	0.02	0.04	0.07	0.12	0.17	0.23	0.29	0.37	0.46	0.56	0.65	0.76	0.86	0.97	1.09
58	0.00	0.00	0.02	0.04	0.07	0.12	0.17	0.23	0.30	0.38	0.46	0.56	0.66	0.77	0.87	0.99	1.11
59	0.00	0.00	0.02	0.04	0.07	0.11	0.16	0.22	0.29	0.37	0.46	0.56	0.65	0.77	0.86	0.98	1.09

Table B.5 4D Secondary Phase (#1) Matrix Constructed from the Experimental Results for Global Optimization Method (17-33 A).

This is the experimental data matrix set developed using the raw machine data for the unsaturated region of the electromagnetic characteristics in terms of torque contribution of the up-coming phase (secondary phase # 1) vs. excitation current(A) in the secondary phase and the active position (θ°) of the rotor close to the primary phase stator. The position of the upcoming secondary rotor with respect to the secondary phase stator, $\left(\phi_1 = \theta - 15^{o}\right)$.

Angle (θ°)/ Current (A)	17	18	19	20	21	22	23	24	25	26	27	28	29	30	31	32	33
0	1.21	1.34	1.45	1.56	1.67	1.79	1.91	2.03	2.15	2.29	2.39	2.50	2.63	2.76	2.87	2.98	3.11
1	1.21	1.33	1.46	1.56	1.67	1.78	1.92	2.04	2.15	2.27	2.40	2.51	2.63	2.76	2.87	2.99	3.11
2	1.20	1.32	1.48	1.55	1.67	1.79	1.90	2.02	2.15	2.27	2.39	2.49	2.61	2.72	2.83	2.94	3.06
3	1.20	1.32	1.40	1.52	1.64	1.76	1.88	2.00	2.12	2.24	2.36	2.50	2.59	2.72	2.83	2.94	3.06
4	1.24	1.31	1.42	1.54	1.66	1.80	1.91	2.02	2.13	2.25	2.36	2.46	2.58	2.69	2.80	2.91	3.01
5	1.18	1.29	1.41	1.54	1.63	1.76	1.87	1.98	2.10	2.20	2.30	2.41	2.52	2.64	2.73	2.82	2.92
6	1.18	1.32	1.49	1.52	1.61	1.72	1.86	1.95	2.07	2.14	2.25	2.35	2.45	2.55	2.65	2.74	2.84
7	1.14	1.25	1.38	1.47	1.57	1.68	1.79	1.86	1.99	2.07	2.15	2.25	2.34	2.44	2.53	2.62	2.71
8	1.15	1.24	1.37	1.41	1.57	1.60	1.69	1.78	1.87	1.98	2.02	2.11	2.20	2.30	2.37	2.46	2.55
9	1.10	1.16	1.31	1.34	1.38	1.47	1.57	1.70	1.74	1.79	1.88	1.95	2.03	2.13	2.18	2.25	2.31
10	1.10	1.15	1.22	1.31	1.27	1.35	1.44	1.56	1.56	1.63	1.70	1.76	1.83	1.88	1.93	1.98	2.03
11	0.90	0.93	1.13	1.08	1.14	1.21	1.42	1.30	1.35	1.41	1.45	1.50	1.54	1.59	1.62	1.66	1.70
12	0.81	0.88	0.95	0.99	0.97	1.08	1.01	1.07	1.12	1.13	1.18	1.20	1.23	1.26	1.28	1.31	1.33
13	0.67	0.69	0.80	0.74	0.77	0.75	0.77	0.79	0.81	0.82	0.85	0.86	0.88	0.89	0.91	0.93	0.94
14	0.30	0.32	0.33	0.33	0.32	0.33	0.33	0.34	0.35	0.36	0.36	0.36	0.37	0.38	0.38	0.39	0.39
15	0.00	0.00	0.00	0.00	0.00	0.00	0.00	0.00	0.00	0.00	0.00	0.00	0.00	0.00	0.00	0.00	0.00
16	-0.30	-0.32	-0.33	-0.33	-0.32	-0.33	-0.33	-0.34	-0.35	-0.36	-0.36	-0.36	-0.37	-0.38	-0.38	-0.39	-0.39
17	-0.67	-0.69	-0.80	-0.74	-0.77	-0.75	-0.77	-0.79	-0.81	-0.82	-0.85	-0.86	-0.88	-0.89	-0.91	-0.93	-0.94
18	-0.81	-0.88	-0.95	-0.99	-0.97	-1.08	-1.01	-1.07	-1.12	-1.13	-1.18	-1.20	-1.23	-1.26	-1.28	-1.31	-1.33
19	-0.90	-0.93	-1.13	-1.08	-1.14	-1.21	-1.42	-1.30	-1.35	-1.41	-1.45	-1.50	-1.54	-1.59	-1.62	-1.66	-1.70
20	-1.10	-1.15	-1.22	-1.31	-1.27	-1.35	-1.44	-1.56	-1.56	-1.63	-1.70	-1.76	-1.83	-1.88	-1.93	-1.98	-2.03
21	-1.10	-1.16	-1.31	-1.34	-1.38	-1.47	-1.57	-1.70	-1.74	-1.79	-1.88	-1.95	-2.03	-2.13	-2.18	-2.25	-2.31
22	-1.15	-1.24	-1.37	-1.41	-1.57	-1.60	-1.69	-1.78	-1.87	-1.98	-2.02	-2.11	-2.20	-2.30	-2.37	-2.46	-2.55
23	-1.14	-1.25	-1.38	-1.47	-1.57	-1.68	-1.79	-1.86	-1.99	-2.07	-2.15	-2.25	-2.34	-2.44	-2.53	-2.62	-2.71
24	-1.18	-1.32	-1.49	-1.52	-1.61	-1.72	-1.86	-1.95	-2.07	-2.14	-2.25	-2.35	-2.45	-2.55	-2.65	-2.74	-2.84
25	-1.18	-1.29	-1.41	-1.54	-1.63	-1.76	-1.87	-1.98	-2.10	-2.20	-2.30	-2.41	-2.52	-2.64	-2.73	-2.82	-2.92
26	-1.24	-1.31	-1.42	-1.54	-1.66	-1.80	-1.91	-2.02	-2.13	-2.25	-2.36	-2.46	-2.58	-2.69	-2.80	-2.91	-3.01
27	-1.20	-1.32	-1.48	-1.55	-1.67	-1.79	-1.90	-2.02	-2.15	-2.27	-2.39	-2.49	-2.61	-2.72	-2.83	-2.94	-3.06
28	-1.20	-1.32	-1.40	-1.52	-1.64	-1.76	-1.88	-2.00	-2.12	-2.24	-2.36	-2.50	-2.59	-2.72	-2.83	-2.94	-3.06
29	-1.21	-1.33	-1.46	-1.56	-1.67	-1.78	-1.92	-2.04	-2.15	-2.27	-2.40	-2.51	-2.63	-2.76	-2.87	-2.99	-3.11
30	-1.21	-1.34	-1.45	-1.56	-1.67	-1.79	-1.91	-2.03	-2.15	-2.29	-2.39	-2.50	-2.63	-2.76	-2.87	-2.98	-3.11
31	-1.20	-1.31	-1.44	-1.57	-1.66	-1.77	-1.90	-2.02	-2.14	-2.26	-2.38	-2.48	-2.62	-2.73	-2.85	-2.97	-3.09
32	-1.21	-1.32	-1.44	-1.56	-1.67	-1.82	-1.91	-2.02	-2.16	-2.26	-2.38	-2.49	-2.61	-2.73	-2.85	-2.96	-3.08
33	-1.21	-1.33	-1.46	-1.54	-1.65	-1.77	-1.88	-1.99	-2.11	-2.26	-2.34	-2.45	-2.57	-2.69	-2.80	-2.92	-3.03
34	-1.19	-1.32	-1.41	-1.52	-1.64	-1.75	-1.86	-1.98	-2.10	-2.22	-2.31	-2.44	-2.54	-2.66	-2.77	-2.89	-3.00
35	-1.19	-1.28	-1.42	-1.51	-1.62	-1.73	-1.86	-1.95	-2.07	-2.18	-2.29	-2.40	-2.51	-2.62	-2.74	-2.85	-2.96
36	-1.18	-1.30	-1.41	-1.52	-1.61	-1.75	-1.84	-1.93	-2.04	-2.15	-2.26	-2.36	-2.47	-2.58	-2.69	-2.80	-2.91

37	-1.25	-1.38	-1.43	-1.54	-1.64	-1.75	-1.86	-1.94	-2.04	-2.15	-2.25	-2.35	-2.46	-2.56	-2.66	-2.77	-2.87
38	-1.16	-1.28	-1.40	-1.52	-1.64	-1.78	-1.88	-1.92	-2.02	-2.12	-2.22	-2.32	-2.42	-2.52	-2.61	-2.71	-2.81
39	-0.74	-0.83	-0.92	-1.01	-1.11	-1.21	-1.32	-1.41	-1.51	-1.62	-1.72	-1.83	-1.93	-2.03	-2.12	-2.22	-2.31
40	-0.44	-0.49	-0.55	-0.60	-0.67	-0.73	-0.79	-0.87	-0.94	-1.01	-1.09	-1.17	-1.25	-1.33	-1.42	-1.50	-1.59
41	-0.28	-0.31	-0.35	-0.38	-0.42	-0.46	-0.51	-0.55	-0.59	-0.64	-0.69	-0.74	-0.80	-0.86	-0.91	-0.97	-1.03
42	-0.18	-0.20	-0.22	-0.25	-0.27	-0.30	-0.33	-0.36	-0.39	-0.42	-0.45	-0.48	-0.52	-0.55	-0.59	-0.63	-0.67
43	-0.11	-0.13	-0.14	-0.16	-0.17	-0.19	-0.21	-0.22	-0.24	-0.26	-0.28	-0.31	-0.33	-0.35	-0.37	-0.40	-0.42
44	-0.06	-0.07	-0.08	-0.09	-0.09	-0.10	-0.11	-0.12	-0.13	-0.15	-0.16	-0.17	-0.18	-0.19	-0.21	-0.22	-0.23
45	0.02	0.02	0.03	0.03	0.03	0.03	0.04	0.04	0.04	0.05	0.05	0.06	0.06	0.06	0.07	0.07	0.08
46	0.06	0.07	0.08	0.09	0.09	0.10	0.11	0.12	0.13	0.15	0.16	0.17	0.18	0.19	0.21	0.22	0.23
47	0.11	0.13	0.14	0.16	0.17	0.19	0.21	0.22	0.24	0.26	0.28	0.31	0.33	0.35	0.37	0.40	0.42
48	0.18	0.20	0.22	0.25	0.27	0.30	0.33	0.36	0.39	0.42	0.45	0.48	0.52	0.55	0.59	0.63	0.67
49	0.28	0.31	0.35	0.38	0.42	0.46	0.51	0.55	0.59	0.64	0.69	0.74	0.80	0.86	0.91	0.97	1.03
50	0.44	0.49	0.55	0.60	0.67	0.73	0.79	0.87	0.94	1.01	1.09	1.17	1.25	1.33	1.42	1.50	1.59
51	0.74	0.83	0.92	1.01	1.11	1.21	1.32	1.41	1.51	1.62	1.72	1.83	1.93	2.03	2.12	2.22	2.31
52	1.16	1.28	1.40	1.52	1.64	1.78	1.88	1.92	2.02	2.12	2.22	2.32	2.42	2.52	2.61	2.71	2.81
53	1.25	1.38	1.43	1.54	1.64	1.75	1.86	1.94	2.04	2.15	2.25	2.35	2.46	2.56	2.66	2.77	2.87
54	1.18	1.30	1.41	1.52	1.61	1.75	1.84	1.93	2.04	2.15	2.26	2.36	2.47	2.58	2.69	2.80	2.91
55	1.19	1.28	1.42	1.51	1.62	1.73	1.86	1.95	2.07	2.18	2.29	2.40	2.51	2.62	2.74	2.85	2.96
56	1.19	1.32	1.41	1.52	1.64	1.75	1.86	1.98	2.10	2.22	2.31	2.44	2.54	2.66	2.77	2.89	3.00
57	1.21	1.33	1.46	1.54	1.65	1.77	1.88	1.99	2.11	2.26	2.34	2.45	2.57	2.69	2.80	2.92	3.03
58	1.21	1.32	1.44	1.56	1.67	1.82	1.91	2.02	2.16	2.26	2.38	2.49	2.61	2.73	2.85	2.96	3.08
59	1.20	1.31	1.44	1.57	1.66	1.77	1.90	2.02	2.14	2.26	2.38	2.48	2.62	2.73	2.85	2.97	3.09

Table B.6 4D Secondary Phase (#1) Matrix Constructed from the Experimental Results for Global Optimization Method (34-50 A).

This is the experimental data matrix set developed using the raw machine data for the saturation region of the electromagnetic characteristics in terms of torque contribution of the up-coming phase (secondary phase # 1) vs. excitation current(A) in the secondary phase and the active position (θ°) of the rotor close to the primary phase stator. The position of the upcoming secondary rotor with respect to the secondary phase stator, $\left(\phi_1 = \theta - 15^{o}\right)$.

Angle (θ°)/ Current (A)	34	35	36	37	38	39	40	41	42	43	44	45	46	47	48	49	50
0	3.22	3.34	3.46	3.57	3.69	3.81	3.92	4.03	4.15	4.26	4.36	4.47	4.59	4.69	4.80	4.90	5.01
1	3.24	3.34	3.45	3.56	3.68	3.78	3.89	4.01	4.12	4.21	4.33	4.43	4.54	4.65	4.75	4.85	4.96
2	3.18	3.28	3.38	3.49	3.60	3.70	3.81	3.91	4.01	4.12	4.22	4.32	4.42	4.51	4.61	4.71	4.80
3	3.17	3.28	3.39	3.47	3.58	3.70	3.79	3.90	4.01	4.06	4.16	4.27	4.37	4.47	4.57	4.66	4.76
4	3.12	3.22	3.33	3.45	3.53	3.64	3.74	3.84	3.94	4.03	4.13	4.22	4.32	4.41	4.51	4.60	4.69
5	3.04	3.13	3.23	3.33	3.43	3.53	3.62	3.72	3.81	3.90	4.00	4.09	4.18	4.26	4.34	4.42	4.50
6	2.95	3.03	3.13	3.22	3.32	3.41	3.50	3.58	3.67	3.75	3.83	3.91	3.98	4.04	4.11	4.17	4.23
7	2.80	2.89	2.98	3.06	3.15	3.23	3.31	3.37	3.44	3.51	3.57	3.62	3.68	3.74	3.79	3.84	3.89
8	2.63	2.70	2.78	2.84	2.91	2.97	3.02	3.08	3.13	3.18	3.24	3.28	3.33	3.38	3.42	3.47	3.51
9	2.38	2.43	2.49	2.54	2.59	2.64	2.68	2.73	2.77	2.81	2.85	2.89	2.93	2.97	3.01	3.05	3.09
10	2.08	2.12	2.16	2.20	2.24	2.28	2.32	2.35	2.39	2.42	2.46	2.49	2.53	2.56	2.59	2.62	2.66
11	1.73	1.77	1.80	1.83	1.86	1.89	1.92	1.95	1.98	2.01	2.04	2.07	2.09	2.12	2.15	2.17	2.20
12	1.36	1.38	1.41	1.43	1.45	1.48	1.50	1.52	1.54	1.56	1.59	1.61	1.63	1.65	1.67	1.69	1.71
13	0.96	0.97	0.99	1.00	1.02	1.03	1.05	1.06	1.07	1.09	1.10	1.11	1.13	1.14	1.15	1.16	1.18
14	0.40	0.40	0.41	0.41	0.42	0.42	0.43	0.43	0.44	0.44	0.45	0.45	0.46	0.46	0.46	0.47	0.47
15	0.00	0.00	0.00	0.00	0.00	0.00	0.00	0.00	0.00	0.00	0.00	0.00	0.00	0.00	0.00	0.00	0.00
16	-0.40	-0.40	-0.41	-0.41	-0.42	-0.42	-0.43	-0.43	-0.44	-0.44	-0.45	-0.45	-0.46	-0.46	-0.46	-0.47	-0.47
17	-0.96	-0.97	-0.99	-1.00	-1.02	-1.03	-1.05	-1.06	-1.07	-1.09	-1.10	-1.11	-1.13	-1.14	-1.15	-1.16	-1.18
18	-1.36	-1.38	-1.41	-1.43	-1.45	-1.48	-1.50	-1.52	-1.54	-1.56	-1.59	-1.61	-1.63	-1.65	-1.67	-1.69	-1.71
19	-1.73	-1.77	-1.80	-1.83	-1.86	-1.89	-1.92	-1.95	-1.98	-2.01	-2.04	-2.07	-2.09	-2.12	-2.15	-2.17	-2.20
20	-2.08	-2.12	-2.16	-2.20	-2.24	-2.28	-2.32	-2.35	-2.39	-2.42	-2.46	-2.49	-2.53	-2.56	-2.59	-2.62	-2.66
21	-2.38	-2.43	-2.49	-2.54	-2.59	-2.64	-2.68	-2.73	-2.77	-2.81	-2.85	-2.89	-2.93	-2.97	-3.01	-3.05	-3.09
22	-2.63	-2.70	-2.78	-2.84	-2.91	-2.97	-3.02	-3.08	-3.13	-3.18	-3.24	-3.28	-3.33	-3.38	-3.42	-3.47	-3.51
23	-2.80	-2.89	-2.98	-3.06	-3.15	-3.23	-3.31	-3.37	-3.44	-3.51	-3.57	-3.62	-3.68	-3.74	-3.79	-3.84	-3.89
24	-2.95	-3.03	-3.13	-3.22	-3.32	-3.41	-3.50	-3.58	-3.67	-3.75	-3.83	-3.91	-3.98	-4.04	-4.11	-4.17	-4.23
25	-3.04	-3.13	-3.23	-3.33	-3.43	-3.53	-3.62	-3.72	-3.81	-3.90	-4.00	-4.09	-4.18	-4.26	-4.34	-4.42	-4.50
26	-3.12	-3.22	-3.33	-3.45	-3.53	-3.64	-3.74	-3.84	-3.94	-4.03	-4.13	-4.22	-4.32	-4.41	-4.51	-4.60	-4.69
27	-3.18	-3.28	-3.38	-3.49	-3.60	-3.70	-3.81	-3.91	-4.01	-4.12	-4.22	-4.32	-4.42	-4.51	-4.61	-4.71	-4.81

28	-3.17	-3.28	-3.39	-3.47	-3.58	-3.70	-3.79	-3.90	-4.01	-4.06	-4.16	-4.27	-4.37	-4.47	-4.57	-4.66	-4.76
29	-3.24	-3.34	-3.45	-3.56	-3.68	-3.78	-3.89	-4.01	-4.12	-4.21	-4.33	-4.43	-4.54	-4.65	-4.75	-4.85	-4.98
30	-3.22	-3.34	-3.46	-3.57	-3.69	-3.81	-3.92	-4.03	-4.15	-4.26	-4.36	-4.47	-4.59	-4.69	-4.80	-4.90	-5.01
31	-3.21	-3.32	-3.44	-3.56	-3.68	-3.79	-3.91	-4.03	-4.14	-4.25	-4.38	-4.48	-4.59	-4.71	-4.82	-4.93	-5.04
32	-3.20	-3.31	-3.43	-3.55	-3.67	-3.78	-3.89	-4.02	-4.13	-4.24	-4.36	-4.47	-4.59	-4.70	-4.81	-4.92	-5.03
33	-3.15	-3.26	-3.38	-3.49	-3.61	-3.72	-3.84	-3.95	-4.06	-4.18	-4.29	-4.40	-4.51	-4.64	-4.74	-4.85	-4.96
34	-3.11	-3.23	-3.34	-3.45	-3.56	-3.68	-3.79	-3.90	-4.02	-4.13	-4.24	-4.35	-4.46	-4.57	-4.68	-4.92	-4.90
35	-3.07	-3.18	-3.29	-3.39	-3.51	-3.62	-3.73	-3.84	-3.95	-4.06	-4.17	-4.28	-4.38	-4.49	-4.60	-4.72	-4.82
36	-3.01	-3.12	-3.22	-3.33	-3.45	-3.55	-3.65	-3.76	-3.87	-3.98	-4.08	-4.18	-4.29	-4.40	-4.50	-4.61	-4.72
37	-2.97	-3.08	-3.19	-3.31	-3.40	-3.50	-3.63	-3.73	-3.80	-3.93	-4.01	-4.18	-4.22	-4.32	-4.42	-4.57	-4.62
38	-2.91	-3.01	-3.10	-3.23	-3.33	-3.43	-3.53	-3.63	-3.74	-3.79	-3.88	-3.98	-4.08	-4.18	-4.28	-4.37	-4.46
39	-2.40	-2.49	-2.61	-2.70	-2.76	-3.00	-2.96	-3.05	-3.14	-3.24	-3.32	-3.41	-3.50	-3.60	-3.69	-3.77	-3.86
40	-1.68	-1.76	-1.85	-1.89	-1.98	-1.87	-1.95	-2.02	-2.10	-2.18	-2.27	-2.34	-2.42	-2.69	-2.89	-2.86	-2.93
41	-1.10	-1.16	-1.23	-1.29	-1.33	-1.43	-1.47	-1.57	-1.61	-1.69	-1.75	-1.82	-1.88	-1.95	-1.93	-1.98	-2.05
42	-0.71	-0.75	-0.74	-0.78	-0.82	-0.86	-0.96	-1.01	-1.00	-1.05	-1.10	-1.15	-1.20	-1.25	-1.30	-1.35	-1.40
43	-0.45	-0.48	-0.50	-0.53	-0.56	-0.57	-0.62	-0.65	-0.67	-0.72	-0.75	-0.76	-0.80	-0.83	-0.89	-0.93	-0.97
44	-0.25	-0.26	-0.28	-0.29	-0.31	-0.33	-0.34	-0.36	-0.38	-0.40	-0.42	-0.44	-0.46	-0.48	-0.50	-0.52	-0.55
45	0.08	0.09	0.09	0.10	0.10	0.11	0.11	0.12	0.13	0.13	0.14	0.14	0.15	0.16	0.16	0.17	0.18
46	0.25	0.26	0.28	0.29	0.31	0.33	0.34	0.36	0.38	0.40	0.42	0.44	0.46	0.48	0.50	0.52	0.55
47	0.45	0.48	0.50	0.53	0.56	0.57	0.62	0.65	0.67	0.72	0.75	0.76	0.80	0.83	0.89	0.93	0.97
48	0.71	0.75	0.74	0.78	0.82	0.86	0.96	1.01	1.00	1.05	1.10	1.15	1.20	1.25	1.30	1.35	1.40
49	1.10	1.16	1.23	1.29	1.33	1.43	1.47	1.57	1.61	1.69	1.75	1.82	1.88	1.95	1.93	1.98	2.05
50	1.68	1.76	1.85	1.89	1.98	1.87	1.95	2.02	2.10	2.18	2.27	2.34	2.42	2.69	2.58	2.86	2.93
51	2.40	2.49	2.61	2.70	2.76	3.00	2.96	3.05	3.14	3.24	3.32	3.41	3.50	3.60	3.69	3.77	3.86
52	2.91	3.01	3.10	3.23	3.33	3.43	3.53	3.63	3.74	3.79	3.88	3.98	4.08	4.18	4.28	4.37	4.46
53	2.97	3.08	3.19	3.31	3.40	3.50	3.63	3.73	3.80	3.93	4.01	4.18	4.22	4.32	4.42	4.57	4.62
54	3.01	3.12	3.22	3.33	3.45	3.55	3.65	3.76	3.87	3.98	4.08	4.18	4.29	4.40	4.50	4.61	4.72
55	3.07	3.18	3.29	3.39	3.51	3.62	3.73	3.84	3.95	4.06	4.17	4.28	4.38	4.49	4.60	4.72	4.82
56	3.11	3.23	3.34	3.45	3.56	3.68	3.79	3.90	4.02	4.13	4.24	4.35	4.46	4.57	4.68	4.79	4.90
57	3.15	3.26	3.38	3.49	3.61	3.72	3.84	3.95	4.06	4.18	4.29	4.40	4.51	4.64	4.74	4.85	4.96
58	3.20	3.31	3.43	3.55	3.67	3.78	3.89	4.02	4.13	4.24	4.36	4.47	4.59	4.70	4.81	4.92	5.03
59	3.21	3.32	3.44	3.56	3.68	3.79	3.91	4.03	4.14	4.25	4.38	4.48	4.59	4.71	4.82	4.93	5.04

Table B.7 4D Secondary Phase (#2) Matrix Constructed from the Experimental Results for Global Optimization Method (0-16 A).

This is the experimental data matrix set developed using the raw machine data for the low current region of the electromagnetic characteristics in terms of torque contribution of the out-going phase (secondary phase (# 2) vs. excitation current(A) in this secondary phase and the active position (θ°) of the rotor close to the primary phase stator . The position of the out-going secondary rotor with respect to the secondary phase stator, $\left(\phi_2 = \theta + 15^o\right)$.

Angle (θ°) / Current(A)	0	1	2	3	4	5	6	7	8	9	10	11	12	13	14	15	16
1	0.00	0.00	-0.02	-0.04	-0.07	-0.12	-0.17	-0.23	-0.29	-0.37	-0.46	-0.55	-0.66	-0.77	-0.87	-0.98	-1.11
2	0.00	0.00	-0.02	-0.04	-0.07	-0.11	-0.16	-0.22	-0.29	-0.37	-0.46	-0.56	-0.65	-0.77	-0.86	-0.98	-1.09
3	0.00	0.00	-0.02	-0.04	-0.07	-0.12	-0.17	-0.23	-0.30	-0.38	-0.46	-0.56	-0.66	-0.77	-0.87	-0.99	-1.11
4	0.00	0.00	-0.02	-0.04	-0.07	-0.12	-0.17	-0.23	-0.29	-0.37	-0.46	-0.56	-0.65	-0.76	-0.86	-0.97	-1.09
5	0.00	0.00	-0.02	-0.04	-0.07	-0.11	-0.17	-0.22	-0.29	-0.37	-0.46	-0.55	-0.65	-0.75	-0.87	-0.98	-1.08
6	0.00	0.00	-0.02	-0.04	-0.07	-0.11	-0.16	-0.22	-0.29	-0.38	-0.46	-0.55	-0.65	-0.76	-0.87	-0.96	-1.07
7	0.00	0.00	-0.02	-0.04	-0.07	-0.11	-0.16	-0.22	-0.29	-0.38	-0.46	-0.55	-0.65	-0.76	-0.86	-0.99	-1.11
8	0.00	0.00	-0.02	-0.04	-0.07	-0.11	-0.16	-0.22	-0.29	-0.38	-0.45	-0.55	-0.65	-0.76	-0.87	-1.00	-1.12
9	0.00	0.00	-0.02	-0.04	-0.07	-0.11	-0.16	-0.21	-0.28	-0.36	-0.43	-0.52	-0.62	-0.72	-0.82	-0.93	-1.04
10	0.00	0.00	-0.01	-0.02	-0.04	-0.06	-0.09	-0.13	-0.17	-0.22	-0.26	-0.31	-0.37	-0.44	-0.51	-0.58	-0.66
11	0.00	0.00	-0.01	-0.01	-0.02	-0.04	-0.05	-0.07	-0.10	-0.13	-0.15	-0.18	-0.22	-0.26	-0.30	-0.34	-0.39
12	0.00	0.00	0.00	-0.01	-0.02	-0.02	-0.03	-0.05	-0.06	-0.08	-0.10	-0.12	-0.14	-0.16	-0.19	-0.22	-0.24
13	0.00	0.00	0.00	-0.01	-0.01	-0.02	-0.02	-0.03	-0.04	-0.05	-0.06	-0.07	-0.09	-0.10	-0.12	-0.14	-0.16
14	0.00	0.00	0.00	0.00	-0.01	-0.01	-0.01	-0.02	-0.02	-0.03	-0.04	-0.05	-0.06	-0.07	-0.08	-0.09	-0.10
15	0.00	0.00	0.00	0.00	0.00	-0.01	-0.01	-0.01	-0.01	-0.02	-0.02	-0.03	-0.03	-0.04	-0.04	-0.05	-0.06
16	0.00	0.00	0.00	0.00	0.00	0.00	0.00	0.00	0.00	0.01	0.01	0.01	0.01	0.01	0.01	0.02	0.02
17	0.00	0.00	0.00	0.00	0.00	0.01	0.01	0.01	0.01	0.02	0.02	0.03	0.03	0.04	0.04	0.05	0.06
18	0.00	0.00	0.00	0.00	0.01	0.01	0.01	0.02	0.02	0.03	0.04	0.05	0.06	0.07	0.08	0.09	0.10
19	0.00	0.00	0.00	0.01	0.01	0.02	0.02	0.03	0.04	0.05	0.06	0.07	0.09	0.10	0.12	0.14	0.16
20	0.00	0.00	0.00	0.01	0.02	0.02	0.03	0.05	0.06	0.08	0.10	0.12	0.14	0.16	0.19	0.22	0.24
21	0.00	0.00	0.01	0.01	0.02	0.04	0.05	0.07	0.10	0.13	0.15	0.18	0.22	0.26	0.30	0.34	0.39
22	0.00	0.00	0.01	0.02	0.04	0.06	0.09	0.13	0.17	0.22	0.26	0.31	0.37	0.44	0.51	0.58	0.66
23	0.00	0.00	0.02	0.04	0.07	0.11	0.16	0.21	0.28	0.36	0.43	0.52	0.62	0.72	0.82	0.93	1.04
24	0.00	0.00	0.02	0.04	0.073	0.11	0.16	0.22	0.29	0.38	0.45	0.55	0.65	0.76	0.87	1.00	1.12
25	0.00	0.00	0.02	0.04	0.07	0.11	0.16	0.22	0.29	0.38	0.46	0.55	0.65	0.76	0.86	0.99	1.11
26	0.00	0.00	0.02	0.04	0.07	0.11	0.16	0.22	0.29	0.38	0.46	0.55	0.65	0.76	0.87	0.96	1.07
27	0.00	0.00	0.02	0.04	0.07	0.11	0.17	0.22	0.29	0.37	0.46	0.55	0.65	0.75	0.87	0.98	1.08
28	0.00	0.00	0.02	0.04	0.07	0.12	0.17	0.23	0.29	0.37	0.46	0.56	0.65	0.76	0.86	0.97	1.09
29	0.00	0.00	0.02	0.04	0.07	0.12	0.17	0.23	0.30	0.38	0.46	0.56	0.66	0.77	0.87	0.99	1.11
30	0.00	0.00	0.02	0.04	0.07	0.11	0.16	0.22	0.29	0.37	0.46	0.56	0.65	0.77	0.86	0.98	1.09
31	0.00	0.00	0.02	0.04	0.07	0.12	0.17	0.23	0.29	0.37	0.46	0.55	0.66	0.77	0.87	0.98	1.11
32	0.00	0.00	0.02	0.04	0.07	0.12	0.17	0.23	0.29	0.37	0.46	0.55	0.65	0.77	0.86	0.99	1.10
33	0.00	0.00	0.02	0.04	0.07	0.12	0.17	0.23	0.29	0.37	0.46	0.55	0.66	0.77	0.87	0.98	1.13
34	0.00	0.00	0.02	0.04	0.07	0.11	0.15	0.21	0.27	0.34	0.45	0.51	0.61	0.72	0.82	0.93	1.10
35	0.00	0.00	0.02	0.04	0.07	0.11	0.16	0.22	0.29	0.37	0.46	0.55	0.66	0.77	0.86	0.98	1.09

36	0.00	0.00	0.02	0.04	0.07	0.11	0.16	0.22	0.28	0.36	0.45	0.54	0.65	0.76	0.85	0.96	1.07
37	0.00	0.00	0.02	0.04	0.07	0.11	0.16	0.22	0.29	0.37	0.45	0.54	0.65	0.76	0.85	0.96	1.07
38	0.00	0.00	0.02	0.04	0.07	0.11	0.16	0.21	0.28	0.35	0.44	0.53	0.63	0.76	0.84	0.94	1.04
39	0.00	0.00	0.02	0.04	0.07	0.11	0.15	0.21	0.27	0.35	0.43	0.52	0.61	0.73	0.83	0.93	1.06
40	0.00	0.00	0.02	0.04	0.07	0.10	0.15	0.20	0.27	0.34	0.42	0.50	0.61	0.71	0.78	0.90	1.00
41	0.00	0.00	0.02	0.04	0.07	0.11	0.15	0.20	0.27	0.33	0.41	0.50	0.58	0.68	0.76	0.82	1.01
42	0.00	0.00	0.02	0.04	0.06	0.10	0.15	0.20	0.26	0.33	0.40	0.48	0.55	0.65	0.70	0.77	0.79
43	0.00	0.00	0.02	0.03	0.06	0.10	0.14	0.19	0.25	0.31	0.38	0.45	0.51	0.62	0.66	0.68	0.81
44	0.00	0.00	0.01	0.03	0.05	0.08	0.12	0.16	0.21	0.27	0.33	0.39	0.44	0.53	0.50	0.56	0.58
45	0.00	0.00	0.01	0.01	0.03	0.04	0.06	0.08	0.11	0.13	0.16	0.19	0.22	0.26	0.25	0.26	0.28
46	0.00	0.00	0.00	0.00	0.00	0.00	0.00	0.00	0.00	0.00	0.00	0.00	0.00	0.00	0.00	0.00	0.00
47	0.00	0.00	-0.01	-0.01	-0.03	-0.04	-0.06	-0.08	-0.11	-0.13	-0.16	-0.19	-0.22	-0.26	-0.25	-0.26	-0.28
48	0.00	0.00	-0.01	-0.03	-0.05	-0.08	-0.12	-0.16	-0.21	-0.27	-0.33	-0.39	-0.44	-0.53	-0.50	-0.56	-0.58
49	0.00	0.00	-0.02	-0.03	-0.06	-0.10	-0.14	-0.19	-0.25	-0.31	-0.38	-0.45	-0.51	-0.62	-0.66	-0.68	-0.81
50	0.00	0.00	-0.02	-0.04	-0.06	-0.10	-0.15	-0.20	-0.26	-0.33	-0.40	-0.48	-0.55	-0.65	-0.70	-0.77	-0.79
51	0.00	0.00	-0.02	-0.04	-0.07	-0.11	-0.15	-0.20	-0.27	-0.33	-0.41	-0.50	-0.58	-0.68	-0.76	-0.82	-1.01
52	0.00	0.00	-0.02	-0.04	-0.07	-0.10	-0.15	-0.20	-0.27	-0.34	-0.42	-0.50	-0.61	-0.71	-0.78	-0.90	-1.00
53	0.00	0.00	-0.02	-0.04	-0.07	-0.11	-0.15	-0.21	-0.27	-0.35	-0.43	-0.52	-0.61	-0.73	-0.83	-0.93	-1.06
54	0.00	0.00	-0.02	-0.04	-0.07	-0.11	-0.16	-0.21	-0.28	-0.35	-0.44	-0.53	-0.63	-0.76	-0.84	-0.94	-1.04
55	0.00	0.00	-0.02	-0.04	-0.07	-0.11	-0.16	-0.22	-0.29	-0.37	-0.45	-0.54	-0.65	-0.76	-0.85	-0.96	-1.07
56	0.00	0.00	-0.02	-0.04	-0.07	-0.11	-0.16	-0.22	-0.28	-0.36	-0.45	-0.54	-0.65	-0.76	-0.85	-0.96	-1.07
57	0.00	0.00	-0.02	-0.04	-0.07	-0.11	-0.16	-0.22	-0.29	-0.37	-0.46	-0.55	-0.66	-0.77	-0.86	-0.98	-1.09
58	0.00	0.00	-0.02	-0.04	-0.07	-0.12	-0.17	-0.23	-0.29	-0.37	-0.46	-0.55	-0.66	-0.77	-0.87	-0.98	-1.13
59	0.00	0.00	-0.02	-0.04	-0.07	-0.11	-0.15	-0.21	-0.27	-0.34	-0.45	-0.51	-0.61	-0.72	-0.82	-0.93	-1.10

Table B.8 4D Secondary Phase (#2) Matrix Constructed from the Experimental Results for Global Optimization Method (17-33 A).

This is the experimental data matrix set developed using the raw machine data for the unsaturated region of the electromagnetic characteristics in terms of torque contribution of the out-going phase (secondary phase (# 2) vs. excitation current(A) in this secondary phase and the active position (θ°) of the rotor close to the primary phase stator . The position of the out-going secondary rotor with respect to the secondary phase stator, $\left(\phi_2 = \theta + 15^o\right)$.

Angle (θ°)/ Current (A)	17	18	19	20	21	22	23	24	25	26	27	28	29	30	31	32	33
0	-1.21	-1.34	-1.45	-1.56	-1.67	-1.79	-1.91	-2.03	-2.15	-2.29	-2.39	-2.50	-2.63	-2.76	-2.87	-2.98	-3.11
1	-1.20	-1.31	-1.44	-1.57	-1.66	-1.77	-1.90	-2.02	-2.14	-2.26	-2.38	-2.48	-2.62	-2.73	-2.85	-2.97	-3.09
2	-1.21	-1.32	-1.44	-1.56	-1.67	-1.82	-1.91	-2.02	-2.16	-2.26	-2.38	-2.49	-2.61	-2.73	-2.85	-2.96	-3.08
3	-1.21	-1.33	-1.46	-1.54	-1.65	-1.77	-1.88	-1.99	-2.11	-2.26	-2.34	-2.45	-2.57	-2.69	-2.80	-2.92	-3.03
4	-1.19	-1.32	-1.41	-1.52	-1.64	-1.75	-1.86	-1.98	-2.10	-2.22	-2.31	-2.44	-2.54	-2.66	-2.77	-2.89	-3.00
5	-1.19	-1.28	-1.42	-1.51	-1.62	-1.73	-1.86	-1.95	-2.07	-2.18	-2.29	-2.40	-2.51	-2.62	-2.74	-2.85	-2.96
6	-1.18	-1.30	-1.41	-1.52	-1.61	-1.75	-1.84	-1.93	-2.04	-2.15	-2.26	-2.36	-2.47	-2.58	-2.69	-2.80	-2.91
7	-1.25	-1.38	-1.43	-1.54	-1.64	-1.75	-1.86	-1.94	-2.04	-2.15	-2.25	-2.35	-2.46	-2.56	-2.66	-2.77	-2.87
8	-1.16	-1.28	-1.40	-1.52	-1.64	-1.78	-1.88	-1.92	-2.02	-2.12	-2.22	-2.32	-2.42	-2.52	-2.61	-2.71	-2.81
9	-0.74	-0.83	-0.92	-1.01	-1.11	-1.21	-1.32	-1.41	-1.51	-1.62	-1.72	-1.83	-1.93	-2.03	-2.12	-2.22	-2.31
10	-0.44	-0.49	-0.55	-0.60	-0.67	-0.73	-0.79	-0.87	-0.94	-1.01	-1.09	-1.17	-1.25	-1.33	-1.42	-1.50	-1.59
11	-0.28	-0.31	-0.35	-0.38	-0.42	-0.46	-0.51	-0.55	-0.59	-0.64	-0.69	-0.74	-0.80	-0.86	-0.91	-0.97	-1.03
12	-0.18	-0.20	-0.22	-0.25	-0.27	-0.30	-0.33	-0.36	-0.39	-0.42	-0.45	-0.48	-0.52	-0.55	-0.59	-0.63	-0.67
13	-0.11	-0.13	-0.14	-0.16	-0.17	-0.19	-0.21	-0.22	-0.24	-0.26	-0.28	-0.31	-0.33	-0.35	-0.37	-0.40	-0.42
14	-0.06	-0.07	-0.08	-0.09	-0.09	-0.10	-0.11	-0.12	-0.13	-0.15	-0.16	-0.17	-0.18	-0.19	-0.21	-0.22	-0.23
15	0.02	0.02	0.03	0.03	0.03	0.03	0.04	0.04	0.04	0.05	0.05	0.06	0.06	0.06	0.07	0.07	0.08
16	0.06	0.07	0.08	0.09	0.09	0.10	0.11	0.12	0.13	0.15	0.16	0.17	0.18	0.19	0.21	0.22	0.23
17	0.11	0.13	0.14	0.16	0.17	0.19	0.21	0.22	0.24	0.26	0.28	0.31	0.33	0.35	0.37	0.40	0.42
18	0.18	0.20	0.22	0.25	0.27	0.30	0.33	0.36	0.39	0.42	0.45	0.48	0.52	0.55	0.59	0.63	0.67
19	0.28	0.31	0.35	0.38	0.42	0.46	0.51	0.55	0.59	0.64	0.69	0.74	0.80	0.86	0.91	0.97	1.03
20	0.44	0.49	0.55	0.60	0.67	0.73	0.79	0.87	0.94	1.01	1.09	1.17	1.25	1.33	1.42	1.50	1.59
21	0.74	0.83	0.92	1.01	1.11	1.21	1.32	1.41	1.51	1.62	1.72	1.83	1.93	2.03	2.12	2.22	2.31
22	1.16	1.28	1.40	1.52	1.64	1.78	1.88	1.92	2.02	2.12	2.22	2.32	2.42	2.52	2.61	2.71	2.81
23	1.25	1.38	1.43	1.54	1.64	1.75	1.86	1.94	2.04	2.15	2.25	2.35	2.46	2.56	2.66	2.77	2.87
24	1.18	1.30	1.41	1.52	1.61	1.75	1.84	1.93	2.04	2.15	2.26	2.36	2.47	2.58	2.69	2.80	2.91
25	1.19	1.28	1.42	1.51	1.62	1.73	1.86	1.95	2.07	2.18	2.29	2.40	2.51	2.62	2.74	2.85	2.96
26	1.19	1.32	1.41	1.52	1.64	1.75	1.86	1.98	2.10	2.22	2.31	2.44	2.54	2.66	2.77	2.89	3.00
27	1.21	1.33	1.46	1.54	1.65	1.77	1.88	1.99	2.11	2.26	2.34	2.45	2.57	2.69	2.80	2.92	3.03
28	1.21	1.32	1.44	1.56	1.67	1.82	1.91	2.02	2.16	2.26	2.38	2.49	2.61	2.73	2.85	2.96	3.08
29	1.20	1.31	1.44	1.57	1.66	1.77	1.90	2.02	2.14	2.26	2.38	2.48	2.62	2.73	2.85	2.97	3.09
30	1.21	1.34	1.45	1.56	1.67	1.79	1.91	2.03	2.15	2.29	2.39	2.50	2.63	2.76	2.87	2.98	3.11
31	1.21	1.33	1.46	1.56	1.67	1.78	1.92	2.04	2.15	2.27	2.40	2.51	2.63	2.76	2.87	2.99	3.11
32	1.20	1.32	1.48	1.55	1.67	1.79	1.90	2.02	2.15	2.27	2.39	2.49	2.61	2.72	2.83	2.94	3.06
33	1.20	1.32	1.40	1.52	1.64	1.76	1.88	2.00	2.12	2.24	2.36	2.50	2.59	2.72	2.83	2.94	3.06
34	1.24	1.31	1.42	1.54	1.66	1.80	1.91	2.02	2.13	2.25	2.36	2.46	2.58	2.69	2.80	2.91	3.01
35	1.18	1.29	1.41	1.54	1.63	1.76	1.87	1.98	2.10	2.20	2.30	2.41	2.52	2.64	2.73	2.82	2.92
36	1.18	1.32	1.49	1.52	1.61	1.72	1.86	1.95	2.07	2.14	2.25	2.35	2.45	2.55	2.65	2.74	2.84
37	1.14	1.25	1.38	1.47	1.57	1.68	1.79	1.86	1.99	2.07	2.15	2.25	2.34	2.44	2.53	2.62	2.71
38	1.15	1.24	1.37	1.41	1.57	1.60	1.69	1.78	1.87	1.98	2.02	2.11	2.20	2.30	2.37	2.46	2.55

39	1.10	1.16	1.31	1.34	1.38	1.47	1.57	1.70	1.74	1.79	1.88	1.95	2.03	2.13	2.18	2.25	2.31
40	1.10	1.15	1.22	1.31	1.27	1.35	1.44	1.56	1.56	1.63	1.70	1.76	1.83	1.88	1.93	1.98	2.03
41	0.90	0.93	1.13	1.08	1.14	1.21	1.42	1.30	1.35	1.41	1.45	1.50	1.54	1.59	1.62	1.66	1.70
42	0.81	0.88	0.95	0.99	0.97	1.08	1.01	1.07	1.12	1.13	1.18	1.20	1.23	1.26	1.28	1.31	1.33
43	0.67	0.69	0.80	0.74	0.77	0.75	0.77	0.79	0.81	0.82	0.85	0.86	0.88	0.89	0.91	0.93	0.94
44	0.30	0.32	0.33	0.33	0.32	0.33	0.33	0.34	0.35	0.36	0.36	0.36	0.37	0.38	0.38	0.39	0.39
45	0.00	0.00	0.00	0.00	0.00	0.00	0.00	0.00	0.00	0.00	0.00	0.00	0.00	0.00	0.00	0.00	0.00
46	-0.30	-0.32	-0.33	-0.33	-0.32	-0.33	-0.33	-0.34	-0.35	-0.36	-0.36	-0.36	-0.37	-0.38	-0.38	-0.39	-0.39
47	-0.67	-0.69	-0.80	-0.74	-0.77	-0.75	-0.77	-0.79	-0.81	-0.82	-0.85	-0.86	-0.88	-0.89	-0.91	-0.93	-0.94
48	-0.81	-0.88	-0.95	-0.99	-0.97	-1.08	-1.01	-1.07	-1.12	-1.13	-1.18	-1.20	-1.23	-1.26	-1.28	-1.31	-1.33
49	-0.90	-0.93	-1.13	-1.08	-1.14	-1.21	-1.42	-1.30	-1.35	-1.41	-1.45	-1.50	-1.54	-1.59	-1.62	-1.66	-1.70
50	-1.10	-1.15	-1.22	-1.31	-1.27	-1.35	-1.44	-1.56	-1.56	-1.63	-1.70	-1.76	-1.83	-1.88	-1.93	-1.98	-2.03
51	-1.10	-1.16	-1.31	-1.34	-1.38	-1.47	-1.57	-1.70	-1.74	-1.79	-1.88	-1.95	-2.03	-2.13	-2.18	-2.25	-2.31
52	-1.15	-1.24	-1.37	-1.41	-1.57	-1.60	-1.69	-1.78	-1.87	-1.98	-2.02	-2.11	-2.20	-2.30	-2.37	-2.46	-2.55
53	-1.14	-1.25	-1.38	-1.47	-1.57	-1.68	-1.79	-1.86	-1.99	-2.07	-2.15	-2.25	-2.34	-2.44	-2.53	-2.62	-2.71
54	-1.18	-1.32	-1.49	-1.52	-1.61	-1.72	-1.86	-1.95	-2.07	-2.14	-2.25	-2.35	-2.45	-2.55	-2.65	-2.74	-2.84
55	-1.18	-1.29	-1.41	-1.54	-1.63	-1.76	-1.87	-1.98	-2.10	-2.20	-2.30	-2.41	-2.52	-2.64	-2.73	-2.82	-2.92
56	-1.24	-1.31	-1.42	-1.54	-1.66	-1.80	-1.91	-2.02	-2.13	-2.25	-2.36	-2.46	-2.58	-2.69	-2.80	-2.91	-3.01
57	-1.20	-1.32	-1.48	-1.55	-1.67	-1.79	-1.90	-2.02	-2.15	-2.27	-2.39	-2.49	-2.61	-2.72	-2.83	-2.94	-3.06
58	-1.20	-1.32	-1.40	-1.52	-1.64	-1.76	-1.88	-2.00	-2.12	-2.24	-2.36	-2.50	-2.59	-2.72	-2.83	-2.94	-3.06
59	-1.21	-1.33	-1.46	-1.56	-1.67	-1.78	-1.92	-2.04	-2.15	-2.27	-2.40	-2.51	-2.63	-2.76	-2.87	-2.99	-3.11

Table B.9 4D Secondary Phase(#2) Matrix Constructed from the Experimental Results for Global Optimization Method (34-50 A).

This is the experimental data matrix set developed using the raw machine data for the saturated region of the electromagnetic characteristics in terms of torque contribution of the out-going phase (secondary phase (# 2) vs. excitation current(A) in this secondary phase and the active position (θ°) of the rotor close to the primary phase stator . The position of the out-going secondary rotor with respect to the secondary phase stator, $\left(\phi_2 = \theta + 15^o\right)$.

Angle (θ°)/ Current (A)	34	35	36	37	38	39	40	41	42	43	44	45	46	47	48	49	50
0	0.00	0.00	0.00	0.00	0.00	0.00	0.00	0.00	0.00	0.00	0.00	0.00	0.00	0.00	0.00	0.00	0.00
1	-0.40	-0.40	-0.41	-0.41	-0.42	-0.42	-0.43	-0.43	-0.44	-0.44	-0.45	-0.45	-0.46	-0.46	-0.46	-0.47	-0.47
2	-0.96	-0.97	-0.99	-1.00	-1.02	-1.03	-1.05	-1.06	-1.07	-1.09	-1.10	-1.11	-1.13	-1.14	-1.15	-1.16	-1.18
3	-1.36	-1.38	-1.41	-1.43	-1.45	-1.48	-1.50	-1.52	-1.54	-1.56	-1.59	-1.61	-1.63	-1.65	-1.67	-1.69	-1.71
4	-1.73	-1.77	-1.80	-1.83	-1.86	-1.89	-1.92	-1.95	-1.98	-2.01	-2.04	-2.07	-2.09	-2.12	-2.15	-2.17	-2.20
5	-2.08	-2.12	-2.16	-2.20	-2.24	-2.28	-2.32	-2.35	-2.39	-2.42	-2.46	-2.49	-2.53	-2.56	-2.59	-2.62	-2.66
6	-2.38	-2.43	-2.49	-2.54	-2.59	-2.64	-2.68	-2.73	-2.77	-2.81	-2.85	-2.89	-2.93	-2.97	-3.01	-3.05	-3.09
7	-2.63	-2.70	-2.78	-2.84	-2.91	-2.97	-3.02	-3.08	-3.13	-3.18	-3.24	-3.28	-3.33	-3.38	-3.42	-3.47	-3.51
8	-2.80	-2.89	-2.98	-3.06	-3.15	-3.23	-3.31	-3.37	-3.44	-3.51	-3.57	-3.62	-3.68	-3.74	-3.79	-3.84	-3.89
9	-2.95	-3.03	-3.13	-3.22	-3.32	-3.41	-3.50	-3.58	-3.67	-3.75	-3.83	-3.91	-3.98	-4.04	-4.11	-4.17	-4.23
10	-3.04	-3.13	-3.23	-3.33	-3.43	-3.53	-3.62	-3.72	-3.81	-3.90	-4.00	-4.09	-4.18	-4.26	-4.34	-4.42	-4.50
11	-3.12	-3.22	-3.33	-3.45	-3.53	-3.64	-3.74	-3.84	-3.94	-4.03	-4.13	-4.22	-4.32	-4.41	-4.51	-4.60	-4.69
12	-3.18	-3.28	-3.38	-3.49	-3.60	-3.70	-3.81	-3.91	-4.01	-4.12	-4.22	-4.32	-4.42	-4.51	-4.61	-4.71	-4.81
13	-3.17	-3.28	-3.39	-3.47	-3.58	-3.70	-3.79	-3.90	-4.01	-4.06	-4.16	-4.27	-4.37	-4.47	-4.57	-4.66	-4.76
14	-3.24	-3.34	-3.45	-3.56	-3.68	-3.78	-3.89	-4.01	-4.12	-4.21	-4.33	-4.43	-4.54	-4.65	-4.75	-4.85	-4.98
15	-3.22	-3.34	-3.46	-3.57	-3.69	-3.81	-3.92	-4.03	-4.15	-4.26	-4.36	-4.47	-4.59	-4.69	-4.80	-4.90	-5.01
16	-3.21	-3.32	-3.44	-3.56	-3.68	-3.79	-3.91	-4.03	-4.14	-4.25	-4.38	-4.48	-4.59	-4.71	-4.82	-4.93	-5.04
17	-3.20	-3.31	-3.43	-3.55	-3.67	-3.78	-3.89	-4.02	-4.13	-4.24	-4.36	-4.47	-4.59	-4.70	-4.81	-4.92	-5.03
18	-3.15	-3.26	-3.38	-3.49	-3.61	-3.72	-3.84	-3.95	-4.06	-4.18	-4.29	-4.40	-4.51	-4.64	-4.74	-4.85	-4.96
19	-3.11	-3.23	-3.34	-3.45	-3.56	-3.68	-3.79	-3.90	-4.02	-4.13	-4.24	-4.35	-4.46	-4.57	-4.68	-4.92	-4.90
20	-3.07	-3.18	-3.29	-3.39	-3.51	-3.62	-3.73	-3.84	-3.95	-4.06	-4.17	-4.28	-4.38	-4.49	-4.60	-4.72	-4.82
21	-3.01	-3.12	-3.22	-3.33	-3.45	-3.55	-3.65	-3.76	-3.87	-3.98	-4.08	-4.18	-4.29	-4.40	-4.50	-4.61	-4.72
22	-2.97	-3.08	-3.19	-3.31	-3.40	-3.50	-3.63	-3.73	-3.80	-3.93	-4.01	-4.18	-4.22	-4.32	-4.42	-4.57	-4.62
23	-2.91	-3.01	-3.10	-3.23	-3.33	-3.43	-3.53	-3.63	-3.74	-3.79	-3.88	-3.98	-4.08	-4.18	-4.28	-4.37	-4.46
24	-2.40	-2.49	-2.61	-2.70	-2.76	-3.00	-2.96	-3.05	-3.14	-3.24	-3.32	-3.41	-3.50	-3.60	-3.69	-3.77	-3.86
25	-1.68	-1.76	-1.85	-1.89	-1.98	-1.87	-1.95	-2.02	-2.10	-2.18	-2.27	-2.34	-2.42	-2.69	-2.89	-2.86	-2.93
26	-1.10	-1.16	-1.23	-1.29	-1.33	-1.43	-1.47	-1.57	-1.61	-1.69	-1.75	-1.82	-1.88	-1.95	-1.93	-1.98	-2.05
27	-0.71	-0.75	-0.74	-0.78	-0.82	-0.86	-0.96	-1.01	-1.00	-1.05	-1.10	-1.15	-1.20	-1.25	-1.30	-1.35	-1.40
28	-0.45	-0.48	-0.50	-0.53	-0.56	-0.57	-0.62	-0.65	-0.67	-0.72	-0.75	-0.76	-0.80	-0.83	-0.89	-0.93	-0.97

29	-0.25	-0.26	-0.28	-0.29	-0.31	-0.33	-0.34	-0.36	-0.38	-0.40	-0.42	-0.44	-0.46	-0.48	-0.50	-0.52	-0.55
30	0.08	0.09	0.09	0.10	0.10	0.11	0.11	0.12	0.13	0.13	0.14	0.14	0.15	0.16	0.16	0.17	0.18
31	0.25	0.26	0.28	0.29	0.31	0.33	0.34	0.36	0.38	0.40	0.42	0.44	0.46	0.48	0.50	0.52	0.55
32	0.45	0.48	0.50	0.53	0.56	0.57	0.62	0.65	0.67	0.72	0.75	0.76	0.80	0.83	0.89	0.93	0.97
33	0.71	0.75	0.74	0.78	0.82	0.86	0.96	1.01	1.00	1.05	1.10	1.15	1.20	1.25	1.30	1.35	1.40
34	1.10	1.16	1.23	1.29	1.33	1.43	1.47	1.57	1.61	1.69	1.75	1.82	1.88	1.95	1.93	1.98	2.05
35	1.68	1.76	1.85	1.89	1.98	1.87	1.95	2.02	2.10	2.18	2.27	2.34	2.42	2.69	2.58	2.86	2.93
36	2.40	2.49	2.61	2.70	2.76	3.00	2.96	3.05	3.14	3.24	3.32	3.41	3.50	3.60	3.69	3.77	3.86
37	2.91	3.01	3.10	3.23	3.33	3.43	3.53	3.63	3.74	3.79	3.88	3.98	4.08	4.18	4.28	4.37	4.46
38	2.97	3.08	3.19	3.31	3.40	3.50	3.63	3.73	3.80	3.93	4.01	4.18	4.22	4.32	4.42	4.57	4.62
39	3.01	3.12	3.22	3.33	3.45	3.55	3.65	3.76	3.87	3.98	4.08	4.18	4.29	4.40	4.50	4.61	4.72
40	3.07	3.18	3.29	3.39	3.51	3.62	3.73	3.84	3.95	4.06	4.17	4.28	4.38	4.49	4.60	4.72	4.82
41	3.11	3.23	3.34	3.45	3.56	3.68	3.79	3.90	4.02	4.13	4.24	4.35	4.46	4.57	4.68	4.79	4.90
42	3.15	3.26	3.38	3.49	3.61	3.72	3.84	3.95	4.06	4.18	4.29	4.40	4.51	4.64	4.74	4.85	4.96
43	3.20	3.31	3.43	3.55	3.67	3.78	3.89	4.02	4.13	4.24	4.36	4.47	4.59	4.70	4.81	4.92	5.03
44	3.21	3.32	3.44	3.56	3.68	3.79	3.91	4.03	4.14	4.25	4.38	4.48	4.59	4.71	4.82	4.93	5.04
45	3.22	3.34	3.46	3.57	3.69	3.81	3.92	4.03	4.15	4.26	4.36	4.47	4.59	4.69	4.80	4.90	5.01
46	3.24	3.34	3.45	3.56	3.68	3.78	3.89	4.01	4.12	4.21	4.33	4.43	4.54	4.65	4.75	4.85	4.96
47	3.18	3.28	3.38	3.49	3.60	3.70	3.81	3.91	4.01	4.12	4.22	4.32	4.42	4.51	4.61	4.71	4.80
48	3.17	3.28	3.39	3.47	3.58	3.70	3.79	3.90	4.01	4.06	4.16	4.27	4.37	4.47	4.57	4.66	4.76
49	3.12	3.22	3.33	3.45	3.53	3.64	3.74	3.84	3.94	4.03	4.13	4.22	4.32	4.41	4.51	4.60	4.69
50	3.04	3.13	3.23	3.33	3.43	3.53	3.62	3.72	3.81	3.90	4.00	4.09	4.18	4.26	4.34	4.42	4.50
51	2.95	3.03	3.13	3.22	3.32	3.41	3.50	3.58	3.67	3.75	3.83	3.91	3.98	4.04	4.11	4.17	4.23
52	2.80	2.89	2.98	3.06	3.15	3.23	3.31	3.37	3.44	3.51	3.57	3.62	3.68	3.74	3.79	3.84	3.89
53	2.63	2.70	2.78	2.84	2.91	2.97	3.02	3.08	3.13	3.18	3.24	3.28	3.33	3.38	3.42	3.47	3.51
54	2.38	2.43	2.49	2.54	2.59	2.64	2.68	2.73	2.77	2.81	2.85	2.89	2.93	2.97	3.01	3.05	3.09
55	2.08	2.12	2.16	2.20	2.24	2.28	2.32	2.35	2.39	2.42	2.46	2.49	2.53	2.56	2.59	2.62	2.66
56	1.73	1.77	1.80	1.83	1.86	1.89	1.92	1.95	1.98	2.01	2.04	2.07	2.09	2.12	2.15	2.17	2.20
57	1.36	1.38	1.41	1.43	1.45	1.48	1.50	1.52	1.54	1.56	1.59	1.61	1.63	1.65	1.67	1.69	1.71
58	0.96	0.97	0.99	1.00	1.02	1.03	1.05	1.06	1.07	1.09	1.10	1.11	1.13	1.14	1.15	1.16	1.18
59	0.40	0.40	0.41	0.41	0.42	0.42	0.43	0.43	0.44	0.44	0.45	0.45	0.46	0.46	0.46	0.47	0.47

APPENDIX C: COMPARATIVE ANALYSES OF PROPOSED METHOD FOR TORQUE MINIMIZATION WITH CONVENTIONAL METHODS

Table C.1 Instantaneous torque profiles by traditional method (0-16A).

Angle (θ°)/ Current (A)	0	1	2	3	4	5	6	7	8	9	10	11	12	13	14	15	16
0	0.00	0.00	0.02	0.04	0.07	0.12	0.17	0.23	0.29	0.37	0.46	0.55	0.66	0.77	0.87	0.98	1.11
1	0.00	0.00	0.02	0.04	0.07	0.12	0.17	0.23	0.29	0.37	0.46	0.55	0.65	0.77	0.86	0.99	1.10
2	0.00	0.00	0.02	0.04	0.07	0.12	0.17	0.23	0.29	0.37	0.46	0.55	0.66	0.77	0.87	0.98	1.13
3	0.00	0.00	0.02	0.04	0.07	0.11	0.15	0.21	0.27	0.34	0.45	0.51	0.61	0.72	0.82	0.93	1.10
4	0.00	0.00	0.02	0.04	0.07	0.11	0.16	0.22	0.29	0.37	0.46	0.55	0.66	0.77	0.86	0.98	1.09
5	0.00	0.00	0.02	0.04	0.07	0.11	0.16	0.22	0.28	0.36	0.45	0.54	0.65	0.76	0.85	0.96	1.07
6	0.00	0.00	0.02	0.04	0.07	0.11	0.16	0.22	0.29	0.37	0.45	0.54	0.65	0.76	0.85	0.96	1.07
7	0.00	0.00	0.02	0.04	0.07	0.11	0.16	0.21	0.28	0.35	0.44	0.53	0.63	0.76	0.84	0.94	1.04
8	0.00	0.00	0.02	0.04	0.07	0.11	0.15	0.21	0.27	0.35	0.43	0.52	0.61	0.73	0.83	0.93	1.06
9	0.00	0.00	0.02	0.04	0.07	0.10	0.15	0.20	0.27	0.34	0.42	0.50	0.61	0.71	0.78	0.90	1.00
10	0.00	0.00	0.02	0.04	0.07	0.11	0.15	0.20	0.27	0.33	0.41	0.50	0.58	0.68	0.76	0.82	1.01
11	0.00	0.00	0.02	0.04	0.06	0.10	0.15	0.20	0.26	0.33	0.40	0.48	0.55	0.65	0.70	0.77	0.79
12	0.00	0.00	0.02	0.03	0.06	0.10	0.14	0.19	0.25	0.31	0.38	0.45	0.51	0.62	0.66	0.68	0.81
13	0.00	0.00	0.01	0.03	0.05	0.08	0.12	0.16	0.21	0.27	0.33	0.39	0.44	0.53	0.50	0.56	0.58
14	0.00	0.00	0.01	0.01	0.03	0.04	0.06	0.08	0.11	0.13	0.16	0.19	0.22	0.26	0.25	0.26	0.28
15	0.00	0.00	0.02	0.04	0.07	0.12	0.17	0.23	0.29	0.37	0.46	0.55	0.66	0.77	0.87	0.98	1.11
16	0.00	0.00	0.02	0.04	0.07	0.12	0.17	0.23	0.29	0.37	0.46	0.55	0.65	0.77	0.86	0.99	1.10
17	0.00	0.00	0.02	0.04	0.07	0.12	0.17	0.23	0.29	0.37	0.46	0.55	0.66	0.77	0.87	0.98	1.13
18	0.00	0.00	0.02	0.04	0.07	0.11	0.15	0.21	0.27	0.34	0.45	0.51	0.61	0.72	0.82	0.93	1.10
19	0.00	0.00	0.02	0.04	0.07	0.11	0.16	0.22	0.29	0.37	0.46	0.55	0.66	0.77	0.86	0.98	1.09
20	0.00	0.00	0.02	0.04	0.07	0.11	0.16	0.22	0.28	0.36	0.45	0.54	0.65	0.76	0.85	0.96	1.07
21	0.00	0.00	0.02	0.04	0.07	0.11	0.16	0.22	0.29	0.37	0.45	0.54	0.65	0.76	0.85	0.96	1.07
22	0.00	0.00	0.02	0.04	0.07	0.11	0.16	0.21	0.28	0.35	0.44	0.53	0.63	0.76	0.84	0.94	1.04
23	0.00	0.00	0.02	0.04	0.07	0.11	0.15	0.21	0.27	0.35	0.43	0.52	0.61	0.73	0.83	0.93	1.06
24	0.00	0.00	0.02	0.04	0.07	0.10	0.15	0.20	0.27	0.34	0.42	0.50	0.61	0.71	0.78	0.90	1.00
25	0.00	0.00	0.02	0.04	0.07	0.11	0.15	0.20	0.27	0.33	0.41	0.50	0.58	0.68	0.76	0.82	1.01
26	0.00	0.00	0.02	0.04	0.06	0.10	0.15	0.20	0.26	0.33	0.40	0.48	0.55	0.65	0.70	0.77	0.79
27	0.00	0.00	0.02	0.03	0.06	0.10	0.14	0.19	0.25	0.31	0.38	0.45	0.51	0.62	0.66	0.68	0.81
28	0.00	0.00	0.01	0.03	0.05	0.08	0.12	0.16	0.21	0.27	0.33	0.39	0.44	0.53	0.50	0.56	0.58
29	0.00	0.00	0.01	0.01	0.03	0.04	0.06	0.08	0.11	0.13	0.16	0.19	0.22	0.26	0.25	0.26	0.28
30	0.00	0.00	0.02	0.04	0.07	0.12	0.17	0.23	0.29	0.37	0.46	0.55	0.66	0.77	0.87	0.98	1.11
31	0.00	0.00	0.02	0.04	0.07	0.12	0.17	0.23	0.29	0.37	0.46	0.55	0.65	0.77	0.86	0.99	1.10
32	0.00	0.00	0.02	0.04	0.07	0.12	0.17	0.23	0.29	0.37	0.46	0.55	0.66	0.77	0.87	0.98	1.13
33	0.00	0.00	0.02	0.04	0.07	0.11	0.15	0.21	0.27	0.34	0.45	0.51	0.61	0.72	0.82	0.93	1.10
34	0.00	0.00	0.02	0.04	0.07	0.11	0.16	0.22	0.29	0.37	0.46	0.55	0.66	0.77	0.86	0.98	1.09
35	0.00	0.00	0.02	0.04	0.07	0.11	0.16	0.22	0.28	0.36	0.45	0.54	0.65	0.76	0.85	0.96	1.07

36	0.00	0.00	0.02	0.04	0.07	0.11	0.16	0.22	0.29	0.37	0.45	0.54	0.65	0.76	0.85	0.96	1.07
37	0.00	0.00	0.02	0.04	0.07	0.11	0.16	0.21	0.28	0.35	0.44	0.53	0.63	0.76	0.84	0.94	1.04
38	0.00	0.00	0.02	0.04	0.07	0.11	0.15	0.21	0.27	0.35	0.43	0.52	0.61	0.73	0.83	0.93	1.06
39	0.00	0.00	0.02	0.04	0.07	0.10	0.15	0.20	0.27	0.34	0.42	0.50	0.61	0.71	0.78	0.90	1.00
40	0.00	0.00	0.02	0.04	0.07	0.11	0.15	0.20	0.27	0.33	0.41	0.50	0.58	0.68	0.76	0.82	1.01
41	0.00	0.00	0.02	0.04	0.06	0.10	0.15	0.20	0.26	0.33	0.40	0.48	0.55	0.65	0.70	0.77	0.79
42	0.00	0.00	0.02	0.03	0.06	0.10	0.14	0.19	0.25	0.31	0.38	0.45	0.51	0.62	0.66	0.68	0.81
43	0.00	0.00	0.01	0.03	0.05	0.08	0.12	0.16	0.21	0.27	0.33	0.39	0.44	0.53	0.50	0.56	0.58
44	0.00	0.00	0.01	0.01	0.03	0.04	0.06	0.08	0.11	0.13	0.16	0.19	0.22	0.26	0.25	0.26	0.28
45	0.00	0.00	0.02	0.04	0.07	0.12	0.17	0.23	0.29	0.37	0.46	0.55	0.66	0.77	0.87	0.98	1.11
46	0.00	0.00	0.02	0.04	0.07	0.12	0.17	0.23	0.29	0.37	0.46	0.55	0.65	0.77	0.86	0.99	1.10
47	0.00	0.00	0.02	0.04	0.07	0.12	0.17	0.23	0.29	0.37	0.46	0.55	0.66	0.77	0.87	0.98	1.13
48	0.00	0.00	0.02	0.04	0.07	0.11	0.15	0.21	0.27	0.34	0.45	0.51	0.61	0.72	0.82	0.93	1.10
49	0.00	0.00	0.02	0.04	0.07	0.11	0.16	0.22	0.29	0.37	0.46	0.55	0.66	0.77	0.86	0.98	1.09
50	0.00	0.00	0.02	0.04	0.07	0.11	0.16	0.22	0.28	0.36	0.45	0.54	0.65	0.76	0.85	0.96	1.07
51	0.00	0.00	0.02	0.04	0.07	0.11	0.16	0.22	0.29	0.37	0.45	0.54	0.65	0.76	0.85	0.96	1.07
52	0.00	0.00	0.02	0.04	0.07	0.11	0.16	0.21	0.28	0.35	0.44	0.53	0.63	0.76	0.84	0.94	1.04
53	0.00	0.00	0.02	0.04	0.07	0.11	0.15	0.21	0.27	0.35	0.43	0.52	0.61	0.73	0.83	0.93	1.06
54	0.00	0.00	0.02	0.04	0.07	0.10	0.15	0.20	0.27	0.34	0.42	0.50	0.61	0.71	0.78	0.90	1.00
55	0.00	0.00	0.02	0.04	0.07	0.11	0.15	0.20	0.27	0.33	0.41	0.50	0.58	0.68	0.76	0.82	1.01
56	0.00	0.00	0.02	0.04	0.06	0.10	0.15	0.20	0.26	0.33	0.40	0.48	0.55	0.65	0.70	0.77	0.79
57	0.00	0.00	0.02	0.03	0.06	0.10	0.14	0.19	0.25	0.31	0.38	0.45	0.51	0.62	0.66	0.68	0.81
58	0.00	0.00	0.01	0.03	0.05	0.08	0.12	0.16	0.21	0.27	0.33	0.39	0.44	0.53	0.50	0.56	0.58
59	0.00	0.00	0.01	0.01	0.03	0.04	0.06	0.08	0.11	0.13	0.16	0.19	0.22	0.26	0.25	0.26	0.28

Table C.2 Instantaneous Torque Profiles by Traditional Method (17-33 A).

Angle (θ°)/ Current (A)	17	18	19	20	21	22	23	24	25	26	27	28	29	30	31	32	33
0	1.21	1.34	1.45	1.56	1.67	1.79	1.91	2.03	2.15	2.29	2.39	2.50	2.63	2.76	2.87	2.98	3.11
1	1.21	1.33	1.46	1.56	1.67	1.78	1.92	2.04	2.15	2.27	2.40	2.51	2.63	2.76	2.87	2.99	3.11
2	1.20	1.32	1.48	1.55	1.67	1.79	1.90	2.02	2.15	2.27	2.39	2.49	2.61	2.72	2.83	2.94	3.06
3	1.20	1.32	1.40	1.52	1.64	1.76	1.88	2.00	2.12	2.24	2.36	2.50	2.59	2.72	2.83	2.94	3.06
4	1.24	1.31	1.42	1.54	1.66	1.80	1.91	2.02	2.13	2.25	2.36	2.46	2.58	2.69	2.80	2.91	3.01
5	1.18	1.29	1.41	1.54	1.63	1.76	1.87	1.98	2.10	2.20	2.30	2.41	2.52	2.64	2.73	2.82	2.92
6	1.18	1.32	1.49	1.52	1.61	1.72	1.86	1.95	2.07	2.14	2.25	2.35	2.45	2.55	2.65	2.74	2.84
7	1.14	1.25	1.38	1.47	1.57	1.68	1.79	1.86	1.99	2.07	2.15	2.25	2.34	2.44	2.53	2.62	2.71
8	1.15	1.24	1.37	1.41	1.57	1.60	1.69	1.78	1.87	1.98	2.02	2.11	2.20	2.30	2.37	2.46	2.55
9	1.10	1.16	1.31	1.34	1.38	1.47	1.57	1.70	1.74	1.79	1.88	1.95	2.03	2.13	2.18	2.25	2.31
10	1.10	1.15	1.22	1.31	1.27	1.35	1.44	1.56	1.56	1.63	1.70	1.76	1.83	1.88	1.93	1.98	2.03
11	0.90	0.93	1.13	1.08	1.14	1.21	1.42	1.30	1.35	1.41	1.45	1.50	1.54	1.59	1.62	1.66	1.70
12	0.81	0.88	0.95	0.99	0.97	1.08	1.01	1.07	1.12	1.13	1.18	1.20	1.23	1.26	1.28	1.31	1.33
13	0.67	0.69	0.80	0.74	0.77	0.75	0.77	0.79	0.81	0.82	0.85	0.86	0.88	0.89	0.91	0.93	0.94
14	0.30	0.32	0.33	0.33	0.32	0.33	0.33	0.34	0.35	0.36	0.36	0.36	0.37	0.38	0.38	0.39	0.39
15	1.21	1.34	1.45	1.56	1.67	1.79	1.91	2.03	2.15	2.29	2.39	2.50	2.63	2.76	2.87	2.98	3.11
16	1.21	1.33	1.46	1.56	1.67	1.78	1.92	2.04	2.15	2.27	2.40	2.51	2.63	2.76	2.87	2.99	3.11
17	1.20	1.32	1.48	1.55	1.67	1.79	1.90	2.02	2.15	2.27	2.39	2.49	2.61	2.72	2.83	2.94	3.06
18	1.20	1.32	1.40	1.52	1.64	1.76	1.88	2.00	2.12	2.24	2.36	2.50	2.59	2.72	2.83	2.94	3.06
19	1.24	1.31	1.42	1.54	1.66	1.80	1.91	2.02	2.13	2.25	2.36	2.46	2.58	2.69	2.80	2.91	3.01
20	1.18	1.29	1.41	1.54	1.63	1.76	1.87	1.98	2.10	2.20	2.30	2.41	2.52	2.64	2.73	2.82	2.92
21	1.18	1.32	1.49	1.52	1.61	1.72	1.86	1.95	2.07	2.14	2.25	2.35	2.45	2.55	2.65	2.74	2.84
22	1.14	1.25	1.38	1.47	1.57	1.68	1.79	1.86	1.99	2.07	2.15	2.25	2.34	2.44	2.53	2.62	2.71
23	1.15	1.24	1.37	1.41	1.57	1.60	1.69	1.78	1.87	1.98	2.02	2.11	2.20	2.30	2.37	2.46	2.55
24	1.10	1.16	1.31	1.34	1.38	1.47	1.57	1.70	1.74	1.79	1.88	1.95	2.03	2.13	2.18	2.25	2.31
25	1.10	1.15	1.22	1.31	1.27	1.35	1.44	1.56	1.56	1.63	1.70	1.76	1.83	1.88	1.93	1.98	2.03
26	0.90	0.93	1.13	1.08	1.14	1.21	1.42	1.30	1.35	1.41	1.45	1.50	1.54	1.59	1.62	1.66	1.70
27	0.81	0.88	0.95	0.99	0.97	1.08	1.01	1.07	1.12	1.13	1.18	1.20	1.23	1.26	1.28	1.31	1.33
28	0.67	0.69	0.80	0.74	0.77	0.75	0.77	0.79	0.81	0.82	0.85	0.86	0.88	0.89	0.91	0.93	0.94
29	0.30	0.32	0.33	0.33	0.32	0.33	0.33	0.34	0.35	0.36	0.36	0.36	0.37	0.38	0.38	0.39	0.39
30	1.21	1.34	1.45	1.56	1.67	1.79	1.91	2.03	2.15	2.29	2.39	2.50	2.63	2.76	2.87	2.98	3.11
31	1.21	1.33	1.46	1.56	1.67	1.78	1.92	2.04	2.15	2.27	2.40	2.51	2.63	2.76	2.87	2.99	3.11
32	1.20	1.32	1.48	1.55	1.67	1.79	1.90	2.02	2.15	2.27	2.39	2.49	2.61	2.72	2.83	2.94	3.06
33	1.20	1.32	1.40	1.52	1.64	1.76	1.88	2.00	2.12	2.24	2.36	2.50	2.59	2.72	2.83	2.94	3.06
34	1.24	1.31	1.42	1.54	1.66	1.80	1.91	2.02	2.13	2.25	2.36	2.46	2.58	2.69	2.80	2.91	3.01
35	1.18	1.29	1.41	1.54	1.63	1.76	1.87	1.98	2.10	2.20	2.30	2.41	2.52	2.64	2.73	2.82	2.92
36	1.18	1.32	1.49	1.52	1.61	1.72	1.86	1.95	2.07	2.14	2.25	2.35	2.45	2.55	2.65	2.74	2.84
37	1.14	1.25	1.38	1.47	1.57	1.68	1.79	1.86	1.99	2.07	2.15	2.25	2.34	2.44	2.53	2.62	2.71

38	1.15	1.24	1.37	1.41	1.57	1.60	1.69	1.78	1.87	1.98	2.02	2.11	2.20	2.30	2.37	2.46	2.55
39	1.10	1.16	1.31	1.34	1.38	1.47	1.57	1.70	1.74	1.79	1.88	1.95	2.03	2.13	2.18	2.25	2.31
40	1.10	1.15	1.22	1.31	1.27	1.35	1.44	1.56	1.56	1.63	1.70	1.76	1.83	1.88	1.93	1.98	2.03
41	0.90	0.93	1.13	1.08	1.14	1.21	1.42	1.30	1.35	1.41	1.45	1.50	1.54	1.59	1.62	1.66	1.70
42	0.81	0.88	0.95	0.99	0.97	1.08	1.01	1.07	1.12	1.13	1.18	1.20	1.23	1.26	1.28	1.31	1.33
43	0.67	0.69	0.80	0.74	0.77	0.75	0.77	0.79	0.81	0.82	0.85	0.86	0.88	0.89	0.91	0.93	0.94
44	0.30	0.32	0.33	0.33	0.32	0.33	0.33	0.34	0.35	0.36	0.36	0.36	0.37	0.38	0.38	0.39	0.39
45	1.21	1.34	1.45	1.56	1.67	1.79	1.91	2.03	2.15	2.29	2.39	2.50	2.63	2.76	2.87	2.98	3.11
46	1.21	1.33	1.46	1.56	1.67	1.78	1.92	2.04	2.15	2.27	2.40	2.51	2.63	2.76	2.87	2.99	3.11
47	1.20	1.32	1.48	1.55	1.67	1.79	1.90	2.02	2.15	2.27	2.39	2.49	2.61	2.72	2.83	2.94	3.06
48	1.20	1.32	1.40	1.52	1.64	1.76	1.88	2.00	2.12	2.24	2.36	2.50	2.59	2.72	2.83	2.94	3.06
49	1.24	1.31	1.42	1.54	1.66	1.80	1.91	2.02	2.13	2.25	2.36	2.46	2.58	2.69	2.80	2.91	3.01
50	1.18	1.29	1.41	1.54	1.63	1.76	1.87	1.98	2.10	2.20	2.30	2.41	2.52	2.64	2.73	2.82	2.92
51	1.18	1.32	1.49	1.52	1.61	1.72	1.86	1.95	2.07	2.14	2.25	2.35	2.45	2.55	2.65	2.74	2.84
52	1.14	1.25	1.38	1.47	1.57	1.68	1.79	1.86	1.99	2.07	2.15	2.25	2.34	2.44	2.53	2.62	2.71
53	1.15	1.24	1.37	1.41	1.57	1.60	1.69	1.78	1.87	1.98	2.02	2.11	2.20	2.30	2.37	2.46	2.55
54	1.10	1.16	1.31	1.34	1.38	1.47	1.57	1.70	1.74	1.79	1.88	1.95	2.03	2.13	2.18	2.25	2.31
55	1.10	1.15	1.22	1.31	1.27	1.35	1.44	1.56	1.56	1.63	1.70	1.76	1.83	1.88	1.93	1.98	2.03
56	0.90	0.93	1.13	1.08	1.14	1.21	1.42	1.30	1.35	1.41	1.45	1.50	1.54	1.59	1.62	1.66	1.70
57	0.81	0.88	0.95	0.99	0.97	1.08	1.01	1.07	1.12	1.13	1.18	1.20	1.23	1.26	1.28	1.31	1.33
58	0.67	0.69	0.80	0.74	0.77	0.75	0.77	0.79	0.81	0.82	0.85	0.86	0.88	0.89	0.91	0.93	0.94
59	0.30	0.32	0.33	0.33	0.32	0.33	0.33	0.34	0.35	0.36	0.36	0.36	0.37	0.38	0.38	0.39	0.39

Table C.3 Instantaneous Torque Profiles by Traditional Method (34-50 A).

Angle (θ°)/ Current (A)	34	35	36	37	38	39	40	41	42	43	44	45	46	47	48	49	50
0	3.22	3.34	3.46	3.57	3.69	3.81	3.92	4.03	4.15	4.26	4.36	4.47	4.59	4.69	4.80	4.90	5.01
1	3.24	3.34	3.45	3.56	3.68	3.78	3.89	4.01	4.12	4.21	4.33	4.43	4.54	4.65	4.75	4.85	4.96
2	3.18	3.28	3.38	3.49	3.60	3.70	3.81	3.91	4.01	4.12	4.22	4.32	4.42	4.51	4.61	4.71	4.80
3	3.17	3.28	3.39	3.47	3.58	3.70	3.79	3.90	4.01	4.06	4.16	4.27	4.37	4.47	4.57	4.66	4.76
4	3.12	3.22	3.33	3.45	3.53	3.64	3.74	3.84	3.94	4.03	4.13	4.22	4.32	4.41	4.51	4.60	4.69
5	3.04	3.13	3.23	3.33	3.43	3.53	3.62	3.72	3.81	3.90	4.00	4.09	4.18	4.26	4.34	4.42	4.50
6	2.95	3.03	3.13	3.22	3.32	3.41	3.50	3.58	3.67	3.75	3.83	3.91	3.98	4.04	4.11	4.17	4.23
7	2.80	2.89	2.98	3.06	3.15	3.23	3.31	3.37	3.44	3.51	3.57	3.62	3.68	3.74	3.79	3.84	3.89
8	2.63	2.70	2.78	2.84	2.91	2.97	3.02	3.08	3.13	3.18	3.24	3.28	3.33	3.38	3.42	3.47	3.51
9	2.38	2.43	2.49	2.54	2.59	2.64	2.68	2.73	2.77	2.81	2.85	2.89	2.93	2.97	3.01	3.05	3.09
10	2.08	2.12	2.16	2.20	2.24	2.28	2.32	2.35	2.39	2.42	2.46	2.49	2.53	2.56	2.59	2.62	2.66
11	1.73	1.77	1.80	1.83	1.86	1.89	1.92	1.95	1.98	2.01	2.04	2.07	2.09	2.12	2.15	2.17	2.20
12	1.36	1.38	1.41	1.43	1.45	1.48	1.50	1.52	1.54	1.56	1.59	1.61	1.63	1.65	1.67	1.69	1.71
13	0.96	0.97	0.99	1.00	1.02	1.03	1.05	1.06	1.07	1.09	1.10	1.11	1.13	1.14	1.15	1.16	1.18
14	0.40	0.40	0.41	0.41	0.42	0.42	0.43	0.43	0.44	0.44	0.45	0.45	0.46	0.46	0.46	0.47	0.47
15	3.22	3.34	3.46	3.57	3.69	3.81	3.92	4.03	4.15	4.26	4.36	4.47	4.59	4.69	4.80	4.90	5.01
16	3.24	3.34	3.45	3.56	3.68	3.78	3.89	4.01	4.12	4.21	4.33	4.43	4.54	4.65	4.75	4.85	4.96
17	3.18	3.28	3.38	3.49	3.60	3.70	3.81	3.91	4.01	4.12	4.22	4.32	4.42	4.51	4.61	4.71	4.80
18	3.17	3.28	3.39	3.47	3.58	3.70	3.79	3.90	4.01	4.06	4.16	4.27	4.37	4.47	4.57	4.66	4.76
19	3.12	3.22	3.33	3.45	3.53	3.64	3.74	3.84	3.94	4.03	4.13	4.22	4.32	4.41	4.51	4.60	4.69
20	3.04	3.13	3.23	3.33	3.43	3.53	3.62	3.72	3.81	3.90	4.00	4.09	4.18	4.26	4.34	4.42	4.50
21	2.95	3.03	3.13	3.22	3.32	3.41	3.50	3.58	3.67	3.75	3.83	3.91	3.98	4.04	4.11	4.17	4.23
22	2.80	2.89	2.98	3.06	3.15	3.23	3.31	3.37	3.44	3.51	3.57	3.62	3.68	3.74	3.79	3.84	3.89
23	2.63	2.70	2.78	2.84	2.91	2.97	3.02	3.08	3.13	3.18	3.24	3.28	3.33	3.38	3.42	3.47	3.51
24	2.38	2.43	2.49	2.54	2.59	2.64	2.68	2.73	2.77	2.81	2.85	2.89	2.93	2.97	3.01	3.05	3.09
25	2.08	2.12	2.16	2.20	2.24	2.28	2.32	2.35	2.39	2.42	2.46	2.49	2.53	2.56	2.59	2.62	2.66
26	1.73	1.77	1.80	1.83	1.86	1.89	1.92	1.95	1.98	2.01	2.04	2.07	2.09	2.12	2.15	2.17	2.20
27	1.36	1.38	1.41	1.43	1.45	1.48	1.50	1.52	1.54	1.56	1.59	1.61	1.63	1.65	1.67	1.69	1.71
28	0.96	0.97	0.99	1.00	1.02	1.03	1.05	1.06	1.07	1.09	1.10	1.11	1.13	1.14	1.15	1.16	1.18
29	0.40	0.40	0.41	0.41	0.42	0.42	0.43	0.43	0.44	0.44	0.45	0.45	0.46	0.46	0.46	0.47	0.47
30	3.22	3.34	3.46	3.57	3.69	3.81	3.92	4.03	4.15	4.26	4.36	4.47	4.59	4.69	4.80	4.90	5.01
31	3.24	3.34	3.45	3.56	3.68	3.78	3.89	4.01	4.12	4.21	4.33	4.43	4.54	4.65	4.75	4.85	4.96
32	3.18	3.28	3.38	3.49	3.60	3.70	3.81	3.91	4.01	4.12	4.22	4.32	4.42	4.51	4.61	4.71	4.80
33	3.17	3.28	3.39	3.47	3.58	3.70	3.79	3.90	4.01	4.06	4.16	4.27	4.37	4.47	4.57	4.66	4.76
34	3.12	3.22	3.33	3.45	3.53	3.64	3.74	3.84	3.94	4.03	4.13	4.22	4.32	4.41	4.51	4.60	4.69
35	3.04	3.13	3.23	3.33	3.43	3.53	3.62	3.72	3.81	3.90	4.00	4.09	4.18	4.26	4.34	4.42	4.50
36	2.95	3.03	3.13	3.22	3.32	3.41	3.50	3.58	3.67	3.75	3.83	3.91	3.98	4.04	4.11	4.17	4.23
37	2.80	2.89	2.98	3.06	3.15	3.23	3.31	3.37	3.44	3.51	3.57	3.62	3.68	3.74	3.79	3.84	3.89

38	2.63	2.70	2.78	2.84	2.91	2.97	3.02	3.08	3.13	3.18	3.24	3.28	3.33	3.38	3.42	3.47	3.51
39	2.38	2.43	2.49	2.54	2.59	2.64	2.68	2.73	2.77	2.81	2.85	2.89	2.93	2.97	3.01	3.05	3.09
40	2.08	2.12	2.16	2.20	2.24	2.28	2.32	2.35	2.39	2.42	2.46	2.49	2.53	2.56	2.59	2.62	2.66
41	1.73	1.77	1.80	1.83	1.86	1.89	1.92	1.95	1.98	2.01	2.04	2.07	2.09	2.12	2.15	2.17	2.20
42	1.36	1.38	1.41	1.43	1.45	1.48	1.50	1.52	1.54	1.56	1.59	1.61	1.63	1.65	1.67	1.69	1.71
43	0.96	0.97	0.99	1.00	1.02	1.03	1.05	1.06	1.07	1.09	1.10	1.11	1.13	1.14	1.15	1.16	1.18
44	0.40	0.40	0.41	0.41	0.42	0.42	0.43	0.43	0.44	0.44	0.45	0.45	0.46	0.46	0.46	0.47	0.47
45	3.22	3.34	3.46	3.57	3.69	3.81	3.92	4.03	4.15	4.26	4.36	4.47	4.59	4.69	4.80	4.90	5.01
46	3.24	3.34	3.45	3.56	3.68	3.78	3.89	4.01	4.12	4.21	4.33	4.43	4.54	4.65	4.75	4.85	4.96
47	3.18	3.28	3.38	3.49	3.60	3.70	3.81	3.91	4.01	4.12	4.22	4.32	4.42	4.51	4.61	4.71	4.80
48	3.17	3.28	3.39	3.47	3.58	3.70	3.79	3.90	4.01	4.06	4.16	4.27	4.37	4.47	4.57	4.66	4.76
49	3.12	3.22	3.33	3.45	3.53	3.64	3.74	3.84	3.94	4.03	4.13	4.22	4.32	4.41	4.51	4.60	4.69
50	3.04	3.13	3.23	3.33	3.43	3.53	3.62	3.72	3.81	3.90	4.00	4.09	4.18	4.26	4.34	4.42	4.50
51	2.95	3.03	3.13	3.22	3.32	3.41	3.50	3.58	3.67	3.75	3.83	3.91	3.98	4.04	4.11	4.17	4.23
52	2.80	2.89	2.98	3.06	3.15	3.23	3.31	3.37	3.44	3.51	3.57	3.62	3.68	3.74	3.79	3.84	3.89
53	2.63	2.70	2.78	2.84	2.91	2.97	3.02	3.08	3.13	3.18	3.24	3.28	3.33	3.38	3.42	3.47	3.51
54	2.38	2.43	2.49	2.54	2.59	2.64	2.68	2.73	2.77	2.81	2.85	2.89	2.93	2.97	3.01	3.05	3.09
55	2.08	2.12	2.16	2.20	2.24	2.28	2.32	2.35	2.39	2.42	2.46	2.49	2.53	2.56	2.59	2.62	2.66
56	1.73	1.77	1.80	1.83	1.86	1.89	1.92	1.95	1.98	2.01	2.04	2.07	2.09	2.12	2.15	2.17	2.20
57	1.36	1.38	1.41	1.43	1.45	1.48	1.50	1.52	1.54	1.56	1.59	1.61	1.63	1.65	1.67	1.69	1.71
58	0.96	0.97	0.99	1.00	1.02	1.03	1.05	1.06	1.07	1.09	1.10	1.11	1.13	1.14	1.15	1.16	1.18
59	0.40	0.40	0.41	0.41	0.42	0.42	0.43	0.43	0.44	0.44	0.45	0.45	0.46	0.46	0.46	0.47	0.47

Table C.4 Instantaneous Phase Current Profiles by Traditional Method (45 A).

Angle (θ°)/ Current (A)	I1	I2	I3	I4
0	0	0	0	45
1	0	0	0	45
2	0	0	0	45
3	0	0	0	45
4	0	0	0	45
5	0	0	0	45
6	0	0	0	45
7	0	0	0	45
8	0	0	0	45
9	0	0	0	45
10	0	0	0	45
11	0	0	0	45
12	0	0	0	45
13	0	0	0	45
14	0	0	0	45
15	45	0	0	0
16	45	0	0	0
17	45	0	0	0
18	45	0	0	0
19	45	0	0	0
20	45	0	0	0
21	45	0	0	0
22	45	0	0	0
23	45	0	0	0
24	45	0	0	0
25	45	0	0	0
26	45	0	0	0
27	45	0	0	0
28	45	0	0	0
29	45	0	0	0
30	0	45	0	0
31	0	45	0	0
32	0	45	0	0
33	0	45	0	0
34	0	45	0	0
35	0	45	0	0
36	0	45	0	0
37	0	45	0	0

38	0	45	0	0
39	0	45	0	0
40	0	45	0	0
41	0	45	0	0
42	0	45	0	0
43	0	45	0	0
44	0	45	0	0
45	0	0	45	0
46	0	0	45	0
47	0	0	45	0
48	0	0	45	0
49	0	0	45	0
50	0	0	45	0
51	0	0	45	0
52	0	0	45	0
53	0	0	45	0
54	0	0	45	0
55	0	0	45	0
56	0	0	45	0
57	0	0	45	0
58	0	0	45	0
59	0	0	45	0

Table C.5 Instantaneous Torque Profiles by Advanced Critical Angle Method (0-16 A).

Angle (θ°)/ Current (A)	0	1	2	3	4	5	6	7	8	9	10	11	12	13	14	15	16
0	0.00	0.00	0.02	0.04	0.07	0.12	0.17	0.23	0.29	0.37	0.46	0.55	0.66	0.77	0.87	0.98	1.11
1	0.00	0.00	0.02	0.04	0.07	0.12	0.17	0.23	0.29	0.37	0.46	0.55	0.65	0.77	0.86	0.99	1.10
2	0.00	0.00	0.02	0.04	0.07	0.12	0.17	0.23	0.29	0.37	0.46	0.55	0.66	0.77	0.87	0.98	1.13
3	0.00	0.00	0.02	0.04	0.07	0.11	0.15	0.21	0.27	0.34	0.45	0.51	0.61	0.72	0.82	0.93	1.10
4	0.00	0.00	0.02	0.04	0.07	0.11	0.16	0.22	0.29	0.37	0.46	0.55	0.66	0.77	0.86	0.98	1.09
5	0.00	0.00	0.02	0.04	0.07	0.11	0.16	0.22	0.28	0.36	0.45	0.54	0.65	0.76	0.85	0.96	1.07
6	0.00	0.00	0.02	0.04	0.07	0.11	0.16	0.22	0.29	0.37	0.45	0.54	0.65	0.76	0.85	0.96	1.07
7	0.00	0.00	0.02	0.04	0.07	0.11	0.16	0.21	0.28	0.36	0.43	0.52	0.62	0.72	0.82	0.93	1.04
8	0.00	0.00	0.02	0.04	0.07	0.11	0.16	0.22	0.29	0.38	0.45	0.55	0.65	0.76	0.87	1.00	1.12
9	0.00	0.00	0.02	0.04	0.07	0.11	0.16	0.22	0.29	0.38	0.46	0.55	0.65	0.76	0.86	0.99	1.11
10	0.00	0.00	0.02	0.04	0.07	0.11	0.16	0.22	0.29	0.38	0.46	0.55	0.65	0.76	0.87	0.96	1.07
11	0.00	0.00	0.02	0.04	0.07	0.11	0.17	0.22	0.29	0.37	0.46	0.55	0.65	0.75	0.87	0.98	1.08
12	0.00	0.00	0.02	0.04	0.07	0.12	0.17	0.23	0.29	0.37	0.46	0.56	0.65	0.76	0.86	0.97	1.09
13	0.00	0.00	0.02	0.04	0.07	0.12	0.17	0.23	0.30	0.38	0.46	0.56	0.66	0.77	0.87	0.99	1.11
14	0.00	0.00	0.02	0.04	0.07	0.11	0.16	0.22	0.29	0.37	0.46	0.56	0.65	0.77	0.86	0.98	1.09
15	0.00	0.00	0.02	0.04	0.07	0.12	0.17	0.23	0.29	0.37	0.46	0.55	0.66	0.77	0.87	0.98	1.11
16	0.00	0.00	0.02	0.04	0.07	0.12	0.17	0.23	0.29	0.37	0.46	0.55	0.65	0.77	0.86	0.99	1.10
17	0.00	0.00	0.02	0.04	0.07	0.12	0.17	0.23	0.29	0.37	0.46	0.55	0.66	0.77	0.87	0.98	1.13
18	0.00	0.00	0.02	0.04	0.07	0.11	0.15	0.21	0.27	0.34	0.45	0.51	0.61	0.72	0.82	0.93	1.10
19	0.00	0.00	0.02	0.04	0.07	0.11	0.16	0.22	0.29	0.37	0.46	0.55	0.66	0.77	0.86	0.98	1.09
20	0.00	0.00	0.02	0.04	0.07	0.11	0.16	0.22	0.28	0.36	0.45	0.54	0.65	0.76	0.85	0.96	1.07
21	0.00	0.00	0.02	0.04	0.07	0.11	0.16	0.22	0.29	0.37	0.45	0.54	0.65	0.76	0.85	0.96	1.07
22	0.00	0.00	0.02	0.04	0.07	0.11	0.16	0.21	0.28	0.36	0.43	0.52	0.62	0.72	0.82	0.93	1.04
23	0.00	0.00	0.02	0.04	0.07	0.11	0.16	0.22	0.29	0.38	0.45	0.55	0.65	0.76	0.87	1.00	1.12
24	0.00	0.00	0.02	0.04	0.07	0.11	0.16	0.22	0.29	0.38	0.46	0.55	0.65	0.76	0.86	0.99	1.11
25	0.00	0.00	0.02	0.04	0.07	0.11	0.16	0.22	0.29	0.38	0.46	0.55	0.65	0.76	0.87	0.96	1.07
26	0.00	0.00	0.02	0.04	0.07	0.11	0.17	0.22	0.29	0.37	0.46	0.55	0.65	0.75	0.87	0.98	1.08
27	0.00	0.00	0.02	0.04	0.07	0.12	0.17	0.23	0.29	0.37	0.46	0.56	0.65	0.76	0.86	0.97	1.09
28	0.00	0.00	0.02	0.04	0.07	0.12	0.17	0.23	0.30	0.38	0.46	0.56	0.66	0.77	0.87	0.99	1.11
29	0.00	0.00	0.02	0.04	0.07	0.11	0.16	0.22	0.29	0.37	0.46	0.56	0.65	0.77	0.86	0.98	1.09
30	0.00	0.00	0.02	0.04	0.07	0.12	0.17	0.23	0.29	0.37	0.46	0.55	0.66	0.77	0.87	0.98	1.11
31	0.00	0.00	0.02	0.04	0.07	0.12	0.17	0.23	0.29	0.37	0.46	0.55	0.65	0.77	0.86	0.99	1.10
32	0.00	0.00	0.02	0.04	0.07	0.12	0.17	0.23	0.29	0.37	0.46	0.55	0.66	0.77	0.87	0.98	1.13
33	0.00	0.00	0.02	0.04	0.07	0.11	0.15	0.21	0.27	0.34	0.45	0.51	0.61	0.72	0.82	0.93	1.10
34	0.00	0.00	0.02	0.04	0.07	0.11	0.16	0.22	0.29	0.37	0.46	0.55	0.66	0.77	0.86	0.98	1.09
35	0.00	0.00	0.02	0.04	0.07	0.11	0.16	0.22	0.28	0.36	0.45	0.54	0.65	0.76	0.85	0.96	1.07
36	0.00	0.00	0.02	0.04	0.07	0.11	0.16	0.22	0.29	0.37	0.45	0.54	0.65	0.76	0.85	0.96	1.07
37	0.00	0.00	0.02	0.04	0.07	0.11	0.16	0.21	0.28	0.36	0.43	0.52	0.62	0.72	0.82	0.93	1.04
38	0.00	0.00	0.02	0.04	0.07	0.11	0.16	0.22	0.29	0.38	0.45	0.55	0.65	0.76	0.87	1.00	1.12

39	0.00	0.00	0.02	0.04	0.07	0.11	0.16	0.22	0.29	0.38	0.46	0.55	0.65	0.76	0.86	0.99	1.11
40	0.00	0.00	0.02	0.04	0.07	0.11	0.16	0.22	0.29	0.38	0.46	0.55	0.65	0.76	0.87	0.96	1.07
41	0.00	0.00	0.02	0.04	0.07	0.11	0.17	0.22	0.29	0.37	0.46	0.55	0.65	0.75	0.87	0.98	1.08
42	0.00	0.00	0.02	0.04	0.07	0.12	0.17	0.23	0.29	0.37	0.46	0.56	0.65	0.76	0.86	0.97	1.09
43	0.00	0.00	0.02	0.04	0.07	0.12	0.17	0.23	0.30	0.38	0.46	0.56	0.66	0.77	0.87	0.99	1.11
44	0.00	0.00	0.02	0.04	0.07	0.11	0.16	0.22	0.29	0.37	0.46	0.56	0.65	0.77	0.86	0.98	1.09
45	0.00	0.00	0.02	0.04	0.07	0.12	0.17	0.23	0.29	0.37	0.46	0.55	0.66	0.77	0.87	0.98	1.11
46	0.00	0.00	0.02	0.04	0.07	0.12	0.17	0.23	0.29	0.37	0.46	0.55	0.65	0.77	0.86	0.99	1.10
47	0.00	0.00	0.02	0.04	0.07	0.12	0.17	0.23	0.29	0.37	0.46	0.55	0.66	0.77	0.87	0.98	1.13
48	0.00	0.00	0.02	0.04	0.07	0.11	0.15	0.21	0.27	0.34	0.45	0.51	0.61	0.72	0.82	0.93	1.10
49	0.00	0.00	0.02	0.04	0.07	0.11	0.16	0.22	0.29	0.37	0.46	0.55	0.66	0.77	0.86	0.98	1.09
50	0.00	0.00	0.02	0.04	0.07	0.11	0.16	0.22	0.28	0.36	0.45	0.54	0.65	0.76	0.85	0.96	1.07
51	0.00	0.00	0.02	0.04	0.07	0.11	0.16	0.22	0.29	0.37	0.45	0.54	0.65	0.76	0.85	0.96	1.07
52	0.00	0.00	0.02	0.04	0.07	0.11	0.16	0.21	0.28	0.36	0.43	0.52	0.62	0.72	0.82	0.93	1.04
53	0.00	0.00	0.02	0.04	0.07	0.11	0.16	0.22	0.29	0.38	0.45	0.55	0.65	0.76	0.87	1.00	1.12
54	0.00	0.00	0.02	0.04	0.07	0.11	0.16	0.22	0.29	0.38	0.46	0.55	0.65	0.76	0.86	0.99	1.11
55	0.00	0.00	0.02	0.04	0.07	0.11	0.16	0.22	0.29	0.38	0.46	0.55	0.65	0.76	0.87	0.96	1.07
56	0.00	0.00	0.02	0.04	0.07	0.11	0.17	0.22	0.29	0.37	0.46	0.55	0.65	0.75	0.87	0.98	1.08
57	0.00	0.00	0.02	0.04	0.07	0.12	0.17	0.23	0.29	0.37	0.46	0.56	0.65	0.76	0.86	0.97	1.09
58	0.00	0.00	0.02	0.04	0.07	0.12	0.17	0.23	0.30	0.38	0.46	0.56	0.66	0.77	0.87	0.99	1.11
59	0.00	0.00	0.02	0.04	0.07	0.11	0.16	0.22	0.29	0.37	0.46	0.56	0.65	0.77	0.86	0.98	1.09

Table C.6 Instantaneous Torque Profiles by Advanced Critical Angle Method (17-33 A).

Angle (θ°)/ Current (A)	17	18	19	20	21	22	23	24	25	26	27	28	29	30	31	32	33
0	1.21	1.34	1.45	1.56	1.67	1.79	1.91	2.03	2.15	2.29	2.39	2.50	2.63	2.76	2.87	2.98	3.11
1	1.21	1.33	1.46	1.56	1.67	1.78	1.92	2.04	2.15	2.27	2.40	2.51	2.63	2.76	2.87	2.99	3.11
2	1.20	1.32	1.48	1.55	1.67	1.79	1.90	2.02	2.15	2.27	2.39	2.49	2.61	2.72	2.83	2.94	3.06
3	1.20	1.32	1.40	1.52	1.64	1.76	1.88	2.00	2.12	2.24	2.36	2.50	2.59	2.72	2.83	2.94	3.06
4	1.24	1.31	1.42	1.54	1.66	1.80	1.91	2.02	2.13	2.25	2.36	2.46	2.58	2.69	2.80	2.91	3.01
5	1.18	1.29	1.41	1.54	1.63	1.76	1.87	1.98	2.10	2.20	2.30	2.41	2.52	2.64	2.73	2.82	2.92
6	1.18	1.32	1.49	1.52	1.61	1.72	1.86	1.95	2.07	2.14	2.25	2.35	2.45	2.55	2.65	2.74	2.84
7	1.16	1.28	1.40	1.52	1.64	1.78	1.88	1.92	2.02	2.12	2.22	2.32	2.42	2.52	2.61	2.71	2.81
8	1.25	1.38	1.43	1.54	1.64	1.75	1.86	1.94	2.04	2.15	2.25	2.35	2.46	2.56	2.66	2.77	2.87
9	1.18	1.30	1.41	1.52	1.61	1.75	1.84	1.93	2.04	2.15	2.26	2.36	2.47	2.58	2.69	2.80	2.91
10	1.19	1.28	1.42	1.51	1.62	1.73	1.86	1.95	2.07	2.18	2.29	2.40	2.51	2.62	2.74	2.85	2.96
11	1.19	1.32	1.41	1.52	1.64	1.75	1.86	1.98	2.10	2.22	2.31	2.44	2.54	2.66	2.77	2.89	3.00
12	1.21	1.33	1.46	1.54	1.65	1.77	1.88	1.99	2.11	2.26	2.34	2.45	2.57	2.69	2.80	2.92	3.03
13	1.21	1.32	1.44	1.56	1.67	1.82	1.91	2.02	2.16	2.26	2.38	2.49	2.61	2.73	2.85	2.96	3.08
14	1.20	1.31	1.44	1.57	1.66	1.77	1.90	2.02	2.14	2.26	2.38	2.48	2.62	2.73	2.85	2.97	3.09
15	1.21	1.34	1.45	1.56	1.67	1.79	1.91	2.03	2.15	2.29	2.39	2.50	2.63	2.76	2.87	2.98	3.11
16	1.21	1.33	1.46	1.56	1.67	1.78	1.92	2.04	2.15	2.27	2.40	2.51	2.63	2.76	2.87	2.99	3.11
17	1.20	1.32	1.48	1.55	1.67	1.79	1.90	2.02	2.15	2.27	2.39	2.49	2.61	2.72	2.83	2.94	3.06
18	1.20	1.32	1.40	1.52	1.64	1.76	1.88	2.00	2.12	2.24	2.36	2.50	2.59	2.72	2.83	2.94	3.06
19	1.24	1.31	1.42	1.54	1.66	1.80	1.91	2.02	2.13	2.25	2.36	2.46	2.58	2.69	2.80	2.91	3.01
20	1.18	1.29	1.41	1.54	1.63	1.76	1.87	1.98	2.10	2.20	2.30	2.41	2.52	2.64	2.73	2.82	2.92
21	1.18	1.32	1.49	1.52	1.61	1.72	1.86	1.95	2.07	2.14	2.25	2.35	2.45	2.55	2.65	2.74	2.84
22	1.16	1.28	1.40	1.52	1.64	1.78	1.88	1.92	2.02	2.12	2.22	2.32	2.42	2.52	2.61	2.71	2.81
23	1.25	1.38	1.43	1.54	1.64	1.75	1.86	1.94	2.04	2.15	2.25	2.35	2.46	2.56	2.66	2.77	2.87
24	1.18	1.30	1.41	1.52	1.61	1.75	1.84	1.93	2.04	2.15	2.26	2.36	2.47	2.58	2.69	2.80	2.91
25	1.19	1.28	1.42	1.51	1.62	1.73	1.86	1.95	2.07	2.18	2.29	2.40	2.51	2.62	2.74	2.85	2.96
26	1.19	1.32	1.41	1.52	1.64	1.75	1.86	1.98	2.10	2.22	2.31	2.44	2.54	2.66	2.77	2.89	3.00
27	1.21	1.33	1.46	1.54	1.65	1.77	1.88	1.99	2.11	2.26	2.34	2.45	2.57	2.69	2.80	2.92	3.03
28	1.21	1.32	1.44	1.56	1.67	1.82	1.91	2.02	2.16	2.26	2.38	2.49	2.61	2.73	2.85	2.96	3.08
29	1.20	1.31	1.44	1.57	1.66	1.77	1.90	2.02	2.14	2.26	2.38	2.48	2.62	2.73	2.85	2.97	3.09
30	1.21	1.34	1.45	1.56	1.67	1.79	1.91	2.03	2.15	2.29	2.39	2.50	2.63	2.76	2.87	2.98	3.11
31	1.21	1.33	1.46	1.56	1.67	1.78	1.92	2.04	2.15	2.27	2.40	2.51	2.63	2.76	2.87	2.99	3.11
32	1.20	1.32	1.48	1.55	1.67	1.79	1.90	2.02	2.15	2.27	2.39	2.49	2.61	2.72	2.83	2.94	3.06
33	1.20	1.32	1.40	1.52	1.64	1.76	1.88	2.00	2.12	2.24	2.36	2.50	2.59	2.72	2.83	2.94	3.06
34	1.24	1.31	1.42	1.54	1.66	1.80	1.91	2.02	2.13	2.25	2.36	2.46	2.58	2.69	2.80	2.91	3.01
35	1.18	1.29	1.41	1.54	1.63	1.76	1.87	1.98	2.10	2.20	2.30	2.41	2.52	2.64	2.73	2.82	2.92
36	1.18	1.32	1.49	1.52	1.61	1.72	1.86	1.95	2.07	2.14	2.25	2.35	2.45	2.55	2.65	2.74	2.84
37	1.16	1.28	1.40	1.52	1.64	1.78	1.88	1.92	2.02	2.12	2.22	2.32	2.42	2.52	2.61	2.71	2.81

38	1.25	1.38	1.43	1.54	1.64	1.75	1.86	1.94	2.04	2.15	2.25	2.35	2.46	2.56	2.66	2.77	2.87
39	1.18	1.30	1.41	1.52	1.61	1.75	1.84	1.93	2.04	2.15	2.26	2.36	2.47	2.58	2.69	2.80	2.91
40	1.19	1.28	1.42	1.51	1.62	1.73	1.86	1.95	2.07	2.18	2.29	2.40	2.51	2.62	2.74	2.85	2.96
41	1.19	1.32	1.41	1.52	1.64	1.75	1.86	1.98	2.10	2.22	2.31	2.44	2.54	2.66	2.77	2.89	3.00
42	1.21	1.33	1.46	1.54	1.65	1.77	1.88	1.99	2.11	2.26	2.34	2.45	2.57	2.69	2.80	2.92	3.03
43	1.21	1.32	1.44	1.56	1.67	1.82	1.91	2.02	2.16	2.26	2.38	2.49	2.61	2.73	2.85	2.96	3.08
44	1.20	1.31	1.44	1.57	1.66	1.77	1.90	2.02	2.14	2.26	2.38	2.48	2.62	2.73	2.85	2.97	3.09
45	1.21	1.34	1.45	1.56	1.67	1.79	1.91	2.03	2.15	2.29	2.39	2.50	2.63	2.76	2.87	2.98	3.11
46	1.21	1.33	1.46	1.56	1.67	1.78	1.92	2.04	2.15	2.27	2.40	2.51	2.63	2.76	2.87	2.99	3.11
47	1.20	1.32	1.48	1.55	1.67	1.79	1.90	2.02	2.15	2.27	2.39	2.49	2.61	2.72	2.83	2.94	3.06
48	1.20	1.32	1.40	1.52	1.64	1.76	1.88	2.00	2.12	2.24	2.36	2.50	2.59	2.72	2.83	2.94	3.06
49	1.24	1.31	1.42	1.54	1.66	1.80	1.91	2.02	2.13	2.25	2.36	2.46	2.58	2.69	2.80	2.91	3.01
50	1.18	1.29	1.41	1.54	1.63	1.76	1.87	1.98	2.10	2.20	2.30	2.41	2.52	2.64	2.73	2.82	2.92
51	1.18	1.32	1.49	1.52	1.61	1.72	1.86	1.95	2.07	2.14	2.25	2.35	2.45	2.55	2.65	2.74	2.84
52	1.16	1.28	1.40	1.52	1.64	1.78	1.88	1.92	2.02	2.12	2.22	2.32	2.42	2.52	2.61	2.71	2.81
53	1.25	1.38	1.43	1.54	1.64	1.75	1.86	1.94	2.04	2.15	2.25	2.35	2.46	2.56	2.66	2.77	2.87
54	1.18	1.30	1.41	1.52	1.61	1.75	1.84	1.93	2.04	2.15	2.26	2.36	2.47	2.58	2.69	2.80	2.91
55	1.19	1.28	1.42	1.51	1.62	1.73	1.86	1.95	2.07	2.18	2.29	2.40	2.51	2.62	2.74	2.85	2.96
56	1.19	1.32	1.41	1.52	1.64	1.75	1.86	1.98	2.10	2.22	2.31	2.44	2.54	2.66	2.77	2.89	3.00
57	1.21	1.33	1.46	1.54	1.65	1.77	1.88	1.99	2.11	2.26	2.34	2.45	2.57	2.69	2.80	2.92	3.03
58	1.21	1.32	1.44	1.56	1.67	1.82	1.91	2.02	2.16	2.26	2.38	2.49	2.61	2.73	2.85	2.96	3.08
59	1.20	1.31	1.44	1.57	1.66	1.77	1.90	2.02	2.14	2.26	2.38	2.48	2.62	2.73	2.85	2.97	3.09

Table C.7 Instantaneous Torque Profiles by Advanced Critical Angle Method (34-50 A).

Angle (θ°)/ Current (A)	34	35	36	37	38	39	40	41	42	43	44	45	46	47	48	49	50
0	3.22	3.34	3.46	3.57	3.69	3.81	3.92	4.03	4.15	4.26	4.36	4.47	4.59	4.69	4.80	4.90	5.01
1	3.24	3.34	3.45	3.56	3.68	3.78	3.89	4.01	4.12	4.21	4.33	4.43	4.54	4.65	4.75	4.85	4.96
2	3.18	3.28	3.38	3.49	3.60	3.70	3.81	3.91	4.01	4.12	4.22	4.32	4.42	4.51	4.61	4.71	4.80
3	3.17	3.28	3.39	3.47	3.58	3.70	3.79	3.90	4.01	4.06	4.16	4.27	4.37	4.47	4.57	4.66	4.76
4	3.12	3.22	3.33	3.45	3.53	3.64	3.74	3.84	3.94	4.03	4.13	4.22	4.32	4.41	4.51	4.60	4.69
5	3.04	3.13	3.23	3.33	3.43	3.53	3.62	3.72	3.81	3.90	4.00	4.09	4.18	4.26	4.34	4.42	4.50
6	2.95	3.03	3.13	3.22	3.32	3.41	3.50	3.58	3.67	3.75	3.83	3.91	3.98	4.04	4.11	4.17	4.23
7	2.91	3.01	3.10	3.23	3.33	3.43	3.53	3.63	3.74	3.79	3.88	3.98	4.08	4.18	4.28	4.37	4.46
8	2.97	3.08	3.19	3.31	3.40	3.50	3.63	3.73	3.80	3.93	4.01	4.18	4.22	4.32	4.42	4.57	4.62
9	3.01	3.12	3.22	3.33	3.45	3.55	3.65	3.76	3.87	3.98	4.08	4.18	4.29	4.40	4.50	4.61	4.72
10	3.07	3.18	3.29	3.39	3.51	3.62	3.73	3.84	3.95	4.06	4.17	4.28	4.38	4.49	4.60	4.72	4.82
11	3.11	3.23	3.34	3.45	3.56	3.68	3.79	3.90	4.02	4.13	4.24	4.35	4.46	4.57	4.68	4.79	4.90
12	3.15	3.26	3.38	3.49	3.61	3.72	3.84	3.95	4.06	4.18	4.29	4.40	4.51	4.64	4.74	4.85	4.96
13	3.20	3.31	3.43	3.55	3.67	3.78	3.89	4.02	4.13	4.24	4.36	4.47	4.59	4.70	4.81	4.92	5.03
14	3.21	3.32	3.44	3.56	3.68	3.79	3.91	4.03	4.14	4.25	4.38	4.48	4.59	4.71	4.82	4.93	5.04
15	3.22	3.34	3.46	3.57	3.69	3.81	3.92	4.03	4.15	4.26	4.36	4.47	4.59	4.69	4.80	4.90	5.01
16	3.24	3.34	3.45	3.56	3.68	3.78	3.89	4.01	4.12	4.21	4.33	4.43	4.54	4.65	4.75	4.85	4.96
17	3.18	3.28	3.38	3.49	3.60	3.70	3.81	3.91	4.01	4.12	4.22	4.32	4.42	4.51	4.61	4.71	4.80
18	3.17	3.28	3.39	3.47	3.58	3.70	3.79	3.90	4.01	4.06	4.16	4.27	4.37	4.47	4.57	4.66	4.76
19	3.12	3.22	3.33	3.45	3.53	3.64	3.74	3.84	3.94	4.03	4.13	4.22	4.32	4.41	4.51	4.60	4.69
20	3.04	3.13	3.23	3.33	3.43	3.53	3.62	3.72	3.81	3.90	4.00	4.09	4.18	4.26	4.34	4.42	4.50
21	2.95	3.03	3.13	3.22	3.32	3.41	3.50	3.58	3.67	3.75	3.83	3.91	3.98	4.04	4.11	4.17	4.23
22	2.91	3.01	3.10	3.23	3.33	3.43	3.53	3.63	3.74	3.79	3.88	3.98	4.08	4.18	4.28	4.37	4.46
23	2.97	3.08	3.19	3.31	3.40	3.50	3.63	3.73	3.80	3.93	4.01	4.18	4.22	4.32	4.42	4.57	4.62
24	3.01	3.12	3.22	3.33	3.45	3.55	3.65	3.76	3.87	3.98	4.08	4.18	4.29	4.40	4.50	4.61	4.72
25	3.07	3.18	3.29	3.39	3.51	3.62	3.73	3.84	3.95	4.06	4.17	4.28	4.38	4.49	4.60	4.72	4.82
26	3.11	3.23	3.34	3.45	3.56	3.68	3.79	3.90	4.02	4.13	4.24	4.35	4.46	4.57	4.68	4.79	4.90
27	3.15	3.26	3.38	3.49	3.61	3.72	3.84	3.95	4.06	4.18	4.29	4.40	4.51	4.64	4.74	4.85	4.96
28	3.20	3.31	3.43	3.55	3.67	3.78	3.89	4.02	4.13	4.24	4.36	4.47	4.59	4.70	4.81	4.92	5.03
29	3.21	3.32	3.44	3.56	3.68	3.79	3.91	4.03	4.14	4.25	4.38	4.48	4.59	4.71	4.82	4.93	5.04
30	3.22	3.34	3.46	3.57	3.69	3.81	3.92	4.03	4.15	4.26	4.36	4.47	4.59	4.69	4.80	4.90	5.01
31	3.24	3.34	3.45	3.56	3.68	3.78	3.89	4.01	4.12	4.21	4.33	4.43	4.54	4.65	4.75	4.85	4.96
32	3.18	3.28	3.38	3.49	3.60	3.70	3.81	3.91	4.01	4.12	4.22	4.32	4.42	4.51	4.61	4.71	4.80
33	3.17	3.28	3.39	3.47	3.58	3.70	3.79	3.90	4.01	4.06	4.16	4.27	4.37	4.47	4.57	4.66	4.76
34	3.12	3.22	3.33	3.45	3.53	3.64	3.74	3.84	3.94	4.03	4.13	4.22	4.32	4.41	4.51	4.60	4.69
35	3.04	3.13	3.23	3.33	3.43	3.53	3.62	3.72	3.81	3.90	4.00	4.09	4.18	4.26	4.34	4.42	4.50
36	2.95	3.03	3.13	3.22	3.32	3.41	3.50	3.58	3.67	3.75	3.83	3.91	3.98	4.04	4.11	4.17	4.23
37	2.91	3.01	3.10	3.23	3.33	3.43	3.53	3.63	3.74	3.79	3.88	3.98	4.08	4.18	4.28	4.37	4.46
38	2.97	3.08	3.19	3.31	3.40	3.50	3.63	3.73	3.80	3.93	4.01	4.18	4.22	4.32	4.42	4.57	4.62

39	3.01	3.12	3.22	3.33	3.45	3.55	3.65	3.76	3.87	3.98	4.08	4.18	4.29	4.40	4.50	4.61	4.72
40	3.07	3.18	3.29	3.39	3.51	3.62	3.73	3.84	3.95	4.06	4.17	4.28	4.38	4.49	4.60	4.72	4.82
41	3.11	3.23	3.34	3.45	3.56	3.68	3.79	3.90	4.02	4.13	4.24	4.35	4.46	4.57	4.68	4.79	4.90
42	3.15	3.26	3.38	3.49	3.61	3.72	3.84	3.95	4.06	4.18	4.29	4.40	4.51	4.64	4.74	4.85	4.96
43	3.20	3.31	3.43	3.55	3.67	3.78	3.89	4.02	4.13	4.24	4.36	4.47	4.59	4.70	4.81	4.92	5.03
44	3.21	3.32	3.44	3.56	3.68	3.79	3.91	4.03	4.14	4.25	4.38	4.48	4.59	4.71	4.82	4.93	5.04
45	3.22	3.34	3.46	3.57	3.69	3.81	3.92	4.03	4.15	4.26	4.36	4.47	4.59	4.69	4.80	4.90	5.01
46	3.24	3.34	3.45	3.56	3.68	3.78	3.89	4.01	4.12	4.21	4.33	4.43	4.54	4.65	4.75	4.85	4.96
47	3.18	3.28	3.38	3.49	3.60	3.70	3.81	3.91	4.01	4.12	4.22	4.32	4.42	4.51	4.61	4.71	4.80
48	3.17	3.28	3.39	3.47	3.58	3.70	3.79	3.90	4.01	4.06	4.16	4.27	4.37	4.47	4.57	4.66	4.76
49	3.12	3.22	3.33	3.45	3.53	3.64	3.74	3.84	3.94	4.03	4.13	4.22	4.32	4.41	4.51	4.60	4.69
50	3.04	3.13	3.23	3.33	3.43	3.53	3.62	3.72	3.81	3.90	4.00	4.09	4.18	4.26	4.34	4.42	4.50
51	2.95	3.03	3.13	3.22	3.32	3.41	3.50	3.58	3.67	3.75	3.83	3.91	3.98	4.04	4.11	4.17	4.23
52	2.91	3.01	3.10	3.23	3.33	3.43	3.53	3.63	3.74	3.79	3.88	3.98	4.08	4.18	4.28	4.37	4.46
53	2.97	3.08	3.19	3.31	3.40	3.50	3.63	3.73	3.80	3.93	4.01	4.18	4.22	4.32	4.42	4.57	4.62
54	3.01	3.12	3.22	3.33	3.45	3.55	3.65	3.76	3.87	3.98	4.08	4.18	4.29	4.40	4.50	4.61	4.72
55	3.07	3.18	3.29	3.39	3.51	3.62	3.73	3.84	3.95	4.06	4.17	4.28	4.38	4.49	4.60	4.72	4.82
56	3.11	3.23	3.34	3.45	3.56	3.68	3.79	3.90	4.02	4.13	4.24	4.35	4.46	4.57	4.68	4.79	4.90
57	3.15	3.26	3.38	3.49	3.61	3.72	3.84	3.95	4.06	4.18	4.29	4.40	4.51	4.64	4.74	4.85	4.96
58	3.20	3.31	3.43	3.55	3.67	3.78	3.89	4.02	4.13	4.24	4.36	4.47	4.59	4.70	4.81	4.92	5.03
59	3.21	3.32	3.44	3.56	3.68	3.79	3.91	4.03	4.14	4.25	4.38	4.48	4.59	4.71	4.82	4.93	5.04

Table C.8 Instantaneous Phase Current Profiles by Advanced Critical Angle Method

(45 A).

Angle (θ°)/ Current (A)	I1	I2	I3	I4
0	0	0	0	45
1	0	0	0	45
2	0	0	0	45
3	0	0	0	45
4	0	0	0	45
5	0	0	0	45
6	0	0	0	45
7	0	0	0	45
8	45	0	0	0
9	45	0	0	0
10	45	0	0	0
11	45	0	0	0
12	45	0	0	0
13	45	0	0	0
14	45	0	0	0
15	45	0	0	0
16	45	0	0	0
17	45	0	0	0
18	45	0	0	0
19	45	0	0	0
20	45	0	0	0
21	45	0	0	0
22	45	0	0	0
23	0	45	0	0
24	0	45	0	0
25	0	45	0	0
26	0	45	0	0
27	0	45	0	0
28	0	45	0	0
29	0	45	0	0
30	0	45	0	0
31	0	45	0	0
32	0	45	0	0
33	0	45	0	0
34	0	45	0	0
35	0	45	0	0

36	0	45	0	0
37	0	45	0	0
38	0	0	45	0
39	0	0	45	0
40	0	0	45	0
41	0	0	45	0
42	0	0	45	0
43	0	0	45	0
44	0	0	45	0
45	0	0	45	0
46	0	0	45	0
47	0	0	45	0
48	0	0	45	0
49	0	0	45	0
50	0	0	45	0
51	0	0	45	0
52	0	0	45	0
53	0	0	0	45
54	0	0	0	45
55	0	0	0	45
56	0	0	0	45
57	0	0	0	45
58	0	0	0	45
59	0	0	0	45

Table C.9 Instantaneous Torque Profiles by Additional Boost Method.

(0-50 A with an increment of 5 A).

The method employs a single phase multi-level current. Therefore torque profile is summarized to show the trend while for a series of current values are shown at all rotor positions

Angle (θ°)/ Current (A)	0	5	10	15	20	25	30	35	40	45	50
0	0	3.92	5.01	5.01	5.01	5.01	5.01	5.01	5.01	4.47	5.01
1	0	1.92	4.54	4.96	4.96	4.96	4.96	4.96	4.96	4.43	4.96
2	0	1.20	3.28	4.80	4.80	4.80	4.80	4.80	4.80	4.42	4.80
3	0	0.82	2.36	4.01	4.76	4.76	4.76	4.76	4.76	4.47	4.76
4	0	0.55	1.80	3.01	3.84	4.69	4.69	4.69	4.69	4.51	4.69
5	0	0.28	1.18	2.20	2.92	3.90	4.26	4.50	4.50	4.50	4.50
6	0	0.22	0.76	1.52	2.14	2.74	3.22	3.83	4.23	4.23	4.23
7	0	0.11	0.44	1.04	1.57	2.15	2.62	3.15	3.57	3.89	3.89
8	0	0.11	0.43	0.93	1.41	1.98	2.46	2.84	3.18	3.51	3.51
9	0	0.10	0.42	0.90	1.34	1.79	2.18	2.54	2.77	3.09	3.09
10	0	0.11	0.41	0.82	1.31	1.63	1.93	2.16	2.39	2.66	2.66
11	0	0.10	0.40	0.77	1.08	1.35	1.62	1.80	1.95	2.20	2.20
12	0	0.10	0.38	0.68	0.99	1.12	1.26	1.41	1.52	1.71	1.71
13	0	0.08	0.33	0.56	0.74	0.81	0.89	0.97	1.05	1.18	1.18
14	0	0.04	0.16	0.26	0.33	0.35	0.38	0.40	0.43	0.47	0.47
15	0	3.92	5.01	5.01	5.01	5.01	5.01	5.01	5.01	4.47	5.01
16	0	1.92	4.54	4.96	4.96	4.96	4.96	4.96	4.96	4.43	4.96
17	0	1.20	3.28	4.80	4.80	4.80	4.80	4.80	4.80	4.42	4.80
18	0	0.82	2.36	4.01	4.76	4.76	4.76	4.76	4.76	4.47	4.76
19	0	0.55	1.80	3.01	3.84	4.69	4.69	4.69	4.69	4.51	4.69
20	0	0.28	1.18	2.20	2.92	3.90	4.26	4.50	4.50	4.50	4.50
21	0	0.22	0.76	1.52	2.14	2.74	3.22	3.83	4.23	4.23	4.23
22	0	0.11	0.44	1.04	1.57	2.15	2.62	3.15	3.57	3.89	3.89
23	0	0.11	0.43	0.93	1.41	1.98	2.46	2.84	3.18	3.51	3.51
24	0	0.10	0.42	0.90	1.34	1.79	2.18	2.54	2.77	3.09	3.09
25	0	0.11	0.41	0.82	1.31	1.63	1.93	2.16	2.39	2.66	2.66
26	0	0.10	0.40	0.77	1.08	1.35	1.62	1.80	1.95	2.20	2.20
27	0	0.10	0.38	0.68	0.99	1.12	1.26	1.41	1.52	1.71	1.71
28	0	0.08	0.33	0.56	0.74	0.81	0.89	0.97	1.05	1.18	1.18
29	0	0.04	0.16	0.26	0.33	0.35	0.38	0.40	0.43	0.47	0.47
30	0	3.92	5.01	5.01	5.01	5.01	5.01	5.01	5.01	4.47	5.01
31	0	1.92	4.54	4.96	4.96	4.96	4.96	4.96	4.96	4.43	4.96

32	0	1.20	3.28	4.80	4.80	4.80	4.80	4.80	4.80	4.42	4.80
33	0	0.82	2.36	4.01	4.76	4.76	4.76	4.76	4.76	4.47	4.76
34	0	0.55	1.80	3.01	3.84	4.69	4.69	4.69	4.69	4.51	4.69
35	0	0.28	1.18	2.20	2.92	3.90	4.26	4.50	4.50	4.50	4.50
36	0	0.22	0.76	1.52	2.14	2.74	3.22	3.83	4.23	4.23	4.23
37	0	0.11	0.44	1.04	1.57	2.15	2.62	3.15	3.57	3.89	3.89
38	0	0.11	0.43	0.93	1.41	1.98	2.46	2.84	3.18	3.51	3.51
39	0	0.10	0.42	0.90	1.34	1.79	2.18	2.54	2.77	3.09	3.09
40	0	0.11	0.41	0.82	1.31	1.63	1.93	2.16	2.39	2.66	2.66
41	0	0.10	0.40	0.77	1.08	1.35	1.62	1.80	1.95	2.20	2.20
42	0	0.10	0.38	0.68	0.99	1.12	1.26	1.41	1.52	1.71	1.71
43	0	0.08	0.33	0.56	0.74	0.81	0.89	0.97	1.05	1.18	1.18
44	0	0.04	0.16	0.26	0.33	0.35	0.38	0.40	0.43	0.47	0.47
45	0	3.92	5.01	5.01	5.01	5.01	5.01	5.01	5.01	4.47	5.01
46	0	1.92	4.54	4.96	4.96	4.96	4.96	4.96	4.96	4.43	4.96
47	0	1.20	3.28	4.80	4.80	4.80	4.80	4.80	4.80	4.54	4.80
48	0	0.82	2.36	4.01	4.76	4.76	4.76	4.76	4.76	4.47	4.76
49	0	0.55	1.80	3.01	3.84	4.69	4.69	4.69	4.69	4.51	4.69
50	0	0.28	1.18	2.20	2.92	3.90	4.26	4.50	4.50	4.50	4.50
51	0	0.22	0.76	1.52	2.14	2.74	3.22	3.83	4.23	4.23	4.23
52	0	0.11	0.44	1.04	1.57	2.15	2.62	3.15	3.57	3.89	3.89
53	0	0.11	0.43	0.93	1.41	1.98	2.46	2.84	3.18	3.51	3.51
54	0	0.10	0.42	0.90	1.34	1.79	2.18	2.54	2.77	3.09	3.09
55	0	0.11	0.41	0.82	1.31	1.63	1.93	2.16	2.39	2.66	2.66
56	0	0.10	0.40	0.77	1.08	1.35	1.62	1.80	1.95	2.20	2.20
57	0	0.10	0.38	0.68	0.99	1.12	1.26	1.41	1.52	1.71	1.71
58	0	0.08	0.33	0.56	0.74	0.81	0.89	0.97	1.05	1.18	1.18
59	0	0.04	0.16	0.26	0.33	0.35	0.38	0.40	0.43	0.47	0.47

Table C.10 Instantaneous Torque Profiles by Additional Boost Method (0-10 A).

The method employs a single phase multi-level current. Therefore current profiles are of much more importance. Excitation current values are shown at all rotor positions

Angle (θ°)/ Current (A)	0	1	2	3	4	5	6	7	8	9	10
0	0	8	15	25	32	40	49	50	50	50	50
1	0	5	9	14	18	23	28	32	37	42	46
2	0	4	7	10	13	17	21	24	28	31	35
3	0	3	6	8	11	14	16	19	22	25	27
4	0	2	4	7	9	11	13	15	18	20	22
5	0	2	4	5	7	8	10	12	14	16	17
6	0	1	3	4	5	7	8	9	11	12	13
7	0	1	2	3	4	5	6	7	8	9	10
8	0	1	2	3	4	5	6	7	8	9	10
9	0	1	2	3	4	5	6	7	8	9	10
10	0	1	2	3	4	5	6	7	8	9	10
11	0	1	2	3	4	5	6	7	8	9	10
12	0	1	2	3	4	5	6	7	8	9	10
13	0	1	2	3	4	5	6	7	8	9	10
14	0	1	2	3	4	5	6	7	8	9	10
15	0	8	15	25	32	40	49	50	50	50	50
16	0	5	9	14	18	23	28	32	37	42	46
17	0	4	7	10	13	17	21	24	28	31	35
18	0	3	6	8	11	14	16	19	22	25	27
19	0	2	4	7	9	11	13	15	18	20	22
20	0	2	4	5	7	8	10	12	14	16	17
21	0	1	3	4	5	7	8	9	11	12	13
22	0	1	2	3	4	5	6	7	8	9	10
23	0	1	2	3	4	5	6	7	8	9	10
24	0	1	2	3	4	5	6	7	8	9	10
25	0	1	2	3	4	5	6	7	8	9	10
26	0	1	2	3	4	5	6	7	8	9	10
27	0	1	2	3	4	5	6	7	8	9	10
28	0	1	2	3	4	5	6	7	8	9	10
29	0	1	2	3	4	5	6	7	8	9	10
30	0	8	15	25	32	40	49	50	50	50	50
31	0	5	9	14	18	23	28	32	37	42	46
32	0	4	7	10	13	17	21	24	28	31	35

33	0	3	6	8	11	14	16	19	22	25	27
34	0	2	4	7	9	11	13	15	18	20	22
35	0	2	4	5	7	8	10	12	14	16	17
36	0	1	3	4	5	7	8	9	11	12	13
37	0	1	2	3	4	5	6	7	8	9	10
38	0	1	2	3	4	5	6	7	8	9	10
39	0	1	2	3	4	5	6	7	8	9	10
40	0	1	2	3	4	5	6	7	8	9	10
41	0	1	2	3	4	5	6	7	8	9	10
42	0	1	2	3	4	5	6	7	8	9	10
43	0	1	2	3	4	5	6	7	8	9	10
44	0	1	2	3	4	5	6	7	8	9	10
45	0	8	15	25	32	40	49	50	50	50	50
46	0	5	9	14	18	23	28	32	37	42	46
47	0	4	7	10	13	17	21	24	28	31	35
48	0	3	6	8	11	14	16	19	22	25	27
49	0	2	4	7	9	11	13	15	18	20	22
50	0	2	4	5	7	8	10	12	14	16	17
51	0	1	3	4	5	7	8	9	11	12	13
52	0	1	2	3	4	5	6	7	8	9	10
53	0	1	2	3	4	5	6	7	8	9	10
54	0	1	2	3	4	5	6	7	8	9	10
55	0	1	2	3	4	5	6	7	8	9	10
56	0	1	2	3	4	5	6	7	8	9	10
57	0	1	2	3	4	5	6	7	8	9	10
58	0	1	2	3	4	5	6	7	8	9	10
59	0	1	2	3	4	5	6	7	8	9	10

Table C.11: Instantaneous Torque Profiles by Additional Boost Method. (11 A to 50 A)

The method employs a single phase multi-level current. Therefore current profiles are of much more importance. Excitation current values are shown at all rotor positions (15-50 A with an increment of 5 A).

Angle (θ°)/ Current (A)	15	20	25	30	35	40	45	50
0	15	50	50	30	50	50	45	50
1	15	50	50	30	50	50	45	50
2	15	50	50	30	50	50	46	50
3	15	50	50	30	50	50	47	50
4	15	41	50	31	50	50	48	50
5	15	33	43	31	50	50	50	50
6	15	26	32	32	44	50	50	50
7	16	21	27	33	38	44	50	50
8	16	20	26	36	37	43	50	50
9	16	20	26	42	37	42	50	50
10	16	20	26	50	36	42	50	50
11	18	20	25	50	36	41	50	50
12	20	20	25	50	36	40	50	50
13	37	20	25	50	35	40	50	50
14	50	20	25	50	35	40	50	50
15	15	50	50	30	50	50	45	50
16	15	50	50	30	50	50	45	50
17	15	50	50	30	50	50	46	50
18	15	50	50	30	50	50	47	50
19	15	41	50	31	50	50	48	50
20	15	33	43	31	50	50	50	50
21	15	26	32	32	44	50	50	50
22	16	21	27	33	38	44	50	50
23	16	20	26	36	37	43	50	50
24	16	20	26	42	37	42	50	50
25	16	20	26	50	36	42	50	50
26	18	20	25	50	36	41	50	50
27	20	20	25	50	36	41	50	50
28	37	20	25	50	35	40	50	50
29	50	20	25	50	35	40	50	50
30	15	50	50	30	50	50	45	50
31	15	50	50	30	50	50	45	50
32	15	50	50	30	50	50	46	50

33	15	50	50	30	50	50	47	50
34	15	41	50	31	50	50	48	50
35	15	33	43	31	50	50	50	50
36	15	26	32	32	44	50	50	50
37	16	21	27	33	38	44	50	50
38	16	20	26	36	37	43	50	50
39	16	20	26	42	37	42	50	50
40	16	20	26	50	36	42	50	50
41	18	20	25	50	36	41	50	50
42	20	20	25	50	36	40	50	50
43	37	20	25	50	35	40	50	50
44	50	20	25	50	35	40	50	50
45	15	50	50	30	50	50	45	50
46	15	50	50	30	50	50	45	50
47	15	50	50	30	50	50	46	50
48	15	50	50	30	50	50	47	50
49	15	41	50	31	50	50	48	50
50	15	33	43	31	50	50	50	50
51	15	26	32	32	44	50	50	50
52	16	21	27	33	38	44	50	50
53	16	20	26	36	37	43	50	50
54	16	20	26	42	37	42	50	50
55	16	20	26	50	36	42	50	50
56	18	20	25	50	36	41	50	50
57	20	20	25	50	36	40	50	50
58	37	20	25	50	35	40	50	50
59	50	20	25	50	35	40	50	50

Table C.12 Desired Torque (T_D) Profiles by Proposed Global NLP Optimization Method (0-16 A).

Angle (θ°)/ Current (A)	0	1	2	3	4	5	6	7	8	9	10	11	12	13	14	15	16
0	0.00	0.00	0.02	0.04	0.07	0.11	0.16	0.22	0.29	0.37	0.46	0.56	0.65	0.77	0.86	0.98	1.09
1	0.00	0.00	0.02	0.04	0.07	0.11	0.16	0.22	0.29	0.37	0.46	0.56	0.65	0.77	0.86	0.98	1.09
2	0.00	0.00	0.02	0.04	0.07	0.11	0.16	0.22	0.29	0.37	0.46	0.56	0.65	0.77	0.86	0.98	1.09
3	0.00	0.00	0.02	0.04	0.07	0.11	0.16	0.22	0.29	0.37	0.46	0.56	0.65	0.77	0.86	0.98	1.09
4	0.00	0.00	0.02	0.04	0.07	0.11	0.16	0.22	0.29	0.37	0.46	0.56	0.65	0.77	0.86	0.98	1.09
5	0.00	0.00	0.02	0.04	0.07	0.11	0.16	0.22	0.29	0.37	0.46	0.56	0.65	0.77	0.86	0.98	1.09
6	0.00	0.00	0.02	0.04	0.07	0.11	0.16	0.22	0.29	0.37	0.46	0.56	0.65	0.77	0.86	0.98	1.09
7	0.00	0.00	0.02	0.04	0.07	0.11	0.16	0.22	0.29	0.37	0.46	0.56	0.65	0.77	0.86	0.98	1.09
8	0.00	0.00	0.02	0.04	0.07	0.11	0.16	0.22	0.29	0.37	0.46	0.56	0.65	0.77	0.86	0.98	1.09
9	0.00	0.00	0.02	0.04	0.07	0.11	0.16	0.22	0.29	0.37	0.46	0.56	0.65	0.77	0.86	0.98	1.09
10	0.00	0.00	0.02	0.04	0.07	0.11	0.16	0.22	0.29	0.37	0.46	0.56	0.65	0.77	0.86	0.98	1.09
11	0.00	0.00	0.02	0.04	0.07	0.11	0.16	0.22	0.29	0.37	0.46	0.56	0.65	0.77	0.86	0.98	1.09
12	0.00	0.00	0.02	0.04	0.07	0.11	0.16	0.22	0.29	0.37	0.46	0.56	0.65	0.77	0.86	0.98	1.09
13	0.00	0.00	0.02	0.04	0.07	0.11	0.16	0.22	0.29	0.37	0.46	0.56	0.65	0.77	0.86	0.98	1.09
14	0.00	0.00	0.02	0.04	0.07	0.11	0.16	0.22	0.29	0.37	0.46	0.56	0.65	0.77	0.86	0.98	1.09
15	0.00	0.00	0.02	0.04	0.07	0.11	0.16	0.22	0.29	0.37	0.46	0.56	0.65	0.77	0.86	0.98	1.09
16	0.00	0.00	0.02	0.04	0.07	0.11	0.16	0.22	0.29	0.37	0.46	0.56	0.65	0.77	0.86	0.98	1.09
17	0.00	0.00	0.02	0.04	0.07	0.11	0.16	0.22	0.29	0.37	0.46	0.56	0.65	0.77	0.86	0.98	1.09
18	0.00	0.00	0.02	0.04	0.07	0.11	0.16	0.22	0.29	0.37	0.46	0.56	0.65	0.77	0.86	0.98	1.09
19	0.00	0.00	0.02	0.04	0.07	0.11	0.16	0.22	0.29	0.37	0.46	0.56	0.65	0.77	0.86	0.98	1.09
20	0.00	0.00	0.02	0.04	0.07	0.11	0.16	0.22	0.29	0.37	0.46	0.56	0.65	0.77	0.86	0.98	1.09
21	0.00	0.00	0.02	0.04	0.07	0.11	0.16	0.22	0.29	0.37	0.46	0.56	0.65	0.77	0.86	0.98	1.09
22	0.00	0.00	0.02	0.04	0.07	0.11	0.16	0.22	0.29	0.37	0.46	0.56	0.65	0.77	0.86	0.98	1.09
23	0.00	0.00	0.02	0.04	0.07	0.11	0.16	0.22	0.29	0.37	0.46	0.56	0.65	0.77	0.86	0.98	1.09
24	0.00	0.00	0.02	0.04	0.07	0.11	0.16	0.22	0.29	0.37	0.46	0.56	0.65	0.77	0.86	0.98	1.09
25	0.00	0.00	0.02	0.04	0.07	0.11	0.16	0.22	0.29	0.37	0.46	0.56	0.65	0.77	0.86	0.98	1.09
26	0.00	0.00	0.02	0.04	0.07	0.11	0.16	0.22	0.29	0.37	0.46	0.56	0.65	0.77	0.86	0.98	1.09
27	0.00	0.00	0.02	0.04	0.07	0.11	0.16	0.22	0.29	0.37	0.46	0.56	0.65	0.77	0.86	0.98	1.09
28	0.00	0.00	0.02	0.04	0.07	0.11	0.16	0.22	0.29	0.37	0.46	0.56	0.65	0.77	0.86	0.98	1.09
29	0.00	0.00	0.02	0.04	0.07	0.11	0.16	0.22	0.29	0.37	0.46	0.56	0.65	0.77	0.86	0.98	1.09
30	0.00	0.00	0.02	0.04	0.07	0.11	0.16	0.22	0.29	0.37	0.46	0.56	0.65	0.77	0.86	0.98	1.09
31	0.00	0.00	0.02	0.04	0.07	0.11	0.16	0.22	0.29	0.37	0.46	0.56	0.65	0.77	0.86	0.98	1.09
32	0.00	0.00	0.02	0.04	0.07	0.11	0.16	0.22	0.29	0.37	0.46	0.56	0.65	0.77	0.86	0.98	1.09
33	0.00	0.00	0.02	0.04	0.07	0.11	0.16	0.22	0.29	0.37	0.46	0.56	0.65	0.77	0.86	0.98	1.09
34	0.00	0.00	0.02	0.04	0.07	0.11	0.16	0.22	0.29	0.37	0.46	0.56	0.65	0.77	0.86	0.98	1.09
35	0.00	0.00	0.02	0.04	0.07	0.11	0.16	0.22	0.29	0.37	0.46	0.56	0.65	0.77	0.86	0.98	1.09
36	0.00	0.00	0.02	0.04	0.07	0.11	0.16	0.22	0.29	0.37	0.46	0.56	0.65	0.77	0.86	0.98	1.09

37	0.00	0.00	0.02	0.04	0.07	0.11	0.16	0.22	0.29	0.37	0.46	0.56	0.65	0.77	0.86	0.98	1.09
38	0.00	0.00	0.02	0.04	0.07	0.11	0.16	0.22	0.29	0.37	0.46	0.56	0.65	0.77	0.86	0.98	1.09
39	0.00	0.00	0.02	0.04	0.07	0.11	0.16	0.22	0.29	0.37	0.46	0.56	0.65	0.77	0.86	0.98	1.09
40	0.00	0.00	0.02	0.04	0.07	0.11	0.16	0.22	0.29	0.37	0.46	0.56	0.65	0.77	0.86	0.98	1.09
41	0.00	0.00	0.02	0.04	0.07	0.11	0.16	0.22	0.29	0.37	0.46	0.56	0.65	0.77	0.86	0.98	1.09
42	0.00	0.00	0.02	0.04	0.07	0.11	0.16	0.22	0.29	0.37	0.46	0.56	0.65	0.77	0.86	0.98	1.09
43	0.00	0.00	0.02	0.04	0.07	0.11	0.16	0.22	0.29	0.37	0.46	0.56	0.65	0.77	0.86	0.98	1.09
44	0.00	0.00	0.02	0.04	0.07	0.11	0.16	0.22	0.29	0.37	0.46	0.56	0.65	0.77	0.86	0.98	1.09
45	0.00	0.00	0.02	0.04	0.07	0.11	0.16	0.22	0.29	0.37	0.46	0.56	0.65	0.77	0.86	0.98	1.09
46	0.00	0.00	0.02	0.04	0.07	0.11	0.16	0.22	0.29	0.37	0.46	0.56	0.65	0.77	0.86	0.98	1.09
47	0.00	0.00	0.02	0.04	0.07	0.11	0.16	0.22	0.29	0.37	0.46	0.56	0.65	0.77	0.86	0.98	1.09
48	0.00	0.00	0.02	0.04	0.07	0.11	0.16	0.22	0.29	0.37	0.46	0.56	0.65	0.77	0.86	0.98	1.09
49	0.00	0.00	0.02	0.04	0.07	0.11	0.16	0.22	0.29	0.37	0.46	0.56	0.65	0.77	0.86	0.98	1.09
50	0.00	0.00	0.02	0.04	0.07	0.11	0.16	0.22	0.29	0.37	0.46	0.56	0.65	0.77	0.86	0.98	1.09
51	0.00	0.00	0.02	0.04	0.07	0.11	0.16	0.22	0.29	0.37	0.46	0.56	0.65	0.77	0.86	0.98	1.09
52	0.00	0.00	0.02	0.04	0.07	0.11	0.16	0.22	0.29	0.37	0.46	0.56	0.65	0.77	0.86	0.98	1.09
53	0.00	0.00	0.02	0.04	0.07	0.11	0.16	0.22	0.29	0.37	0.46	0.56	0.65	0.77	0.86	0.98	1.09
54	0.00	0.00	0.02	0.04	0.07	0.11	0.16	0.22	0.29	0.37	0.46	0.56	0.65	0.77	0.86	0.98	1.09
55	0.00	0.00	0.02	0.04	0.07	0.11	0.16	0.22	0.29	0.37	0.46	0.56	0.65	0.77	0.86	0.98	1.09
56	0.00	0.00	0.02	0.04	0.07	0.11	0.16	0.22	0.29	0.37	0.46	0.56	0.65	0.77	0.86	0.98	1.09
57	0.00	0.00	0.02	0.04	0.07	0.11	0.16	0.22	0.29	0.37	0.46	0.56	0.65	0.77	0.86	0.98	1.09
58	0.00	0.00	0.02	0.04	0.07	0.11	0.16	0.22	0.29	0.37	0.46	0.56	0.65	0.77	0.86	0.98	1.09
59	0.00	0.00	0.02	0.04	0.07	0.11	0.16	0.22	0.29	0.37	0.46	0.56	0.65	0.77	0.86	0.98	1.09

Table C.13 Desired Torque(T_D) Profiles by Proposed Global NLP Optimization Method (17-33A).

Angle (θ°)/ Current (A)	17	18	19	20	21	22	23	24	25	26	27	28	29	30	31	32	33
0	1.20	1.31	1.44	1.57	1.66	1.77	1.90	2.02	2.14	2.26	2.38	2.48	2.62	2.73	2.85	2.97	3.09
1	1.20	1.31	1.44	1.57	1.66	1.77	1.90	2.02	2.14	2.26	2.38	2.48	2.62	2.73	2.85	2.97	3.09
2	1.20	1.31	1.44	1.57	1.66	1.77	1.90	2.02	2.14	2.26	2.38	2.48	2.62	2.73	2.85	2.97	3.09
3	1.20	1.31	1.44	1.57	1.66	1.77	1.90	2.02	2.14	2.26	2.38	2.48	2.62	2.73	2.85	2.97	3.09
4	1.20	1.31	1.44	1.57	1.66	1.77	1.90	2.02	2.14	2.26	2.38	2.48	2.62	2.73	2.85	2.97	3.09
5	1.20	1.31	1.44	1.57	1.66	1.77	1.90	2.02	2.14	2.26	2.38	2.48	2.62	2.73	2.85	2.97	3.09
6	1.20	1.31	1.44	1.57	1.66	1.77	1.90	2.02	2.14	2.26	2.38	2.48	2.62	2.73	2.85	2.97	3.09
7	1.20	1.31	1.44	1.57	1.66	1.77	1.90	2.02	2.14	2.26	2.38	2.48	2.62	2.73	2.85	2.97	3.09
8	1.20	1.31	1.44	1.57	1.66	1.77	1.90	2.02	2.14	2.26	2.38	2.48	2.62	2.73	2.85	2.97	3.09
9	1.20	1.31	1.44	1.57	1.66	1.77	1.90	2.02	2.14	2.26	2.38	2.48	2.62	2.73	2.85	2.97	3.09
10	1.20	1.31	1.44	1.57	1.66	1.77	1.90	2.02	2.14	2.26	2.38	2.48	2.62	2.73	2.85	2.97	3.09
11	1.20	1.31	1.44	1.57	1.66	1.77	1.90	2.02	2.14	2.26	2.38	2.48	2.62	2.73	2.85	2.97	3.09
12	1.20	1.31	1.44	1.57	1.66	1.77	1.90	2.02	2.14	2.26	2.38	2.48	2.62	2.73	2.85	2.97	3.09
13	1.20	1.31	1.44	1.57	1.66	1.77	1.90	2.02	2.14	2.26	2.38	2.48	2.62	2.73	2.85	2.97	3.09
14	1.20	1.31	1.44	1.57	1.66	1.77	1.90	2.02	2.14	2.26	2.38	2.48	2.62	2.73	2.85	2.97	3.09
15	1.20	1.31	1.44	1.57	1.66	1.77	1.90	2.02	2.14	2.26	2.38	2.48	2.62	2.73	2.85	2.97	3.09
16	1.20	1.31	1.44	1.57	1.66	1.77	1.90	2.02	2.14	2.26	2.38	2.48	2.62	2.73	2.85	2.97	3.09
17	1.20	1.31	1.44	1.57	1.66	1.77	1.90	2.02	2.14	2.26	2.38	2.48	2.62	2.73	2.85	2.97	3.09
18	1.20	1.31	1.44	1.57	1.66	1.77	1.90	2.02	2.14	2.26	2.38	2.48	2.62	2.73	2.85	2.97	3.09
19	1.20	1.31	1.44	1.57	1.66	1.77	1.90	2.02	2.14	2.26	2.38	2.48	2.62	2.73	2.85	2.97	3.09
20	1.20	1.31	1.44	1.57	1.66	1.77	1.90	2.02	2.14	2.26	2.38	2.48	2.62	2.73	2.85	2.97	3.09
21	1.20	1.31	1.44	1.57	1.66	1.77	1.90	2.02	2.14	2.26	2.38	2.48	2.62	2.73	2.85	2.97	3.09
22	1.20	1.31	1.44	1.57	1.66	1.77	1.90	2.02	2.14	2.26	2.38	2.48	2.62	2.73	2.85	2.97	3.09
23	1.20	1.31	1.44	1.57	1.66	1.77	1.90	2.02	2.14	2.26	2.38	2.48	2.62	2.73	2.85	2.97	3.09
24	1.20	1.31	1.44	1.57	1.66	1.77	1.90	2.02	2.14	2.26	2.38	2.48	2.62	2.73	2.85	2.97	3.09
25	1.20	1.31	1.44	1.57	1.66	1.77	1.90	2.02	2.14	2.26	2.38	2.48	2.62	2.73	2.85	2.97	3.09
26	1.20	1.31	1.44	1.57	1.66	1.77	1.90	2.02	2.14	2.26	2.38	2.48	2.62	2.73	2.85	2.97	3.09
27	1.20	1.31	1.44	1.57	1.66	1.77	1.90	2.02	2.14	2.26	2.38	2.48	2.62	2.73	2.85	2.97	3.09
28	1.20	1.31	1.44	1.57	1.66	1.77	1.90	2.02	2.14	2.26	2.38	2.48	2.62	2.73	2.85	2.97	3.09
29	1.20	1.31	1.44	1.57	1.66	1.77	1.90	2.02	2.14	2.26	2.38	2.48	2.62	2.73	2.85	2.97	3.09
30	1.20	1.31	1.44	1.57	1.66	1.77	1.90	2.02	2.14	2.26	2.38	2.48	2.62	2.73	2.85	2.97	3.09
31	1.20	1.31	1.44	1.57	1.66	1.77	1.90	2.02	2.14	2.26	2.38	2.48	2.62	2.73	2.85	2.97	3.09
32	1.20	1.31	1.44	1.57	1.66	1.77	1.90	2.02	2.14	2.26	2.38	2.48	2.62	2.73	2.85	2.97	3.09
33	1.20	1.31	1.44	1.57	1.66	1.77	1.90	2.02	2.14	2.26	2.38	2.48	2.62	2.73	2.85	2.97	3.09
34	1.20	1.31	1.44	1.57	1.66	1.77	1.90	2.02	2.14	2.26	2.38	2.48	2.62	2.73	2.85	2.97	3.09
35	1.20	1.31	1.44	1.57	1.66	1.77	1.90	2.02	2.14	2.26	2.38	2.48	2.62	2.73	2.85	2.97	3.09
36	1.20	1.31	1.44	1.57	1.66	1.77	1.90	2.02	2.14	2.26	2.38	2.48	2.62	2.73	2.85	2.97	3.09

37	1.20	1.31	1.44	1.57	1.66	1.77	1.90	2.02	2.14	2.26	2.38	2.48	2.62	2.73	2.85	2.97	3.09
38	1.20	1.31	1.44	1.57	1.66	1.77	1.90	2.02	2.14	2.26	2.38	2.48	2.62	2.73	2.85	2.97	3.09
39	1.20	1.31	1.44	1.57	1.66	1.77	1.90	2.02	2.14	2.26	2.38	2.48	2.62	2.73	2.85	2.97	3.09
40	1.20	1.31	1.44	1.57	1.66	1.77	1.90	2.02	2.14	2.26	2.38	2.48	2.62	2.73	2.85	2.97	3.09
41	1.20	1.31	1.44	1.57	1.66	1.77	1.90	2.02	2.14	2.26	2.38	2.48	2.62	2.73	2.85	2.97	3.09
42	1.20	1.31	1.44	1.57	1.66	1.77	1.90	2.02	2.14	2.26	2.38	2.48	2.62	2.73	2.85	2.97	3.09
43	1.20	1.31	1.44	1.57	1.66	1.77	1.90	2.02	2.14	2.26	2.38	2.48	2.62	2.73	2.85	2.97	3.09
44	1.20	1.31	1.44	1.57	1.66	1.77	1.90	2.02	2.14	2.26	2.38	2.48	2.62	2.73	2.85	2.97	3.09
45	1.20	1.31	1.44	1.57	1.66	1.77	1.90	2.02	2.14	2.26	2.38	2.48	2.62	2.73	2.85	2.97	3.09
46	1.20	1.31	1.44	1.57	1.66	1.77	1.90	2.02	2.14	2.26	2.38	2.48	2.62	2.73	2.85	2.97	3.09
47	1.20	1.31	1.44	1.57	1.66	1.77	1.90	2.02	2.14	2.26	2.38	2.48	2.62	2.73	2.85	2.97	3.09
48	1.20	1.31	1.44	1.57	1.66	1.77	1.90	2.02	2.14	2.26	2.38	2.48	2.62	2.73	2.85	2.97	3.09
49	1.20	1.31	1.44	1.57	1.66	1.77	1.90	2.02	2.14	2.26	2.38	2.48	2.62	2.73	2.85	2.97	3.09
50	1.20	1.31	1.44	1.57	1.66	1.77	1.90	2.02	2.14	2.26	2.38	2.48	2.62	2.73	2.85	2.97	3.09
51	1.20	1.31	1.44	1.57	1.66	1.77	1.90	2.02	2.14	2.26	2.38	2.48	2.62	2.73	2.85	2.97	3.09
52	1.20	1.31	1.44	1.57	1.66	1.77	1.90	2.02	2.14	2.26	2.38	2.48	2.62	2.73	2.85	2.97	3.09
53	1.20	1.31	1.44	1.57	1.66	1.77	1.90	2.02	2.14	2.26	2.38	2.48	2.62	2.73	2.85	2.97	3.09
54	1.20	1.31	1.44	1.57	1.66	1.77	1.90	2.02	2.14	2.26	2.38	2.48	2.62	2.73	2.85	2.97	3.09
55	1.20	1.31	1.44	1.57	1.66	1.77	1.90	2.02	2.14	2.26	2.38	2.48	2.62	2.73	2.85	2.97	3.09
56	1.20	1.31	1.44	1.57	1.66	1.77	1.90	2.02	2.14	2.26	2.38	2.48	2.62	2.73	2.85	2.97	3.09
57	1.20	1.31	1.44	1.57	1.66	1.77	1.90	2.02	2.14	2.26	2.38	2.48	2.62	2.73	2.85	2.97	3.09
58	1.20	1.31	1.44	1.57	1.66	1.77	1.90	2.02	2.14	2.26	2.38	2.48	2.62	2.73	2.85	2.97	3.09
59	1.20	1.31	1.44	1.57	1.66	1.77	1.90	2.02	2.14	2.26	2.38	2.48	2.62	2.73	2.85	2.97	3.09

Table C.14 Desired Torque (T_D) Profiles by Proposed Global NLP Optimization Method (34-50 A).

Angle (θ°)/ Current (A)	34	35	36	37	38	39	40	41	42	43	44	45	46	47	48	49	50
0	3.21	3.32	3.44	3.56	3.68	3.79	3.91	4.03	4.14	4.25	4.38	4.48	4.59	4.71	4.82	4.93	5.04
1	3.21	3.32	3.44	3.56	3.68	3.79	3.91	4.03	4.14	4.25	4.38	4.48	4.59	4.71	4.82	4.93	5.04
2	3.21	3.32	3.44	3.56	3.68	3.79	3.91	4.03	4.14	4.25	4.38	4.48	4.59	4.71	4.82	4.93	5.04
3	3.21	3.32	3.44	3.56	3.68	3.79	3.91	4.03	4.14	4.25	4.38	4.48	4.59	4.71	4.82	4.93	5.04
4	3.21	3.32	3.44	3.56	3.68	3.79	3.91	4.03	4.14	4.25	4.38	4.48	4.59	4.71	4.82	4.93	5.04
5	3.21	3.32	3.44	3.56	3.68	3.79	3.91	4.03	4.14	4.25	4.38	4.48	4.59	4.71	4.82	4.93	5.04
6	3.21	3.32	3.44	3.56	3.68	3.79	3.91	4.03	4.14	4.25	4.38	4.48	4.59	4.71	4.82	4.93	5.04
7	3.21	3.32	3.44	3.56	3.68	3.79	3.91	4.03	4.14	4.25	4.38	4.48	4.59	4.71	4.82	4.93	5.04
8	3.21	3.32	3.44	3.56	3.68	3.79	3.91	4.03	4.14	4.25	4.38	4.48	4.59	4.71	4.82	4.93	5.04
9	3.21	3.32	3.44	3.56	3.68	3.79	3.91	4.03	4.14	4.25	4.38	4.48	4.59	4.71	4.82	4.93	5.04
10	3.21	3.32	3.44	3.56	3.68	3.79	3.91	4.03	4.14	4.25	4.38	4.48	4.59	4.71	4.82	4.93	5.04
11	3.21	3.32	3.44	3.56	3.68	3.79	3.91	4.03	4.14	4.25	4.38	4.48	4.59	4.71	4.82	4.93	5.04
12	3.21	3.32	3.44	3.56	3.68	3.79	3.91	4.03	4.14	4.25	4.38	4.48	4.59	4.71	4.82	4.93	5.04
13	3.21	3.32	3.44	3.56	3.68	3.79	3.91	4.03	4.14	4.25	4.38	4.48	4.59	4.71	4.82	4.93	5.04
14	3.21	3.32	3.44	3.56	3.68	3.79	3.91	4.03	4.14	4.25	4.38	4.48	4.59	4.71	4.82	4.93	5.04
15	3.21	3.32	3.44	3.56	3.68	3.79	3.91	4.03	4.14	4.25	4.38	4.48	4.59	4.71	4.82	4.93	5.04
16	3.21	3.32	3.44	3.56	3.68	3.79	3.91	4.03	4.14	4.25	4.38	4.48	4.59	4.71	4.82	4.93	5.04
17	3.21	3.32	3.44	3.56	3.68	3.79	3.91	4.03	4.14	4.25	4.38	4.48	4.59	4.71	4.82	4.93	5.04
18	3.21	3.32	3.44	3.56	3.68	3.79	3.91	4.03	4.14	4.25	4.38	4.48	4.59	4.71	4.82	4.93	5.04
19	3.21	3.32	3.44	3.56	3.68	3.79	3.91	4.03	4.14	4.25	4.38	4.48	4.59	4.71	4.82	4.93	5.04
20	3.21	3.32	3.44	3.56	3.68	3.79	3.91	4.03	4.14	4.25	4.38	4.48	4.59	4.71	4.82	4.93	5.04
21	3.21	3.32	3.44	3.56	3.68	3.79	3.91	4.03	4.14	4.25	4.38	4.48	4.59	4.71	4.82	4.93	5.04
22	3.21	3.32	3.44	3.56	3.68	3.79	3.91	4.03	4.14	4.25	4.38	4.48	4.59	4.71	4.82	4.93	5.04
23	3.21	3.32	3.44	3.56	3.68	3.79	3.91	4.03	4.14	4.25	4.38	4.48	4.59	4.71	4.82	4.93	5.04
24	3.21	3.32	3.44	3.56	3.68	3.79	3.91	4.03	4.14	4.25	4.38	4.48	4.59	4.71	4.82	4.93	5.04
25	3.21	3.32	3.44	3.56	3.68	3.79	3.91	4.03	4.14	4.25	4.38	4.48	4.59	4.71	4.82	4.93	5.04
26	3.21	3.32	3.44	3.56	3.68	3.79	3.91	4.03	4.14	4.25	4.38	4.48	4.59	4.71	4.82	4.93	5.04
27	3.21	3.32	3.44	3.56	3.68	3.79	3.91	4.03	4.14	4.25	4.38	4.48	4.59	4.71	4.82	4.93	5.04
28	3.21	3.32	3.44	3.56	3.68	3.79	3.91	4.03	4.14	4.25	4.38	4.48	4.59	4.71	4.82	4.93	5.04
29	3.21	3.32	3.44	3.56	3.68	3.79	3.91	4.03	4.14	4.25	4.38	4.48	4.59	4.71	4.82	4.93	5.04
30	3.21	3.32	3.44	3.56	3.68	3.79	3.91	4.03	4.14	4.25	4.38	4.48	4.59	4.71	4.82	4.93	5.04
31	3.21	3.32	3.44	3.56	3.68	3.79	3.91	4.03	4.14	4.25	4.38	4.48	4.59	4.71	4.82	4.93	5.04
32	3.21	3.32	3.44	3.56	3.68	3.79	3.91	4.03	4.14	4.25	4.38	4.48	4.59	4.71	4.82	4.93	5.04
33	3.21	3.32	3.44	3.56	3.68	3.79	3.91	4.03	4.14	4.25	4.38	4.48	4.59	4.71	4.82	4.93	5.04
34	3.21	3.32	3.44	3.56	3.68	3.79	3.91	4.03	4.14	4.25	4.38	4.48	4.59	4.71	4.82	4.93	5.04
35	3.21	3.32	3.44	3.56	3.68	3.79	3.91	4.03	4.14	4.25	4.38	4.48	4.59	4.71	4.82	4.93	5.04
36	3.21	3.32	3.44	3.56	3.68	3.79	3.91	4.03	4.14	4.25	4.38	4.48	4.59	4.71	4.82	4.93	5.04

37	3.21	3.32	3.44	3.56	3.68	3.79	3.91	4.03	4.14	4.25	4.38	4.48	4.59	4.71	4.82	4.93	5.04
38	3.21	3.32	3.44	3.56	3.68	3.79	3.91	4.03	4.14	4.25	4.38	4.48	4.59	4.71	4.82	4.93	5.04
39	3.21	3.32	3.44	3.56	3.68	3.79	3.91	4.03	4.14	4.25	4.38	4.48	4.59	4.71	4.82	4.93	5.04
40	3.21	3.32	3.44	3.56	3.68	3.79	3.91	4.03	4.14	4.25	4.38	4.48	4.59	4.71	4.82	4.93	5.04
41	3.21	3.32	3.44	3.56	3.68	3.79	3.91	4.03	4.14	4.25	4.38	4.48	4.59	4.71	4.82	4.93	5.04
42	3.21	3.32	3.44	3.56	3.68	3.79	3.91	4.03	4.14	4.25	4.38	4.48	4.59	4.71	4.82	4.93	5.04
43	3.21	3.32	3.44	3.56	3.68	3.79	3.91	4.03	4.14	4.25	4.38	4.48	4.59	4.71	4.82	4.93	5.04
44	3.21	3.32	3.44	3.56	3.68	3.79	3.91	4.03	4.14	4.25	4.38	4.48	4.59	4.71	4.82	4.93	5.04
45	3.21	3.32	3.44	3.56	3.68	3.79	3.91	4.03	4.14	4.25	4.38	4.48	4.59	4.71	4.82	4.93	5.04
46	3.21	3.32	3.44	3.56	3.68	3.79	3.91	4.03	4.14	4.25	4.38	4.48	4.59	4.71	4.82	4.93	5.04
47	3.21	3.32	3.44	3.56	3.68	3.79	3.91	4.03	4.14	4.25	4.38	4.48	4.59	4.71	4.82	4.93	5.04
48	3.21	3.32	3.44	3.56	3.68	3.79	3.91	4.03	4.14	4.25	4.38	4.48	4.59	4.71	4.82	4.93	5.04
49	3.21	3.32	3.44	3.56	3.68	3.79	3.91	4.03	4.14	4.25	4.38	4.48	4.59	4.71	4.82	4.93	5.04
50	3.21	3.32	3.44	3.56	3.68	3.79	3.91	4.03	4.14	4.25	4.38	4.48	4.59	4.71	4.82	4.93	5.04
51	3.21	3.32	3.44	3.56	3.68	3.79	3.91	4.03	4.14	4.25	4.38	4.48	4.59	4.71	4.82	4.93	5.04
52	3.21	3.32	3.44	3.56	3.68	3.79	3.91	4.03	4.14	4.25	4.38	4.48	4.59	4.71	4.82	4.93	5.04
53	3.21	3.32	3.44	3.56	3.68	3.79	3.91	4.03	4.14	4.25	4.38	4.48	4.59	4.71	4.82	4.93	5.04
54	3.21	3.32	3.44	3.56	3.68	3.79	3.91	4.03	4.14	4.25	4.38	4.48	4.59	4.71	4.82	4.93	5.04
55	3.21	3.32	3.44	3.56	3.68	3.79	3.91	4.03	4.14	4.25	4.38	4.48	4.59	4.71	4.82	4.93	5.04
56	3.21	3.32	3.44	3.56	3.68	3.79	3.91	4.03	4.14	4.25	4.38	4.48	4.59	4.71	4.82	4.93	5.04
57	3.21	3.32	3.44	3.56	3.68	3.79	3.91	4.03	4.14	4.25	4.38	4.48	4.59	4.71	4.82	4.93	5.04
58	3.21	3.32	3.44	3.56	3.68	3.79	3.91	4.03	4.14	4.25	4.38	4.48	4.59	4.71	4.82	4.93	5.04
59	3.21	3.32	3.44	3.56	3.68	3.79	3.91	4.03	4.14	4.25	4.38	4.48	4.59	4.71	4.82	4.93	5.04

Table C.15 Ripples in Instantaneous Torque Profiles (ΔT Profile) Determined for Fast Filling by Proposed Global NLP Optimization Method.(0-16 A).

Angle (θ°)/ Current (A)	0	1	2	3	4	5	6	7	8	9	10	11	12	13	14	15	16
0	0.00	0.00	0.00	0.00	0.00	0.00	0.00	0.00	0.00	0.00	0.00	0.00	-0.01	0.00	-0.01	-0.01	-0.02
1	0.00	0.00	0.00	0.00	0.00	0.00	0.00	0.00	0.00	0.00	0.00	0.00	-0.01	0.00	0.00	-0.01	-0.01
2	0.00	0.00	0.00	0.00	0.00	0.00	0.00	0.00	0.00	0.00	0.00	0.00	-0.01	0.00	-0.01	0.00	-0.04
3	0.00	0.00	0.00	0.00	0.01	0.01	0.01	0.02	0.02	0.03	0.00	0.04	0.04	0.05	0.05	0.05	-0.01
4	0.00	0.00	0.00	0.00	0.00	0.00	0.00	0.00	0.00	0.00	0.00	0.01	-0.01	0.00	0.00	0.00	0.00
5	0.00	0.00	0.00	0.00	0.00	0.00	0.00	0.01	0.01	0.01	0.01	0.01	0.00	0.01	0.01	0.02	0.02
6	0.00	0.00	0.00	0.00	0.00	0.00	0.00	0.00	0.00	0.01	0.01	0.01	0.00	0.01	0.01	0.02	0.02
7	0.00	0.00	0.00	0.00	0.00	0.01	0.01	0.01	0.01	0.01	0.02	0.03	0.03	0.05	0.04	0.05	0.05
8	0.00	0.00	0.00	0.00	0.00	0.00	0.00	0.00	0.00	-0.01	0.00	0.01	0.00	0.01	-0.01	-0.02	-0.03
9	0.00	0.00	0.00	0.00	0.00	0.00	0.00	0.00	0.00	-0.01	0.00	0.01	0.00	0.01	0.00	-0.01	-0.02
10	0.00	0.00	0.00	0.00	0.00	0.00	0.00	0.00	0.00	-0.01	0.00	0.01	-0.01	0.01	-0.01	0.02	0.02
11	0.00	0.00	0.00	0.00	0.00	0.00	0.00	0.00	0.00	0.00	0.00	0.00	0.00	0.02	-0.01	0.00	0.01
12	0.00	0.00	0.00	0.00	0.00	0.00	0.00	0.00	0.00	0.00	-0.01	0.00	-0.01	0.01	0.00	0.01	0.00
13	0.00	0.00	0.00	0.00	0.00	0.00	0.00	0.00	-0.01	-0.01	-0.01	0.00	-0.01	0.00	-0.01	-0.01	-0.02
14	0.00	0.00	0.00	0.00	0.00	0.00	0.00	0.00	0.00	0.00	0.00	0.00	0.00	0.00	0.00	0.00	0.00
15	0.00	0.00	0.00	0.00	0.00	0.00	0.00	0.00	0.00	0.00	0.00	0.00	-0.01	0.00	-0.01	-0.01	-0.02
16	0.00	0.00	0.00	0.00	0.00	0.00	0.00	0.00	0.00	0.00	0.00	0.00	-0.01	0.00	0.00	-0.01	-0.01
17	0.00	0.00	0.00	0.00	0.00	0.00	0.00	0.00	0.00	0.00	0.00	0.00	-0.01	0.00	-0.01	0.00	-0.04
18	0.00	0.00	0.00	0.00	0.01	0.01	0.01	0.02	0.02	0.03	0.00	0.04	0.04	0.05	0.05	0.05	-0.01
19	0.00	0.00	0.00	0.00	0.00	0.00	0.00	0.00	0.00	0.00	0.00	0.01	-0.01	0.00	0.00	0.00	0.00
20	0.00	0.00	0.00	0.00	0.00	0.00	0.00	0.01	0.01	0.01	0.01	0.01	0.00	0.01	0.01	0.02	0.02
21	0.00	0.00	0.00	0.00	0.00	0.00	0.00	0.00	0.00	0.01	0.01	0.01	0.00	0.01	0.01	0.02	0.02
22	0.00	0.00	0.00	0.00	0.00	0.01	0.01	0.01	0.01	0.01	0.02	0.03	0.03	0.05	0.04	0.05	0.05
23	0.00	0.00	0.00	0.00	0.00	0.00	0.00	0.00	0.00	-0.01	0.00	0.01	0.00	0.01	-0.01	-0.02	-0.03
24	0.00	0.00	0.00	0.00	0.00	0.00	0.00	0.00	0.00	-0.01	0.00	0.01	0.00	0.01	0.00	-0.01	-0.02
25	0.00	0.00	0.00	0.00	0.00	0.00	0.00	0.00	0.00	-0.01	0.00	0.01	-0.01	0.01	-0.01	0.02	0.02
26	0.00	0.00	0.00	0.00	0.00	0.00	0.00	0.00	0.00	0.00	0.00	0.00	0.00	0.02	-0.01	0.00	0.01
27	0.00	0.00	0.00	0.00	0.00	0.00	0.00	0.00	0.00	0.00	-0.01	0.00	-0.01	0.01	0.00	0.01	0.00
28	0.00	0.00	0.00	0.00	0.00	0.00	0.00	0.00	-0.01	-0.01	-0.01	0.00	-0.01	0.00	-0.01	-0.01	-0.02
29	0.00	0.00	0.00	0.00	0.00	0.00	0.00	0.00	0.00	0.00	0.00	0.00	0.00	0.00	0.00	0.00	0.00
30	0.00	0.00	0.00	0.00	0.00	0.00	0.00	0.00	0.00	0.00	0.00	0.00	-0.01	0.00	-0.01	-0.01	-0.02
31	0.00	0.00	0.00	0.00	0.00	0.00	0.00	0.00	0.00	0.00	0.00	0.00	-0.01	0.00	0.00	-0.01	-0.01
32	0.00	0.00	0.00	0.00	0.00	0.00	0.00	0.00	0.00	0.00	0.00	0.00	-0.01	0.00	-0.01	0.00	-0.04
33	0.00	0.00	0.00	0.00	0.01	0.01	0.01	0.02	0.02	0.03	0.00	0.04	0.04	0.05	0.05	0.05	-0.01
34	0.00	0.00	0.00	0.00	0.00	0.00	0.00	0.00	0.00	0.00	0.00	0.01	-0.01	0.00	0.00	0.00	0.00
35	0.00	0.00	0.00	0.00	0.00	0.00	0.00	0.01	0.01	0.01	0.01	0.01	0.00	0.01	0.01	0.02	0.02

36	0.00	0.00	0.00	0.00	0.00	0.00	0.00	0.00	0.00	0.01	0.01	0.01	0.00	0.01	0.01	0.02	0.02
37	0.00	0.00	0.00	0.00	0.00	0.01	0.01	0.01	0.01	0.01	0.02	0.03	0.03	0.05	0.04	0.05	0.05
38	0.00	0.00	0.00	0.00	0.00	0.00	0.00	0.00	0.00	-0.01	0.00	0.01	0.00	0.01	-0.01	-0.02	-0.03
39	0.00	0.00	0.00	0.00	0.00	0.00	0.00	0.00	0.00	-0.01	0.00	0.01	0.00	0.01	0.00	-0.01	-0.02
40	0.00	0.00	0.00	0.00	0.00	0.00	0.00	0.00	0.00	-0.01	0.00	0.01	-0.01	0.01	-0.01	0.02	0.02
41	0.00	0.00	0.00	0.00	0.00	0.00	0.00	0.00	0.00	0.00	0.00	0.00	0.00	0.02	-0.01	0.00	0.01
42	0.00	0.00	0.00	0.00	0.00	0.00	0.00	0.00	0.00	0.00	-0.01	0.00	-0.01	0.01	0.00	0.01	0.00
43	0.00	0.00	0.00	0.00	0.00	0.00	0.00	0.00	-0.01	-0.01	-0.01	0.00	-0.01	0.00	-0.01	-0.01	-0.02
44	0.00	0.00	0.00	0.00	0.00	0.00	0.00	0.00	0.00	0.00	0.00	0.00	0.00	0.00	0.00	0.00	0.00
45	0.00	0.00	0.00	0.00	0.00	0.00	0.00	0.00	0.00	0.00	0.00	0.00	-0.01	0.00	-0.01	-0.01	-0.02
46	0.00	0.00	0.00	0.00	0.00	0.00	0.00	0.00	0.00	0.00	0.00	0.00	-0.01	0.00	0.00	-0.01	-0.01
47	0.00	0.00	0.00	0.00	0.00	0.00	0.00	0.00	0.00	0.00	0.00	0.00	-0.01	0.00	-0.01	0.00	-0.04
48	0.00	0.00	0.00	0.00	0.01	0.01	0.01	0.02	0.02	0.03	0.00	0.04	0.04	0.05	0.05	0.05	-0.01
49	0.00	0.00	0.00	0.00	0.00	0.00	0.00	0.00	0.00	0.00	0.00	0.01	-0.01	0.00	0.00	0.00	0.00
50	0.00	0.00	0.00	0.00	0.00	0.00	0.00	0.01	0.01	0.01	0.01	0.01	0.00	0.01	0.01	0.02	0.02
51	0.00	0.00	0.00	0.00	0.00	0.00	0.00	0.00	0.00	0.01	0.01	0.01	0.00	0.01	0.01	0.02	0.02
52	0.00	0.00	0.00	0.00	0.00	0.01	0.01	0.01	0.01	0.01	0.02	0.03	0.03	0.05	0.04	0.05	0.05
53	0.00	0.00	0.00	0.00	0.00	0.00	0.00	0.00	0.00	-0.01	0.00	0.01	0.00	0.01	-0.01	-0.02	-0.03
54	0.00	0.00	0.00	0.00	0.00	0.00	0.00	0.00	0.00	-0.01	0.00	0.01	0.00	0.01	0.00	-0.01	-0.02
55	0.00	0.00	0.00	0.00	0.00	0.00	0.00	0.00	0.00	-0.01	0.00	0.01	-0.01	0.01	-0.01	0.02	0.02
56	0.00	0.00	0.00	0.00	0.00	0.00	0.00	0.00	0.00	0.00	0.00	0.00	0.00	0.02	-0.01	0.00	0.01
57	0.00	0.00	0.00	0.00	0.00	0.00	0.00	0.00	0.00	0.00	-0.01	0.00	-0.01	0.01	0.00	0.01	0.00
58	0.00	0.00	0.00	0.00	0.00	0.00	0.00	0.00	-0.01	-0.01	-0.01	0.00	-0.01	0.00	-0.01	-0.01	-0.02
59	0.00	0.00	0.00	0.00	0.00	0.00	0.00	0.00	0.00	0.00	0.00	0.00	0.00	0.00	0.00	0.00	0.00

Table C.16 Ripples in Instantaneous Torque Profile (ΔT profile) Determined for Fast Filling by Proposed Global NLP Optimization Method.(17-33 A).

Angle (θ°)/ Current (A)	17	18	19	20	21	22	23	24	25	26	27	28	29	30	31	32	33
0	-0.01	-0.03	-0.01	0.01	-0.01	-0.02	-0.01	-0.01	-0.01	-0.03	-0.01	-0.02	-0.01	-0.03	-0.02	-0.01	-0.02
1	-0.01	-0.02	-0.02	0.01	-0.01	-0.01	-0.02	-0.02	-0.01	-0.01	-0.02	-0.03	-0.01	-0.03	-0.02	-0.02	-0.02
2	0.00	-0.01	-0.04	0.02	-0.01	-0.02	0.00	0.00	-0.01	-0.01	-0.01	-0.01	0.01	0.01	0.02	0.03	0.03
3	0.00	-0.01	0.04	0.05	0.02	0.01	0.02	0.02	0.02	0.02	0.02	-0.02	0.03	0.01	0.02	0.03	0.03
4	-0.04	0.00	0.02	0.03	0.00	-0.03	-0.01	0.00	0.01	0.01	0.02	0.02	0.04	0.04	0.05	0.06	0.08
5	0.02	0.02	0.03	0.03	0.03	0.01	0.03	0.04	0.04	0.06	0.08	0.07	0.10	0.09	0.12	0.15	0.17
6	0.02	-0.01	-0.05	0.05	0.05	0.05	0.04	0.07	0.07	0.12	0.13	0.13	0.17	0.18	0.20	0.23	0.25
7	0.04	0.03	0.04	0.05	0.02	-0.01	0.02	0.10	0.12	0.14	0.16	0.16	0.20	0.21	0.24	0.26	0.28
8	-0.05	-0.07	0.01	0.03	0.02	0.02	0.04	0.08	0.10	0.11	0.13	0.13	0.16	0.17	0.19	0.20	0.22
9	0.02	0.01	0.03	0.05	0.05	0.02	0.06	0.09	0.10	0.11	0.12	0.12	0.15	0.15	0.16	0.17	0.18
10	0.01	0.03	0.02	0.06	0.04	0.04	0.04	0.07	0.07	0.08	0.09	0.08	0.11	0.11	0.11	0.12	0.13
11	0.01	-0.01	0.03	0.05	0.02	0.02	0.04	0.04	0.04	0.04	0.07	0.04	0.08	0.07	0.08	0.08	0.09
12	-0.01	-0.02	-0.02	0.03	0.01	0.00	0.02	0.03	0.03	0.00	0.04	0.03	0.05	0.04	0.05	0.05	0.06
13	-0.01	-0.01	0.00	0.01	-0.01	-0.05	-0.01	0.00	-0.02	0.00	0.00	-0.01	0.01	0.00	0.00	0.01	0.01
14	0.00	0.00	0.00	0.00	0.00	0.00	0.00	0.00	0.00	0.00	0.00	0.00	0.00	0.00	0.00	0.00	0.00
15	-0.01	-0.03	-0.01	0.01	-0.01	-0.02	-0.01	-0.01	-0.01	-0.03	-0.01	-0.02	-0.01	-0.03	-0.02	-0.01	-0.02
16	-0.01	-0.02	-0.02	0.01	-0.01	-0.01	-0.02	-0.02	-0.01	-0.01	-0.02	-0.03	-0.01	-0.03	-0.02	-0.02	-0.02
17	0.00	-0.01	-0.04	0.02	-0.01	-0.02	0.00	0.00	-0.01	-0.01	-0.01	-0.01	0.01	0.01	0.02	0.03	0.03
18	0.00	-0.01	0.04	0.05	0.02	0.01	0.02	0.02	0.02	0.02	0.02	-0.02	0.03	0.01	0.02	0.03	0.03
19	-0.04	0.00	0.02	0.03	0.00	-0.03	-0.01	0.00	0.01	0.01	0.02	0.02	0.04	0.04	0.05	0.06	0.08
20	0.02	0.02	0.03	0.03	0.03	0.01	0.03	0.04	0.04	0.06	0.08	0.07	0.10	0.09	0.12	0.15	0.17
21	0.02	-0.01	-0.05	0.05	0.05	0.05	0.04	0.07	0.07	0.12	0.13	0.13	0.17	0.18	0.20	0.23	0.25
22	0.04	0.03	0.04	0.05	0.02	-0.01	0.02	0.10	0.12	0.14	0.16	0.16	0.20	0.21	0.24	0.26	0.28
23	-0.05	-0.07	0.01	0.03	0.02	0.02	0.04	0.08	0.10	0.11	0.13	0.13	0.16	0.17	0.19	0.20	0.22
24	0.02	0.01	0.03	0.05	0.05	0.02	0.06	0.09	0.10	0.11	0.12	0.12	0.15	0.15	0.16	0.17	0.18
25	0.01	0.03	0.02	0.06	0.04	0.04	0.04	0.07	0.07	0.08	0.09	0.08	0.11	0.11	0.11	0.12	0.13
26	0.01	-0.01	0.03	0.05	0.02	0.02	0.04	0.04	0.04	0.04	0.07	0.04	0.08	0.07	0.08	0.08	0.09
27	-0.01	-0.02	-0.02	0.03	0.01	0.00	0.02	0.03	0.03	0.00	0.04	0.03	0.05	0.04	0.05	0.05	0.06
28	-0.01	-0.01	0.00	0.01	-0.01	-0.05	-0.01	0.00	-0.02	0.00	0.00	-0.01	0.01	0.00	0.00	0.01	0.01
29	0.00	0.00	0.00	0.00	0.00	0.00	0.00	0.00	0.00	0.00	0.00	0.00	0.00	0.00	0.00	0.00	0.00
30	-0.01	-0.03	-0.01	0.01	-0.01	-0.02	-0.01	-0.01	-0.01	-0.03	-0.01	-0.02	-0.01	-0.03	-0.02	-0.01	-0.02
31	-0.01	-0.02	-0.02	0.01	-0.01	-0.01	-0.02	-0.02	-0.01	-0.01	-0.02	-0.03	-0.01	-0.03	-0.02	-0.02	-0.02
32	0.00	-0.01	-0.04	0.02	-0.01	-0.02	0.00	0.00	-0.01	-0.01	-0.01	-0.01	0.01	0.01	0.02	0.03	0.03
33	0.00	-0.01	0.04	0.05	0.02	0.01	0.02	0.02	0.02	0.02	0.02	-0.02	0.03	0.01	0.02	0.03	0.03
34	-0.04	0.00	0.02	0.03	0.00	-0.03	-0.01	0.00	0.01	0.01	0.02	0.02	0.04	0.04	0.05	0.06	0.08
35	0.02	0.02	0.03	0.03	0.03	0.01	0.03	0.04	0.04	0.06	0.08	0.07	0.10	0.09	0.12	0.15	0.17
36	0.02	-0.01	-0.05	0.05	0.05	0.05	0.04	0.07	0.07	0.12	0.13	0.13	0.17	0.18	0.20	0.23	0.25

37	0.04	0.03	0.04	0.05	0.02	-0.01	0.02	0.10	0.12	0.14	0.16	0.16	0.20	0.21	0.24	0.26	0.28
38	-0.05	-0.07	0.01	0.03	0.02	0.02	0.04	0.08	0.10	0.11	0.13	0.13	0.16	0.17	0.19	0.20	0.22
39	0.02	0.01	0.03	0.05	0.05	0.02	0.06	0.09	0.10	0.11	0.12	0.12	0.15	0.15	0.16	0.17	0.18
40	0.01	0.03	0.02	0.06	0.04	0.04	0.04	0.07	0.07	0.08	0.09	0.08	0.11	0.11	0.11	0.12	0.13
41	0.01	-0.01	0.03	0.05	0.02	0.02	0.04	0.04	0.04	0.04	0.07	0.04	0.08	0.07	0.08	0.08	0.09
42	-0.01	-0.02	-0.02	0.03	0.01	0.00	0.02	0.03	0.03	0.00	0.04	0.03	0.05	0.04	0.05	0.05	0.06
43	-0.01	-0.01	0.00	0.01	-0.01	-0.05	-0.01	0.00	-0.02	0.00	0.00	-0.01	0.01	0.00	0.00	0.01	0.01
44	0.00	0.00	0.00	0.00	0.00	0.00	0.00	0.00	0.00	0.00	0.00	0.00	0.00	0.00	0.00	0.00	0.00
45	-0.01	-0.03	-0.01	0.01	-0.01	-0.02	-0.01	-0.01	-0.01	-0.03	-0.01	-0.02	-0.01	-0.03	-0.02	-0.01	-0.02
46	-0.01	-0.02	-0.02	0.01	-0.01	-0.01	-0.02	-0.02	-0.01	-0.01	-0.02	-0.03	-0.01	-0.03	-0.02	-0.02	-0.02
47	0.00	-0.01	-0.04	0.02	-0.01	-0.02	0.00	0.00	-0.01	-0.01	-0.01	-0.01	0.01	0.01	0.02	0.03	0.03
48	0.00	-0.01	0.04	0.05	0.02	0.01	0.02	0.02	0.02	0.02	0.02	-0.02	0.03	0.01	0.02	0.03	0.03
49	-0.04	0.00	0.02	0.03	0.00	-0.03	-0.01	0.00	0.01	0.01	0.02	0.02	0.04	0.04	0.05	0.06	0.08
50	0.02	0.02	0.03	0.03	0.03	0.01	0.03	0.04	0.04	0.06	0.08	0.07	0.10	0.09	0.12	0.15	0.17
51	0.02	-0.01	-0.05	0.05	0.05	0.05	0.04	0.07	0.07	0.12	0.13	0.13	0.17	0.18	0.20	0.23	0.25
52	0.04	0.03	0.04	0.05	0.02	-0.01	0.02	0.10	0.12	0.14	0.16	0.16	0.20	0.21	0.24	0.26	0.28
53	-0.05	-0.07	0.01	0.03	0.02	0.02	0.04	0.08	0.10	0.11	0.13	0.13	0.16	0.17	0.19	0.20	0.22
54	0.02	0.01	0.03	0.05	0.05	0.02	0.06	0.09	0.10	0.11	0.12	0.12	0.15	0.15	0.16	0.17	0.18
55	0.01	0.03	0.02	0.06	0.04	0.04	0.04	0.07	0.07	0.08	0.09	0.08	0.11	0.11	0.11	0.12	0.13
56	0.01	-0.01	0.03	0.05	0.02	0.02	0.04	0.04	0.04	0.04	0.07	0.04	0.08	0.07	0.08	0.08	0.09
57	-0.01	-0.02	-0.02	0.03	0.01	0.00	0.02	0.03	0.03	0.00	0.04	0.03	0.05	0.04	0.05	0.05	0.06
58	-0.01	-0.01	0.00	0.01	-0.01	-0.05	-0.01	0.00	-0.02	0.00	0.00	-0.01	0.01	0.00	0.00	0.01	0.01
59	0.00	0.00	0.00	0.00	0.00	0.00	0.00	0.00	0.00	0.00	0.00	0.00	0.00	0.00	0.00	0.00	0.00

Table C.17 Ripples in Instantaneous Torque Profile (ΔT profile) Determined for Fast Filling by Proposed Global NLP Optimization Method.(34-50 A).

Angle (θ°)/ Current (A)	34	35	36	37	38	39	40	41	42	43	44	45	46	47	48	49	50
0	-0.01	-0.02	-0.02	-0.01	-0.02	-0.02	-0.01	0.00	-0.01	-0.01	0.02	0.01	0.00	0.02	0.02	0.03	0.03
1	-0.03	-0.02	-0.01	0.00	0.00	0.01	0.02	0.02	0.02	0.04	0.05	0.05	0.05	0.06	0.07	0.08	0.08
2	0.03	0.04	0.06	0.07	0.08	0.09	0.10	0.12	0.13	0.13	0.16	0.16	0.17	0.20	0.21	0.22	0.24
3	0.04	0.04	0.05	0.09	0.10	0.09	0.12	0.13	0.13	0.19	0.22	0.21	0.22	0.24	0.25	0.27	0.28
4	0.09	0.10	0.11	0.11	0.15	0.15	0.17	0.19	0.20	0.22	0.25	0.26	0.27	0.30	0.31	0.33	0.35
5	0.17	0.19	0.21	0.23	0.25	0.26	0.29	0.31	0.33	0.35	0.38	0.39	0.41	0.45	0.48	0.51	0.54
6	0.26	0.29	0.31	0.34	0.36	0.38	0.41	0.45	0.47	0.50	0.55	0.57	0.61	0.67	0.71	0.76	0.81
7	0.30	0.31	0.34	0.33	0.35	0.36	0.38	0.40	0.40	0.46	0.50	0.50	0.51	0.53	0.54	0.56	0.58
8	0.24	0.24	0.25	0.25	0.28	0.29	0.28	0.30	0.34	0.32	0.37	0.30	0.37	0.39	0.40	0.36	0.42
9	0.20	0.20	0.22	0.23	0.23	0.24	0.26	0.27	0.27	0.27	0.30	0.30	0.30	0.31	0.32	0.32	0.32
10	0.14	0.14	0.15	0.17	0.17	0.17	0.18	0.19	0.19	0.19	0.21	0.20	0.21	0.22	0.22	0.21	0.22
11	0.10	0.09	0.10	0.11	0.12	0.11	0.12	0.13	0.12	0.12	0.14	0.13	0.13	0.14	0.14	0.14	0.14
12	0.06	0.06	0.06	0.07	0.07	0.07	0.07	0.08	0.08	0.07	0.09	0.08	0.08	0.07	0.08	0.08	0.08
13	0.01	0.01	0.01	0.01	0.01	0.01	0.02	0.01	0.01	0.01	0.02	0.01	0.00	0.01	0.01	0.01	0.01
14	0.00	0.00	0.00	0.00	0.00	0.00	0.00	0.00	0.00	0.00	0.00	0.00	0.00	0.00	0.00	0.00	0.00
15	-0.01	-0.02	-0.02	-0.01	-0.01	-0.02	-0.01	0.00	-0.01	-0.01	0.02	0.01	0.00	0.02	0.02	0.03	0.03
16	-0.03	-0.02	-0.01	0.00	0.00	0.01	0.02	0.02	0.02	0.04	0.05	0.05	0.05	0.06	0.07	0.08	0.08
17	0.03	0.04	0.06	0.07	0.08	0.09	0.10	0.12	0.13	0.13	0.16	0.16	0.17	0.20	0.21	0.22	0.24
18	0.04	0.04	0.05	0.09	0.10	0.09	0.12	0.13	0.13	0.19	0.22	0.21	0.22	0.24	0.25	0.27	0.28
19	0.09	0.10	0.11	0.11	0.15	0.15	0.17	0.19	0.20	0.22	0.25	0.26	0.27	0.30	0.31	0.33	0.35
20	0.17	0.19	0.21	0.23	0.25	0.26	0.29	0.31	0.33	0.35	0.38	0.39	0.41	0.45	0.48	0.51	0.54
21	0.26	0.29	0.31	0.34	0.36	0.38	0.41	0.45	0.47	0.50	0.55	0.57	0.61	0.67	0.71	0.76	0.81
22	0.30	0.31	0.34	0.33	0.35	0.36	0.38	0.40	0.40	0.46	0.50	0.50	0.51	0.53	0.54	0.56	0.58
23	0.24	0.24	0.25	0.25	0.28	0.29	0.28	0.30	0.34	0.32	0.37	0.30	0.37	0.39	0.40	0.36	0.42
24	0.20	0.20	0.22	0.23	0.23	0.24	0.26	0.27	0.27	0.27	0.30	0.30	0.30	0.31	0.32	0.32	0.32
25	0.14	0.14	0.15	0.17	0.17	0.17	0.18	0.19	0.19	0.19	0.21	0.20	0.21	0.22	0.22	0.21	0.22
26	0.10	0.09	0.10	0.11	0.12	0.11	0.12	0.13	0.12	0.12	0.14	0.13	0.13	0.14	0.14	0.14	0.14
27	0.06	0.06	0.06	0.07	0.07	0.07	0.07	0.08	0.08	0.07	0.09	0.08	0.08	0.07	0.08	0.08	0.08
28	0.01	0.01	0.01	0.01	0.01	0.01	0.02	0.01	0.01	0.01	0.02	0.01	0.00	0.01	0.01	0.01	0.01
29	0.00	0.00	0.00	0.00	0.00	0.00	0.00	0.00	0.00	0.00	0.00	0.00	0.00	0.00	0.00	0.00	0.00
30	-0.01	-0.02	-0.02	-0.01	-0.01	-0.02	-0.01	0.00	-0.01	-0.01	0.02	0.01	0.00	0.02	0.02	0.03	0.03
31	-0.03	-0.02	-0.01	0.00	0.00	0.01	0.02	0.02	0.02	0.04	0.05	0.05	0.05	0.06	0.07	0.08	0.08
32	0.03	0.04	0.06	0.07	0.08	0.09	0.10	0.12	0.13	0.13	0.16	0.16	0.17	0.20	0.21	0.22	0.24
33	0.04	0.04	0.05	0.09	0.10	0.09	0.12	0.13	0.13	0.19	0.22	0.21	0.22	0.24	0.25	0.27	0.28
34	0.09	0.10	0.11	0.11	0.15	0.15	0.17	0.19	0.20	0.22	0.25	0.26	0.27	0.30	0.31	0.33	0.35
35	0.17	0.19	0.21	0.23	0.25	0.26	0.29	0.31	0.33	0.35	0.38	0.39	0.41	0.45	0.48	0.51	0.54
36	0.26	0.29	0.31	0.34	0.36	0.38	0.41	0.45	0.47	0.50	0.55	0.57	0.61	0.67	0.71	0.76	0.81

37	0.30	0.31	0.34	0.33	0.35	0.36	0.38	0.40	0.40	0.46	0.50	0.50	0.51	0.53	0.54	0.56	0.58
38	0.24	0.24	0.25	0.25	0.28	0.29	0.28	0.30	0.34	0.32	0.37	0.30	0.37	0.39	0.40	0.36	0.42
39	0.20	0.20	0.22	0.23	0.23	0.24	0.26	0.27	0.27	0.27	0.30	0.30	0.30	0.31	0.32	0.32	0.32
40	0.14	0.14	0.15	0.17	0.17	0.17	0.18	0.19	0.19	0.19	0.21	0.20	0.21	0.22	0.22	0.21	0.22
41	0.10	0.09	0.10	0.11	0.12	0.11	0.12	0.13	0.12	0.12	0.14	0.13	0.13	0.14	0.14	0.14	0.14
42	0.06	0.06	0.06	0.07	0.07	0.07	0.07	0.08	0.08	0.07	0.09	0.08	0.08	0.07	0.08	0.08	0.08
43	0.01	0.01	0.01	0.01	0.01	0.01	0.02	0.01	0.01	0.01	0.02	0.01	0.00	0.01	0.01	0.01	0.01
44	0.00	0.00	0.00	0.00	0.00	0.00	0.00	0.00	0.00	0.00	0.00	0.00	0.00	0.00	0.00	0.00	0.00
45	-0.01	-0.02	-0.02	-0.01	-0.01	-0.02	-0.01	0.00	-0.01	-0.01	0.02	0.01	0.00	0.02	0.02	0.03	0.03
46	-0.03	-0.02	-0.01	0.00	0.00	0.01	0.02	0.02	0.02	0.04	0.05	0.05	0.05	0.06	0.07	0.08	0.08
47	0.03	0.04	0.06	0.07	0.08	0.09	0.10	0.12	0.13	0.13	0.16	0.16	0.17	0.20	0.21	0.22	0.24
48	0.04	0.04	0.05	0.09	0.10	0.09	0.12	0.13	0.13	0.19	0.22	0.21	0.22	0.24	0.25	0.27	0.28
49	0.09	0.10	0.11	0.11	0.15	0.15	0.17	0.19	0.20	0.22	0.25	0.26	0.27	0.30	0.31	0.33	0.35
50	0.17	0.19	0.21	0.23	0.25	0.26	0.29	0.31	0.33	0.35	0.38	0.39	0.41	0.45	0.48	0.51	0.54
51	0.26	0.29	0.31	0.34	0.36	0.38	0.41	0.45	0.47	0.50	0.55	0.57	0.61	0.67	0.71	0.76	0.81
52	0.30	0.31	0.34	0.33	0.35	0.36	0.38	0.40	0.40	0.46	0.50	0.50	0.51	0.53	0.54	0.56	0.58
53	0.24	0.24	0.25	0.25	0.28	0.29	0.28	0.30	0.34	0.32	0.37	0.30	0.37	0.39	0.40	0.36	0.42
54	0.20	0.20	0.22	0.23	0.23	0.24	0.26	0.27	0.27	0.27	0.30	0.30	0.30	0.31	0.32	0.32	0.32
55	0.14	0.14	0.15	0.17	0.17	0.17	0.18	0.19	0.19	0.19	0.21	0.20	0.21	0.22	0.22	0.21	0.22
56	0.10	0.09	0.10	0.11	0.12	0.11	0.12	0.13	0.12	0.12	0.14	0.13	0.13	0.14	0.14	0.14	0.14
57	0.06	0.06	0.06	0.07	0.07	0.07	0.07	0.08	0.08	0.07	0.09	0.08	0.08	0.07	0.08	0.08	0.08
58	0.01	0.01	0.01	0.01	0.01	0.01	0.02	0.01	0.01	0.01	0.02	0.01	0.00	0.01	0.01	0.01	0.01
59	0.00	0.00	0.00	0.00	0.00	0.00	0.00	0.00	0.00	0.00	0.00	0.00	0.00	0.00	0.00	0.00	0.00

Table C.18 Instantaneous Excitation Phase Current Profiles by Proposed Global Optimization Method (5 A, 10 A, 15 A, 20 A, 25 A).

Angle (θ°)/ Current (A)	5A				10A				15A				20A				25A			
	I1	I2	I3	I4	I1	I2	I3	I4	I1	I2	I3	I4	I1	I2	I3	I4	I1	I2	I3	I4
0	0	0	0	5	0	0	3	10	0	0	4	15	0	0	3	20	0	0	5	25
1	0	0	0	5	0	0	2	10	0	0	2	15	0	0	2	20	0	0	5	25
2	0	0	0	5	0	0	2	10	0	0	2	15	0	0	3	20	0	0	5	25
3	0	0	0	5	0	0	2	10	0	0	3	15	0	0	3	20	0	0	4	25
4	0	0	0	5	0	0	2	10	0	0	3	15	0	0	3	20	0	0	3	25
5	0	0	0	5	0	0	2	10	0	0	3	15	0	0	2	20	0	0	3	25
6	0	0	0	5	0	0	2	10	0	0	2	15	0	0	1	20	0	0	1	25
7	0	0	0	5	2	0	0	10	4	0	0	15	1	0	0	20	1	0	0	25
8	0	0	0	5	2	0	0	10	5	0	0	15	1	0	0	20	1	0	0	25
9	0	0	0	5	2	0	0	10	3	0	0	15	1	0	0	20	1	0	0	25
10	0	0	0	5	2	0	0	10	3	0	0	15	2	0	0	20	1	0	0	25
11	0	0	0	5	2	0	0	10	4	0	0	15	3	0	0	20	3	0	0	25
12	0	0	0	5	3	0	0	10	2	0	0	15	2	0	0	20	2	0	0	25
13	0	0	0	5	3	0	0	10	3	0	0	15	2	0	0	20	3	0	0	25
14	0	0	0	5	3	0	0	10	3	0	0	15	3	0	0	20	4	0	0	25
15	5	0	0	0	10	0	0	3	15	0	0	4	20	0	0	3	25	0	0	5
16	5	0	0	0	10	0	0	2	15	0	0	2	20	0	0	2	25	0	0	5
17	5	0	0	0	10	0	0	2	15	0	0	2	20	0	0	3	25	0	0	5
18	5	0	0	0	10	0	0	2	15	0	0	3	20	0	0	3	25	0	0	4
19	5	0	0	0	10	0	0	2	15	0	0	3	20	0	0	3	25	0	0	3
20	5	0	0	0	10	0	0	2	15	0	0	3	20	0	0	2	25	0	0	3
21	5	0	0	0	10	0	0	2	15	0	0	2	20	0	0	1	25	0	0	1
22	5	0	0	0	10	2	0	0	15	4	0	0	20	1	0	0	25	1	0	0
23	5	0	0	0	10	2	0	0	15	5	0	0	20	1	0	0	25	1	0	0
24	5	0	0	0	10	2	0	0	15	3	0	0	20	1	0	0	25	1	0	0
25	5	0	0	0	10	2	0	0	15	3	0	0	20	2	0	0	25	1	0	0
26	5	0	0	0	10	2	0	0	15	4	0	0	20	3	0	0	25	3	0	0
27	5	0	0	0	10	3	0	0	15	2	0	0	20	2	0	0	25	2	0	0
28	5	0	0	0	10	3	0	0	15	3	0	0	20	2	0	0	25	3	0	0
29	5	0	0	0	10	3	0	0	15	3	0	0	20	3	0	0	25	4	0	0
30	0	5	0	0	3	10	0	0	4	15	0	0	3	20	0	0	5	25	0	0
31	0	5	0	0	2	10	0	0	2	15	0	0	2	20	0	0	5	25	0	0
32	0	5	0	0	2	10	0	0	2	15	0	0	3	20	0	0	5	25	0	0
33	0	5	0	0	2	10	0	0	3	15	0	0	3	20	0	0	4	25	0	0
34	0	5	0	0	2	10	0	0	3	15	0	0	3	20	0	0	3	25	0	0
35	0	5	0	0	2	10	0	0	3	15	0	0	2	20	0	0	3	25	0	0
36	0	5	0	0	2	10	0	0	2	15	0	0	1	20	0	0	1	25	0	0
37	0	5	0	0	0	10	2	0	0	15	4	0	0	20	1	0	0	25	1	0
38	0	5	0	0	0	10	2	0	0	15	5	0	0	20	1	0	0	25	1	0
39	0	5	0	0	0	10	2	0	0	15	3	0	0	20	1	0	0	25	1	0

40	0	5		0	0	10	2	0	0	15	3	0	0	20	2	0	0	25	1	0
41	0	5		0	0	10	2	0	0	15	4	0	0	20	3	0	0	25	3	0
42	0	5		0	0	10	3	0	0	15	2	0	0	20	2	0	0	25	2	0
43	0	5		0	0	10	3	0	0	15	3	0	0	20	2	0	0	25	3	0
44	0	5		0	0	10	3	0	0	15	3	0	0	20	3	0	0	25	4	0
45	0	0	5	0	0	3	10	0	0	4	15	0	0	3	20	0	0	5	25	0
46	0	0	5	0	0	2	10	0	0	2	15	0	0	2	20	0	0	5	25	0
47	0	0	5	0	0	2	10	0	0	2	15	0	0	3	20	0	0	5	25	0
48	0	0	5	0	0	2	10	0	0	3	15	0	0	3	20	0	0	4	25	0
49	0	0	5	0	0	2	10	0	0	3	15	0	0	3	20	0	0	3	25	0
50	0	0	5	0	0	2	10	0	0	3	15	0	0	2	20	0	0	3	25	0
51	0	0	5	0	0	2	10	0	0	2	15	0	0	1	20	0	0	1	25	0
52	0	0	5	0	0	0	10	2	0	0	15	4	0	0	20	1	0	0	25	1
53	0	0	5	0	0	0	10	2	0	0	15	5	0	0	20	1	0	0	25	1
54	0	0	5	0	0	0	10	2	0	0	15	3	0	0	20	1	0	0	25	1
55	0	0	5	0	0	0	10	2	0	0	15	3	0	0	20	2	0	0	25	1
56	0	0	5	0	0	0	10	2	0	0	15	4	0	0	20	3	0	0	25	3
57	0	0	5	0	0	0	10	3	0	0	15	2	0	0	20	2	0	0	25	2
58	0	0	5	0	0	0	10	3	0	0	15	3	0	0	20	2	0	0	25	3
59	0	0	5	0	0	0	10	3	0	0	15	3	0	0	20	3	0	0	25	4

Table C.19 Instantaneous Excitation Phase Current Profiles by Proposed Global Optimization Method (30 A, 35 A, 40 A, 45 A, 50 A).

Angle (θ°)/ Current (A)	30A				35A				40A				45A				50A			
	I1	I2	I3	I4	I1	I2	I3	I4	I1	I2	I3	I4	I1	I2	I3	I4	I1	I2	I3	I4
0	0	0	7	30	0	0	9	35	0	0	9	40	0	0	8	45	0	0	12	50
1	0	0	6	30	0	0	8	35	0	0	8	40	0	0	8	45	0	0	10	50
2	0	0	6	30	0	0	7	35	0	0	8	40	0	0	7	45	0	0	9	50
3	0	0	5	30	0	0	6	35	0	0	6	40	0	0	5	45	0	0	8	50
4	0	0	4	30	0	0	5	35	0	0	5	40	0	0	4	45	0	0	6	50
5	0	0	3	30	0	0	4	35	0	0	4	40	0	0	2	45	0	0	5	50
6	0	0	1	30	0	0	2	35	0	0	3	40	0	0	1	45	0	0	4	50
7	1	0	0	30	0	0	0	35	0	0	0	40	12	0	0	45	4	0	0	50
8	0	0	0	30	0	0	0	35	0	0	0	40	15	0	0	45	5	0	0	50
9	1	0	0	30	0	0	0	35	0	0	0	40	20	0	0	45	7	0	0	50
10	1	0	0	30	4	0	0	35	5	0	0	40	19	0	0	45	9	0	0	50
11	1	0	0	30	4	0	0	35	5	0	0	40	17	0	0	45	9	0	0	50
12	3	0	0	30	5	0	0	35	6	0	0	40	16	0	0	45	10	0	0	50
13	5	0	0	30	7	0	0	35	8	0	0	40	15	0	0	45	12	0	0	50
14	7	0	0	30	8	0	0	35	10	0	0	40	11	0	0	45	15	0	0	50
15	30	0	0	7	35	0	0	9	40	0	0	9	45	0	0	8	50	0	0	12
16	30	0	0	6	35	0	0	8	40	0	0	8	45	0	0	8	50	0	0	10
17	30	0	0	6	35	0	0	7	40	0	0	8	45	0	0	7	50	0	0	9
18	30	0	0	5	35	0	0	6	40	0	0	6	45	0	0	5	50	0	0	8
19	30	0	0	4	35	0	0	5	40	0	0	5	45	0	0	4	50	0	0	6
20	30	0	0	3	35	0	0	4	40	0	0	4	45	0	0	2	50	0	0	5
21	30	0	0	1	35	0	0	2	40	0	0	3	45	0	0	1	50	0	0	4
22	30	1	0	0	35	0	0	0	40	0	0	0	45	12	0	0	50	4	0	0
23	30	0	0	0	35	0	0	0	40	0	0	0	45	15	0	0	50	5	0	0
24	30	1	0	0	35	0	0	0	40	0	0	0	45	20	0	0	50	7	0	0
25	30	1	0	0	35	4	0	0	40	5	0	0	45	19	0	0	50	9	0	0
26	30	1	0	0	35	4	0	0	40	5	0	0	45	17	0	0	50	9	0	0
27	30	3	0	0	35	5	0	0	40	6	0	0	45	16	0	0	50	10	0	0
28	30	5	0	0	35	7	0	0	40	8	0	0	45	15	0	0	50	12	0	0
29	30	7	0	0	35	8	0	0	40	10	0	0	45	11	0	0	50	15	0	0
30	7	30	0	0	9	35	0	0	9	40	9	0	8	45	0	0	12	50	0	0
31	6	30	0	0	8	35	0	0	8	40	8	0	8	45	0	0	10	50	0	0
32	6	30	0	0	7	35	0	0	8	40	8	0	7	45	0	0	9	50	0	0
33	5	30	0	0	6	35	0	0	6	40	6	0	5	45	0	0	8	50	0	0
34	4	30	0	0	5	35	0	0	5	40	5	0	4	45	0	0	6	50	0	0
35	3	30	0	0	4	35	0	0	4	40	4	0	2	45	0	0	5	50	0	0
36	1	30	0	0	2	35	0	0	3	40	3	0	1	45	0	0	4	50	0	0
37	0	30	1	0	0	35	0	0	0	40	0	0	0	45	12	0	0	50	4	0
38	0	30	0	0	0	35	0	0	0	40	0	0	0	45	15	0	0	50	5	0
39	0	30	1	0	0	35	0	0	0	40	0	0	0	45	20	0	0	50	7	0
40	0	30	1	0	0	35	4	0	0	40	5	0	0	45	19	0	0	50	9	0
41	0	30	1	0	0	35	4	0	0	40	5	0	0	45	17	0	0	50	9	0

42	0	30	3	0	0	35	5	0	0	40	6	0	0	45	16	0	0	50	10	0
43	0	30	5	0	0	35	7	0	0	40	8	0	0	45	15	0	0	50	12	0
44	0	30	7	0	0	35	8	0	0	40	10	0	0	45	11	0	0	50	15	0
45	0	7	30	0	0	9	35	0	0	9	40	0	0	8	45	0	0	12	50	0
46	0	6	30	0	0	8	35	0	0	8	40	0	0	8	45	0	0	10	50	0
47	0	6	30	0	0	7	35	0	0	8	40	0	0	7	45	0	0	9	50	0
48	0	5	30	0	0	6	35	0	0	6	40	0	0	5	45	0	0	8	50	0
49	0	4	30	0	0	5	35	0	0	5	40	0	0	4	45	0	0	6	50	0
50	0	3	30	0	0	4	35	0	0	4	40	0	0	2	45	0	0	5	50	0
51	0	1	30	0	0	2	35	0	0	3	40	0	0	1	45	0	0	4	50	0
52	0	0	30	1	0	0	35	0	0	0	40	0	0	0	45	12	0	0	50	4
53	0	0	30	0	0	0	35	0	0	0	40	0	0	0	45	15	0	0	50	5
54	0	0	30	1	0	0	35	0	0	0	40	0	0	0	45	20	0	0	50	7
55	0	0	30	1	0	0	35	4	0	0	40	5	0	0	45	19	0	0	50	9
56	0	0	30	1	0	0	35	4	0	0	40	5	0	0	45	17	0	0	50	9
57	0	0	30	3	0	0	35	5	0	0	40	6	0	0	45	16	0	0	50	10
58	0	0	30	5	0	0	35	7	0	0	40	8	0	0	45	15	0	0	50	12
59	0	0	30	7	0	0	35	8	0	0	40	10	0	0	45	11	0	0	50	15

APPENDIX D: PERFORMANCE EVALUATION OF MATRIX CONVERTER

Table D.1 Comparison of Instantaneous Phase Current Profiles by Proposed Method with the Results of the 3 Switching Schemes of Matrix Converter Design. (at 45 A)

Angle (θ°)/ Current (A)	Optimal Solution (22-DC Levels)				Matrix Converter with 7 DC-Levels				Matrix Converter with 9 DC-Levels				Matrix Converter with 12 DC-Levels			
	I1	I2	I3	I4	I1	I2	I3	I4	I1	I2	I3	I4	I1	I2	I3	I4
0	11	0	0	45	12	0	0	45	12	0	0	45	12	0	0	45
1	45	0	0	8	45	0	0	8	45	0	0	9	45	0	0	8
2	45	0	0	8	45	0	0	8	45	0	0	9	45	0	0	8
3	45	0	0	7	45	0	0	8	45	0	0	6	45	0	0	6
4	45	0	0	5	45	0	0	4	45	0	0	6	45	0	0	4
5	45	0	0	4	45	0	0	4	45	0	0	3	45	0	0	4
6	45	0	0	2	45	0	0	4	45	0	0	3	45	0	0	2
7	45	0	0	1	45	0	0	0	45	0	0	0	45	0	0	0
8	45	12	0	0	45	12	0	0	45	12	0	0	45	12	0	0
9	45	15	0	0	45	16	0	0	45	15	0	0	45	14	0	0
10	45	20	0	0	45	20	0	0	45	21	0	0	45	20	0	0
11	45	19	0	0	45	20	0	0	45	18	0	0	45	18	0	0
12	45	17	0	0	45	16	0	0	45	18	0	0	45	16	0	0
13	45	16	0	0	45	16	0	0	45	15	0	0	45	16	0	0
14	45	15	0	0	45	16	0	0	45	15	0	0	45	14	0	0
15	45	11	0	0	45	12	0	0	45	12	0	0	45	10	0	0
16	8	45	0	0	8	45	0	0	9	45	0	0	8	45	0	0
17	8	45	0	0	8	45	0	0	9	45	0	0	8	45	0	0
18	7	45	0	0	8	45	0	0	6	45	0	0	6	45	0	0
19	5	45	0	0	4	45	0	0	6	45	0	0	4	45	0	0
20	4	45	0	0	4	45	0	0	3	45	0	0	4	45	0	0
21	2	45	0	0	4	45	0	0	3	45	0	0	2	45	0	0
22	1	45	0	0	0	45	0	0	0	45	0	0	0	45	0	0
23	0	45	12	0	0	45	12	0	0	45	12	0	0	45	12	0
24	0	45	15	0	0	45	16	0	0	45	15	0	0	45	14	0
25	0	45	20	0	0	45	20	0	0	45	21	0	0	45	20	0
26	30	1	0	0	0	45	20	0	0	45	18	0	0	45	18	0
27	0	45	19	0	0	45	16	0	0	45	18	0	0	45	16	0
28	0	45	17	0	0	45	16	0	0	45	15	0	0	45	16	0
29	0	45	16	0	0	45	16	0	0	45	15	0	0	45	14	0
30	0	45	15	0	0	45	12	0	0	45	12	0	0	45	10	0
31	0	45	11	0	0	8	45	0	0	9	45	0	0	8	45	0

32	0	8	45	0	0	8	45	0	0	9	45	0	0	8	45	0
33	0	8	45	0	0	8	45	0	0	6	45	0	0	6	45	0
34	0	7	45	0	0	4	45	0	0	6	45	0	0	4	45	0
35	0	5	45	0	0	4	45	0	0	3	45	0	0	4	45	0
36	0	4	45	0	0	4	45	0	0	3	45	0	0	2	45	0
37	0	2	45	0	0	0	45	0	0	0	45	0	0	0	45	0
38	0	1	45	0	0	0	45	12	0	0	45	12	0	0	45	12
39	0	0	45	12	0	0	45	16	0	0	45	15	0	0	45	14
40	0	0	45	15	0	0	45	20	0	0	45	21	0	0	45	20
41	0	0	45	19	0	0	45	20	0	0	45	18	0	0	45	18
42	0	0	45	17	0	0	45	16	0	0	45	18	0	0	45	16
43	0	0	45	16	0	0	45	16	0	0	45	15	0	0	45	16
44	0	0	45	15	0	0	45	16	0	0	45	15	0	0	45	14
45	0	0	45	11	0	0	45	12	0	0	45	12	0	0	45	10
46	0	0	8	45	0	0	8	45	0	0	9	45	0	0	8	45
47	0	0	8	45	0	0	8	45	0	0	9	45	0	0	8	45
48	0	0	7	45	0	0	8	45	0	0	6	45	0	0	6	45
49	0	0	5	45	0	0	4	45	0	0	6	45	0	0	4	45
50	0	0	4	45	0	0	4	45	0	0	3	45	0	0	4	45
51	0	0	2	45	0	0	4	45	0	0	3	45	0	0	2	45
52	0	0	1	45	0	0	0	45	0	0	0	45	0	0	0	45
53	12	0	0	45	12	0	0	45	12	0	0	45	12	0	0	45
54	15	0	0	45	16	0	0	45	15	0	0	45	14	0	0	45
55	20	0	0	45	20	0	0	45	21	0	0	45	20	0	0	45
56	19	0	0	45	20	0	0	45	18	0	0	45	18	0	0	45
57	17	0	0	45	16	0	0	45	18	0	0	45	16	0	0	45
58	16	0	0	45	16	0	0	45	15	0	0	45	16	0	0	45
59	15	0	0	45	16	0	0	45	15	0	0	45	14	0	0	45

Table D.2 Comparison of Instantaneous Initial (T_i), ΔT and Final Torque (T_f) with Ripple (R) Profiles by Proposed Global Optimization Method with 3 Switching Schemes of Matrix Converter. (at 45 A)

Angle (θ°)/ Current (A)	After Adv.θ	Optimal Solution (22-DC Levels)			Matrix Converter with 7 DC-Levels			Matrix Converter with 9 DC-Levels			Matrix Converter with 12 DC-Levels		
	T_i	ΔT	T_f	R	ΔT	T_f	R	ΔT	T_f	R	ΔT	T_f	R
0	4.47	0.01	4.48	0.00	0.01	4.48	-0.02	0.01	4.48	-0.04	0.01	4.48	0.02
1	4.43	0.05	4.48	0.00	0.06	4.49	-0.01	0.05	4.48	-0.04	0.06	4.49	0.03
2	4.32	0.16	4.48	0.00	0.16	4.48	-0.02	0.17	4.49	-0.03	0.16	4.48	0.02
3	4.27	0.22	4.49	0.01	0.25	4.52	0.02	0.2	4.47	-0.05	0.2	4.47	0.01
4	4.22	0.28	4.50	0.02	0.24	4.46	-0.04	0.31	4.53	0.01	0.24	4.46	0.00
5	4.09	0.39	4.48	0.00	0.39	4.48	-0.02	0.49	4.58	0.06	0.39	4.48	0.02
6	3.91	0.58	4.49	0.01	0.66	4.57	0.07	0.58	4.49	-0.03	0.51	4.42	-0.04
7	3.98	0.52	4.50	0.02	0.62	4.60	0.10	0.62	4.60	0.08	0.43	4.41	-0.05
8	4.18	0.29	4.47	-0.01	0.29	4.47	-0.03	0.38	4.56	0.04	0.29	4.47	0.01
9	4.18	0.29	4.47	-0.01	0.29	4.47	-0.03	0.38	4.56	0.04	0.29	4.47	0.01
10	4.28	0.22	4.50	0.02	0.29	4.57	0.07	0.17	4.45	-0.07	0.17	4.45	-0.01
11	4.35	0.11	4.46	-0.02	0.07	4.42	-0.08	0.16	4.51	-0.01	0.07	4.42	-0.04
12	4.40	0.07	4.47	-0.01	0.07	4.47	-0.03	0.17	4.57	0.05	0.07	4.47	0.01
13	4.47	0.02	4.49	0.01	0.07	4.54	0.04	0.04	4.51	-0.01	0.02	4.49	0.03
14	4.48	0	4.48	0.00	0	4.48	-0.02	0	4.48	-0.04	0	4.48	0.02
15	4.47	0.01	4.48	0.00	0.01	4.48	-0.02	0.01	4.48	-0.04	0.01	4.48	0.02
16	4.43	0.05	4.48	0.00	0.06	4.49	-0.01	0.05	4.48	-0.04	0.06	4.49	0.03
17	4.32	0.16	4.48	0.00	0.16	4.48	-0.02	0.17	4.49	-0.03	0.16	4.48	0.02
18	4.27	0.22	4.49	0.01	0.25	4.52	0.02	0.2	4.47	-0.05	0.2	4.47	0.01
19	4.22	0.28	4.50	0.02	0.24	4.46	-0.04	0.31	4.53	0.01	0.24	4.46	0.00
20	4.09	0.39	4.48	0.00	0.39	4.48	-0.02	0.49	4.58	0.06	0.39	4.48	0.02
21	3.91	0.58	4.49	0.01	0.66	4.57	0.07	0.58	4.49	-0.03	0.51	4.42	-0.04
22	3.98	0.52	4.50	0.02	0.62	4.60	0.10	0.62	4.60	0.08	0.43	4.41	-0.05
23	4.18	0.29	4.47	-0.01	0.29	4.47	-0.03	0.38	4.56	0.04	0.29	4.47	0.01
24	4.18	0.29	4.47	-0.01	0.29	4.47	-0.03	0.38	4.56	0.04	0.29	4.47	0.01
25	4.28	0.22	4.50	0.02	0.29	4.57	0.07	0.17	4.45	-0.07	0.17	4.45	-0.01
26	4.35	0.11	4.46	-0.02	0.07	4.42	-0.08	0.16	4.51	-0.01	0.07	4.42	-0.04
27	4.40	0.07	4.47	-0.01	0.07	4.47	-0.03	0.17	4.57	0.05	0.07	4.47	0.01
28	4.47	0.02	4.49	0.01	0.07	4.54	0.04	0.04	4.51	-0.01	0.02	4.49	0.03
29	4.48	0	4.48	0.00	0	4.48	-0.02	0	4.48	-0.04	0	4.48	0.02
30	4.47	0.01	4.48	0.00	0.01	4.48	-0.02	0.01	4.48	-0.04	0.01	4.48	0.02
31	4.43	0.05	4.48	0.00	0.06	4.49	-0.01	0.05	4.48	-0.04	0.06	4.49	0.03

32	4.32	0.16	4.48	0.00	0.16	4.48	-0.02	0.17	4.49	-0.03	0.16	4.48	0.02
33	4.27	0.22	4.49	0.01	0.25	4.52	0.02	0.2	4.47	-0.05	0.2	4.47	0.01
34	4.22	0.28	4.50	0.02	0.24	4.46	-0.04	0.31	4.53	0.01	0.24	4.46	0.00
35	4.09	0.39	4.48	0.00	0.39	4.48	-0.02	0.49	4.58	0.06	0.39	4.48	0.02
36	3.91	0.58	4.49	0.01	0.66	4.57	0.07	0.58	4.49	-0.03	0.51	4.42	-0.04
37	3.98	0.52	4.50	0.02	0.62	4.60	0.10	0.62	4.60	0.08	0.43	4.41	-0.05
38	4.18	0.29	4.47	-0.01	0.29	4.47	-0.03	0.38	4.56	0.04	0.29	4.47	0.01
39	4.18	0.29	4.47	-0.01	0.29	4.47	-0.03	0.38	4.56	0.04	0.29	4.47	0.01
40	4.28	0.22	4.50	0.02	0.29	4.57	0.07	0.17	4.45	-0.07	0.17	4.45	-0.01
41	4.35	0.11	4.46	-0.02	0.07	4.42	-0.08	0.16	4.51	-0.01	0.07	4.42	-0.04
42	4.40	0.07	4.47	-0.01	0.07	4.47	-0.03	0.17	4.57	0.05	0.07	4.47	0.01
43	4.47	0.02	4.49	0.01	0.07	4.54	0.04	0.04	4.51	-0.01	0.02	4.49	0.03
44	4.48	0	4.48	0.00	0	4.48	-0.02	0	4.48	-0.04	0	4.48	0.02
45	4.47	0.01	4.48	0.00	0.01	4.48	-0.02	0.01	4.48	-0.04	0.01	4.48	0.02
46	4.43	0.05	4.48	0.00	0.06	4.49	-0.01	0.05	4.48	-0.04	0.06	4.49	0.03
47	4.32	0.16	4.48	0.00	0.16	4.48	-0.02	0.17	4.49	-0.03	0.16	4.48	0.02
48	4.27	0.22	4.49	0.01	0.25	4.52	0.02	0.2	4.47	-0.05	0.2	4.47	0.01
49	4.22	0.28	4.50	0.02	0.24	4.46	-0.04	0.31	4.53	0.01	0.24	4.46	0.00
50	4.09	0.39	4.48	0.00	0.39	4.48	-0.02	0.49	4.58	0.06	0.39	4.48	0.02
51	3.91	0.58	4.49	0.01	0.66	4.57	0.07	0.58	4.49	-0.03	0.51	4.42	-0.04
52	3.98	0.52	4.50	0.02	0.62	4.60	0.10	0.62	4.60	0.08	0.43	4.41	-0.05
53	4.18	0.29	4.47	-0.01	0.29	4.47	-0.03	0.38	4.56	0.04	0.29	4.47	0.01
54	4.18	0.29	4.47	-0.01	0.29	4.47	-0.03	0.38	4.56	0.04	0.29	4.47	0.01
55	4.28	0.22	4.50	0.02	0.29	4.57	0.07	0.17	4.45	-0.07	0.17	4.45	-0.01
56	4.35	0.11	4.46	-0.02	0.07	4.42	-0.08	0.16	4.51	-0.01	0.07	4.42	-0.04
57	4.40	0.07	4.47	-0.01	0.07	4.47	-0.03	0.17	4.57	0.05	0.07	4.47	0.01
58	4.47	0.02	4.49	0.01	0.07	4.54	0.04	0.04	4.51	-0.01	0.02	4.49	0.03
59	4.48	0	4.48	0.00	0	4.48	-0.02	0	4.48	-0.04	0	4.48	0.02

LIST OF PUBLICATIONS

1. S. F. Ghousia and N. C. Kar, “Performance analysis of an 8/6 switched reluctance machine using finite element method,” *Proc. of the IEEE Power Engineering Society General Meeting*, 24-28 June 2007.

2. S. F. Ghousia and N. C. Kar, “Investigation of electromagnetic force using tunable volume integration method in a switched reluctance motor,” *Electrimacs International Conference on Theory and Application of Modeling and Simulation in Electrical Power Engineering*, Quebec, June 8-11 2008.

3. S. F.Ghousia, N. C. Kar, “A novel optimized instantaneous torque ripple minimization method with current profiling in switched reluctance motors,” *Proceedings of The 12th Joint MMM/Intermag Conference*, Chicago, IL Jan 14-18, 2013.

4. S. F.Ghousia, N. C. Kar, “A Novel torque ripple elimination method for switched reluctance motors using modified flood fill algorithm,” *IEEE Transactions on Industrial Informatics*, 2013 (Submitted).

VITA AUCTORIS

Syeda Fatima Ghousia was born in 1971 at Karachi, Pakistan. She received her bachelor degree in electronics engineering from Dawood College of Engineering and Technology, NED University, Karachi, Pakistan in 1992. She received her masters of nuclear engineering degree from Quaid-e-Azam University, Islamabad, Pakistan in 1995. She received her master of engineering degree in electrical power engineering in 2005 from University of Alberta, Edmonton, Canada. She is currently working towards the PhD degree at the Department of Electrical and Computer Engineering, University of Windsor, Ontario, Canada. Her research interests includes design and control of switched reluctance motors and drives in electric vehicle and wind energy applications, matrix converter topologies and applications in renewable energy generation applications.